# Photocatalytic and Biological Applications of Titania based Nanostructures

*Thesis submitted to*
*the University of Calicut in  partial fulfillment of the*
*requirements for the award of the degree of*

**Doctor of Philosophy**
*in Chemistry under the Faculty of Sciences*

*by*

## NIKHILA  M. P.

*Under the guidance of*

**Dr. Renuka N.K.**

**DEPARTMENT OF CHEMISTRY**
**UNIVERSITY OF CALICUT**
**KERALA–673 635**
**NOVEMBER 2017**

# CERTIFICATE

This is to certify that the thesis entitled **"Photocatalytic and Biological Applications of Titania based Nanostructures"** is an authentic record of the research work carried out by Nikhila M.P., under my guidance for the award of the degree of Doctor of Philisophy in Chemistry under the faculty of Sciencs, University of Calicut, Kerala and the same has not been submitted elsewhere for a degree or diploma. Certified that all the modifications suggested by the examiners have been incorporated in the thesis.

Calicut University                                   **Dr. Renuka N.K**
Date                                               (Supervising Teacher)

# DECLARATION

I hereby declare that the thesis entitled **"Photocatalytic and Biological Applications of Titania based Nanostructures"** is the bonafide report of the original work carried out by me under the supervision of Dr. N.K. Renuka, Asst. Professor, Department of Chemistry, University of Calicut for the award of the degree of Doctor of Philosophy in Chemistry Under the Faculty of Sciences, University of Calicut, Kerala. The content of this thesis have not been submitted to any other institute or University for the award of any degree or diploma.


Calicut University                                    **NIKHILA M. P.**
Date

# ACKNOWLEDGEMENT

*Thasleena Panakkal for their supportive nature and trust on me which have been crucial factors in the successful completion of my Ph.D work. They have been like a family to me and it was and will remain always a great pleasure to have such helpful and understanding friends with me. Special thanks to research scholars Anu Antony, Anju Ajayan, Shivanandan C.K., Vineeth M., Jyothy P.R., Nusrath Riyas, Aparna K. Balan, Jency, Soumya, Rajeena Puthoor, Dr. Sarada Karangadan, Shahnas Beegam M., Dr. K. Shijina, Bintu Thomas, Nonu Devis, Babina, Niji, Anju Paulson, Suja, Sagitha, of same and other departments for the co-operation offered to me during the work.*

*I extend my gratitude to Dr. Mrinal R Pai, BARC Mumbai, Dr. K. Vimala of Department of Zoology, Periyar University, Dr.K. Anas, Sud-Chemie India Pvt Ltd., Dr.Kuttan, Preetha of Amala Cancer research centre Thrissur, Dr. T Radhika, C-Met Thrissur, Vimala College Thrissur, St.Joseph's College Irinjalakuda, STIC Cochin (CUSAT), SAIF (IIT Bombay), for helping with  characterisation part.*

*My biggest source of strength has been my family: My Parents. They are the one who really stood by me to complete this venture. I salute you both for the love, care and sacrifice you did to shape my life and thank you for giving me freedom to realise my own potential. I am thankful to my brother Hari, cousin sisters, brothers, other elders of my family especially vallichan Aravindhakshan who encouraged me and sustained my will power. Dears, your love, care, affection, and moral support helped me to achieve this position. The words fall short to express the affection and support shown by my husband, Mr.Dijeesh; I greatly value his contribution and appreciate his belief in me. I thank*

**To my Parents................**

# PREFACE

Nanotechnology bullet train has the power to take us to magical places we have barely even dreamed of, and the increased understanding of both its potential benefits and dangers will retain it on track allowing the journey toward newer discoveries to continue. Studies which contribute to this area by design paradigms enable the scientists to design innovative functional materials, and thus broadening the fields to address major societal needs and challenges. Among various nanostructures, Nano Titania possesses numerous unique features such as low cost, non-toxicity, good stability, favorable band edge positions, and facile preparation routes with diverse morphologies. The uniqueness in each lattice structure of titania bestows it with multifaceted physico-chemical and opto-electronic properties and thus provide different functionalities for thair performance in various applications. Accordingly, synthesising crystalline titania with tunable phase/particle size/morphology has opened the grand research avenue. All the functional applications of $TiO_2$ fall in the scope of energy, environment and health, which are undeniably considered as the three important and challenging themes human race faces which are to be addressed in the present scenerio.

Here we have attempted to synthesise five nano titania structures with different morphologies; namely multishelled titania hollow nanospheroids, titania nanotubes, titania nanobelts, mesoporous assembled titania nanocuboids and titania nanoparticles. Analysis of physico-chemical characteristics and formation mechanisms of these

nanostructures provide a good understanding of morphology, crystal phases, porosities etc. The applicability of the systems in photocatalytic and biological fields has to been investigated.

Thesis is consists of 6 chapters

The first chapter comprises general introduction on the topic with special emphasis to nanotitania, crystal structures, synthesis, applications etc; An exhaustive review of literature in this area has been provided in this section. Second chapter dicusses the experimental aspects of synthesis, characterisation and application studies of titanium dioxide nanostructures. Titanium dioxide nanostructures with diverse morphologies are prepared by adopting different synthetic routes. Modification of the high surface area nanostrctures with copper and silver has been done. For biomedical applications, modifications are trialed with folic acid along with the incorporation of an anticancer drug 5-Fluorouracil [5FU]. Fundamental aspects of charactersation tools, X-Ray Diffraction (small and wide angle), Electron Spectroscopy (TEM, HRTEM, SEM,FEG-SEM), Nitrogen adsorption study (surface area and pore size distribution), Fourier Transform Infra-Red (FTIR) spectroscopy, UV-Visible Diffuse Reflectance Spectroscopy (UV-Vis DRS), Photoluminescent spectroscopy (PL) and Dynamic light scattering (DLS) are briefly explained. The utilization of these techniques for the characterisation of the prepared nanostructures and its mofied analouges are also discussed.

A detailed analysis of various chatacterization techniques of the five nanostructured systems are presented in chapter 3. A brief description related to formation mechanisms of the nanostructures is also provided. The fourth chapter discussing the applications is divided into two sections. First section deals with the photocatalytic removal of organic pollutant using the synthesied nanostructured photocatalysts. The antibacterial as well as antifungal properties of the systems as well as superhydrophilicity character of titania surface is also investigated, so as to examine the applicability of the system as a self-cleaning material. In the second section, photocatalytic watersplitting reaction to produce Hydrogen has been discussed using catalysts modified titania nanostructures.

The fifth chapter comprises the invitro cytotoxic studies of the synthesised nanostructures towards MCF-7 Cancer cell lines. Also cytotoxicities of anticancer drug encapsulated systems are compared with those systems which are functionalised with folic acid to support the targeted drug delivery. Further the intracellular mechanisms leading to cell death is assessed using a selected system. Chapter 7 summarizes the major results and outcomes of the present study. The scope of future aspect of the work based on these studies is also provided.

# TABLE OF CONTENTS

**CHAPTER II**
**Experimental methods and characterisation techniques**

**CHAPTER VI**
**SUMMARY AND SCOPE OF FUTURE WORK**

# CHAPTER I
# GENERAL INTRODUCTION

CONTENTS

*The ever increasing development of research in nanoscience and nanotechnology continually brings on new physical and chemical properties of TiO$_2$ nanomaterials. Titania based photo catalysts have been most widely investigated in the past decades. Basically photocatalysis underpins the important renewable energy and environmental technologies like photocatalytic water water/air purification, hydrogen production from water splitting, solar cells as well as in medical fields. The wide application range of nanotitania relies not only on the characteristics like non toxicity, cheapness and tunable band gap, but also on the capability of being nanostructured with ease. Surface-tuning strategies for synthesis and modification of oxides in nanometer scale for efficient photocatalysis have progressed at a fast pace. Titania can be shaped in a large class of nanostructures which include nanoparticles, nanorods, nanowires, nanotubes, nanobelts etc. It can also be aggregated to form mesoporous materials, aerogels, opals, interconnected architectures and photonic crystals. This chapter gives a brief introduction to nano sized titanium dioxide, various methods of preparation, relevant applications and appropriate modification techniques.*

## 1.1 Introduction

Earth has a natural environment called Ecosystem which included not only human life but also a series of numbers including plant life, atmosphere, rivers, seas, glaciers, other natural resources etc. The rise in human population and his over desire for luxurious life increased the reliance on technology. Though technology is providing us an easier and comfortable living, its over dependence poses a great threat to the environment. The threat is due to pollution, radiation hazards, exploitation of various natural resources, energy shortage etc. It is high time for human beings to address the various issues prudently and seriously. These environmental problems make us vulnerable to disasters and tragedies, and thus curb human existence in near future. Industrial development is filling our rivers, seas and oceans with toxic pollutants. Unabated release of toxic agents and industrial waste into the air and waterways has resulted in pollution-related diseases, global warming, and abnormal climatic changes. The removal of many emerging anthropogenic organic pollutants needs novel techniques to chemically convert them into non-hazardous compounds.

In addition to the environmental issues aforementioned, energy considerations also have greatly attracted attention nowadays. Natural resource depletion is another crucial current environmental problem. Inspite of the massive and unrampant use of available resources, the voracious appetite for energy is also raising world wide. Depletion of fossil fuel reserves results in the emission of Greenhouse gases, global warming and climate change. Recently people are taking efforts to utilise the renewable sources of energy like solar, wind, biogas,

geothermal energy etc. While most of us cry aloud about dirty air, polluted water and energy shortage, we should not close eyes to the fact that it is "us" who is responsible for these unfavorable circumstances. It should therefore be our duty to contribute to the development of renewable technologies for environmental remediation and sustainable energy production to deal with the global energy crisis and environmental issues related to various human activities. Interestingly, use of engineered nanoscale materials in this aspect usually meets the requirements for the current issues related to environment and energy. In this study, we focus on some of the aspects of nanomaterial applications in energy and environmental regimes. Nanoscale materials are of interest for various environmental applications due to their high surface area to volume ratio. Related to the same material of large size, these nano scale materials exhibit enhanced reactivity in chemical or biological surface mediated reactions.

Development of nanotechnology has its impact in medical field also. The use of nanotechnology paved the way to revolutionary changes in the field of medicine. Many techniques which were only in imagination a few years ago are being realised with the advent of Nanotechnology. Nanotechnology in medicine application includes drug delivery, therapy techniques, diagnostic techniques, antimicrobial techniques, etc. Nano medicines used for drug delivery are made up of nano scale particles or molecules which can improve drug bioavailability. Given the vast scope of nanomedicines we will also

focus on the therapeutic applications, in particular, cytotoxic applications of nanoparticles.

## 1.2 Nanotechnology- applied to metal oxides

Nanotechnology is manipulation of matter on an atomic, molecular, and supramolecular scale. Here we exploit the augmented physical and chemical properties offered by the materials in nanoscale dimension that are not accomplished in their bulk counterparts [1-2]. It is indeed a multidisciplinary and interdisciplinary field which extends over a number of fields (Figure 1) [3]. Nanotechnology may be able to produce new devices and materials with a massive range of applications in fields like in nanomedicine, biomaterials energy production, nanoelectronics and consumer products.
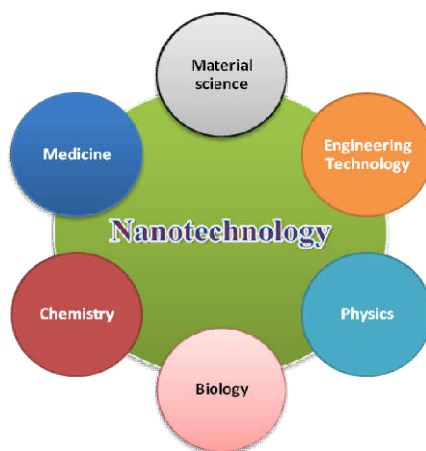


**Figure 1**. Nanotechnology - an inter disciplinary science

Development of Nanotechnology and nanoscience created a new space in the scienctific world where the superior properties of nanostructured materials (Optical, chemical, electronic, photoelectrochemical properties, mechanical etc;) are exploited for innovative applications. As an important family among this group, nanostructured metal oxides have recieved significant scientific attention and importance due to their unique functionalities when their structural feature size is down to nanoscale. For example, the bending of bulk copper in wire/ribbon, forms etc occur with movement of copper atoms/clusters at about the 50 nm scale. When copper nanoparticles smaller than 50 nm are exhibiting different maleability and ductility than the bulk copper atoms instead they are considered super hard materials. since nanoparticles are small enough to confine their electrons and produce quantum effects, often have unexpected visual properties. For example, in solution, gold nanoparticles appear deep red to black. The properties and applications of nanostructured semiconductors are determined by the morphology, structure and organization of nanostructured architectures to a great extent [4]. Nanotechnology applied to health sciences includes fabrication of devices used in surgery, design of new chips for better diagnostics, new functional materials for substituting body structures, and structures capable of carrying drugs through the body for the treatment of a lot of diseases called as nanocarriers. The use of nanoparticles has revealed therapeutic potential in almost every branch of medicine such as oncology, neurology, cardiology, endocrinology, immunology, ophthalmology, orthopedics, pulmonary and dentistry. The nanosize of these materials enable them to cross the cell tissue barriers with desired

effect and its lodging depends on temperature, ROS, pH etc of the microenvironment of the desired cell [5]. Reports based on the biological effects of these nanostrctures are controversial in many ways. Nanotechnologists continue fabricating newer nanomaterials and the toxicologists continue to assess the possible potential effects [6-7].

The change in properties is not always desirable. But Purposeful exploitation of such nanosized semiconductor metal oxides gives unprecedented growth of novel materials with breath taking performances. More explorations of fascinating and enhanced properties of these nano metal oxides are needed for focusing more on their applications [Figure 2]. A spectrum of applications have been identified utilising the enhanced properties of these nanosized metal oxides.
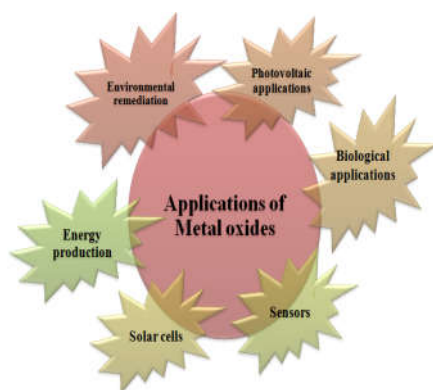


**Figure 2.** Applications of Metal oxides

Focussing on the other applications of metal oxides, Environmental cleanup / energy production using semiconductor mediated photocatalysis is a well explored area. A photocatalyst is defined as a material that is capable of absorbing light, thereby

generating electron–hole pairs which enable chemical transformations of the reaction participants, and can be regenerated after each cycle [8]. By using the principles of photoelctrochemistry, semiconductor particles convert light energy into electrical and chemical energy. Many binary compounds are classified as semiconductors but not all are suitable for semiconductor photocatalysis. An appropriate semiconductor to be used as photocatalyst should satisfy the following conditions. Proper band gap energies (1.7- 3.20 eV), good light absorption, efficient charge carrier mobility, defiinte band edge positions that straddle water redox potential, innocuous and chemically durable. Possible applications of semiconductor mediated photocatalysis are found mainly in four aspects: (i) photocatalytic removal of organic pollutants, (ii) $H_2$ and $O_2$ by photocatalytic water splitting, (iii) photocatalytic reduction of $CO_2$,(iv) photocatalytic synthesis for organic substances. Examples of some semiconductor metaloxide photocatalyst are $Fe_3O_4$, $TiO_2$, ZnO, $SnO_2$, $CeO_2$ , $V_2O_5$, $WO_3$.

Semiconductors can be classified into different categories according to their ability to split water as (i) oxidative/ O type, (ii) reductive/ R type, (iii) OR type and (iv) X-type. O type has strong oxidising power to oxidise water but reducing power is less to reduce water examples include $WO_3$, $Fe_2O_3$ etc. R-type is just the reverse of the aforementioned type where the reducing power is high whereas oxidation power is low. In X Type semiconductors, since the conduction and valence bands are located between $H^+/H_2$ and $O_2/H_2O$ levels both oxidation and reduction powers are weak hence no production of oxygen, hydrogen can be observed. OR type is characterised by its strong oxidising and reducing power to split water.

The most popular among this series being $TiO_2$. It is the most popular semiconductor and blessed with numerous unique features such as high redox potential, inexpensiveness, nontoxicity, good photochemical stability towards adverse environment. Other features include hydrophilicity, humidity and gas sensing, dielectric character, favorable band edge positions, facile preparation methods, synthesis of diverse morphologies, etc. CdS and ZnO are well known for their photcatalytic activity. But CdS decomposes to environmentally harmful $Cd^{2+}$ while ZnO is more liable to photcorossion due to self oxidation [9]. Moreover, thermodynamically favourable condition of the valence and conduction band position of titanium dioxide in which the reduction potential of superoxide radical and oxidation potential of hydroxyl radical are with in the bandgap.
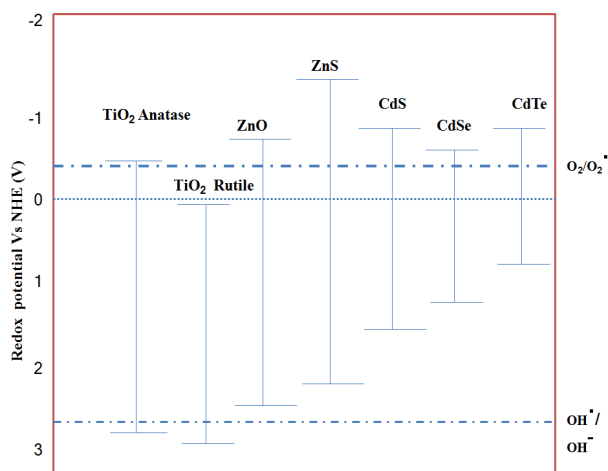


**Figure 3.** Valence band and Concuction band edges of some common semiconductors and their standard redox potentials (versus NHE: normal hydrogen electrode) of the ($O_2/O_2\bullet$) and ($\bullet OH/{-}OH$) redox couple.

From ancient times, Titanium dioxide has been widely used as an white pigment and its low toxicity is quite established from ancient times [10]. Only in the early part of 20 [th] centuary, scientific reports based on the photoactivity of titanium dioxide was observed. Photobleaching of dyes by $TiO_2$ has been reported where they suggested that the active oxygen species formed on $TiO_2$ upon UV absorption is responsible for this bleaching and $TiO_2$ was called as photosensitizer [11]. Works by Mashio et al, entitled ''Auto oxidation by $TiO_2$ as a photocatalyst''[12] observed the autooxidation of various organic solvents such as alcohol, hydrocarbons in presence of UV irradiation and Titania powders simultaneously generating $H_2O_2$ under ambient conditions. The same group had compared the photocatalytic activities of twelve types of commercial anatase and three types of rutile, $TiO_2$ powders and concluded that the anatase activity of the autooxidation is much higher than that of rutile [13]. In 1972 Fujishima and Honda discovered that water can be split when a bias potential is applied to an UV illuminated $TiO_2$ single crystal electrode and a platinum black counter electrode simultaneously oxidized to oxygen and reduced to hydrogen [14]. In those days of oil crisis, this astonishing report received attention of scientists in broad area. Soon after this discovery numerous studies related to this effect were reported.

**1972**

**A.Fujishima**                    **K.Honda**

In the late 1970s, the research was shifted more on utilising the oxidation power of photogenerated charge carriers of titania for the degradation of toxic pollutants. First report in this direction was by Frank and Bard in 1977 decomposing cyanide, a frequent industrial pollutant by $TiO_2$ suspension [15]. The photocatalytic decomposition reaction can be applicable to deactivate microorganisms. For example, Escherichia coli (E.coli) cells can completely disappear when treated with $TiO_2$ after about one week under a UV irradiation of 1 mW/cm$^2$ [16]. It is important to note that $TiO_2$ photocatalysis for using practical applications does not require any chemicals and but only with sunlight and rainwater. Important keys for these successes are (ii) the utilization of nano $TiO_2$ dispersed on substrates with extremely large surface areas and (ii) spreading them to collect sunlight to the maximum. As the concentrations of environmental pollutants are usually low, the portion of UV light contained in sunlight is sufficient enough to decompose them by $TiO_2$ photocatalysis. Absorption in UV region and its rapid electron hole recombination are considered as a major demerit of using Titania as a photocatalyst. Various modifications to increase the photocatalytic activity of titania have been practised including

modification of crystal structure, morphology, introducing metals/ nonmetals either as a dopant or surface deposite, dye sensitization, etc. These modifications are either indended to reduce the recombination of photogenerated charge carriers/ increase their life time/ increase the absorption to visible region so as to utilize the freely available solar energy for its light harvesting applications.

## 1.3 Nano Titania

Titanium dioxide was discovered in 1821 and holds position in the list of top 20 inorganic chemicals of industrial importance. Titania was given the name after the 'titans' who in Greek mythodology were 'the sons of earth'. Moreover, it is the 9th most abundant element in the earth crust and is the 4th most abundant structural element [17]. Titanium is well known for its unique combination of properties such as 'lighter than iron', 'stronger than aluminium' and 'corrosion resistant as platinum' and has been called as the 'wonder metal'. This low density material is having high melting point of $1667^0C$ and is very hard. It is never found in the metallic form in nature and is always found combined with oxygen and other metal oxides.

Materials in the nanoregime notices an increase of surface area with its decrease of the primary particle size thus resulting in the enhancement of chemical activity. It is obvious that by decreasing the particle size, the bandgap also widens as reflected by the blue shift in the absorption edge. The shift of Conduction Band towards more negative potential and Valence Band to more positive potentials favours the redox process that cannot occur in their bulk counterparts

[18-19]. In addition to this the added advantages of nanomaterials are modified electrical and optical properties definitely improve the efficiency of any photocatalytic process. The movement of charge carriers in semiconductor nanomaterials is primarily governed by the well known quantum confinement and transport properties related to phonons and photons which are largely affected by the size and geometry of the materials [20-21]. Obviously nanocrystalline $TiO_2$ exhibits distinctive properties such as quantum size effect, high surface area, short interface migration distance and visible light response. All the application potential of nanotitania lies in the scope of energy, environment, health which are the most challenging issues of the present centuary.

## 1.4 Crystal structure of Titania

Anatase, rutile and brookite are the most relevant modifications of titanium dioxide with the following crystallographic properties:[22-26].

1) Anatase (space group- I41/amd, crystal system – tetragonal, symmetry -$D_{4h}$)

2) Rutile (space group -P42/mnm, crystal system – tetragonal, symmetry- $D_{4h}$)

3) Brookite (space group- Pbca, crystal system – orthorhombic, symmetry- $D_{2h}$)

Other modifications, that have been synthesized, are [127]:

4)      $TiO_2$ II ("columbite", ($\alpha$-$PbO_2$),crystal system – orthorhombic, space group -Pbcn),

5)      $TiO_2$ III ("baddeleyite", crystal system – monoclinic, space group -P21/c)

6)      $TiO_2$ (H) ("hollandite", crystal system – tetragonal, space group- I4/m),

7)      $TiO_2$ (R) ("ramsdellite", crystal system – orthorhombic, space group- Pbnm)

8)      $TiO_2$ (B) ("bronze", crystal system – monoclinic, space group- $C_2$/m)

Except $TiO_2$ (B), none of the latter modifications occur in nature and have been synthesized by high pressure treatment of anatase or rutile. The local order in each phase is represented by an octahedron constituting oxygen ions at its vertices and titanium atoms at the center with different spatial arrangements sharing the edges and corners in a different manner. Each $Ti^{4+}$ ion is surrounded by an octahedron of six $O^{2-}$ ions. Each [$TiO_6$] in anatase is surrounded by eight octahedra (four edge-shared and four corner-shared) while Rutile is composed of corner-sharing octahedra with each octahedron surrounded by ten octahedral (two are edge-shared, eight corner-shared) The fraction of edge-sharing octahedra required to form anatase is greater compared to rutile [27-28]. In orthorhombic Brookite the octahedra share three edges and one of the edges determine the crystal distribution along the [100] direction and the other two edges the crystal distribution along

the [001] direction with tunnels along the c-axis [29]. The metastable monoclinic $TiO_2$ (B) has edge- and corner-shared octahedra with perovskite- like windows between the sites and a relatively open structure [30]. Rutile is the most common natural form of $TiO_2$ and thermodynamically the most stable phase at all temperatures and pressures, while metastable anatase and brookite are kinetic products. It is obvious that rutile is more symmetric and compact compared to other titania polymorphs. Rutile is commonly used as a white pigment in paints. Of the three minerals of titanium dioxide, anatase is the rarest form of titanium dioxide and tends to transform to rutile at high temperatures, approximately 723 K.

Each crystalline form, due to the lattice structure differences in turn affects the electronic structure and bulk diffusion ability of charge carriers. physico-chemical properties, opto-electronic properties are different in different polymorphs. For example, the high refractive index, excellent light scattering efficiency and UV absorptivity enables Rutile its use as a filter in solar creams, pigments, opacifiers and optical communication devices (isolators, modulators and switches) [31]. Anatase phase of titania is largely preferred in the fields of photocatalysis and photovoltaics. The other polymorphs brookite and $TiO_2$(B) are are nowadays gaining importance in photocatalysis, photovoltaics and lithium ion insertion recently [32-34]. Some peculiar structural features of the polymorphs serve beneficial depending on the applications. Size or surface area to volume ratio is important in catalysis while manipulation of size and shape (exposed facet) is vital for fabricating photonic crystals which provides more flexibility and

options for the design of nanostructures to assure distinctive requirements. The synergetic effect of mixed crystal framework of titania which is beneficial for achieving optimized performances is achieved through controlling the phase composition. The dissimilarity in band gaps, along with the position of CB and VB edges, is responsible for the formation of a stable heterojunction allowing the absorption of a wide spectral range and modifies the charge carrier generation, separation and transfer process. In light induced photoreactions, the inimate contact between the different phases affects the charge carrier transfer dynamics to an extent [35-37].

## 1.5 Synthesis methods for Titania nanostructures

According to Ardson, "Catalyst preparation is the secret of achieving the desired activity, selectivity and life time" [38]. In the case of metal oxides, the said fact is true as suggested by many reports [39-40]. Appropriate control of the desired properties, particularly morphology and crystallite structure in the synthesis of nanosized $TiO_2$ is still considered as key issues in this field. Generally there are two approaches for the synthesis of nanoparticles: top-down (physical method), and bottom-up (chemical method). The top-down approach includes ball milling and the nanoparticles synthesized by physical method possess relatively broad size distribution and diverse particle shapes. On the other hand, nanoparticles synthesised using the bottom-up approaches are observed to be uniform [41]. Some of the common methods for the synthesis of nanotitania are discussed below.

## 1.5.1 Sol-Gel method

Sol-gel is a versatile method for the synthesis of various ceramic Materials. Hydrolysis or polymerisation reactions of precursor solution, most probably an alkoxide results in the formation of sol. The loss of solvent leads to solid gel which can be converted in to a film on a substrate by spin or dip coating. Or it can be casted into a mould, forming a wet gel. Further, when this wet gel on drying and heat treatment leads to a dense ceramic. An aerogel can be obtained when the solvent in this wet gel is removed under supercritical conditions. When the viscosity of the sol is in a particular range, ceramic fibers can be drawn. Precipitation, spray pyrolysis, emulsion methods etc are used to obtain ultrafine and uniform ceramic powders. Sol-gel method to synthesise $TiO_2$ nanomaterials from a titanium precursor normally proceeds through an acid-catalyzed hydrolysis of precursor (Titanium (IV) alkoxide) followed by condensation. Low content of water, low hydrolysis rates, and excess titanium alkoxide in the reaction mixture favoured the formation of Ti-O-Ti chains. Development of Ti-O-Ti chains leads to 3D polymeric skeletons with close packing. Hydrolysis in a higher rate with medium amount of water result in the formation of $Ti(OH)_4$, while large quantity of Ti-OH and insufficient development of three-dimensional polymeric skeletons form loosely packed first-order particles. Presence of large excess of water leads to the development of polymeric Ti-O-Ti chains. Closely packed first order particles are yielded via a three-dimensionally developed gel skeleton.

## 1.5.2 Hydrothermal method

Hydrothermal method is usually conducted with aqueous solutions with controlled temperature and pressure in autoclave with or without teflon liners. The development of this technique was to mimic the formation of rocks and minerals in the nature [42]. In this method the temperature is normally chosen above the boiling point of water, reaching the pressure of vapor saturation. The amount of solution added and the temperature of the experiment detetmines the internal pressure developed in the vessel. Morphologies like titania naoparticles, nanorods, nanowires, nanaotubes, nanobelts, nanosheets can be synthesised by this method depending on precursors and additives. Because of the low cost and environmentally friendly nature, this method of synthesising nanostructures has received considerable interest which can be used on large area and/or flexible substrates, as well as fabrication of free standing nanostructures. The hydrothermal method has been extensively used to synthesise $TiO_2$ nanotubes since it was introduced by Kasuga et al. in 1998 [43]. Nanostructures including titania nanotubes, nanofibers, nanowires, nanoribbons and nanorods can be successfully obtained by controlling various parameters during hydrothermal synthetic conditions. For example, $TiO_2$ nanowires and nanobelts have been obtained by hydrothermal method by different groups [44-45]. $TiO_2$ nanorods are obtained by treating a dilute $TiCl_4$ solution at 333-423 K for 12 h in the presence of acid or inorganic salts [46]. Yang et al. [47] prepared $TiO_2$ nanoparticles by hydrothermal treatment of peptized precipitates of a titanium precursor with water.

### 1.5.3 Solvothermal method

Solvothermal method has been identified as a versatile method for the preparation of a variety of nanoparticles with narrow size distribution and dispersity.The solvothermal method is almost identical to the hydrothermal method, the only difference being that the precursor solution is usually not aqueous. This method combines the benefit of both the sol-gel and hydrothermal routes. Solvothermal synthesis allows for the precise control over the size, shape and crystallinity of nanostructures when compared to hydrothermal method. These features can be altered by the variation of experimental parameters. Solvothermal treatment of titania suspension in 5 M NaOH water-ethanol solution maintained at 170-200°C in an autoclave for 24 h produce $TiO_2$ nanowires followed by acid treatment and overnight drying. The physical and chemical properties of solvents significantly influence the solubility, reactivity, and diffusion behavior of the reactants and morphology and the crystallization behavior of products. Introduction of solvent ethanol at a higher concentration can result in the change in polarity of the solvent and increases solution viscosity. Wide and short flake like morphology was observed in the absence of ethanol and $TiO_2$ nanorods are formed when chloroform is used [48].

### 1.5.4 Vapour deposition (Chemical vapour deposition and Physical vapour deposition)

In vapour deposition, materials in a vapor state are condensed to form a solid-phase material and this processes usually take place within a vacuum chamber. These methods are usually done to form

coatings to modify the properties like optical, mechanical, thermal, electrical, wear resistance and corrosion resistance of various substrates. Semiconductor industry usually uses this method to produce thin films. If no chemical reaction is there, the process is called physical vapor deposition (PVD) and if otherwise; it is called chemical vapor deposition (CVD). In CVD processes, thermal energy heats the gases in the coating chamber and drives the deposition reaction. Methods such as ultrasonic spray pyrolysis, electrostatic spray hydrolysis, thermal plasma pyrolysis, diffusion flame pyrolysis, laser-induced pyrolysis, and ultronsic assisted hydrolysis etc. are the common CVD methods for the preparation of titania nano materials. Djerdja et al. reported CVD of nanocrystalline $TiO_2$ films on various substrates at relatively low temperature of 320°C with $TiCl_4$ as a precursor and observed that the size and distribution of nanomaterial largly depends on the substrate used [49]. Common PVD methods to synthesise titania nanomaterials included methods like thermal deposition, sputtering, cathodic arc deposition, ion plating, ion implantation, laser vaporization, and laser surface alloying etc. The most common PVD processes are sputtering and evaporation. $TiO_2$ nanowire arrays have been fabricated by a simple PVD method [50-52].

## 1.5.5 Electro deposition method

In electrodeposition coating, usually metallic, is done on a surface by the of reduction at the cathode. Cathode in the process is the substrate to be coated which was immersed into a solution which is the salt of the metal to be deposited. When electricity is applied, the

metallic ions in the solution are attracted towards the cathode and reduced to metallic form. An example for this method being the synthesis of titania nanowires using an anodic alumina membrane (AAM) as template [53-54]. When pulsed electrodeposition is carried out in 0.2 M $TiCl_3$ solution of pH= 2, titanium is deposited into the pores of the AAM. When the deposited template was heated at 500 ° C for 4 h, the removal of template takes place resulting in the formation of pure anatase $TiO_2$ nanowires [55].

## 1.5.6 Microwave method [MW]

MW heating is a promising new method for the one-pot synthesis of metallic nanostructures in solutions. By microwave irradiation, the energy is transferred to the reactants through molecular interactions with the electromagneticfield. Nanostructures with small sizes with narrow range of size distributions and a higher degree of crystallization have been achieved via MW heating than by conventional methods. Achievement of nanomaterials with narrow size distributions is due to the rapid consumption of starting materials which reduces the possibility of agglomorations in MW-assisted methods. In conventional thermal techniques the reaction vessel transfers energy from the heating mantle to the solvent then to the reactant molecules. As these steps rely on the thermal conductivity of various materials, the temperature of the reaction vessel may be higher than that of the reaction mixture. Resulting sharp thermal gradient all over the bulk solution and inefficient, non uniform reaction conditions has been a problem in the preparation of nanomaterials where uniform nucleation and growth rates are mandetary for material quality. The

dipolar mechanism and the electrical conductor mechanism are the basic principles of microwave chemistry. The dipolar mechanism occurs when a polar molecule attempts to follow the field in the same alignment under a very high frequency electric field. To drive the reaction forward, the molecules release enough heat. In the second mechanism, at lower microwave frequencies, conductive currents flowing within the material due to the movement of ionic constituents can transfer energy from the microwave field to the material. These induced currents and any electrical resistance will heat the sample. Microwave irradiation generates efficient internal heating by direct coupling of microwave energy with the molecules in the reaction mixtures. The reaction vessels employed are usually microwave transparent materials (borosilicate glass, quartz, or Teflon). Different morphologies like spheres, sheets, rods, tubes, and varying sizes can be synthesised by proper manipulation of exprimental parameters. Corradi et al. observed that microwave treatment of 1-2 h result in formation of colloidal titania nanoparticle suspensions whereas conventional techniques required 1 to 32 h with forced hydrolysis at 195 °C [56].

## 1.5.7 Direct oxidation method

Nanostructured $TiO_2$ can be synthesised by oxidizing titanium metal with oxidants or under anodization. For example, direct oxidation of titanium metal plate with hydrogen peroxide yeild crystalline $TiO_2$ nanorods. In a typical synthesis, A cleaned Ti plate was immersed in 50 mL of 30 wt% solution for 72 h at $353^{°}$K [57-58]. Addition of inorganic salts like Na (X) X= $F^-$, $Cl^-$, $SO_4^{2-}$) helps in

controlling the crystalline phase. while addition of $F^-$ and $SO_4^{2-}$ produces anatase phase, rutile phase is favoured in presence of $Cl^-$ [59]. Synthesis of Titania nanotube by anodization method is well studied [60-62]. Titania nanotubes are obtained when a clean Ti plate is anodized under the potential of 10-20V for 10-30 minutes [63]. Here counter electrodes used were platinum. Annealing at 500°C for 6 h in oxygen, results in the formation of crystallized $TiO_2$ nanotubes. Usually all anodizing experiments were done at an ambient temperature (22±2°C).

## 1.5.8 Sonochemical method

Sonochemical method produces nanostructured material of high surface area using ultra sound. Sonochemistry develop from acoustic cavitation: the formation, growth, and implosive collapse of bubbles in a liquid. Zhu et al. [64] developed Titania whiskers and nanotubes with the assistance of sonication. Yu et al [65] reported the sonochemical method for the synthesis of highly active $TiO_2$ nanoparticle photocatalysts with anatase and brookite phases by the hydrolysis of titanium tetraisoproproxide in pure water or in a 1:1 EtOH-$H_2O$ solution. Cavitational collapse produces intense local heating of about 5000 K and high pressures of about 1000 atm, vast heating and cooling rates ( >109 K/s). Rapid heat transfer, volumetric and selective heating are the advantages of using this method in industrial purposes.

## 1.6 Applications of Nanotitania

$TiO_2$ nanomaterials have been used in wide range of applications. Earlier applications include paint, sunscreens, toothpaste, UV protection, oinments etc. Later on after the discovery of photocatalytic splitting of water on a $TiO_2$ electrode in presence of UV light, much effort has been devoted to the development and application of $TiO_2$ materials in photovoltaics, photocatalysis, photo-electrochromics and sensors as well as photochromics.

### 1.6.1 Self cleaning and antifogging functions

If the water-surface contact angle is larger than 130° or less than 5°, the surface is defined as superhydrophilic or superhydrophobic respectively [66]. Depending on the surface conditions, $TiO_2$ thin film exhibits an initial CA of several tens of degrees. But when the $TiO_2$ coated surface is exposed to UV light, the contact angle decreases almost to zero [67]. At this stage, the surface becomes totally non-water-repellant and is termed ''super hydrophilic''. In 1992, first demonstration of self cleaning concept on a titania coated ceramic tile was done by Watanabe, Hashimoto and Fujishima [68]. More or less similar idea was showed independently by Heller [69] . One of such first commercialized products using this technique was the self cleaning cover glass for highway tunnel lamps [70]. Usually this type of lamp, is a sodium lamp in Japan, emits UV light of about 3 mW cm$^{-2}$ at the position of the cover glass. The chemical conformation changes of $TiO_2$ surface resulted in the phenomenon of superhydrophilicity [71]. Majority of photogenerated holes react with adsorbed water

molecules or contaminants producing •OH radicals and a small portion are trapped at the lattice oxygen sites. The interaction of these holes with $TiO_2$ itself is responsible for result in the reduction of strength of the bonds between the lattice titanium and oxygen ions. Then water molecules can interrupt these bonds, generating new hydroxyl groups which are singly coordinated and these are thermodynamically unstable and possess high surface energy, leading to the formation of a superhydrophilic surface. The discovery of photo-induced superhydrophilicity has markedly extended the application potential of $TiO_2$-coated materials. The deposition of various types of dirt, soot, vehicular exhaust and other particulates results in the requirement of cleaning the surfaces of buildings. Though the amount of photons is not adequate to decompose the adsorbed stains, the surface is maintained clean after water is supplied there. It is because water soaks between the molceular level spacing of stain/dirt and the super hydrophilic $TiO_2$ surface therefore, stains/dirt adsorbed on the $TiO_2$ surface can easily be washed by water. Such ''photocatalytic building materials'', e.g., exterior tiles, glass, plastic films, aluminum walls, PVC fabric, cement have been fabricated commercially [72]. TOTO, Ltd., the pioneer of self-cleaning technology, estimated that a building covered by ordinary tiles in a Japanese city need to be cleaned at least every five years to have a fine appearance, while those covered with self-cleaning tiles appeared cleaned with no maintanance cost over a period of twenty years. For example, the photocatalytic exterior glass with an area of 20,000 $m^2$ was installed in the terminal building of Chubu International Airport opened in 2005. Beading of rainwater on automobile side-view mirrors is a severe trouble which can be solved

by by constructing anti beading mirrors and windows using this technique.

The fogging of surfaces of glass occurs when moist air from the surrounding environment cools and forms water droplet on their surfces. Since these droplets scatter light or reflect or refract it, adversly affects the visual clarity. The study related to this effect was done by Watanabe and co-workers. They observed that under UV light illumination, a $TiO_2\backslash SiO_2$ surface become extremely hydrophilic. Thus water can spread evenly over the surface. The first commercial application of this effect has been employed for automobile side-view mirrors [73]. Takata et al. [74] have shown that when humid air was passed through the cooled fins, compared to ordinary fins, the volume of water flowing off the $TiO_2$-coated fins was 20% higher which hinder fogging and increase the heat exchange efficiency.

## 1.6.2 Electrochromic devices

Titania is widely employed in electrochromic windows and displays. It is basically the capability of a material to undergo color change upon oxidation or reduction [75]. When a small voltage applied to the windows causes them to be darken and reversing the voltage causes them to lighten. In this way the amount of energy entering through the window can be controlled which decreases the need of air conditioning in a cooled building. Among the two types of electrochromism of nanocrystalline thin film $TiO_2$ electrodes, the first type is that of nanocrystalline $TiO_2$ electrodes in $Li^+$ containing electrolytes where the reversible insertion of Li into the anatase lattice

of the nanoparticles takesplace. Hagfeldt et al observed forward biasing of nanocrystalline $TiO_2$ films in lithium ion-containing organic electrolytes resulted in the quick and reversible coloration owing to the electron accumulation and $Li^+$ intercalation in the anatase lattice [76]. The second type is the electrochromism of nanocrystalline $TiO_2$ electrodes in which viologens and/or anthrachinons equipped with a surface anchoring group. Moeller et al. observed electrochromic pictures with extraordinary resolution in transparent and reflective electrochromic displays (ECD) based on ink-jet printing technology. Here cascade-type crosslinking reactions of viologens in the mesopores of a $TiO_2$ electrode are explained with counter electrode based on mesoporous antimony tin oxide coated with $CeO_2$ [77].

## 1.6.3 Photocatalytic Applications towards water and air purification

Titania is known as the most efficient and environmentally friendly photocatalyst. Photocatalysis is generally thought of as the catalysis of a photochemical reaction on a solid surface, most probably a semiconductor. This definition simply not takes the full meaning. This process involves participation of two reactions oxidation and reduction occurring simultaneously. Oxidation, is from photogenerated holes and the second reaction involving reduction, is from photogenerated electrons. Both of these processes must be balanced in a proper way and the photocatalyst itself should not undergo any physical or chemical change, which is one of the essential property of a catalyst.The main advantage of this method for water decontamination is being the requirement of the $TiO_2$ photocatalyst and UV light (solar

light or artificial light) only and thus it is economical related to other kinds of advanced oxidation techniques. In addition to this, the process is devoid of the generation of any toxic products. Many endocrine disrupting chemicals like dioxins, bisphenol-A etc released into the aquatic environment are found to disturb normal endocrine functions. Chemical oxidation methods are costly and other biological methods require long periods of treatment time thus limiting their usage. But photocatalytic treatment is effective in the complete remediation of these chemicals. Water treatment plants adopting photocatalytic techniques have been in use for years. For example, Nakashima et al. fabricated a photocatalytic reactor with $TiO_2$-modified-PTFE mesh sheets to treat the water discharged from the Kitano sewage treatment plant, situated near to the Tama River near Tokyo [78]. Other important water-purification applications of $TiO_2$ photocatalysis include water decontamination, water disinfection, remediation of metal contamination etc. Rincón et al. [79] found that a CPC reactor and a $TiO_2$ slurry catalyst can effectively remove E. coli K12 in real lake water within 3 h on a clear day in summer. When solar light alone is used, it was ineffective and the self-repair action of microbes also complicates the disinfection process. Alternatively in $TiO_2$ catalysis, many reactive oxygen species, such as hydroxyl radicals, superoxide, hydrogen peroxide, etc participate in the disinfection process. Other water purification facility available in market using photocatalytic principle include those designed to remove volatile organic compounds. VOCs such as dichloromethane, trichloroethylene, tetrachloroethylene, and 1, 3-dichlorobenzene etc, are extracting solvents in industrial processes and in dry cleaning. They are

discharged into underground water or soil in considerable quantities. Suctioning up the polluted water in a deep well is followed by converting the VOCs to the gas phase. This photocatalytic air-cleaning unit decompose the gaseous VOCs at concentration levels ranging from several hundreds to several thousands of parts per million. Maximum treatment capability is 5 kg VOCs in a day with a 15-kW facility. $TiO_2$ treatment was effective for a range of water pollutants like hydrocarbons, halohydrocarbons, nitrocompounds, insecticides, fungicides, herbicides, toxic heavy metals,dyes etc.

Another area where $TiO_2$ photocatalysis is largly used is to deodorise or decontaminate the indoor air. Volatile organic contaminants like formaldehyde, toluene discharged from the interior funishing etc are harmful if inhaled. Also the indoor air in the public facilities are highly contaminated due to the presence of various microorganisms which are necesserily disinfected. Unlike conventianal active carbon filters, the use of photocatalytic air-cleaning filters, instead of accumulaing the organic contaminants, degrade it to less harmful products and therefore show commendable performance. These photocatalytic filter effectively kills the bacteria in indoor air, thus assisting in indoor air purification [80-81]. In Europe, a paint was developed based on metal oxide called as ecopaint which soaks up various poisonous gases from vehicle exhausts. It will provide the town planners a reliable tool to prevent pollution, is basically a silicon-based polymer with spherical 30 nm wide nanoparticles of titanium dioxide and calcium carbonate embedded in it. Since polysiloxane base is porous NOx diffuse through its pores and attached to the titanium

dioxide particles which absorb UV light from sunlight converting them to nitric acid which either washed out by rain or neutralised by alkaline calcium carbonate particles [82].

$TiO_2$ photocatalysts can be used for photocatalytic sterilisation and bactericidal activity. Kikuchi et al [83] succeeded in the removal of E. coli bacteria within hours using $TiO_2$ coated glass plate. Thus food poisoning from E. coli, can be prevented. Disinfection by titania resulted in the removal/deactivation of various pathogenic bacteria/ viruses/ protozoa/ fungi etc. By serving both as an antibacterial and detoxifying agent, $TiO_2$ photocatalyst is unique in its environmental applications. In collaboration with TOTO Ltd., Fujishima et al. fabricated an antibacterial tile covered with a $TiO_2/Cu$ composite coating [84-85]. The experiment conducted towards anti bacterial activity revealed that the bacteria were completely killed within an hour of illumination. Not only the bacterial colonies are decreased to a substantial amount, but also the air surrounding them also showed diminished amount of microbes. Thus showing the applicability of such tiles on the floor and walls of a hotels, restuarents, hospitals, operating room anywhere sterile environment are vital. Unlike other chemical antibacterial agents, these photocatalytic surfcaes are environmentally friendly.

## 1.6.4 Sensor applications

$TiO_2$ nanomaterials are promising candidates for sensing of Hydrogen, Oxygen, Carbonmonoxide, methanol and ethanol sensing. In the early years of fabricating oxygen sensors for automotive exhaust

gases, various semiconductor oxides including $TiO_2$ were considered as a good alternative to zirconia. Grimes et al. carried out a number of studies on sensing using $TiO_2$ nanotubes and they found that $TiO_2$ nanotubes exhibited outstanding performance as room-temperature hydrogen sensors with high sensitivity. Usually the elevated temperature hydrogen sensors observe the electrical resistance change with hydrogen concentration. Birkefeld et al. [86] found that at temperatures above 500°C, the resistance of anatase $TiO_2$ varied in presence of CO and $H_2$ and later on doping with 10% alumina it became selective for hydrogen only. Gao et al. [87] has seen that unlike microscale $TiO_2$, nanoscale $TiO_2$ showed higher performance in $H_2$ sensing because of its larger surface area. Devi et al. [88] observed that $H_2$ and CO sensitivities shown by ordered mesoporous $TiO_2$ are higher than sensors made from common $TiO_2$ powders due to the enhanced surface area offered by these mesoporous structures. Upon loading with 0.5 mol % $Nb_2O_5$, enhanced the sensitivity was achieved towards Oxygen.In the case of Ta- $TiO_2$, the oxygen vacancies created by the photoirradiation acted as oxygen-sensing sites. Sotter et al. [89] found Nb-doped $TiO_2$ nanomaterials to be good sensor materials for $O_2$. The oxygen sensitivity shown by Nb- and Cr-doped $TiO_2$ nanocrystalline films are higher than pure $TiO_2$ based films [90]. Cu- or Co-doped $TiO_2$ nanoparticles were found to be good candidates for CO sensing by Ruiz et al. [91]. Garzella et al. [92] found that related to pure $TiO_2$, W-doped system displayed better performance for ethanol sensing. An optical humidity sensor fabricated by Yadav et al. using $TiO_2$ nanocrystalline films [93] which is based on the variations in the intensity of light with humidity changes.

## 1.6.5 Anticorrosion applications

Prevention of metals from corrosion is another hot topic of relevance. Passive compound layer and paint coating required complete and perfect covering of metal surface to resist corrosion. Alternatively, sacrificial coating dissolves gradually in life time. Nowadays the photocatalytic technology has been applied to anticorrosion field also [94-96]. Anticorrosion effects of a $TiO_2$ coating for Type 304 stainless steel were studied by Ohko et al. [97] in cooperation with the Koyo Electrical Construction Co. The photogenerated electrons are ejected into steel preventing it from corrosion whereas the holes produced performs self cleaning function. $TiO_2$ coupled with $WO_3$, maintained excellent anticorrosion effect even in the dark for certain time period though the UVlight has ceased off [95]. Under irradiation, the ejected electrons are injected into the metal making its potential more negative than the corrosion potential. Due to the lower conduction band edge favours the accumulation of excess electrons in the "electron pool" of $WO_3$. Meta stable tungston bronze are formed when the protons adsorbed on the surface interact with reduced $WO_3$. The reductive energy produced during this process can be stored. Under dark condition, the metastable tungsten bronze slowly releases electrons into the metal through a self-discharge process and untill the discharge process is completed, the metal remains protected from corrosion in the dark [98]. Practical semiconductor coating for metal corrosion protection has been attaining tremendous attention. $TiO_2$ - Phosphotungstic acid exhibit longer self discharge time and

maintain anticorrosion effect over 12 h in electrolyte solution, after irradiation with a UV light for about 1 h [99].

## 1.6.6 Photovoltaic Applications

It has been reported that renewable sources comprise about 13% of all energy production[100]. Among these, photovoltaic technology is considered to be the most promising one. A solar cell, or photovoltaic cell (PV), is basically an electrical device which converts the energy of light directly into electricity by the photovoltaic effect. First silicon based solar cells demonstrated by Chapin et al. at Bell Lab in 1954 exhibited 6% efficiency [101]. Though these first generation solar cells of mono and poly crystalline silicon cells have good power conversion efficiency, high production costs and environmently benign nature increased the quest for low cost devices. The second-generation solar cells included compound films such as gallium arsenide, cadmium telluride, copper indium gallium selenide etc. Though these have similar performances as that of silicon based devices, the high production costs limited its practical usage. After 20 years of research, the third generation solar cells enriched the photovoltaic technology with devices of lower processing cost and small environmental influences though they are not showing efficiency upto the silicon based systems. Gratzel and O'Regan in 1991 discovered dye-sensitized titania nanocrystalline solar cell which is different from that of conventional photovoltaic system [102]. In DSSC, the semiconductor never performs both photoreceptor and charge transfer functions instead it is done by separate components. Due to this low cost, flexible mode of preparation, environmentally benign nature, and

commendable performance gave DSSCs intense interest among the third-generation PV technologies. Titania is the most commonly used photoanode material. Usually a typical DSSC consists of the following: (i) a transparent glass sheet covered with indium doped tin oxide (ITO) or fluorine-doped tin oxide (FTO) layer (ii) a semiconductor oxide layer deposited on the substrate which transfer electrons; (iii) a monomolecular coating of dye adsorbed on the semiconductor surface to absorb light [ i−iii compose the photoanode in the DSSC] (iv) an electrolyte (iodide/triiodide couple) (v) counter electrode, anode is also made of ITO or FTO conductive glass sheet coated with platinum catalyst. The photoexcitation of dye molecules transfer electrons to conduction band of titania and these electrons are collected at the conducting glass surface via movement cross the disordered network of titania nanoparticles. The dye which is in the oxidised form accepts electrons (Iodide ions from electrolyte) and is regenerated whereas the generated triiodide ions are reduced at the counter electrode. Thus the device generates electric power from light without undergoing any permanent chemical transformation. Many factors like structure, porosity of titania etc. are crucial for the enhancement of photovoltaic efficiency. In order to facilitate the reaction between titania, and interacting media, maximising the surface area of titania is one approach. Along with the surface area, defects in $TiO_2$ materials which exists in grain boundaries are also decisive inwhich the nanoparticle's contact serve as electron traps. Therefore utilising interconnected a network structure with $TiO_2$ single-crystal-like nanowires instead of $TiO_2$ nanoparticles certainly improve the electron transportation.

## 1.6.7 Photocatalytic Water Splitting

Enormous research has been done towards the applications of $TiO_2$ under light illumination since the discovery of photocatalytic splitting of water on a $TiO_2$ electrode in 1972 by Fujishima and Honda. The exploration and progress of clean and renewable energy are crucial to solve the energy crisis of future generation due to fast depletion of fossil fuels. Hydrogen has been identified to possess great potential as a source of energy from the aspects of environmental preservation and sustainable energy security in the near future. Currently, about 95% hydrogen production along world wide is obtained from natural gas through steam–methane reforming, generating massive amounts of carbon dioxide; a main contributor to global warming. Photocatalysis via solar energy has been widely considered as a possible system to produce hydrogen from water. Titania in various forms, shapes with and without modifications have been studied towards hydrogen production by water splitting. Properties, size, geometry and compositions of the materials are the keys to alter the material activity to advanced hydrogen production. Modification of $TiO_2$ surface by noble metals, non-metals, transition metals dyes etc can enhance the energy range of photo excitation as well as its photocatalytic activity towards hydrogen production. The photo efficiency of the process can be enhanced by the addition of sacrificial reagents [methanol, ethanol, EDTA, $Na_2S$, and $Na_2SO_4$ or ions such as $I^-$, $IO_3^-$, $CN^-$, and $Fe^{3+}$]. which help in the separation of the photoexcited electrons and holes. When the photocatalytic reaction is performed in aqueous solutions including readily oxidizable

reducing reagents, the target of the photogenerated holes are the reducing reagents instead of water. This process makes the photocatalyst electron-rich, and rate of hydrogen production was found to be higher. Alternatively, electron acceptors such as $Ag^+$ and $Fe^{3+}$, consume the photogenerated electrons and therefore $O_2$ evolution reaction is enhanced. Thus, a sacrificial reagent helps to control the electron-hole recombination process.

## 1.6.8 Biological applications

Majority the studies of titania circled around its photocatalytic activity towards pollutant removal and energy applications. Use of $TiO_2$ in biomedical appliance is comparatively new. This field, which began in 1990s, has gained increased attention of various scientists for future medical innovations. The earlier report came when the increased usage of titanium in implants raised queries regarding its interaction of living tissues [103]. First use of titania for photoinduced cell death was soon published by Cai et al [104]. After this discovery this field is growing exponentially and has now expanded into an area of great importance and impact. Alternatively, another study reported application of nano titania as a redox agent in medical implants [103]. Nanotechnology basically relies on the engineering science at molecular level, and when used in biomedicine for theraputics and diagnostics, is called as theranostics [105]. In industry, titania nanomaterials are usually employed as consumer products. But their smaller size and large surface area provide more active species on the surface which enhances its reactivity. Nowadays, gold and silver nanoclusters, platinum, mutiwalled carbon nanotubes, iridium and

titanium are among the series of candidates used for nano inorganic drug delivery systems (NI-DDS) with multiple therapies. Among them titanium has been proven as noble one with promising sonodynamic, photodynamic therapeutic and drug carrier for cancer other contagious diseases [106].

Nano titania is largly explored as photdynamic-therapeutic agent has become accepted for cancer therapies, microbial infections and food safety. It is utilised as photosensitizer in PDT as it becomes super hydrophilic on exposure to UV light and this functionality can be reversed, depending upon the exposed light. This treatment involves administration of photosensitizer and when the desired concentration was achieved at the specific tissue, it is followed by the excitation with electromagnetic radiation. The reactive oxygen species generated on their surface is responsible for the eradication of cancerous growth. Deep penetration ability and capability to eradiacate deep seated tumors make sonodynamic therapy to gain popularity among various diagnostic methods. Singlet oxygen and other ROS were generated by $TiO_2$ nanoparticle with coreshell type polyallylamines micelles in HeLa cancer cells after sonoactivation [107]. Sonodynamic and photodynamic therapeutic effect of $TiO_2$-PEG nanoparticles have been evaluated by Yamaguchi et al. [108] to find their effect on human glioblastoma cells U251. After activation (5.0 mW/cm$^2$), MTT assay evaluation demonstrated that $TiO_2$-PEG sonosensitizers decrease the viability and membrane integrity in the tumor cell line. Considering the orthopaedic implants based on titania, where the autoimmune reactions are relevant, the usual approach is to coat the surface with thin

passivation layer of nano or submicron titania particles which reduces the macrophages chemotaxis and delayed the chances of thrombosis as postoperative complications [109].

The titanate has got significant attention in recent years among various active forms of titania. Formerly it was designed for the cleansing of nuclear waste materials due to their good ion exchange ability. Later it was found that they can be effectively attached to the biologically active metals [110]. The monosodium titanate (MST) particles are efficient for biomedical applications, and recently Drury et al found the efficient biological activity of nano monosodium titaniate especially as suppressor of human squamous cells carcinoma and observed non-lethal effects on the oral bacterial infections [111]. During topical applications, $TiO_2$ nanoparticles serve as photoprotectant in sunscreens, and as vehicle in drug delivery system to release the drug.

## 1.7 Stategies in the modification of Titania nanomaterials for enhanced application potential

The betterment of the performance of titania for various application can be accomplished by a number of approaches like control over the morphology, crystal structure, particle size, introduction of various additives like anions, cations noble metals or other semiconductors, sensitizing with dyes, tuning the active facetes on the surface, pore volume, pore structure, etc.

Thus, structural dimensionality is a crucial factor which has a significant influence on various properties of Titania [112]. While

considering photocatalysis and hydrophilicity, it is quite interesting to see that the types of photochemistry involved for photocatalysis and hydrophilicity are completely different, even if both these processes occur simultaneously on the same $TiO_2$ surface. Nanotitania with different morphologies exhibit different photocatalytic activities [113]. The above said observations diverted the attention of researchers to synthesise nanotitania with various morphologies and shapes such as nanorods [114] nanotubes [115] nanowires, sheets [116-117], inter connected architectures [118-119], nanospheres [120] etc. The right choice of appropriate dimensionality for desired applications enables to utilise their unique properties. For example, photocatalytic applications of the material largely depends on the chemical reactions occuring on their surface and therfore, the structural features definitely influence the light harvesting abilities of the material and thereby activity. Zhang et al. synthesized tri-phase (anatase, rutile and brookite), bi-phase (anatase and rutile) and mono-phase (rutile) $TiO_2$ nanomaterials with diverse morphologies adopting a hydrothermal-hydrolysis method and adjusting the $Ti^{4+}/Ti^{3+}$ molar ratio in a precursor solution. They have observed that purely rutile nanorods are inferior to Tri-phase $TiO_2$ nanorods and bi-phase $TiO_2$ nanoparticles towards methylene blue degradation ability under irradiation from a medium mercury lamp at ambient temperatures [121]

Nanostructured $TiO_2$ materials are extensively used not only in photocatalysis, but also in many applications like dye-sensitized solar cells (DSSCs) [122], lithium-ion batteries [123] and electrochromic displays [124]. An effective way to increase the application potential

of titania in heterogenous catalysis is increasing the specific surface area by creating porosity within the structure. Researchers strived to produce high surface area catalysts by various methods. In this direction, fabrications of mesostructured semiconductors have given considerable attention as they have proven to increase the photocatalytic activity on account of their large number of active sites in their surface provided by their high surface area [125-126]. According to IUPAC, porous materials can be categorised into three types depending on their pore sizes: microporous ( pore size below 2 nm), mesoporous (pore size between 2 and 50 nm), and macroporous ( pore size larger than 50 nm) [127]. The large pore volumes have shown promise in the loading of guest species within the mesopores, that are not achieved by microporus materials. Kim et al. [128] have found that mesoporous titania exhibits 5.8 times higher activity than P25 $TiO_2$ towards methylene blue dye degradation. Besides, the possibility to synthesise mesoporous nanoparticles (NPs) helps to obtain a material which is highly dispersible in water. Therefore, the application of mesoporous- $TiO_2$ is not limited in environmental photocatalytic processes. The flexibility in nanoparticle morphology and size during the synthesis make it suitable for applications in biomedicine, sensing, bioelectronic devices etc. When we try to increase the crystallinity by high temperature treatment, mesoporous $TiO_2$ there is undesirable grain growth and a total collapse of the ordered mesoporous network. This can be overcome by the addition of various dopants. Recently, Zhou et al have reported ordered thermally stable mesoporous anatase $TiO_2$ with high crystallinity, large surface area and a large pore size by evaporation-

induced self-assembly (EISA). Its photocatalytic activity for the degradation of toxic 2,4-dichlorophenol was found to be good under UV irradiation [129]. Khan et al [130] prepared nanocrystalline mesoporous titania of the anatase crystal phase for DSSC applications and demonstrated that the surface area indeed affects the conversion efficiency of the DSSCs. Mesoporous $TiO_2$ film platforms can be used for high-sensitivity conductometric gas sensor materials and the high sensitivity of the film is atributed to the large internal surface area in the mesoporous structure [131]. Wu et al [132] showed the biocompactibility of synthesised mesoporous titania by cell viability assay in human breast cancer cell line (BT—20] and showed its good biocompatibility at concentrations as high as $0.4 \, g \, L^{-1}$.

One dimensional (1D) materials are another category of nanostructured materials which have been extensively researched with various special structures such as nanotubes, nanosheets, nanorods, nanowires, nanobelts etc. Apart from the scientific curiosity, another reason for this interest is the expected economic impact in the form of applications owing to the definite physical and chemical characteristics of these 1D (or extremely high aspect ratio) structures. Particularly, one-dimensional (1D) hierarchical structures with hollow or porous interiors provide longitudnal pathways to transport electrons efficiently [133]. When compared to $TiO_2$ nanoparticles, these one dimensional $TiO_2$ nanostructures are proven to be efficient for photocatalytic degradation of air pollutants owing to their large specific surface area and low recombination of electrons/holes [134]. Very recently, Camposeco et al. [135] examined the dye degradation abilities of $TiO_2$

nanomaterials with different structures and shapes and they found that the photocatalytic activities depend on the various kind of $TiO_2$ nanostructures [nano-tubes, nanofibers, nanowires and nanoparticles] showing a strong correlation between their structure and the medium. The water splitting activity also depends on the shape of nanostructures because of the variation in the charge transfer ability as morphology changes. Alternatively, compared to nanoparticles, their specific geometric features enable these one-dimensional (1D) nanostructures (nanowires, nanorods, nanotubes, nanobelts) for faster electron transport and Li-ion insertion/extraction. [136-137]. $TiO_2$ nanotubes possess several advantages like large specific surface area, single step method of preparation etc. [138]. Grimes and coworkers observed that higher life time for electron enhances the charge separation efficiency benefit the use of $TiO_2$ nanotube arrays for photoelectrochemical (PEC) water splitting [139-141]. This one dimensional materials exhibited good response mainly to ethanol, acetone and hydrogen and thus are used for sensor applications also [142]. Similarly, shape effects of anatase titania nanospheres and nanorods are examined by Yun et al for $H_2$ generation from aqueous ethanol solution in UV light and they found that $Pt/TiO_2$ nanorods generated $H_2$ gas which is 1.6 folds more that accomplished by nanospheres under identical experimental conditions [143].

One drawback of using titania for various applications includes the easy recombination of photogenerated holes and electrons. The rate of recombination is affected by many factors like charge trapping, the chemisorption/physorption of target molecules, the intensity of

incident light etc. Use of sacrificial electron and hole scavengers which increase the life time of charge carriers are often used to decrease the electron- hole recombination in photocatalytic processes. The life time of photogenerated holes can be extended by adsorbed molecular oxygen which readily accepts electrons to form superoxide ion. The hole scavengers include, methanol, ethanol, glycerol etc.

Contrains on the performance due to single phase  leading to fast electron hole recombinations, low surface area etc can be tolerated by the fabrication of one dimensional nanostrctures with second phases or introducing dopants (metals, non-metals, semiconductors). [144-146].  Actually development of $TiO_2$ crystals with specific facets is also an attractive area where immense research is going on. This type of fabrication of heterostructures is attractive as it not only helps to improve the performance of the individual materials but also helps to introduce some new and unusual properties the individual materials do not possess. Its quite interesting to see that different facets with different surface atomic structures  are shown to possess distinct abilities in hosting guest materials.  For example, because of the different surface energy levels of two facets of rutile $TiO_2$, selective photodeposition of Pt  occurs on the {110} facets and while for $PbO_2$ particles it occurs on the {011} facets. Though, $TiO_2$ nanostructures with various shapes have been realized in the past decades,  the synthetic $TiO_2$ crystals with high-energy facets were very rare before 2008 [147]. Mi et al. [148] also proved that presence of mixed phase of anatase and rutile exhibited enhanced photocatalytic performance than a pure one-phase crystal structure.

Poor activiy in the visible region is another important drawback of titania based systems. Since the band gap of bulk $TiO_2$ lies in the UV regime, which utilises only a small fraction of the sun's energy, the improvement in the performance can be accomplished by increasing the onset of absorption to the visible region. The second limitation was overcome by various modifications like (i) coupling with other semiconductors or sensitized with dyes, (ii) doping with metals and (iii) doping with nonmetals. Dye sensitization of $TiO_2$ is capable of extending the absorption by the excitation of electrons from the dye molecule to the conduction band of semiconductor. It has been observed that when titania is doped with an appropriate metal, the rate of recombination was reduced to a considerable extent and the photocatalytic activity is correspondingly enhanced. Photo-oxidation of oxalic acid over $TiO_2$ surface in the presence of silver ion was studied by Bardos et al, who observed that after silver deposition, the photooxidation of oxalic acid is enhanced by a factor of 5 [149]. Recently Songara et al [150] studied the photochromic behaviour of films of vanadium doped titania in alkyd resin. They observed a reversible color change from beige- yellow to brownish violet upon UV treatment. Yamazaki et al prepared Cu-deposited $TiO_2$ films by photoreduction of Cu (II) in the presence of sodium formate and these films exhibited higher photocatalytic activity compared to pure $TiO_2$ for the degradation of methylene blue [151].

Asahi et al. [152] was the first to report the idea of doping titania with non-metal such as Nitrogen. They also carried out theoretical studies related to the substitution of C, N, F, P or S for

oxygen atoms in the titania lattice. The great success of anion doped titania with high activity in the visible region is due to the decrease of their band gap either by mixing p orbital of the dopant with O 2p orbital of titania that generates a state which is just above the valence band, or generate a mid-gap stage of dopants between the valence band and conduction band. Later years observed research related to the the chemical state and composition of the dopants using modern techniques which concluded that the defects generated by inculcation of these impurities on titania network reduces the recombination of the photo generated species and thereby enhance the photocatalytic activity [152-155]. Bessekhouad et al [156] experimented the photocatalytic activity of $TiO_2$, CdS and coupled $CdS/TiO_2$ powders and concluded that under visible light, the coupled semiconductor $CdS/TiO_2$ exhibits faster degradation rate related to both isolated components.

Modifications to titania based systems are also favaourable when they are applied in biological applicarions. In addition to the non toxic nature, the possibility of precise control over the size and shape along with the functionalisation flexibility makes them a good candidate in biomedical field. For example, compared to titania nanoparticles, $TiO_2$ nanowhiskers possess unique advantages that they exhibit better photocatalytic activity than nanoparticles. Besides, their charge transportation abilities makes them suitable candidate for solar cells, in wind screens and the synergetic effect offered by its photocatalytic activity make them a good phototheraputic agent [157]. Furthermore, they are good basement for excellent drug delivery

systems owing to their large surface area and reactivity. Recently, carbon coated titania nanotubes have found to applications in biomedical field as reported by Gracia-valverde et al [158]. Besides this modification of the nanomaterial with antibodies, active ligands, peptides, folic acids , PEG, etc imparts them many desired properties and improve therapy effectiveness [159-160]. Recently, Chennell et al [161] observed the loading and eluting of the Cefuroxime as antibiotic on the orthopedic implants by various titania based nanostructures, $TiO_2$ nano fibers, tubes and smooth surfaces and found that titania nanotubes exhibited peak drug release at two minutes time interval with highest concentration release. The pristine nano $TiO_2$ are liable to photoactivation at UV range light (400 nm) but a relatively higher wave length (more than 600 nm) has been approved by WHO for therapeutic window to start. It is because of the fact that biological molecules like proteins, haemoglobin and melanin are also vulnerable to excitation in UV range causing serious disavantages. So it is better to modify pristine $TiO_2$ with upconverting surface modifiers or coat with other molecules for better results in the desired range [162]. Nano $TiO_2$ when used in combination with other nanomaterials and macro molecules exhibited good synergistic effect. For example, for the neoplastic disease theranostics, Zheng et al used nanocomposites of $TiO_2$-$Fe_3O_4$, where nano $TiO_2$ acts as Photosensitizer for Photodynamic therapy and $Fe_3O_4$ as contrast agent for Magnetic resonance Imaging (MRI) [163]. The therapeutic efficiency of $TiO_2$ is expected to be, independent of their shape or crystalline form. But it depends on the produced ROS including $HO_2^{\cdot}$, $O_2^{\cdot-}$, $OH^-$ and $^1O_2$. Nevertheless its isomorphs can effect the extent of the ROS generation

as they vary in their reactivity. for example anatase has been reported to be more reactive than rutile. Similarly $^1O_2$ is reported to be successfully generated from nano $TiO_2$ with size more than 10 nm by NIR phosphorescence. When the size was less than 10 nm, they are unable to generate $^1O_2$ .

## 1.8    Present work Relevance and Objectives

Environmental pollution and energy scarcity are the serious day-to-day problems faced by all the developing and the developed nations in the world. Photocatalysis is identified as a major advance in this direction where the abundant/clean/safe energy of the sun can be utilised for sustainable, nonhazardous, and economically viable technologies. Titanium-oxide, an ideal and powerful photocatalyst has been proven to have high potential in this direction. Our ecosystem is constantly facing imbalance from air, water and solid waste pollution caused by  anthropogenic sources. Titania based photocatalysis has been proven to effectively remove a wide range of common pollutants, including dyes, detergents, surfactants, insecticides, pesticides and herbicides, disinfection byproducts, chlorinated /nonchlorinated, aliphatic / aromatic compounds, volatile organic compounds, plastics, inorganic compounds like heavy metals, harmful gases like NOx, SOx, CO and $NH_3$, and pathogens like bacteria, fungi and viruses. Here we tried to address the UV light assisted photocatalytic degradation and antimicrobial activity of different morphologies of Titania based nanostructures. The model pollutant chosen is methylene blue dye. Moreover, its application as antibacterial and antifungal agent ensure it

as good self-cleaning products for domestic, medical and industrial applications in large-scale.

Similarly, efficient and low cost hydrogen production with minimum environmental and social adverse effect is the objective of successful transition to hydrogen economy which can also be achieved by titania based visible light through photocatalytic water splitting reaction. Among many modification techniques cocatalyst loading on semiconductor is proven to be effective to reduce the charge carrier recombination, high electron availability, enhance its absorption to visible region etc. Alternative cocatalysts based on nonprecious metals and metal-free materials have been actively pursued owing to the expensive conventional noble metal based cocatalysts. In the present study, copper and silver are employed as cocatalyst for photocatalytic water splitting using titania.

The nontoxicity and biocompactible nature of titanium dioxide extent its applications in biomedical relms also. It has been used in bone implants, treatment of cancer, as drug carrier etc. The development of nanoscience and nanotechnology effectively utilised nanosized materials for cancer treatment due to the wide application potential of materials confined to nanorange. Nanotitania also imparts its surface functionalities for cancer treatment with appropriate modifications. Moreover attachment of targetting moeties has found to enhance the uptake of cytotoxic agents into the cell thereby effectively killing the cancer cells leaving the healthy tissues behind. In the present work $TiO_2$ is used for analysing cytotoxicity towards cancer cells. It is used as a drug carrier also.

**The specific objectives**

➢ Present work aims at synthesizing morphologically diverse Titanium dioxide nanostructures; (i) multi shelled titania hollow nanospheroids, (ii) mesoporous assembled titania nanocuboids, (iii) titania nanotubes, (iv) titania nanobelts, (v) titania nanoparticles

➢ Characterization of the prepared systems using various analytical and spectroscopic techniques such as Scanning Electron Microscopy (SEM), Transmission Electron Microscopy (TEM), Fourier Transform Infra Red spectroscopy (FTIR), X-Ray Diffraction analysis (XRD), UV Diffuse Reflectance spectroscopy, Raman spectroscopy, Photoluminescence spectroscopy, and BET surface area analysis.

➢ Modification of the morphologies mesoporous assembled titania and titania nanotubes with co-catalysts silver and copper followed by their well characterization studies for Hydrogen production by water splitting.

➢ Anticancer drug incorporation of the synthesised nanostructures and folate attachment for targeted drug delivery.

➢ Application studies of titanium dioxide nanostructures and the modified systems in

- Photocatalytic Applications

❖ Photocatalytic removal of organic pollutant

❖ Photocatalytic Antimicrobial activity studies (Antibacterial and anti fungal studies)

❖ Photocatalytic Water splitting reaction for Hydrogen production

- Biological Applications

➢ Invitro cytotoxic studies of synthesised titania nanostructures in cancer cell lines

➢ Invitro cytotoxic studies of Anticancer drug embeddedd titania nanostructures in cancer cell lines

➢ Invitro cytotoxic studies of Folate targeted Anticancer drug loaded titania nanostructures in cancer cell lines.

➢ Mechanistic pathway underlying the cell death are examined with various apoptotic studies.

## References

1.      N. Bertrand and J.C. Leroux, J. Control Release, 2012, 161, 152.

2.      Z.F. Yin, L. Wu, H.G. Yang and Y.H. Su, Phys Chem. 2013, 15, 4844.

3.      A. S. Aricò, P. Bruce, B. Scrosati, J. M. Tarascon and W. Van Schalkwijk. Nat. Mater. 2005, 4, 366.

4.      T. Jia, W. Wang, F. Long, Z. Fu, H. Wang and Q. Zhang, J. Phys. Chem. , 2009, 113, 9071.

5.      J. L. Wang, G. Zhang, Q. W. Li, H. Jiang, C. Y. Liu, C. Amatore and X. M. Wang, Sci Rep, 2013, 3, 6.

6.      J.J. Escobar-Chávez, I.M. Rodriguez-Cruz and C.L. Dominguez-Delgado, Chemical and Physical Enhancers for Transdermal Drug Delivery, In: L.Gallelli, editor. Pharmacology, ISBN 978-953-51-0222-9, InTech, 2012, 397.

7.      R. Díaz-Torres, Transdermal nanocarriers. In: J.J. Escobar-Chávez, editor. Current Technologies to Increase the Transdermal Delivery of Drugs. Bussum: Bentham Science; 978-1-60805-385-8, 2010, 120.

8.      S.H.S. Chan, T.Y. Wu, J.C. Juan and C.Y. Teh, J. Chem. Technol. Biotechnol., 2011, 86, 1130.

9.      V. Ramamurthy, Organic Photochemistry, CRC Press, - Science – 295, 1997, ISBN 9780824700126 - CAT# DK1359.

10.     K. Hashimoto, H. Irie and A. Fujishima, Jpn. J. Appl. Phys., Part 1, 2005, 44, 8269.

11.     C. F. Doodeve and J. A. Kitchener: Trans. Faraday Soc., 1938, 34, 902.

12.     S. Kato and F. Mashio: Abtr. Book Annu. Meet. Chemical Society of Japan, 1956, 223.

13.     S. Kat and F. Masuo: Kogyo Kagaku Zasshi, 1964, 67, 1136 [in Japanese].

14.     A. Fujishima and K. Honda, Nature 1972, 238, 37.

15.     S. N. Frank and A. J. Bard: J. Am. Chem. Soc., 1977, 99, 303.

16.     K. Sunada, Y. Kikuchi, K. Hashimoto and A. Fujishima: Environ. Sci. Technol., 1998, 32, 726.

17.  Jelks Barksdale, "Titanium- its Occurrence, Chemistry and Technology", The Ronald Press Co. USA, 1949, 966.

18.  A. L. Stroyuk, A. I. Kryukov, S. Y. Kuchmii and V. D. Pokhodenko, Theor. Exp. Chem., 2005, 41, 67.

19.  D. Beydoun, R. Amal, G. Low and S. McEvoy, J. Nanopart. Res., 1999, 1, 439.

20.  A.P. Alivisatos, J. Phys. Chem., 1996, 100, 13226.

21.  C. Burda, X. Chen, R. Narayanan, R. and M.A. El Sayed, Chem. Rev., 2005, 105, 1025.

22.  R. Marchand, L. Brohan and M. Tournoux, Mater.Res.Bull., 1980, 15, 1129.

23.  M. Latroche, L. Brohan, R. Marchand and M. Tournoux, J.Solid State Chem., 1989, 81, 78.

24.  J. Akimoto, Y. Gotoh, Y. Oosawa, N. Nonose, T. Kumagai, K. Aoki and H. Takei, J.Solid State Chem., 1994, 113, 27.

25.  P.Y. Simons and F. Dachille, Acta Cryst., 1967, 23, 334.

26.  H. Sato, S. Endo, M. Sugiyama, T. Kikegawa, O. Shimomura and K. Kusaba, Science., 1991, 251, 786.

27.  H. Cheng, J. Ma, Z. Zhao and L. Qi, Chem. Mater., 1995, 7, 663.

28.  S. D. Mo and W. Y. Ching, Phys. Rev. B: Condens. Matter Mater. Phys., 1995, 51, 13023.

29.  X. Bokhimi, A. Morales, M. Aguilar, J. A. T. Antonio and F. Pedraza, Int. J. Hydrogen Energy, 2001, 26, 1279.

30.  W. Li, Y. Bai, W. Zhuang, K. Y. Chan, C. Liu, Z. Yang, X. Feng and X. Lu, J. Phys. Chem. C, 2014, 118, 3049.

31.   M. N. Tahir, P. Theato, P. Oberle, G. Melnyk, S. Faiss, U. Kolb, A. Janshoff, M. Stepputat and W. Tremel, Langmuir, 2006, 22, 5209.

32.  T. Beuvier, M. R. Plouet and L. Brohan, J. Phys. Chem. C, 2009, 113, 13703.

33.  G. Xiang, T. Li, J. Zhuang and X. Wang, Chem. Commun., 2010, 46, 6801.

34.  K. Li, J. Xu, W. Shi, Y. Wang and T. Peng, J. Mater. Chem. A, 2014, 2, 1886.

35. W. Zhou, L. Gai, P. Hu, J. Cui, X. Liu, D. Wang, G. Li, H. Jiang, D. Liu, H. Liu and J. Wang, Cryst.Eng.Comm., 2011, 13, 6643.

36. J. Yu, M. Zhou, B. Cheng, H. Yu and X. Zhao, J. Mol. Catal. A: Chem., 2005, 227, 75.

37. S. G. Kumar and K. S. R. K. Rao, Energy Environ. Sci., 2014, 7, 45.

38. B. lmelik, J.C. Vedrine (Eds), Catalyst Characterization: Physical Techniques for Solid Materials, Plenum Press, New York 1994, ISBN 978-1-4757-9589-9.

39. M.J. Holgado, S. SanRoman, P. Malet, and V. Rives, Mater. Chem. Phys, 2000, 89, 49.

40. Q. Fu, A. Weber and M. Flytzani-Stephanopoulos, Catal. 1ett. , 2001, 77, 87.

41. X. Wang, J. Zhuang, Q. Peng and Y. Li, Nature, 2005, 437, 121.

42. B.D. Aleksandra, Y.X. Yan, F.H. Yan and K.C. Wai K. Chan, Recent Patents on Nanotechnology 2007, 1, 121.

43. T. Kasuga, M. Hiramatsu, A. Hoson, T. Sekino and K. Niihara, Langmuir 1998, 14, 3160.

44. A.R. Armstrong, G. Armstrong, J. Canales, R. Garcı´a and P.G. Bruce, AdV. Mater. 2005, 7, 862.

45. Y.X. Zhang, G.H. Li, Y.X. Jin, Y. Zhang, J. Zhang and L.D. Zhang, Chem. Phys. Lett. 2002, 365, 300.

46. Q. Zhang, L. Gao, Langmuir 2003, 19, 967.

47. J. Yang, S. Mei, J.M.F. Ferreira, Mater. Sci. Eng., C 2001, C15, 183.

48. B. Wen, C. Liu, Y. Liu, Y. New J. Chem. 2005, 29, 969.

49. I. Djerdj, A.M. Tonej, M. Bijelic, V. Vranesa and A. Turkovic, Vacuum., 2005, 80, 371.

50. J.M. Wu, H.C. Shih and W.T. Wu, Chem. Phys. Lett. 2005, 413, 490.

51. J.M. Wu, H.C. Shih, W.T. Wu, Y.K. Tseng and I.C. Chen, J. Cryst. Growth 2005, 281, 384.

52. B. Xiang, Y. Zhang, Z. Wang, X.H. Luo, Y.W. Zhu, H.Z. Zhang and D.P. Yu, J. Phys. D, 2005, 38, 1152.

53. J.H. Lee, H.S. Choi, J.H. Lee, Y.J. Kim, S.J. Suh, C.S. Chi and H.J. Oh, J. Cryst. Growth., 2009, 311, 638.

54.    J. Liu, J. Xu, R. Che, H. Chen, M. Liu and Z. Liu, Chem – A. Eur. J., 2013, 19, 6746.

55.    S. Liu and K. Huang, Sol. Energy Mater. Sol. Cells 2004, 85, 125.

56.    A.B. Corradi, F. Bondioli, B. Focher, A.M. Ferrari, C. Grippo, E. Mariani and C. Villa, J. Am. Ceram. Soc. 2005, 88, 2639.

57.    J.M. Wu and T.W.  Zhang, J. Photochem. Photobiol., A 2004, 162, 171.

58.    J.M. Wu, S. Hayakawa, K. Tsuru and A. Osaka, Cryst. Growth Des. 2002, 2, 147.

59.    J.M. Wu, S. Hayakawa, K. Tsuru and A. Osaka, Scripta Mater. 2002, 46, 101.

60.    S. Vemury and S.E. Pratsinis, Appl. Phys. Lett. 1995, 66, 3275.

61.    G.K. Mor, O.K. Varghese, M. Paulose and C.A. Grimes, AdV. Funct. Mater. 2005, 15, 1291.

62.    J.M. Macak, H. Tsuchiya and P. Schmuki, Angew. Chem., Int. Ed. 2005, 44, 2100.

63.    O.K. Varghese, D. Gong, M. Paulose, C.A. Grimes and E.C. Dickey, J. Mater. Res. 2003, 18, 156.

64.    Y. Zhu, H. Li, Y. Koltypin, Y.R. Hacohen and A. Gedanken, Chem. Commun., 2001, 12, 2616.

65.    J.C. Yu, J. Yu, W. Ho and L.  Zhang, Chem. Commun. 2001, 1942.

66.    S. Meng, Z.Y. Zhang and E. Kaxiras,  Phys. ReV. Lett. 2006, 97.

67.    R. Wang, K. Hashimoto A. Fujishima, M. Chikuni, E. Kojima, A. Kitamura, M. Shimohigoshi and T. Watanabe: Nature, 1997, 388, 431.

68.    T. Watanabe, K. Hashimoto and A. Fujishima, 1st International Conference on $TiO_2$ Photocatalytic Purification and Treatment of Water and Air, 1992.

69.    A. Heller, Acc. Chem. Res., 1995, 28, 503.

70.    K. Hashimoto, H. Irie and A. Fujishima, J. Appl. Phys., 2005, 44, 8269.

71.    K. Ikeda, H. Sakai, R. Baba, K. Hashimoto and A. Fujishima, J. Phys. Chem. B., 1997, 101, 2617.

72.    A. Fujishima and X. Zhang, C. R. Chimie, 2006, 9, 750.

73.     K. Hashimoto, H. Irie, and A. Fujishima, Japan. J. Appl. Phys. , 2005, 44, 8269 .

74.     Y. Takata, S. Hidaka, J. M. Cao, T. Nakamura, H. Yamamoto, M. Masuda and T. Ito, Energy, 2005, 30, 209.

75.     P.V. Kamat, Electrochem. Nanomater. 2001, 229.

76.     A. Hagfeldt, N. Vlachopoulos and M. Gra¨tzel, J. Electrochem. Soc. 1994, 141, L82.

77.     M. Moeller, S. Asaftei, D. Corr, M. Ryan and L. Walder, AdV. Mater. 2004, 16, 1558.

78.     T. Nakashima, Y. Ohko, D.A. Tryk and A. Fujishima, J. Photochem. Photobiol. A Chem., 2002, 151, 207.

79.     A.G. Rincón and C. Pulgarin, Solar Energy, 2004, 77, 635.

80.     P. Pichat, J. Disdier, C. Hoang-Van, D. Mas, G. Goutailler and C. Gaysse, Catal. Today , 2000, 63, 363.

81.     C. H. Ao and S. C. Lee, J. Photochem. Photobiol. A: Chem., 2004, 161, 131.

82.     T. Maggos, J. G. Bartzis, M. Liakou and C. Gobin, J. Hazard. Mater., 2007, 146, 668.

83.     Y. Kikuchi, K. Sunada, T. Iyoda, K. Hashimoto and A. Fujishima, J. Photochem. and Photobiol. A: Chem., 1997, 106, 51.

84.     A. Fujishima, K. Hashimoto and T. Watanabe, BKC, Inc. Tokyo, 1999, 29, 354.

85.     T. N. Rao, A. Fujishima, D. A. Tryk, in: A. J. Bard, M. Stratmann, S. Licht (Eds.), Encyclopedia of Electrochemistry, in: Semiconductor Electrodes and Photoelectrochemistry, Weinheim, Wiley-VCH, 2002, 6.

86.     L.D. Birkefeld, A.M.  Azad and S.A. Akbar, J. Am. Ceram. Soc. 1992, 75, 2964.

87.     L. Gao, Q. Li, Z. Song and  J. Wang, Sens. Actuators, B , 2000, B71, 179.

88.     G.S. Devi, T. Hyodo, Y. Shimizu and M. Egashira, Sens. Actuators, B 2002, B87, 122.

89.     S. Hasegawa, Y. Sasaki and S. Matsuhara, Sens. Actuators, B 1993, 14, 509.

90. R.K. Sharma and M. C. Bhatnagar, Sens. Actuators, B 1999, B56, 215.

91. A.M. Ruiz, A. Cornet, K. Shimanoe, J.R. Morante and N. Yamazoe, Sens. Actuators, B 2005, B109, 7.

92. C. Garzella, E. Bontempi, L.E. Depero, A. Vomiero, G. la Mea and G. Sberveglieri, Sens. Actuators, B 2003, B93, 495.

93. B.C. Yadav, R.K. Shukla and L.M. Bali, Indian J. Pure Appl. Phys. 2005, 43, 51.

94. P. Ngaotrakanwiwat and T. Tatsuma, J. Electroanalyt. Chem., 2004, 573, 263.

95. T. Tatsuma, S. Saitoh, P. Ngaotrakanwiwat, Y. Ohko and A. Fujishima, Langmuir, 2002, 18, 7777.

96. H. Park, K.Y. Kim and W. Choi, J. Phys. Chem. B, 2002, 106, 4775.

97. Y. Ohko, S. Saitoh, T. Tatsuma and A. Fujishima, J. Electrochem. Soc. 2001, B24, 148.

98. Y. Takahashi, P. Ngaotrakanwiwat and T. Tatsuma, Electrochim. Acta, 2004, 49, 2025.

99. P. Ngaotrakanwiwat, S. Saitoh, Y. Ohko, T. Tatsuma and A. Fujishima, J.Electrochem. Soc., 2003, 150, A1405.

100. http://en.wikipedia.org/wiki/World energy consumption; accessed Oct 2009.

101. D. Chapin, C. Fuller and G. Pearson, J. Appl. Phys. 1954, 25, 676.

102. B. O'Regan and M. Gratzel, Nature 1991, 353, 737.

103. J.E. Ellingsen, Biomaterials 1991, 12, 593.

104. R. Cai, K. Hashimoto, K. Itoh, Y. Kubota and A. Fujishima, Bull. Chem. Soc. Jpn. 1991, 64, 1268.

105. J. V. Jokerst and S. S. Gambhir, Accounts Chem Res, 2011, 44, 1050.

106. K. Ninomiya, C. Ogino, S. Oshima, S. Sonoke, S.-i. Kuroda and N. Shimizu, Ultrason Sonochem, 2012, 19, 607.

107. A. Harada, M. Ono, E. Yuba and K. Kono, Biomater Sci, 2013, 1, 65.

108.    S. Yamaguchi, H. Kobayashi, T. Narita, K. Kanehira, S. Sonezaki, N. Kudo, Y. Kubota, S. Terasaka and K. Houkin, Ultrason Sonochem, 2011, 18, 1197.

109.    A. Biesiekierski, J. Wang, M. A.-H. Gepreel and C. Wen, Acta Biomater, 2012, 8, 1661.

110.    D. Hobbs, R. Messer, J. Lewis, D. Click, P. Lockwood and J. C. Wataha, J. Biomed. Mater. Res. Part B, 2006, 78, 296.

111.    J. L. Drury, Y.W. Chen, J. J. Wong, M. C. Elvington, R. B. Rutherford, D. T. Hobbs and J. C. Wataha, J Exp Clin Med, 2014, 6, 21.

112.    K. Nakata and A. Fujishima, J.Photochem.Photobiol.,C, 2012, 13, 169.

113.    T. Suprabha, H. G. Roy , J. Thomas, K. P. Kumar and S. Mathew, Nanoscale Res. Lett., 2009,  4, 144.

114.    H.J. Yun, H. Lee, J.B. Joo, W. Kim and J. Yi, J. Phys. Chem. C., 2009, 113, 3050.

115.    H.F. Zhuang, C.J. Lin, Y.K. Lai, L. Sun and J. Li, Environ. Sci. Technol., 2007, 41, 4735.

116.    Y. Chen, G. Tian, Z. Ren, C. Tian, K. Pan, W. Zhou and H. Fu, Eur. J. Inorg. Chem. 2011, 5, 754.

117.     G. Xiang, T. Li, J. Zhuang and X. Wang, Chem. Commun. , 2010, 46, 6801.

118.    Y. Lai, C. Lin, J. Huang, H. Zhuang, L. Sun and T. Nguyen, Langmuir , 2008, 24, 3867.

119.    G. Tian, Y. Chen, W. Zhou, K. Pan, C. Tian, X.-r. Huang and H. Fu, Cryst. Eng. Comm., 2011, 13, 2994.

120.    J.S. Chen, C. Chen, J. Liu, R. Xu, S.Z. Qiao and X.W. Lou, Chem. Commun., 2011, 47, 2631.

121.    J. Zhang, X. Xiao and J. Nan, J. Hazard. Mater., 2010, 176, 617.

122.    W.G. Yang, F.R. Wan, Q.W. Chen, J.J. Li and D.S. Xu, J. Mater. Chem., 2010, 20, 2870.

123.    S. Ding, J.S. Chen, Z. Wang, Y.L. Cheah, S. Madhavi, X. Hu and X.W. Lou, J. Mater. Chem., 2011, 21, 1677.

124.    P. Periyat, N. Leyland, D.E. McCormack, J. Colreavy, D. Corr and S.C. Pillai, J. Mater. Chem., 2010, 20, 3650.

125. F. E. Osterloh, Chem. Soc. Rev., 2013, 42, 2294.

126. M. R. Gholipour, C.-T. Dinh, F. B´elandb and T.O. Do, Nanoscale, 2015, 7, 8187.

127. T. Kimura and K. Kuroda, Adv. Funct. Mater. 2009, **19,** 511.

128. E.Y. Kim, D.S. Kim and B.T. Ahn, Bull. Korean Chem. Soc. , 2009, 30, 193.

129. W. Zhou, F. Sun, K. Pan, G. Tian, B. Jiang, Z. Ren, C. Tian and H. Fu, Adv. Funct. Mater., 2011, 21, 1922.

130. M.A. Khan, M.S. Akhtar and O.B. Yang, Sol. Energy, 2010, 2195, 84.

131. K.D. Benkstein and S. Semancik, Sensors Actuators B, 2006, 113, 445.

132. K.C.W. Wu, Yamauchi, C.Y. Hong, Y.H. Yang, Y.H. Liang, T. Funatsu and M. Tsunoda,Chem. Commun., 2011, 47 , 5232.

133. L. Xin, Y. Liu, B. Li, X. Zhou, H. Shen, W. Zhao, C. Liang and Sci. Rep., 2014, 4, 4479 .

134. X. Y. Fan, F. M. Qiu, H. S. Yang, W. Tian, T. F. Hou and X. B. Zhang, Catal. Chem., 2011, 12, 1298.

135. R. Camposeco, S. Castillo, J. Navarrete and R. Gomez, Catal. Today, 2016, 266, 90.

136. J.M. Li, W. Wan, H.H. Zhou, J.J. Li and D.S. Xu, Chem. Commun. 2011, 47, 3439.

137. J.N. Nian, H.S. Teng, J. Phys. Chem. B 2006, 110, 4193.

138. A. Thorne, A. Kruth, D. Tunstall, J.T.S. Irvine, W.J. Zhou, Phys. Chem. B 2005, 109, 5439.

139. S. Rani, S.C. Roy, M. Paulose, O.K. Varghese, G.K. Mor, S. Kim, S. Yoriya, T.J. Latempa and C.A. Grimes, Phys. Chem. Chem. Phys., 2010, 12, 2780.

140. G.K. Mor, K. Shankar, M. Paulose, O.K. Varghese and C.A. Grimes, Nano Lett., 2005, 5, 191.

141. M. Paulose, K. Shankar, S. Yoriya, H.E. Prakasam, O.K. Varghese, G.K. Mor, T.A. Latempa, A. Fitzgerald and C.A. Grimes, J. Phys. Chem. B , 2006, 110 , 16179.

142.    V. Galstyan, E. Comini, G. Faglia and G. Sberveglieri, Sensors 2013, 13, 14813.

143.    H.J. Yun, H. Lee, J.B. Joo, N.D. Kim and J. Yi, J. Nanosci. Nanotechnol., 2011, 11,1.

144.    A. N. Banerjee, Nanotechnol., Sci. Appl., 2011, 4, 35.

145.    M. A. Hossain, J. Park, J. Y. Ahn, C. Park, Y. Kim, S. H. Kim and D. Lee, Electrochim. Acta, 2015, 173, 665.

146.    M. Z. Ge, C. Y. Cao, J. Y. Huang, S. H. Li, S. N. Zhang, S. Deng, Q. S. Li, K. Q. Zhang and Y. K. Lai, Nanotechnol. Rev., 2016, 5, 75.

147.    G.Liu, H.G. Yang, J. Pan, Y.Q. Yang, G.Q. Lu, H.M. Cheng, *Chem. Rev.* 2014, 114, 9559.

148.    Y. Mi ,Y. X. Weng, *Sci. Rep.*, 2015, 5, 11482

149.    E. Bardos, S.H. Czili, and A. Horvath, J.Photochem. Photobiol. A: Chem., 2003, 154, 195.

150.    S. Songara, M.K. Patra, M. Manoth, L. Saini, V. Gupta, G.S. Gowd, S.R. Vadera and N. Kumar, J.Photochem. Photobiol. A: Chem., 2010, 209, 68.

151.    S. Yamazaki, M. Sugihara, E. Yasunaga, T. Shimooka and K. Adachi, J.Photochem. Photobiol. A: Chem., 2010, 209, 74.

152.    R. Asahi, T. Morikawa, T. Ohwaki, K. Aoki and Y. Taga, Science, 2001, 293, 269.

153.    T. Morikawa, R. Asahi, T. Ohwaki, A. Aoki and Y. Taga, Jap. J. Appl. Phys. , 2001, 40, 561.

154.    C.D. Valentin, G. Pacchioni, A. Selloni, S. Livraghi and E.J. Giamello , J. Phys. Chem. B., 2005, 109, 11414.

155.    H. Irie, Y. Watanabe and K. Hashimoto, J. Phys. Chem. B., 2003, 107, 5483.

156.    Y. Bessekhouad, N. Chaoui, M. Trzpit, N. Ghazzal, D. Robert, and J.V. Weber, J. Photochem. Photobiol. A: Chem., 2006, 183, 218.

157.    N. Wu, J. Wang, D. N. Tafen, H. Wang, J.-G. Zheng, J. P. Lewis, X. Liu, S. S. Leonard and A. Manivannan, J Am Chem Soc, 2010, 132, 6679.

158.    M. Garcia-Valverde, R. Lucena, F. Galan-Cano, S. Cardenas and M. Valcarcel, J Chromatogr A, 2014, 1343, 26.

159.  Y. Matsumura and H. Maeda, Cancer Res, 1986, 46, 6387.

160.  A. Z. Wilczewska, K. Niemirowicz, K. H. Markiewicz and H. Car, Pharmacol Rep, 2012, 64, 1020.

161.  P. Chennell, E. Feschet-Chassot, T. Devers, K. Awitor, S. Descamps and V. Sautou, Int J Pharm, 2013, 455, 298.

162.  M. Pacia, P. Warszyński and W. Macyk, Dalton T, 2014, 43, 12480.

163.  L. Zeng, W. Ren, L. Xiang, J. Zheng, B. Chen and A. Wu, Nanoscale, 2013, 5, 2107.

# CHAPTER II
# EXPERIMENTAL METHODS AND CHARACTERIZATION TECHNIQUES

CONTENTS

*The preparation and characterization of solid catalysts are one of the vital areas of major interest in chemistry/ chemical engineering. Even small variations in the preparation conditions alter the properties and performance of the catalyst. Characterisation of the catalysts is the main backbone to analyse the expected properties for various applications. This chapter presents brief discription regarding the experimental aspects of (i) synthesis, (ii) principles uderlying the characterisation techniques used and (iii) application studies of the prepared catalysts.*

## 2.1    Introduction

The experimental conditions used for the synthesis are important in determining the physiochemical characteristics of a semiconductor catalyst. Variation of the synthesis conditions radically modifies the performance of the catalyst. Hence care must be taken during the selection of materials and preparation of various systems. Characterization techniques are primary processes in the field of materials science, without which no scientific understanding of engineering materials could be ascertained. Details of experimental procedures adopted for synthesis, the principles of various characterization techniques and application studies employed using the synthesised nanostructures are presented in this chapter.

## 2.2    Chemicals and Reagents used

| Chemicals/Reagents | Company |
|---|---|
| TiO$_2$ powder | Sigma- Aldrich |
| P123 | Sigma- Aldrich |
| Tetrabutyltitanate | Sigma- Aldrich |
| Acetylacetone | Sigma- Aldrich |
| HCl | Merck |
| NaOH | Merck |
| Methanol | Sigma Aldrich |
| Ethanol | Sigma Aldrich |
| Methylene Blue Dye | Merck |
| 5Fluoro uracil | Sigma Aldrich |
| Folic acid | Sigma aldrich |
| Human breat cancer cells (MCF-7) | National centre for cell science, Pune |
| 3-(4,5-dimethylthiazol-2yl)-2,5-diphenyltetrazolium bromide | Sigma Aldrich |

| | |
|---|---|
| **L-glutamine** | Sigma Aldrich |
| **Glucose** | Sigma Aldrich |
| **4- (2-hydroxyethyl)−1-piperazineethane sulfonic acid (HEPES)** | Sigma Aldrich |
| **Sodium bicarbonate** | Sigma Aldrich |
| **sodium pyruate** | Sigma Aldrich |
| **Earles BSS** | Sigma Aldrich |
| **EDTA** | Sigma Aldrich |
| **DMSO** | Sigma Aldrich |
| **Acetic acid** | Sigma Aldrich |
| **Acridine Orange (AO)** | Sigma Aldrich |
| **Ethidium Bromide (EtBr)** | Sigma Aldrich |
| **nitrocellulose membrane** | Millipore Banglore |
| **Protein assay Kit** | Bio-Rad |
| **LIVE-DEAD double staining Kits** | Sigma Aldrich |
| **Paraformaldehyde** | Sigma aldrich |
| **DAPI (4'-6-diamidino-2-phenylindole )** | Sigma |
| **Rhodamine 123 stain** | Sigma Aldrich |
| **Phenol** | Sigma Aldrich |
| **Choloroform** | Sigma Aldrich |
| **Isoamyl alcohol** | Sigma Aldrich |
| **Phosphate buffered saline** | Sigma Aldrich |
| **2', 7'- dichlorofluoresein diacetate (DCFH-DA)** | Sigma Aldrich |
| **Potassium dichromate** | Sigma Aldrich |
| **Sulfuric acid** | Sigma Aldrich |
| **Ferrous ammonium sulphate** | Sigma Aldrich |
| **Ferroin indicator** | Sigma Aldrich |

## 2.3 Synthesis of titanium dioxide nanostructures

Different morphologies of titanium dioxide in the nanolevel have been synthesized through different procedures. The naming was done in accordance with their morphology

### 2.3.1 Synthesis of multishelled hollow nanospheroids [MHS]

In a typical synthesis, about 1 g of $TiO_2$ powder (technical grade Sigma- Aldrich) was mixed with 100 mL of 2 M NaOH (Merck) in methanol(Nice, Assay GLC 99%), in a tightly closed steel autoclave at 90 °C for 7 h. It was then allowed to cool at room temperature. The precipitate was separated through proper filtration and washed thoroughly with distilled water several times until the pH of the filtrate reached 7. The resulting sample was dried overnight in air oven at $100°C$ and calcined at $500°C$ for 2 hours. The system thus obtained was called as multiwalled hollow nano spheroid.

### 2.3.2 Synthesis of mesoporous assembled titania nanocuboids [MT]

Here, we use nonionic triblock copolymer P123 $(EO_{20}PO_{70}EO_{20})$ as the structure-directing agent because it can promote the cooperative assembly with relatively weak interactions at the titanium/surfactant interface, and yield mesostructured titania with good thermal stability. To a premixed ethanol (Merck) P123 (Sigma Aldrich) solution, HCl (Merck) was added. Tetrabutyltitanate (Sigma Aldrich) and acetylacetone (Sigma Aldrich) were added to the above solution under vigorous mechanical stirring. After 30 minutes, distilled

water was added. The molar ratio P123/ TBOT/ Ethanol/ Water/ Acetylacetone/ HCl was maintained as 0.025:1:28.5:30:0.5:0.005. Solution was stirred for 6 hours at room temperature, followed by aging at $40^0$C for 9 days. The gel was collected, dried overnight at $110^0$C, and calcined at $500^0$C for 4 hours to obtain mesoporous assembled titania nanocuboids.

### 2.3.3   Synthesis of tiania nanotubes [TNT]

Titania nanotubes were synthesized following Hydrothermal method. About 5 g of Commercial $TiO_2$ powder was dispersed in 175 ml of NaOH (10 N) solution using mechanical stirrer for 1 hour and the suspension was transferred into a Teflon-lined stainless steel autoclave and sealed. The autoclave was maintained at a temperature of 130 $^0$C for 48 h and then allowed to cool to room temperatures. The white precipitate obtained from the hydrothermal treatment was vacuum-filtered and washed with 0.1 N HCl and deionized water until the pH was around 7. The sample was then dried at 100 ∘C overnight and calcined at $400^0$C to obtain the titania nanotubes.

### 2.3.4   Synthesis of titania nanobelts [TNB]

Same procedure as that of Titania nanotubes was adopted for the synthesis of titania nanobelts except that treatment temperature and time were varied. About 5 g of Commercial $TiO_2$ powder was dispersed in 175 ml of NaOH (10N) solution using mechanical stirrer for 1 hour and the suspension was transferred into a Teflon-lined stainless steel autoclave and sealed. The autoclave was maintained at a temperature of 220$^°$C for 18 h and then allowed to cool to room

temperatures. The white precipitate obtained from the hydrothermal treatment was vacuum-filtered and washed with 0.1 N HCl and deionized water until the pH was around 7. The sample was then dried at $100^{\circ}C$ overnight and calcined at $400^{0}C$ to obtain the titania nanobelts.

### 2.3.5   Synthesis of titania nanoparticles [TNP]

10mL of Titanium butoxide is mixed with 10 mL of acetylacetone.To this mixtrure, 10mL of ethanol containing 0.5mL HCl was added under sonication. 4 mL of distilled water was also added meanwhile. The solution is allowed to stand for 24 hours at room temperature and then 30 mL of distilled water was added and sonicated again. The gel formed is dried at $100^{\circ}C$ for 12 hours and the dried sample was calcined at $500^{\circ}C$

## 2.4   Synthesis of modified analogues of titania nanostructures for Hydrogen energy production

Visible light harvesting of titania has become an important topic nowadays. Co-doping with metals are proven to be effective for reducing the recombination of photogenerated charge carriers and also for visible light absorption. Thus introducing cost effective metals in appropriate amounts will bestow the nanostructures with many desired properties to be used in wide applications. Since surface area also plays a significant role in the Hydrogen production by water splitting reaction. Two systems with high surface area values were chosen and they are incorporated with 0.5 wt % copper and silver metal as cocatalysts. Precursor compounds chosen for metal ions were copper nitrate and silver nitrate. Photo deposition method was adopted for the

incorporation of the doped systems. Required quantities of titania nanostructures were dispersed in water and ethanol mixture in the ratio (2:1) and stirred for 15 minutes under UV radiation. Sufficient amount of precursor solutions was added, sonicated and again illuminated with UV light for 2 hours with continuous stirring. After filtration, the precipitates obtained were washed with water and dried for 12 hour at $80^0$C.

## 2.5 Modification of synthesised nanostructures for biological applications

### 2.5.1 Anticancer drug [5-Fluorouracil] modified titania nanostructures

Definite amount of titania nanostructures was incubated with 1mg/mL of drug solution [5-Fluorouracil] overnight with continuous stirring at 50 rpm. The resulting drug encorporated solution was centrifuged and washed with double distilled water and dried. All the experimental procedures were carried out in dark conditions.

### 2.5.2 Folic acid modified/anticancer drug incorporated titania nanostructures

Specific amount of folic acid was dissolved in DMSO and to this transparent yelow solution, desired quantity of Titania nanostructures was added and stirred for 4 hours. The resultion suspension was centrifuged, washed with distilled water and dried. Dark conditions were maintained throughout the preparation and preservation of modified $TiO_2$. For drug loading, folic acid modified systems were added to 1 mg/mL drug solution and stirred at 50 rpm over night in dark. It was centrifuged and washed with ditilled water to remove the unbound drug from surface and dried.

## 2.6    Catalyst Notations

| | |
|---|---|
| **MHS** | Multishelled titania hollow nanospheroids |
| **MT** | mesoporous assembled titania naocuboids |
| **TNT** | Titania nanotubes |
| **TNB** | Titania nanobelts |
| **TNP** | Titania nanoparticles |
| **CTiO$_2$** | Commercial titania |
| **CuMT** | Copper modified mesoporous assembled titania nanocuboids |
| **AgMT** | Silver modified mesoporous assembled titania nanocuboids |
| **CuTNT** | Copper modified Titania nanotubes |
| **AgTNT** | Silver modified Titania nanotubes |
| **5-FU** | 5Fluorouracil |
| **DMHS** | 5Fluorouracil drug loaded Multishelled titania hollow nanospheroids |
| **DMT** | 5Fluorouracil drug loaded mesoporous assembled titania nanocuboids |
| **DTNT** | 5Fluorouracil drug loaded Titania nanotubes |
| **DTNB** | 5Fluorouracil drug loaded Titania naobelt |
| **DTNP** | 5Fluorouracil drug loaded Titania naoparticle |
| **FDMHS** | Folic acid modified 5 Fluorouracil loaded Multishelled titania hollow nanospheroids |
| **FDMT** | Folic acid modified 5 Fluorouracil loaded mesoporous assembled titania nanocuboids |
| **FDTNT** | Folic acid modified 5 Fluorouracil loaded Titania nanotubes |
| **FDTNB** | Folic acid modified 5 Fluorouracil loaded Titania naobelts |
| **FDTNP** | Folic acid modified 5 Fluorouracil loaded Titania naoparticles |

## 2.7    Characterization techniques

World of catalysis is nothing without the characterization of the synthesised systems. They are the powerful tools which unreveal most of the informations of the catalysts into lime light. Appropriate techniques are needed to assess the structure and properties of materials, depending upon the nature of material under study. Some of them are qualitative, providing information about presence of particular ions; morphology etc while quantitative techniques reveal the concentration, chemical composition, size etc. Various characterization techniques used in this study are

Small And Wide Angle X-ray Diffraction Pattern

Fourier Transform Infra Red Spectroscopy

Raman Spectroscopy

SEM,FEG-SEM

TEM,HRTEM

Dynamic Light Scattering Analysis

Photo Luminescence Spectroscopy

$N_2$ Adsorption Desorption Study-Surface Area Analysis

Uv-visible Spectroscopy And UV-DRS

## 2.7.1   **Scanning electron microscopy [SEM]**

Scanning electron microscopy is widely used for characterizing the texture, size and morphology of the catalysts. Image is produced by scanning the surface with a focussed beam of electrons. During the scanning ofthe surface with a beam of electrons emitted from an electron gun, their interaction with surface leads to the generation of secondary electrons, back scattered electrons, auger electrons etc, The back scattered electrons and secondary electrons are captured by a detector to form a three dimensional image. Secondary electrons arise due to inelastic collision between primary electrons (the beam) and loosely bound electrons of the conduction band/ tightly bound valence electrons, whereas the elastic collisions between the incoming electrons and the nucleus of target atom resulted in back scattered electrons which increase with increase of atomic number.

The typical componets of SEM constitutes electron column, scanning system, detector(s), display, vacuum system and electronics controls. An accelerated beam of electrons (0.2 - 40KeV) generated from the electron gun (tungsten filament cathode) and two or more electromagnetic lenses operating in vacuum constitutes the electron column. Designing the lenses often involves space for the scanning coils, the stigmator, and the beam limiting aperture.  The role of these lenses is controlling the diameter of the beam and focusing the beam to surface of the specimen. The lenses are metal cylinders with cylindrical hole, which operate in vacuum. Scanning coils are provided to focus the energized electron beams on to the sample. Signals are emitted in the form of electromagnetic radiation when struck by these accelerated electrons. Various types of signals are produced including secondary    electrons (SE),    reflected    or back-scattered

electrons (BSE), characteristic X-rays and light (cathodoluminescence) (CL), absorbed current (specimen current) and transmitted electrons. These probes, usually secondary (SE) and/or backscattered electrons (BSE), are collected by a detector which is then amplified by electronic amplifiers and typical image is displayed on a computer monitor. The final lens in the column called "objective" focuses the probe on the sample. As high currents are flowing through the lenses which may produce excessive heat, they are cooled usually by circulating water. The final lens aperture has three important effects on the final probe. i) An optimum aperture angle minimizes aberrations. ii) The size of the aperture is one factor which controls the current in the final probe iii) the probe convergence angle, α controls the depth of field. Smaller α creates greater depth of field. Spot size in SEM is minimized at the expense of current [1-2]. Schematic diagram has been shown in figure 1.
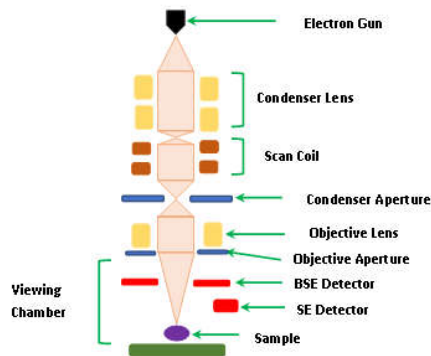


**Figure 1**. Schematic diagram of SEM

The combination of higher magnification, larger depth of focus with large number of sample to be in focus and greater resolution make the FEG-SEM as one of the most widely used instruments in various research areas. The high resolution images produced by FESEM imply that with high magnification, closely spaced features can be examined. Recently, three-dimensional features also can be observed due to the large depth of field available in the FESEM. The electrons which are generated by a field emission source are accelerated in a field gradient under vacuum. After passing through the electromagnetic lenses, the beam is focussed  onto the sample resulting in the emission of different types of electrons. A detector catches the secondary electrons and an image of the sample surface is constructed by comparing the intensity of these secondary electrons to the scanning primary electron beam [3-4].   SEM analysis was done using instrument JEOL, Model JSM-6390LV

## 2.7.2   Transmission electron microscopy

The only difference between SEM and TEM is that, in the former one back scattered electrons or secondary electrons are analyzed whereas in the TEM, the transmitted electrons through the sample is detected. The possibility for high magnification has made the TEM a valuable tool in both medical, biological and materials research. The TEM uses electromagnetic lens to focus the electrons into a very thin beam. As the sample is bombarded with a highly-energetic beam of electrons in vaccum, black and white images are formed by the passage of some electrons through the sample. The condenser lenses (2-4 depending on the microscope) are responsible

for the amount of illumination that reaches the sample and controlling the beam intensity/ brightness. The transmitted electrons through the sample are focused on a fluorescent screen by objective lenses and generate corresponding images applying a small amount of magnification. Finally the intermediate and projector lenses magnify the beam and project it onto the camera (CCD or film) or screen to form an image. The microscopic image (micrograph) is obtained in a short time. Transmitted electrons are detected as light areas in the micrograph; electrons have been scattered or absorbed by the sample appear as darker areas as the number of electrons reaching to the destination are reduced. The finest details of the internal structure of the sample are revealed by TEM analysis. At present, the highest point resolution realized in phase contrast TEM is around $0.5A^0$ (0.050 nm) [5]. Sample preparation is another important factor in TEM analysis as the sample must be thin to transmit more electrons without much energy loss. The sample dispersed in suitable solvent the dispersion was coated on a copper grid on carbon tape for TEM analysis. The sample is placed in a sample holder in the path of the electron beam. Thus the high energy electron can be focused on the specimen using the condenser lenses and aperture. A schematic representation of TEM experimental set up has been shown in figure 2. The morphology of the samples was investigated using Transmission electron microscopy, TEM model FEI TECNAI 30 G2, 300KV.

The Crystallographic experimental technique selected area (electron) diffraction can be performed inside a transmission electron microscope. The term "selected" means the user has the freedom to

choose from which part of the sample to obtain the diffraction pattern. On the TEM column, located below the sample holder, there is selected area aperture which can be inserted into the beam path. This thin strip of metal contained different sized holes allows the electron beam to pass through only one of the hole. As the aperture can be moved by the user, the indended area can be selected to get selected area electron diffraction pattern on the screen. As the high energy electrons passes through the sample, the atoms act as diffraction gratings to the electrons which means some fraction of the beam will be scattered in particular angles while the rest of them without any deflection, passes through it. The image on the screen be a series of spots. Each spot matches a satisfied diffraction condition of the sample's crystal structure. From the selected electron diffraction, we are able to get an idea about the crystal structure, crystal defects, lattice parameters, of the sample. An electron density map may be obtained and a three dimensional model can be set up with a series of SAED patterns from different orientations taken on a selected particle and combining all reflections [6].
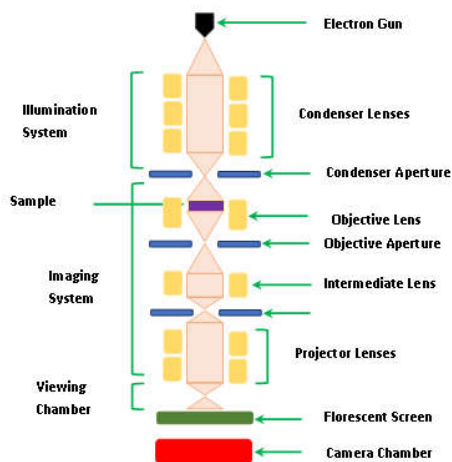
**Figure 2**. Schematic picture of TEM experimental setup

## 2.7.3 Fourier transform infrared spectroscopy (FTIR)

Fourier transform infra red spectroscopy is a multidisciplinary analytical technique used for the Identification of the structural features of the catalysts such as adsorbed and dispersed species and their structure, surface characteristics such as acidity, metal-metal interaction, reaction intermediates on the catalyst surface etc. In the electromagnetic spectrum, the term infrared spectrum covers the range between 12800-10 cm$^{-1}$ [near (12800-4000 cm$^{-1}$), mid (4000-200cm$^{-1}$) and far (200-10 cm$^{-1}$)]. In which the most useful IR region lies between 4000-670 cm$^{-1}$ and the region between 1430-910 cm$^{-1}$ is called as the finger print region. Since each molecule possesses discrete vibrational energy levels, absorption of photons in the IR region resulted in the transition between these vibrational levels. The selctron rule for vibrational transitions being $\Delta V = \pm 1$ and the vibrational energy of a chemical bond which is quantized having the value, $E_{vib} = \left(v + \frac{1}{2}\right)h\nu$ where, 'v' is the number of the vibrational level

and can have values 0, 1, 2, 3………… 'h' is the Planck's constant, and 'v' is the vibrational frequency of the bond.

Thus if a bond is subjected to infrared radiation of a specific frequency, it will absorb the energy, and the bond will move from the lowest vibrational state, to the next highest. A s the number of atoms increases, there will be more number of bonds therefore more modes of vibrations. For a linear molecule with 'n' atoms there are 3n-5 vibrational modes, if it is nonlinear, it will have 3n-6 modes. Considering a catalyst system, which have surface adsorbed reactants, short-lived species or the reaction products, the calculation of overall vibration modes in these systems are not possible. But, the functional group vibrations are open to to characterization by IR spectroscopy. Every functional group has unique vibrational energy, the IR spectra can be seen as their fingerprints.

IR spectra represent a plot of absorption ( % Transmittance) as a function of wavelength (cm$^{-1}$). The experimental set up includes; IR source, interferometer, holder which holds the sample, a detector and a computer [Figure 3]. The modern Fourier–Transform Infrared (FTIR) spectrometer uses the principle of Michelson Interferometer to cause interference pattern. In which light from the polychromatic infrared source is collimated (made parallel) and directed to a beam splitter. Ideally each of 50% of the light is refracted and transmitted towards the fixed mirror and the moving mirror respectively. These two mirrors refelcts these beams back to beamsplitter. The two beams unite constructively or destructively depending up on their optical path difference as the moving mirror is moved. These combined beam when transmitted through the sample, it is detected as an interfergram which contains all the information about the sample. By a mathematical

process of Fourier transformation, ihis interferogram give the infrared spectrum of the sample [7].

Jasco FTIR - 4100 spectrometer using KBr disc method is used for recording the FTIR spectra of synthesised catalysts in our work. This method exploits the property that alkali halides become plastic when subjected to pressure and form a sheet which is transparent in the infrared region. Potassium bromide is the commonest alkali halide used. The pellet foin this technique. Pellet for analysis is prepard by grinding 150 mg of special grade KBr with sample well in a mortar and pelletizing in a hydraulic press. This pellet was used for recording the spectrum in mid infrared region (4000-400 cm$^{-1}$). Background measurements were done on a pellet holder with a pellet of KBr only, which can correct for infrared light scattering losses in the pellet and for moisture adsorbed on the KBr.
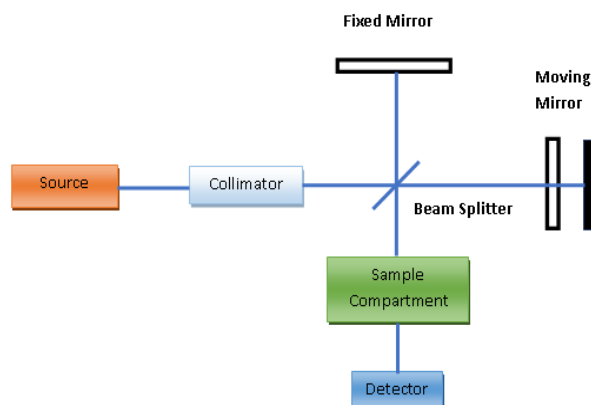


**Figure 3**. Representation of Experimental setup for FTIR

## 2.7.4 Powder X-ray diffraction analysis

X-ray diffraction (XRD) is one of the most unambiguous non-destructive tools to investigate all kinds of matter -ranging from fluids, to powders and crystals. Degree of crystallinity, crystallite size, phase purity and its composition, lattice parameters, geometry, impurities, lattice defects etc of a solid material can be determined with this analytical tool. The conventional X-ray source consists of a target which is bombarded with high energy electrons. Usually CuKα radiation with energy of 8.04 keV and wavelength of 0.154 nm is used as the X-ray source. In this method X-rays interact with crystalline matter with atoms in periodic lattice and undergoes diffraction. A diffraction peak is observed when there is constructive interference occurs from these scattered X-rays. We can calculate distance between two planes knowing the angle of diffraction using the expression, $n\lambda = 2d\sin\theta$ where n is an integer called order of diffraction, $\lambda$ is the wavelength of Xray, d is the distance between lattice planes [8]. Figure 4 (Left) signifies the typical bragg's diffraction of Xrays from crystal planes .

The average crystallite size of a material can also be obtained from the broadening of an X-ray diffraction peak, the formula being $d = 0.9\lambda/ \beta \cos\theta$ where $\beta$ is full width at half maximum. As each crystalline powder gives a unique diffraction diagram, we can determine the purity of sample and degree of crystallisation by comparing with a standard (a pattern), taken from any X-ray powder data file catalogues. [Published by the American Society for Testing

Materials (JCPDS)] X-ray diffractometers consist of three basic elements: an X-ray tube, a sample holder, and an X-ray detector.
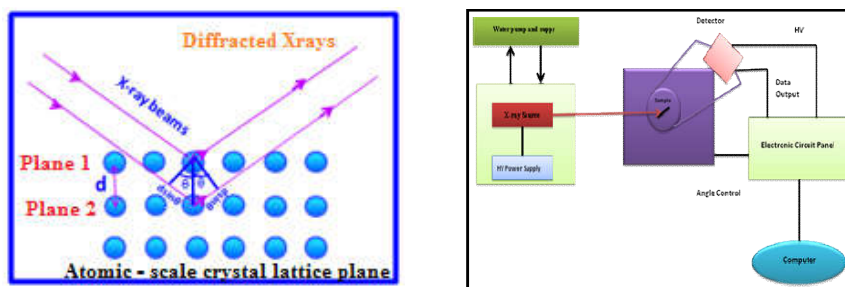


**Figure 4**. Diffraction of X-rays from different planes (Left), Experimental setup for Xray powder diffraction (Right)

When high energy electrons are bombarded on metals like Cu/Mo, it emits Xrays. These X-rays are collimated and directed onto the sample. In X-ray diffractometer , the sample rotates in the path of the collimated X-ray beam at an angle θ whereas the X-ray detector is mounted on an arm to collect the diffracted X-rays and rotates at an angle of 2θ. A goniometer is used to maintain the angle and rotate the sample. Once the X-rays impinge on the sample, they diffract from each of the exposed planes. When the geometry of the incident X-rays impinging the sample satisfies the Bragg law, constructive interference occurs and a peak in intensity occurs. The detector rotating around the sample records the intensities of diffraction at each each angle.The experimental setup has been represented in figure 4 (Right).

The wide angle powder X-Ray Diffraction results of the catalyst samples are collected on Rigaku miniflex 600 diffractometer with a rotating anode using Cu Kα radiation.

Small angle Xray Scattering (SAXS)

From Bragg's law it can be revealed that if the wavelength of X-ray is kept constant, smaller angles leads to the detection of large 'd' spacing. The constructive interference of Xrays from the ordered array of atoms/molecules lead to the formation of strong diffraction peaks. This technique is usually used for examining multilength scale structures such as small peptides, high molecular weight polymers, proteins,nuceic acids, self- assembled suprastructures like mesoporous materials etc; The SAXS measurements are usually done near to the primary beam ("small angles"), so the technique earn greatly from the brilliance of X-ray photon radiations provided by particle accelerators known as synchrotrons. The method used is nondestructive with minimum amount sample preparation.Typically SAXS experiment is simple;monochromatic beam of Xrays stuck on the sample when some of the Xrays scatters and most of them pass through the sample. Small angle scatterring techniques were usually done using hard X-rays with wavelength of 0.07- 0.2nm. The scattered radiation is registered by the detector which situated just behind the sample and perpendicular to the incident Xray beam. The scattering pattern contains the information on the structure of the sample. The scattering was recorded in small angle region that is 0.1-10$^{°}$ hence the name small angle. Uniform pore sized materials often exhibit sharp peak in the low angle region due to the diffraction of X-rays from the pore walls arranged in a regular pattern.

The distance between the pore walls is far greater than the distance between the lattice planes, thus creating diffraction peak at low angle [9]. In the present study, the low angle XRD diffraction pattern of mesoporous titania was obtained by Brucker Nanostar instrument.

## 2.7.5   Surface area and porosity measurement

Surface area and porosity of the material greatly influence the performance of the catalysts as these parameters give an idea about the maximum active sites available and the rate of diffusion of reactants and products in and out of the pores. Gas adsorption analysis is usually used for porosity measurement and surface area analysis. Under appropriate conditions of temperature and pressure, a gas can be progressively adsorbed on the solid surface leading to its complete coverage. An adsorption desorption isotherms signifies the amount of molecules adsorbed on the solid surface as a function of the equilibrium partial pressure at constant temperature [10]. There are five adsorption isotherms have been identified and named by IUPAC [Figure 5, Top left]. Type I, are given by microporous materials having relatively small external surfaces (activated carbon, molecular seive zeolite etc ;). At very low $p/p_0$, a steep uptake of gas molecules can be observed owing to the enhanced interactions and the amount is approaching to a limiting value. Type II Type III and Type VI corresponds to nonporous and macroporous materials. The type II isotherm is the result of unrestricted monolayer-multilayer adsorption up to high $p/p_0$. The completion of monolayer coverage is indicated by the sharp knee just before the middle linear portion in the curve. The overlapping mono and multilayer adsorption and beginning of

multilayer adsorption is indicated by region where the gradual curvature is observed. In the case of a Type III isotherm absence of a sharp knee is an indicative of the absence of monolayer formation. Adsorbate-adsorbate interactions are more than adsorbent-adsorbate interactions and the adsorbate molecules are clustered on the surface. Layer-by-layer adsorption on a highly uniform nonporous surface is shown by the step widse Type VI isotherm. Type IV and Type V isotherms are observed for mesoporous materials. In type IV, monolayer-multilayer adsorption occurs initially on the mesopore walls, followed by pore condensation. In pore condensation a gas condenses to a liquid-like phase in a pore at a pressure less than the saturation pressure $p_0$ of the bulk liquid. The most striking features of the Type IV and V isotherm are the hysteresis loop and the plateau at high $\left(\frac{P}{P_0}\right)$. The shape of Type V is almost similar to that of Type III in the low $p/p_0$ range due to molecular clusturing and at higher $p/p_0$ clusturing is followed by pore filling. Analysis of adsorption data are done adopting various models such as langmier, BET equations, BJH method, t-plot, Horvath–Kavazoe method etc [11-15]. t-plots and the BJH method are employed to calculate total micropore and mesopore volume, respectively. The BET model is usually used for the measurement of total surface areas. Among the different gases ($N_2$, Ar, and $CO_2$ ) used as adsorptive, $N_2$ adsorption at 77K and at sub-atmospheric pressures has remained dominant adsorptive for surface probing. Besides inertness, it forms multilayer isotherm independent of the differences in the surface structure of the adsorbent. Brunauer, Emmett and Teller in 1938 derived the equation for physical

adsorption of gases on solid surfaces that leads to multilayer adsorption, known as BET equation,

$$\frac{p}{(po-p)V} = \frac{1}{CVm} + \frac{C-1}{CVm} \left\lfloor \frac{p}{po} \right\rfloor ;$$

Where p and $p_o$ partial pressure and saturation pressure at experimental temperature, V is the volume of gas adsorbed and Vm volume adsorbed at monolayer coverage, 'C' is the BET constant related to the interaction between solid and the adsorbed gas molecules

$C = \exp\left\lfloor \frac{E1-EL}{RT} \right\rfloor$ ; $E_l$ is the heat of adsoption for the first layer, $E_L$ is the heat of adsoption for the remaining layers.

$\frac{p}{(po-p)V}$ plotted as a function of $\frac{p}{po}$ is called BET plot which is a straight line in the range of $\frac{p}{po} = 0.05$-$0.3$ whose slope is $(C-1)/_{CVm}$ and intercept is $1/_{CVm}$ [Figure 5, Top right]. From this $V_m$ can be formulated as $\frac{1}{(slope+intercept)}$. Thus total and specific surface area can be obtained from the following relations $S_{total} = \frac{Vm\,N\,s}{V}$ ; $S_{BET} = \frac{Stotal}{a}$ N is the avogadro number ($6.023 \times 10^{23}$ mol$^{-1}$), 'a' is the mass of the solid sample or adsorbant, 's' is the adsorption cross section of adsobing species, V is the molar volume of adsorbate gas.

Size and shape of the pores determine the adsoption process to an extend. According to IUPAC, porous materials have been classified as microporous (<2 nm), mesoporous (2-50 nm), and macroporous (>50 nm) materials. In the adsorption-desorption isotherms, the

desorption isotherms do not duplicate the adsorption ones in the case of mesoporous materials instead lie above it over a range of relative pressure, which leads to the formation of a hysteresis loop before rejoining the adsorption isotherms. IUPAC has classified the hysteresis loops observed as types H1, H2, H3 and H4 [Figure 5, bottom].
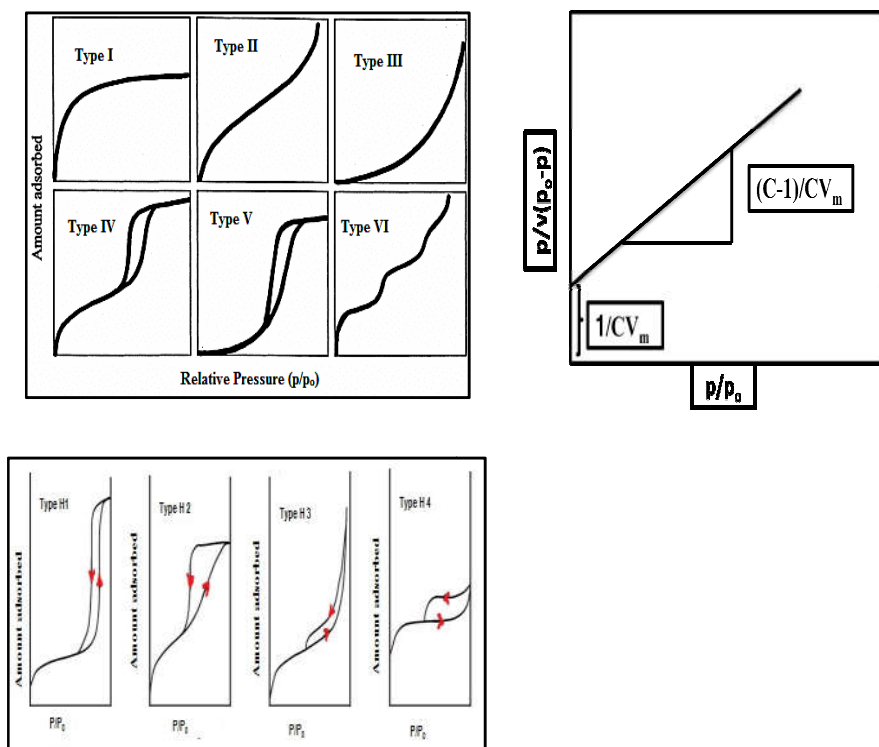


**Figure 5.** BET adsorption isotherm by plotting $p/p_0$ Vs $p/V(p_0-p)$ (Top, Left) and Type of physisorption isotherms (Top, Right) and hysteresis loops (Bottom).

Type H1 is representative of an adsorbent with a narrow distribution of relatively uniform mesopores. The adsorption desorption curves are steep and parallel. Where as, Type H2 is associated with a more

complex pore structure with interconnected networks. Type H2 loop is given by adsorbents containing narrow slit-shaped pores such as activated carbons. Type H3 and Type H4 do not exhibit any limiting adsorption at high relative pressure. Type H3 loops are often given by plate-like materials such as clays and the adsorption brach resembles type II adsorption isotherm. Type H4 adsorption branch is a combination of type I and typr II adsorption isotherm. Many computational procedures have been projected for the derivation of the mesopore size distribution from a physisorption isotherm [16 -18]. Among this BJH method proposed by Barrett, Joyner, and Halenda in 1951 is the one which is widely used. The total pore volume and specific pore volume was calculated using the relations,

$$V_{liq} = \frac{P \, Vads \, Vm}{RT} \text{ and } V_p = \frac{V \, liq}{m}$$

where P and T are the ambient pressure and temperature respectively, $V_{ads}$ is the volume of nitrogen adsorbed, $V_{liq}$ is the volume of liquid nitrogen and m is the weight of adsorbant after degassing. Pore size distribution is calculated from the Kelvin equation in conjunction with the statistical thickness derived from the t-curve equation.

$$r\left(\frac{p}{po}\right) = \frac{2 \, \gamma \, V \, L}{R \, T \, \ln \frac{po}{p}} + t \, \frac{p}{po} + 0.3 \text{ nm}$$

r (p/po) is the pore radius as a function of relative pressure, $\gamma$ is surface tension, VL is the molar volume of the liquid adsorbate, R is the gas constant, T is the absolute temperature (77K) and t is the statistical film thickness (t curve) for nitrogen adsorbed on the pore walls and its

value is calculated as t $\left(^p/_{po}\right)$ [nm] = 0.1 [60.65/0.03071- log $\left(\frac{p}{po}\right)$

0.3968

Nitrogen adsorption-desorption isotherms of the catalyst samples are obtained on a micromeritics Gemini Surface Area Analyser using a static adsorption procedure at 77K.

## 2.7.6 Diffuse reflectance UV - Visible spectroscopy

UV-Visible diffuse reflectance spectroscopy is an excellent and non-invasive technique for understanding electronic structure of materials. The electronic transitions of materials in liquid state is usually studied by UV-visible spectroscopy. While in the case of insoluble solids, UV-Vis. Reflectance or diffuse reflectance methods is used. The UV-Vis. Reflectance is applied for highly reflective materials and diffuse reflectance method is suited for powdered samples and roughened solids. Diffuse reflectance spectroscopy is very closely associated to UV/visible spectroscopy, the only difference is in this method the change in the amount of reflected light is measured instead of transmitted light in the case of UV/visible spectroscopy. In general electronic transitions are of two types. The first type includes the metal centered transitions, ns-np in the main group elements, a d-d and (n-1) d-ns in transition elements, f-f and 4f-5d in rare earth elements and. The second type involves charge transfer (CT) transitions like ligand-to- metal (LMCT) and metal-to-ligand (MLCT) charge transfer, metal-to-metal charge transfer (MMCT) or sometimes called intervalence transitions (e.g., Fe(II) $\leftrightarrow$ Fe(III) in $Fe_3O_4$) , intra-ligand CTs or ligand centered (LC).

When electromagnetic radiation in the UV/Visible wavelength range interacts with a sample, the radiation may be absorbed/ transmitted/ reflected/ scattered. When an UV-Visible instrument is equipped with the proper accessories, it is possible to measure the reflected and scattered energy from a sample. Reflectance, the base quantity that characterizes the process of reflection is defined as the ratio of the reflected radiant flux to the incident radiant flux. Reflected radiation can be either specular or diffuse. Specular reflectance is the mirror like reflectance from a surface with well defined angle of reflection. In diffuse reflectance, the reflected radiant energy that has been partially absorbed, transmitted and partially scattered by a surface with no defined angle of reflection [Figure 6].
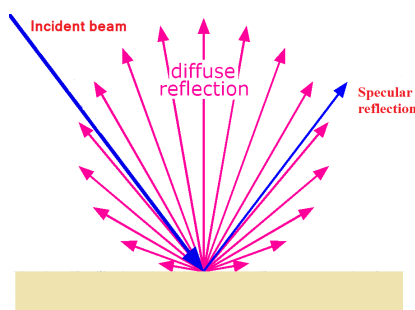


**Figure 6**. Diffuse and secular reflectance from a glossy surface

Instrumentation includes the components, light source, interacting sphere, sample holder, detectors. The integrating sphere is an optical device whose interior is covered with a white reflective coating. There are holes for entrance and exit in that hollow spherical

cavity. Two types of sample holders are used centre –Mount cuvette style and clip and jaw style mount sample holders. Commonly used detector in DR-UV-Vis spectrophotometer is photomultiplier tube which works based on the principle of photoelectric effect. The spectra is a plot of percentage of reflectance againt wavelength[19].

Kubleka-Munk function is used for the determination of band gap of powdered semiconductor nanostructures[20]. The expression is as flows;

$$\frac{k}{s} = \frac{(1 - R\infty)^2}{2R\infty} \equiv F(R\infty)$$

'k' and's' are absorption and scattering coefficients respectively, '$R_\infty$' is the ratio of sample reflectance to the reflectance of reference, F ($R_\infty$) is called Kubelka Munk function. Band gap value is based on the equation, $\propto h\nu = C(h\nu - Eg)^n$, where '$\propto$' is the absorption coefficient, 'hν' is the photon energy, C is a constant [21]. For n=2 and n=1/2 for directly allowed transition and indirectly allowed transition respectively. Titania is a direct band gap semiconductor hence the equation can be written as, $\propto h\nu = C(h\nu - Eg)^2$. The graph between $[F(R) \alpha h\nu]^2$ and (hν) is extrapolated to X axis to get the band gap value.

Jasco V-550 spectrophotometer served the purpose of recording the DR UV–Vis spectra in the range 200–800 nm using $BaSO_4$ as reference.

## 2.7.7 Raman spectroscopy

Raman spectroscopy is a type of molecular spectroscopy which measures the rotational, vibrational and other low frequency modes of molecules. The phase purity of the solid material can be determined by this technique. Raman scattering is an example of inelastic scattering since the energy is transferred between the photons and the molecules during their interaction. These lnteractions leads the energy of laser photons to be increased or decreased. This shift in energy lights to the vibrarional modes in the system. In a Typical raman spectrometer, laser beam focussed with a lens and sent through a monochromator. The monochromatic radiation is passed through the sample and the filter removes the elastically scattered radiations and antistock radiation and the inelastically scattered radiation reaches the detector. Raman effect is based on the interaction between the electron cloud of the sample and the external electric field produced by the monochromatic light creating an induced dipole moment based on its polarizability. In spontaneous raman effect, photon excites the molecule from the ground state to a virtual energy state for a short time before the photon scatters inelastically. When the molecule relaxes, it emits a photon of different energy and returns to another rotational or vibrational state. the shift in energy of laser photon is dependent up on the enrgy difference between the initial and final rovibronic state. If the final vibrational state of the molecule is higher in energy than the initial state, for the total energy of the system to remain balanced, the emitted photon will be shifted to a lower frequency.This shift in frequency is designated as a Stokes shift. If the final vibrational state is

lesser in energy than the initial state, then the emitted photon will be shifted to a higher frequency, and this is designated as an Anti-Stokes shift [Figure 7a]. Each molecule has its own unique Raman spectrum, which can be correlated as a molecular fingerprint. Thus effective for developing databases of known standards which can be consequently used for the identification of unknowns [22-23]. Figure 7b represents typical experimental setup for raman spectroscopy. Raman spectra of the samples were recorded using Bruker multi Ram FT-NIR spectrometer with Nd-YAG Laser source (1064nm).
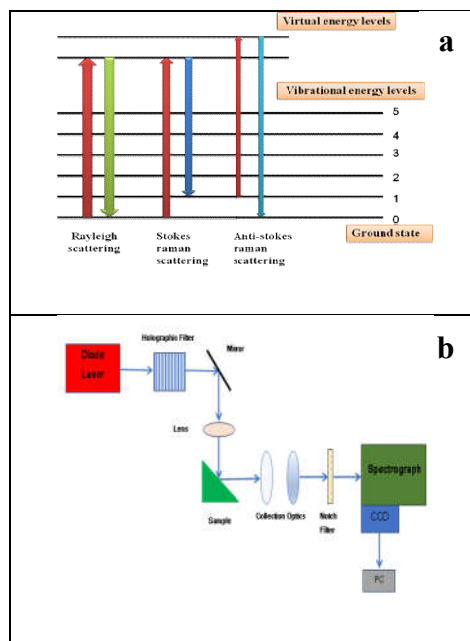


**Figure 7.** Energy diagram showing states involved in Raman spectra (a) Instrumentation seup for raman spectrum measurement (b)

## 2.7.8 Photoluminescence spectroscopy

Photoluminescence spectroscopy is a nondistructive, noncontact tool to probe the discrete electronic levels by optical excitation. Up on excitation by ligth the subsequent procecess may or may not result in emission of light as in figure 8 a. . In PL spectroscopy, when the sample is photoexcited, the energy is dissipated spontaneously through emission of light / photoluminescence (radiative process) is collected and measured. In the case of a semiconductor with valence and conduction bands the most common radiative transition is that between these levels which is called as bandgap. When a semiconductor is photoexcited, the excited charge carriers electrons and holes finally recombines by emission of energy. Thus quantity of this emited light is the relative contrubution of radiative process. Since the radiative transitions in semiconductors also include localized defects or impurity levels,the PL spectrum leads to the identification and the extent of specific defects or impurities. Thus photoluminescence study is useful in the determination of bandgap, excited states, impurity levels, defect dtection, surface structure, along with the recombination mechanism involved [24-25]. A spectrofluorometer is an analytical instrument used to measure and record the fluorescence of a sample. Schematic representation of a typical emission exprement is shown in figure 8 b. The excitation wavelength is selected by the monochomator and luminescence is collected through the second monochomator which collects it to detector. Finally the signal is transferred for processing to a programmed computer.

Here emission characteristics were recorded using RF-5301
PC- Shimadzu Spectro Fluorophotometer.
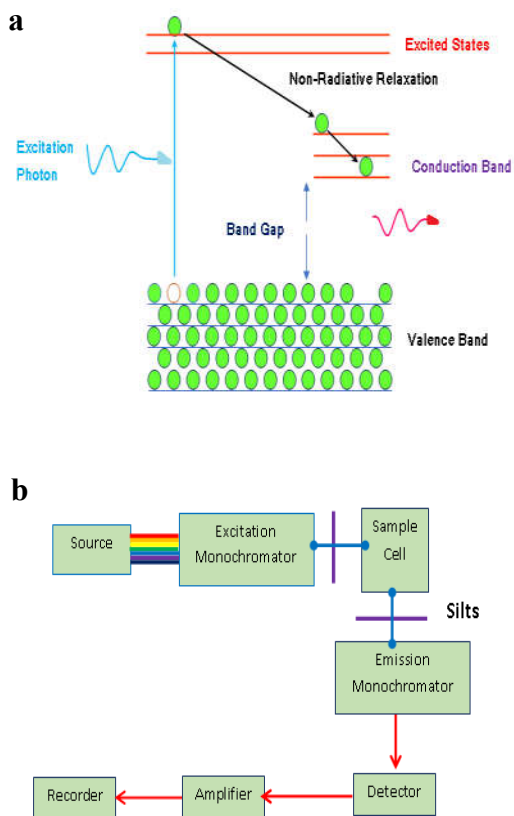


**Figure 8.** Principle of Photoluminescence spectroscopy (a),
Experimental setup for mesurement of fluorescence (b)

## 2.7.9 Dynamic light scattering

Dynamic light scattering also known as photoncorrelation spectroscopy or quasi elastic light scattering is a non- invasive technique for the measurement of small particles in suspension and polymer in solution. Small particles in suspension undergo random thermal motion due to its bombardment with solvent molecules that surround them known as Brownian motion. The Brownian motion of particles or molecules in suspension causes the laser light to be scattered at different intensities. Larger particles have slower brownian motion whereas the smaller particles move fast. Analysis of these intensity fluctuations yields the velocity of the Brownian motion and hence the particle size using the Stokes-Einstein relationship

$$D_h = k_B T / 3 \Pi \, \eta D_t$$

$k_B$ is the Boltzmann constant, T is the absolute temperature, Dt is the translational diffusion coefficient, $\eta$ is the viscosity.

Particles can be dispersed in a variety of liquids provided the liquid refractive index and viscosity is needed for interpreting the measurement results.

Instrumentation
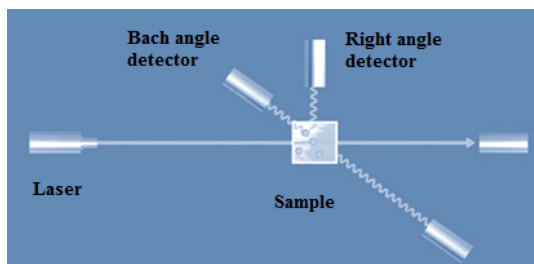


**Figure 9**. Dynamic light scattering layout

Sample in the cell is illuminated by the light from the laser light source. The scattered light signals are collected using one of the two detectors, either at a 90 degree (right angle) or 173 degree (back angle) scattering angle. The obtained optical signal exhibit random changes due to the randomly changing relative position of the particles.

Electrokinetic meaurements are used to characterize the stability of dispersions. There exists a surface potential at the interface between the solid particle and the surrounding liquid due to the presence of a surface charge. Zeta potential is the electric potential in the interfacial double layer at the slipping plane relative to a particular point in the bulk liquid away from interface [Figure 10] . Unlike other interface potentials, this value is measurable and gives charge conditions at the particle surface and colloidal stability. The information regarding the acidic and basic groups on solid surface and the interaction between components of electrolyte solution and solid surface can be identified by this measurement. The magnitude of the

zeta potential is an indication of the extent of electrostatic repulsion between adjacent, similarly charged particles in dispersion. A high zeta potential will bestow stability, the solution or dispersion will resist aggregation. When the potential is small, attractive forces may exceed this repulsion. So, colloids with high zeta potential (negative or positive) are electrically stabilized while colloids with low zeta potentials tend to coagulate or flocculate. Horiba Scientific, Nanopartica, Nano particle analyser SZ-100 was used to analyze the surface charge of the particles
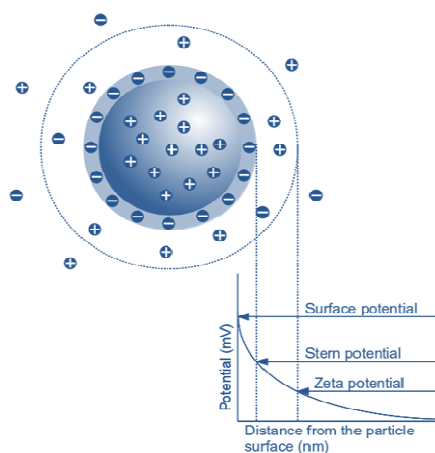


**Figure 10.** Location of the zeta potential relative to the particle surface

## 2.8 Instrumental methods for aplication studies

### 2.8.1 UV-Visible spectrophotometer

Molecules with non bonding / Π electrons when excited with UV or Visible radiation, they absorb energy exciting the electrons to higher

antibonding molecular orbital. The more easily the electronic excitation taking place, longer the wavelength that it can absorb. Usually the three types of transitions observed in UV Visible spectroscopy are Transitions involving s, p and n electrons, Transitions involving charge transfer electrons, Transitions involving 'd' and 'f' electrons. Characterization of specific functional groups can be possible. This method can be used in a quantitative way to determine the concnetration of absorbing species which is basd upon the Beer Lmbert Law. $A = \mathcal{E}Cl = \log_{10}(I/I_0)$ ; Where A is the measured absorbance, $\mathcal{E}$ is the molar absorption coefficient, l is the path length through the sample, $I_0$ is the intensity of incident light at a particular wavelength whereas I is the transmitted light intensity.

The instrumentation [Figure 11] includes, a light source, sample holder, Prism/diffraction grating to separate different wavelengths, detector unit. UV- Visible spectrophotometer can be single or double beam. In sigle beam configuration all the light passes through the sample compartment. In doble beam, the light is splitted in to two, one goes to sample and other to reference. The intensities of these beams are measured and compared. Samples are placed in cuvette which is transparent rectangular cell with internal width of 1cm. Commonly used detectors are photomultiplier tube or charge coupled device.
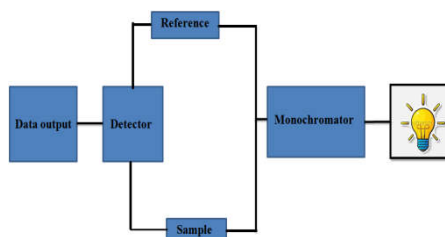
**Figure 11.** Block diagram for the measurement of Absorbance

In this studies, Jasco V-550 spectrophotometer served the purpose of recording the absorption spectrum of the samples in the wavelength range of 200-900 nm using double distilled water as the reference. The reported absorbance maxima were 663 nm for methylene blue dye, 267nm for 5-fluorouracil.

## 2.8.2 High performance Liquid Chromatograph

High performance liquid chromatograph is highly improved form of column liquid chromatography that can be used in both quantitative and qualitative analysis. It has stationary and mobile phases where stationary phase is usually packed with silica gel and the mobile phase with the help of a pump moves the mixture through the stationary phase for separation. HPLC instrument consists of a reservoir of mobile phase, pump, sample injector,column(Stationary phase), detector, data analyser. Here the separation is based on the partition of compounds towards stationary and mobile phase. Under specific pressures, the mobile phase brought in to the pump moved to column and the sample was injected just before colum in to the stream of mobile phase. The sample with greater affinity for mobile phase will detected first. Once the analyte reached the detector, the information is

translated into a chromatogram by the software. Typical diagram of an HPLC column chromatography has been represented in figure 12.
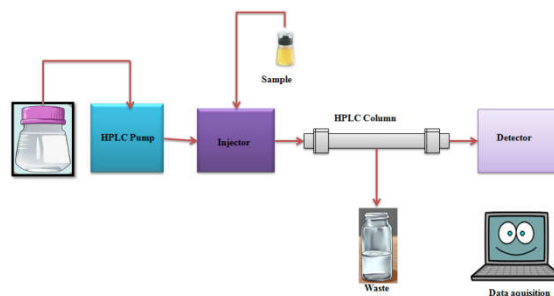


**Figure 12**. Schematic representation of HPLC Unit

## 2.8.3 Chemical Oxygen Demand Measurement (C.O.D)

The chemical oxygen demand test is a commonly adopted technique to measure the amount of organic matter present in water. COD determines the the quantity of Oxygen required to to oxidize the organic matter in samples under specific conditions[Temperature, time,oxidising agent]. It is usually expresses in mg/L indicating mass of oxygen consumed per liter of solution. Applicable range being 3 - 900 mg/L. The present study to determine the COD value, is done using a standard method (IS:3025 2006). It is based on the principle that organic matter in the sample is completely get oxidised by potassium dichromate in the presence of sulphuric acid, mercury sulphate and silver sulphate to produce $CO_2$ and $H_2O$. The amount of oxygen required to oxidise the organic matter in the sample is correlated to the amount of potassium dichromate consumed by the sample. The experimental procedure is given below.

Take three COD vials, two for sample and one for blank. Add 2.5 mL sample to the vials and to the third one, add distilled water. Add 1.5 mL of potassium dichromate solution, then 3.5 mL of sulfuric acid reagent to each of these vials and sealed them tightly. When the temperature and Time are set in the COD digester, place the vials in it for the program to start. When the machine is switched off, the vials are allowed to cool at room temperature. Transfer the contents of blank vial to a conical flask and add few drops of ferroin indicator and the solution becomes bluish green. It is titrated with ferrous ammonium sulfate solution [0.1N] taken in the burrete. End point is the apprearance of a reddish brown colour. The experiment is repeated with the sample solutions and the readings are noted.

COD value was calculated using the expression,

$$COD = \frac{(A-B) \times N \times 8 \times 1000}{V} \text{ where}$$

'A' and 'B' are the volume of ferrous ammonium sulphate for blank and water sample respectively

'N' the normality of ferrous ammonium sulphate  and

'V' the volume of the water sample used.

## 2.9    Applications of titanium dioxide nanostructures in photocatalytic and biological fields

## 2.9.1 Photocatalytic activity studies of titania based nanostructures

### 2.9.1.1 Photocatalytic activity study of synthesised nanostructures towards organic pollutant removal

The photocatalytic activity of the prepared systems was monitored by examining the degradation of an organic dye as a model pollutant. Here methylene blue is chosen as the target pollutant. The degradation studies were carried out in presence of UV lamp 98W ($\lambda$= 380nm) at room temperature in a Luzchem LZC 4X model photoreactor [Figure 13]. The chamber with uniform illuminator is a fan cooled housing set up that offers a temperature controlled, stable environment for the lamp. Continuous stirring is maintained throughout the reaction. All Catalyst dosage was kept as 0.25g/L. In a general procedure, the required amount of catalyst was added to 75 ml of 2.325 x $10^{-5}$ M solution of methylene blue dye. Prior to illumination, the solution was stirred for 30 minutes under dark in order to reach adsorption desorption equilibrium. The aqueous slurry was placed in the center of the reactor and exposed to UV radiation with continuous magnetic stirring. At regular intervals of time (5minutes), the suspension collected was centrifuged at 8,000 rpm for 10 minutes to remove the catalyst particles. The clear solution was analyzed for methylene blue content by measuring the absorbance at 664 nm using a

UV-Visible spectrophotometer. The photocatalytic degradation percentage was calculated using the equation [27].

$$\text{Percentage Degradation} = \frac{(C_\circ\text{-C})}{C_0} \times 100$$

Where 'C$_0$' is the initial concentration of the dye solution and 'C' is the concentration after a definite time 't'.



**Figure 13.** Photograph of Luzchem LZC 4X model photoreactor

Determination of hydroxyl radicals on the surface was performed by fluorescence technique using terephthalic acid. Terephthalic acid reacts with hydroxyl radical generating 2-hydroxy terephthalic acid which is highly fluorescent. The intensity of the peak is directly proportional to the formed hydroxy radicals. 0.0375g of the sample was added to 150 mL terephthalic acid solution ($5\times10^{-4}$M in a diluted NaOH aqueous solution with a concentration of $2\times10^{-3}$ M) followed by UV irradiation. The solution was measured in a fluorescence spectrometer.

2-hydroxy terephthalic acid gave a peak at the wavelength of about 425 nm by the excitation with the wavelength of 315 nm [28].

## 2.9.1.2 Photocatalytic Antimicrobial activity of titania nanostructures

### 2.9.1.2a Antibacterial activity studies

The E. coli were cultured in 5 ml Luria Bertani (LB) broth at 37 °C for 12–16 h in a rotary shaker incubator at 200 rpm. 10 ml of the culture was washed with a 0.9% saline solution by centrifugation (12000 rpm for 15 minutes). After discarding the supernatant, the cells were suspended in 10 ml normal saline. Serial dilution of the suspension give the proper concentration that is number of colonies forming unit/ml (cfu/ml)

Stock $TiO_2$ suspension prepared just before the photocatalytic reaction is used for the experiment. A required amount of the photocatalyst was mixed with 9 ml 0.9% saline solution in a reagent bottle. After sterilization by autoclaving; it was mixed with 1ml of the prepared cell suspension. The $TiO_2$ –Bacteria slurry was stirred with a magnetic stirrer.The sample was illuminated with one 100 W black light bulbs from above. Suspension with no photocatalyst was treated as a control, and the reaction mixture with no light irradiation was used as a dark control. 1mLof the sample after irradiation, was spread on petridish contained nutrient agar and incubated at 37 °C for 24 hours. After the incubation period, the number of viable colonies was counted manually and after multiplication with the dilution factor the results were expressed as mean colony forming units (CFU) per ml. The

counts on the three plates corresponding to a particular sample were averaged.

Anti bacterial efficiency (in percent) was reported using the equation,

$$\frac{(C_0 - C)}{C_0} \times 100$$

where $C_0$ and C are the number of colonies formed before and after irradiation.

### 2.9.1.2b Antifungal activity studies

The antibacterial and antifungal activities were carried out by measuring the optical density (OD) at 600 nm.

### i)      Preparation of fungal culture

Using aseptic techniques a single colony was transferred into a 10 ml of potato dextrose broth, capped and placed in incubator overnight at 37°C. After 24hrs of incubation, using aseptic preparation and with the aid of a centrifuge, a clean sample of Fungus was prepared. The broth was spun down using a centrifuge set at 5000 rpm for 5 min with appropriate aseptic precautions. The supernatant was collected and used as fungal suspension.

### ii)      Preparation of the microtiter plate plates

Plates were prepared under aseptic conditions. A sterile 96 well plate was labeled. A volume of 20 µl, 40µl, 60 µl, 80µl and 100µl solution of test material was pipetted into the wells. 100 µl of potato dextrose broth was added to each well. Finally, 100 µl of fungal suspension was

added to each well. Plate was wrapped loosely with cling film to ensure that fungus did not become dehydrated. Each plate had a set of controls: a column with all solutions with the exception of the test compound, and a column with all solutions with the exception of the fungal solution adding 100 µl of potato dextrose broth instead. The plates were incubated at $37^\circ$C for 24 hours and OD reading was taken (OD600) after sufficient incubation.

Optical density of the samples was measured using ELISA multiplate reader at wavelength of 600 nm.

The % growth inhibition of bacteria was evaluated from the OD values of the control and the test compound using the equation; $\% \, I = \frac{OD_{cont} - OD_{test}}{OD_{cont}} \times 100$ , where $OD_{cont}$ is the optical density of the control and $OD_{test}$ is the optical density of the test compound.

### 2.9.1.3 Photocatalytic water splitting reactions

The activity of the materials towards photocatalytic reduction of water was examined using methanol as a hole scavenger, which serves as sacrificial reagent. Photogenerated holes irreversibly oxidize methanol instead of water therefore no oxygen evolved as a result of oxidation of water. Irradiation is done with a medium pressure mercury lamp (Hg, Ace Glass Inc., 450W) in a closed rectangular quartz cell having both sampling and evacuation ports. The irradiated catalysts were placed in an outer irradiation quartz cell with the lamp which is surrounded with water circulation jacket to absorb IR radiation [typical outer reaction assembly in horizonatal geometry is represented in figure 14. The lamp

produces wide range emission spectra with maxima at both UV and visible range [16% UV -84% visible region]. The catalytic activity experiments were conducted in static mode with water in methanol (2:1 v/v %) mixture, with well dispersed catalyst. The reaction products were analyzed with an interval of 2 hr over the period of 6 hrs. A gas chromatogram (Netel (Michro-1100), India) equipped with a thermal conductivity detector (TCD) and a molecular sieve column (4m length) with argon as the carrier gas was employed in the isothermal temperature mode (50°C).
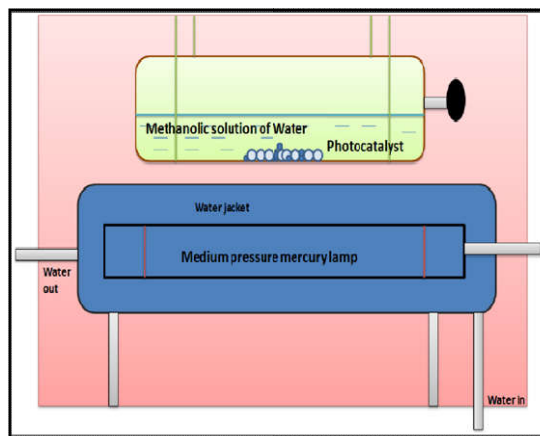


**Figure 14**. The typical outer irradiation reaction assembly in horizontal geometry kept inside a housing equipped with reflectors with water-cooled medium pressure mercury vapour lamp (Hg, Ace Glass Inc., 450W) as light supply.

**Measurement of light intensity (Flux)**

Silicon diode based light meter LX 1108; Lutron Electronic measures the flux of medium pressure mercury lamp. The number of photons

falling on the reaction cell or flux of medium pressure mercury lamp was determined to be $19 \times 10^4$ lx or 278.2 $Wm^{-2}$ in horizontal geometry irradiation of UV-Visible photoirradiator.

## 2.9.2 Biological Applications of Titania nanostructures

At cell culture level, prepared systems are evaluated for their efficiency for this cytotoxicity studies, apoptosis, cell cycle analysis were conducted.

### 2.9.2.1 Cytotoxicity study in Daltons lymphoma ascites (DLA)

The prepared anticancer drug loaded Titania nanostructures were investigated for preliminary cytotoxicity effect by taking cancer model cells (DLA) from tumor bearing mice using Trypan blue exclusion method. Here the plasma isolated from blood of tumor bearing mice was subjected to cytotoxic analysis. In vitro cytotoxic study was carried out using tumor model cells excluded from cancer bearing mice. The drug damages the cell by making small pores on the cell membrane and through the pores trypan blue dye enters into the cell. The dead cells can be distinguished from the live cells from the color developed by the dead cells. Live cells are colorless.

Materials used for the study are Daltons lymphoma ascites (DLA) bearing mice, phosphate buffered saline (PBS) of pH 7.4, distilled water, trypan blue in 1% saline and haemocytometer (Rohan India Pvt. Ltd), drug loaded nanostructures well dispersed in DI water by sonication (10mg/mL).

DLA tumor cells were aspirated from the peritoneal cavity of tumor bearing mice and the excluded cells were washed thrice with phosphate buffered saline (PBS) and normal saline. The viability of the cells was checked using trypan blue (cell viability should be above 98%) then the solution were diluted using PBS solution. A haemocytometer was used to count the number of cells in the diluted sample and the cell number was adjusted to $1 \times 10^7$ cells/mL. The experiment was set up by adding different concentrations of drug loaded Titania nanostructures with $1 \times 10^7$ cells/mL. The final volume of the assay mixture was made up to 1mL using PBS and was incubated at $37^o$C for about 3 hours. 100 microliter of trypan blue was added after incubation and the number of dead cells was counted. The dead cells are blue in color. The number of stained and unstained cells was counted separately. The % cytotoxicity of the drug is calculated using the following expression.

$$\% \text{ Cytotoxicity} = \frac{\text{Number of dead cells}}{\text{Number of live cells} + \text{Number of dead cells}} \times 100$$

## 2.9.2.2 Cell culture and maintenance

Human breast cancer MCF-7cell lines were procured from National Centre for Cell Science (Pune, India). The cells were maintained in Dulbecco's Modified Eagles medium supplemented with 10% FBS, 2 mM l-glutamine and Earle's BSS adjusted to contain 1.5 g/L Na bicarbonate, 0.1 mM nonessential amino acids, and 1.0 mM of Na pyruate in a humidified atmosphere containing 5% $CO_2$ at 37 $^{\circ}$C. The media were changed every two days, and the cells were passaged by trypsinization before confluence.

## 2.9.2.3 In vitro cytotoxicity

Cell viability was determined by MTT ((3-(4,5-dimethylthiazole-2-yl)-2,5-diphenyltetrazoliumbromide) assay. The mitochondrial dehydrogenases in living cells reduce MTT to a blue-magenta colored formazan crystals. The absorption of dissolved formazan in the visible region associated with the number of intact alive cells. Cytotoxic additives have the ability to damage and destroy cells, and consequently diminish the reduction of MTT to formazan The MCF-7cells in the log phase were seeded in 96-well plates at a concentration of 1.0 x $10^4$cells/well and incubated overnight at 37 °C in 5% $CO_2$ humidified environment. The cells were then treated with different concentrations of the nanomaterials (dissolved with RPMI medium1640), respectively. Controls were also cultivated under same conditions without the addition of test compound. The treated cells were incubated for 24 h and then subjected for MTT assay. The stock concentration (5 mg/mL) of MTT-(3-(4, 5-dimethylthiazol-2-yl)-2,5-diphenyltetrazolium bromide) was prepared and 100 µL of MTT was added in each treated wells and incubated for 4h. Purple coloured formazan crystals were observed and these crystals were dissolved in 100 µL of dimethyl sulphoxide (DMSO), and read at 620 nm in a multiwell ELISA plate reader (Thermo Multiskan EX, USA).

The OD value was used to calculate the percentage of viability using the following formula,

$$\% \text{ of Cell viability} =$$

$$\left[\text{Mean OD Value of experimental sample}\right] \Big/ \left[\text{Mean OD Value of experimental }_{\text{control}}\right] \times 100$$

## 2.9.2.4 Morphological study

The MCF-7 cell lines were grown on coverslips ($1\times10^5$ cells/ cover slip) and was incubated with the nanoparticle suspension at $IC_{25}$ and $IC_{50}$ concentrations.They were fixed with methanol and acetic acid solutions in the ratio of 3:1 (V/V). Smoothly, the cover slips were mounted on glass slide for analysis of the morphology. Morphological changes of MCF-7 cells were analyzed under a Nikon (Japan) bright field inverted light microscope at 40x magnification.

## 2.9.2.5 AO/EtBr staining assay

MCF-7 cells were seeded in a 6-well plate at a density of $1\times10^5$ cells per well and grown for 24 h. The culture media were removed and the cells were treated with $IC_{25}$, $IC_{50}$ concentrations of nanomaterials and untreated cells were used as a control. After 48 h post-transfection, the morphology of cells was monitored under a fluorescence microscope (Olympus  IX51, Japan). Apoptosis studies were performed with a staining method utilizing acridine orange (AO) and ethidium bromide (EtBr). Each cell culture was stained with AO/EB solution (100 µg/ml AO, 100µg/mL EtBr). Samples were observed under a fluorescence microscope. Several fields, randomly chosen, were digitalized and at least 600–800 nuclei for each sample were counted and scored. Results are expressed as the relative percentages of viable and apoptotic cells to the total number of cells scored.

## 2.9.2.6 DAPI (4', 6-diamidino-2-phenylindole, dihydrochloride) Staining

For visuaisation of MCF-7 Cells, the nuclei of the cells were stained with DAPI. DAPI (4',6-diamidino-2-phenylindole) is a fluorescent stain that binds strongly to A-T rich regions in DNA (Figure 15). The treated cells at the concentrations corresponding to $IC_{25}$ and $IC_{50}$ values were taken fixed with methanol : acetic acid (3:1 v/v) before washing with PBS 7.4. The washed cells were mixed with 1mg/mL of DAPI for 20 minutes in dark and stained images were recorded with a fluorescent microscope (Nikon Eclipse, Inc., Japan) at 400× magnification with excitation filter at 510–590 nm.
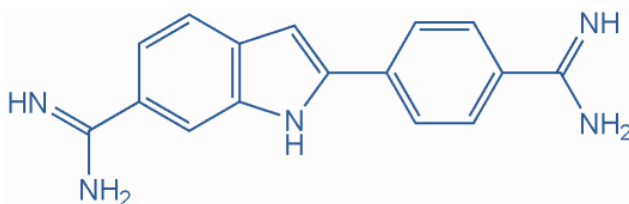


**Figure 15. DAPI (**4',6-diamidino-2-phenylindole**) molecule**

## 2.9.2.7 Analysis of mitochondrial membrane potential ($\Delta\Psi$m) - Rhodamine 123 staining

MCF-7 cell lines were seeded in 6 well plates ($1 \times 10^5$ cells per well) and allowed to grow for a day. Then nanoparticle suspension was added at its $IC_{25}$, $IC_{50}$ concentrations. After 24hours, cells were fixed in 4% paraformaldehyde and washed with PBS twice. Then the cells were exposed to Rhodamine 123 (Rh-123) stain (10 µg/mL) at $37^{\circ}C$ for 30 minutes. The excess stain was washed two times with methanol then with PBS and analyzed for changes in $\Delta\Psi$m using fluorescence microscope with an excitation and emission wavelengths of 505 nm and 534 nm, respectively.

### 2.9.2.8 Comet Assay

The alkaline comet assay (Single Cell Gel Electrophoresis—SCGE) briefly, $1 \times 10^5$ MCF-7 cells/well were seeded in a six-well plate and is grown overnight. The cells were then treated with different concentrations ($IC_{25}$ and $IC_{50}$) of test solution for 24 h. Then the cells were trypsinized and resuspended in cold PBS. 15 µl of cell suspension was mixed with 100 µl of low melting agarose(0.75% , 37 °C) and spread on a frosted glass slide pre- cleaned and pre-coated with a 150 µL layer of normal melting agarose (1.5%). After solidification, it was covered with a third layer of 100 µl of low melting agarose (0.75%), it was covered with coverslip and allowed to solidify on ice for 20 min. Then the coverslip was removed and the slide was immersed in freshly prepared ice-cold lysis solution (10 mM Tris pH 10, 2.5 M NaCl, 100 mM Na2EDTA, with 10% DMSO and 1% Triton X-100 added just

before use) for 2 h at 4 °C. After lysis treatment, slides were kept in an alkaline electrophoresis buffer (300 mM NaOH, 1 mM EDTA, pH > 13) for 20 min in a horizontal gel electrophoresis unit for DNA unwinding and conversion of alkali-labile sites to single-strand breaks. Electrophoresis was carried out for 20 min with an electric field of 25 V and adjusting the current to 300 mA. The slides were neutralized gently with 0.4 M Tris buffer at pH 7.5. All the synthesis steps were conducted in the dark in order to prevent additional DNA damage. Each slide was stained with 75 µl of 20 µg/ml ethidium bromide solution for 3 min. The slides were analyzed under 40× objective lens (excitation wavelength of 515–560 nm and emission wavelength of 590 nm) in a compound fluorescence microscope.

### 2.9.2.9 DNA fragmentation analysis

Cells were treated with $IC_{25}$ and $IC_{50}$ concentrations based on MTT assay results. The cells were pelleted by centrifugation at $1000 \times g$ for 5 min at room temperature. Aliquots from cells were resuspended in 500 µl of digestion buffer (5 mM EDTA, pH 8.0, 20 mM Tris, 0.5% SDS) containing 100 g/ml proteinase K and RNAse followed by incubation at $37°C$ for 3 h and analyzed on 1.5% agarose gel.

### 2.9.2.10 Annexin V-FITC/PI staining

After seeding $5 \times 10^5$ cells/well to a 6-well plate, the cells was pretreated with Titania based system, at $IC_{25}$ and $IC_{50}$ concentrations. The treated cells were suspended in 200 µL of binding buffer, and the suspension was added with 10 µL of Annexin V-FITC and 5 µL of PI followed by incubation for 15 min in the dark at room temperature.

Subsequently, 300 µL of binding buffer was added to the cell suspension and the cells were analyzed by a flow cytometer (BD, FACS Calibur, USA). Cells undergoing early apoptosis bind only to Annexin V/FITC, whereas cells that are either in the late stages of apoptosis or already dead bind to both Annexin V/FITC, and PI and the data were analyzed with FCS Express V3.

### 2.9.2.12 Western blot analysis

Western blotting was performed to detect the regulation of apoptotic and anti-apoptotic proteins in treated cells. The MCF-7 cells ($1 \times 10^6$) were seeded onto 100-mm culture dishes with test solutions for 48 h. The medium was removed Cells were washed with ice-cold PBS two times and incubated in lysis buffer (0.1 ml lysis buffer/each plate). The lysates were centrifuged at $10,000 \times g$ for 5 min at $4^0C$, and were used as the cell protein extracts. The harvested protein concentration was measured using a protein assay kit (Bio-Rad). Each of the extracts was applied to 12% SDS polyacrylamide gel electrophoresis followed by transfer of proteins on to a nitrocellulose membrane, and then blocked for 1 h using 10% skim milk in water. After washing in a PBS containing 0.1% Tween 20 for 3 times, the primary antibodies were added at a v/v ratio of 1:1000. After overnight incubation at 4°C, the primary antibodies were washed away and the secondary antibodies were added for 1 h incubation at room temperature. Finally, the enhanced chemiluminescence detection reagents were used to develop the signal of the membrane.

## 2.9.2.13 The measurement of intracellular ROS formation

It is based on the oxidative conversion of 2' ,7' -dichlorofluorescein-diacetate (DCFH-DA) to fluorescent dichloro flouorescin (DCF). After seeding of $5 \times 10^5$ cells/well to a 6-well plate, the cells were treated with nanomaterials for 24 h at $IC_{25}$ and $IC_{50}$. Subsequently, cells were washed once with ice-cold PBS and incubated with DCFH-DA (50 μM final concentration) at 37 °C for 30 min in the dark. Then, the cells were washed twice and maintained in 1mL of PBS. DCFH-DA was taken up by the cells and deacetylated by cellular esterase to form a non-fluorescent product DCFH, which was converted to a green fluorescent product DCF by intracellular ROS produced by treated MCF cells. The fluorescence intensity of DCF is proportional to the amount of ROS produced by the cells. ROS generation was assessed using a fluorescence microscope (Nikon Eclipse, Inc., Japan) at excitation and emission wavelengths of 488 and 530 nm, respectively, and the mean fluorescence intensity of DCF was evaluated.

# References

1. C.W. Oatley, W.C. Nixon, R.F.W Pease, Scanning electron microscopy. Adv Electronics Electron Phys 21, 1965, 181–247.

2. *D. McMullan, "Scanning electron microscopy 1928–1965". Scanning, 2006, 17 (3): 175–185.*

3. Z. L. Wang, Reflected Electron Microscopy and Spectroscopy for Surface Analysis, Cambridge University Press, Cambridge, Newyork, 1996, ISBN: 0-521-48266-6456.

4. D. Sarid, Scanning Force Microscopy with Applications to Electric, Magnetic and Atomic forces, Oxford University Press, New York ,1991.

5. C. Kisielowski; B. Freitag; M. Bischoff; H. van Lin; S. Lazar; G. Knippels; P. Tiemeijer; M. van der Stam; S. von Harrach; M. Stekelenburg; M. Haider; H. Muller; P. Hartel; B. Kabius; D. Miller; I. Petrov; E. Olson; T. Donchev; E. A. Kenik; A. Lupini; J. Bentley; S. Pennycook; A. M. Minor; A. K. Schmid; T. Duden; V. Radmilovic; Q. Ramasse; R. Erni; M. Watanabe; E. Stach; P. Denes; U. Dahmen "Detection of single atoms and buried defects in three dimensions by aberration-corrected electron microscopy with 0.5 Å information limit". Microscopy and Microanalysis., 2008, 14, 469–477.

6. D.B. Williams, C.B. Carter, Transmission Electron Microscopy: A Textbook For Materials Science. New York, USA: Springer, 2009, p. 35, ISBN 978-0-387-76500-6.

7. P. Griffiths, J.A. de Hasseth, Fourier Transform Infrared Spectrometry (2nd ed.). Wiley-Blackwell., 2007, ISBN 0-471-19404-2.

8. S.G. Podorov, N.N. Faleev, K.M. Pavlov, D.M. Paganin, S.A. Stepanov, and E. Forster, A new approach to wide-angle dynamical X-ray diffraction by deformed crystals" J. Appl. Crystallogr., v.39, 2006.

9. B.C. Lippens, J.H. de Boer, J. Catal. , 1965, 4 , 319.

10. O. Glatter, O. Kratky, eds. Small Angle X-ray Scattering. Academic Press., 1982, ISBN 0-12-286280-5.

11. S. J. Gregg, K. S. W. Sing, Adsorption, Surface Area and Porosity, Academic Press, London etc., 1982.

12.  I. Langmuir, J. Am. Chem. Soc. 1918, 40, 1361.

13.  S. Brunauer, P.H. Emmett, E. Teller, J. Am. Chem. Soc. , 1938, 60, 309.

14.  G. Horvath, K. Kawazoe, J. Chem. Eng. Jpn. , 1983, 16, 470.

15.  E.P. Barrett, L.G. Joyner, P.P. Halenda, J. Am. Chem. Soc. 1951, 73, 373 .

16.  F. Rouquerol, J.Rouquerol , K.Sing ,Adsorption by powders and porous solids; Academic Press:  San Diego, WILEY-VCH, 1999, ISBN 0-12-598920-2.

17.  IUPAC Recommendations Pure Appl..Chem1985, 57,603

18.  Recommendations Pure Appl IUPAC.Chem. 1994, 66,1739.

19.  Z. Bian, J. Zhu, F. Cao, Y. Lu and H. Li, Chem. Commun., 2009,0, 3789

20.  P. Kubelka, F. Munk, Z. Tech. Phys. 12, 1931, 593.

21.  W. N. Delgass, G. L. Haller, R. Kellerman, J. H. Lunsford, Spectroscopy in Heterogeneous Catalysis; Academic Press; New York,1979; p.86.

22.  D.A. Skoog, F.J. Holler, S.R. Crouch  Principles   of   instrumental analysis (6th ed.), Cengage  Learning,Brooks Cole , 2006, ISBN-13: 978-0495012016.

23.   C.V. Raman, K.S. Krishnan A new type of secondary radiation Nature, 1928, 121, 1928, pp. 501-502.

24.  IUPAC, Compendium of Chemical Terminology, 2nd ed. (the "Gold Book") (1997). Online corrected version: (2006–) "photochemistry.

25.   H.J. Kimble, M. Dagenais and L. Mandel, "Photon Antibunching in Resonance Fluorescence", 1977, Phys. Rev. Lett. 39, 691.

26.  J. F. Moulder, W. F. Stickle, P. E. Sobol and K. Bomben, Handbook of X-ray Photoelectron Spectroscopy, Perkin-Elmer Corporation, Physical Electronics Inc., Eden Prairie, USA (1992).

27.  K. Wang, L. Yu, S. Yin, H. Li, Pure Appl. Chem., 2009, 81, 2327.

28.  K. Ishibashi, A. Fujishima, T.Watanabe and K. Hashimoto, Electrochem. Commun. 2000, 2 ,207.

# CHAPTER III
# CHARACTERIZATION OF TITANIA NANOSTRUCTURES

**CONTENTS**

*The world of catalysis is incomplete without proper characterization of systems.The charcterization techniques used suitable agents (electrons light etc;) and the data obtained are processed with appropriate softwares on computer. We can get exact picture about its surface nature size, shape, crystallinity and the possible mechanisms taking place on their surface by gathering these informations. In the present study, different nanostructures of titanium dioxide have been fabricated by various synthesis procedures and the systems are well characterized by X-ray diffraction analysis (XRD, Small angle and Wide angle) Fourier transform infrared spectroscopy (FTIR), electron microscopic techniques; scanning electron microscopy (SEM), Field emission gun scanning electron microscopy (FE-SEM), Transmission electron microscopy (TEM), High resolution transmission electron microscopy (HRTEM), Diffuse reflectance UV spectroscopy (UV-DRS), BET surface area analysis, Raman spectroscopy and Dynamic light scattering analysis.*

The result of various characterisation studies are described in the following sections and the nature of physicochemical characteristics are explained.

## 3.1 Multishelled titania hollow nanostructures [MHS]

The material was synthesised via solvothermal route. The details of synthesis procedure are provided in section 2.3.1. The results of various characterisation techniques are displayed below.

### 3.1.1. Electron Microscopy images

Figure 1 shows the electron microscopy images of the sample achieved via solvotherml reaction for 7 hours. The texture indicated that the surface is composed of aggregation of primary nanoparticles of 4-5 nm in size (Figure 1a). Further investigation of a single sphere is done by high magnification TEM image (Figure 1b), which indicated spheroid geometry of the particle. The clear contrast between different regions is easily recognized, which confirms the multi walled hollow nature of these spheroid structures. A 5-shelled nanostructure is presumed from the image. Another characteristic feature is that even though the thickness is not uniform, the thickness of the shells increases as moving from outer region to interiors. The selected area electron diffraction (SAED) pattern of solvothermally prepared mutishelled system is presented in Figure 1c. Sharp isolated diffraction spots in the pattern revealed the single crystalline nature of the synthesized sample. It is established that when compared to a polycrystalline

material, the single-crystalline nano architectures have improved stability and may give rise to specific applications in advanced fields. Single crystalline nature wipes away the limitations of either polycrystalline /amorphous materials such as poor crystal quality, insufficient close contact between the units etc. To date reports on achieving this type of single crystalline multishelled titania adopting a template free approach is nil, which is projected as the major highlight of this report. This unique shell structure of hollow $TiO_2$ structure is quite different from those of the conventional $TiO_2$ sphere with smooth surface and can greatly contribute to their photocatalytic activity [1]. An over view of the product in the HR-TEM shows the coexistence of 3, 5 shelled hollow structures (Figure 2)
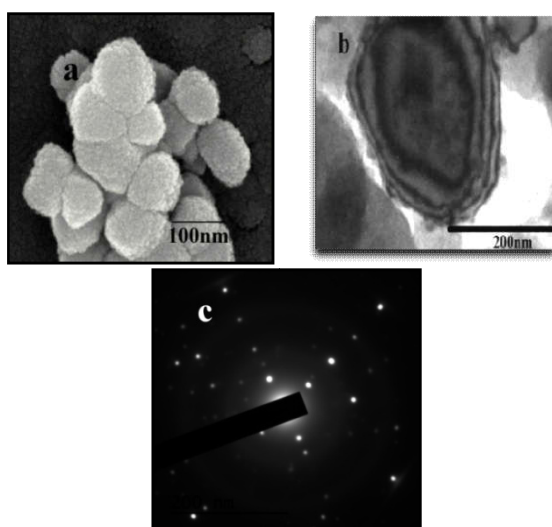


**Figure 1**. (a) FE-SEM image; (b) HR-TEM Image (c) SAED Pattern of five shelled titania structure
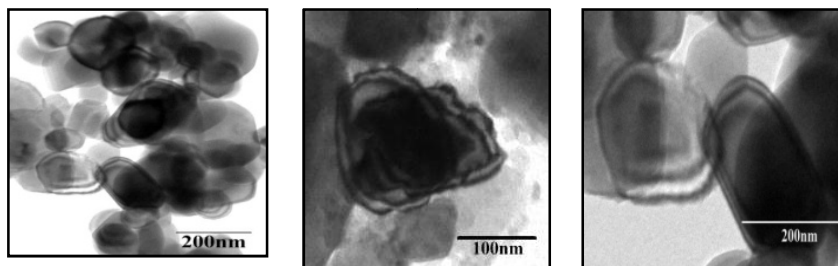
**Figure 2.** An over view of the various multishelled nano spheroids prepared in 7 hours of reaction time as observed in the TEM.

## 3.1.2 Dynamic Light Scattering Analysis

The particle size distribution curve of MHS (figure 3) shows uniform distribution of particles with mean size of 278.2 nm. The measured size is much larger than that measured by TEM. This is ascribed to the fact that this technique measures large aggregate size which are formed by many single $TiO_2$ nanoparticles where as TEM measures a single $TiO_2$ nanoparticle. [2-3]. The Zeta potential value of MHS was found to be − 44.6 mV. It was known that the zeta potential of nanoparticles higher than ± 30mV implies good stability, as this high potential leads to electrostatic repulsion between the nanoparticles [4].The poly dispersity index was 0.279. Practically PDI value should be less than 0.5. PDI is an indicator of aggregation in the particles. A value of PDI closer to zero denotes the monodisperse system. A higher value shows a polydisperse system. Polydisperse systems have greater tendency for aggregation than monodisperse system.
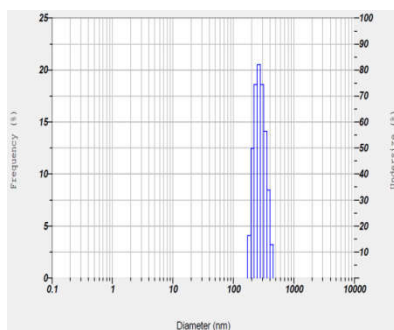
**Figure 3**. Particle size distribution curve of MHS

### 3. 1. 3 X-ray diffraction studies

Further crystallinity and the phase structure of the prepared hollow structures are revealed by XRD study. The X-Ray diffraction pattern indicates highly crystalline nature of the material as indicated by the narrow peaks (Figure 4a). As shown in the figure , major peaks appearing at 2θ values $25.3^\circ$,$37.8^\circ$, and $48.0^\circ$ can be indexed to the characteristic peaks of Anatase $TiO_2$ (JCPDS No. 21-1272, Tetragonal; space group: I41/ *amd* (141)). The peaks corresponds to (101), (004), (200) anatase titania planes. No impurity diffraction peaks were detected. Figure 4b represents the XRD pattern of the solvothermally synthesized sample calcined at different temperatures. With increase in temperature, the intensities of the diffraction peaks also increase indicating the increased order in crystal growth. Absence of diffraction peaks of other phases of titania like rutile, brookite etc., confirms that it maintains the anatase phase even up to $600^\circ$C. The chemical composition of

titania phase and purity are further examined and confirmed by EDX analysis (Figure 4c), which revealed the presence of Titanium metal only.



**(a)**                    **(b)**                    **(c)**
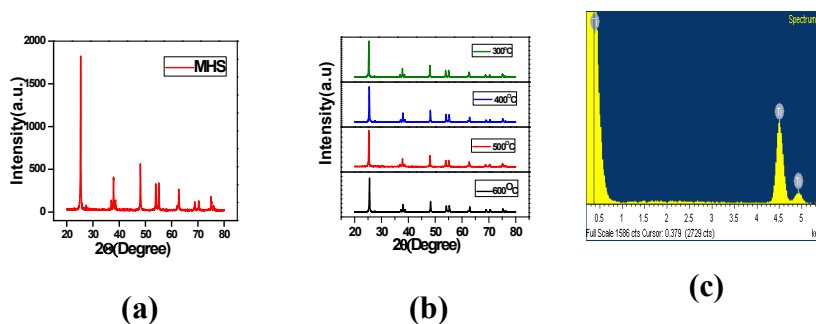
**Figure 4**. X-ray diffraction pattern of the sample (a); XRD pattern of the sample calcined at different temperatures (b); EDX pattern

### 3.1.4   Raman spectroscopy

It is a useful technique to investigate the various phases of titania. Raman spectrum of multishelled titania hollow nanospheroids is represented in figure 5. The peaks around 144 cm$^{-1}$($E_{g(1)}$ mode), 197 cm$^{-1}$($E_{g(2)}$ mode), 397 cm$^{-1}$($B_{1g(1)}$ mode), 514 cm$^{-1}$($A_{1g}$ mode) and 638 cm$^{-1}$($E_{g(3)}$ mode) are characteristic peaks of Anatase. Absence of any other peaks confirms the purity of anatase phase and is in accordance with XRD analysis.
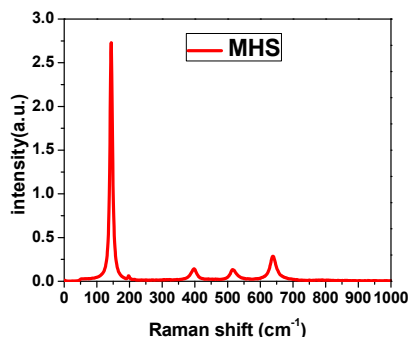
**Figure 5.** Raman spectrum of MHS

### 3.1.5   Fourier Transform Infra Red Spectroscopy

The FTIR spectra (Figure 6) of the uncalcined sample showed strongest absorption in the range 500-900 cm$^{-1}$ confirming the presence of metal oxide. Band noticed at 1631 cm$^{-1}$ is due to the bending vibrations of water molecules and the one at 3437 cm$^{-1}$ is due to the symmetric and asymmetric stretching vibarations of the –OH group of adsorbed water molecules [5]. IR band at 1000-1300 cm$^{-1}$ is due to C-O-C vibrations, which indicates the presence of adhered organic species, preferably an ether, in the uncalcined sample. It is of course noteworthy that there were no such ether linkages in the precursor as well as in reagents. It can be concluded from the IR data that there is existence of small amount of organics, water and hydroxyl groups on the surface of hollow structure.
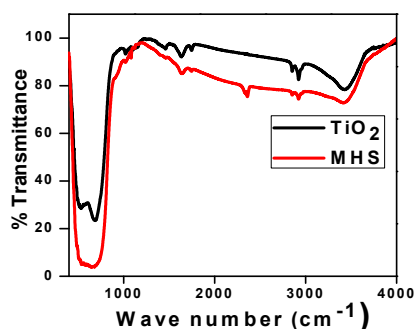
**Figure 6**. FTIR Spectra of TiO$_2$ powder precursor and the multishelled hollow system

### 3.1.6 Diffuse reflectance UV spectroscopy

Further characterisation of the sample is done by measuring the optical absorption property of the system using UV-visible reflectance spactroscopy. Figure 7a represents UV-Visible absorption spectrum of multiwalled structure. The system exhibited broad absorption maximum in the UV region. The band gap energy of the samples has been determined from the reflectance [F(R)] spectra using the KM (Kubelka–Munk) formalism and the Taucplot.

For a semiconductor material, a plot of [F(R).h$\nu$]$^n$ against h$\nu$ should show a linear region just above the optical absorption edge for n=½ if the band gap is a direct transition, or for n= 2 if it is indirect [6-7]. Over the linear region of the plots, the relationship can be described as

$$[F(R) \, h\nu]^{1/2} = K(h\nu - E_g) \quad (1)$$

Where hv is the photon energy, $E_g$ is the band gap energy, and K is a constant characteristic of the semiconductor material. The extrapolation of a Tauc plot (Figure 7b.) to the X-axis should yield the band gap energy which assigns an indirect band gap 3.22 eV for the material.
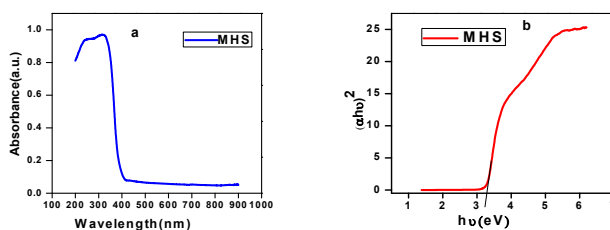


**Figure 7.** UV-Visible absorbance spectrum (a) and corresponding Kubelka-Munk (b) plot of MHS

## 3.1.7 Nitrogen adsorption- desorption study and BET- Surface area Analysis

Nitrogen adsorption-desorption isotherm of the multishelled spheroids and the corresponding Barret-Joyner-Halenda (BJH) pore distribution profile are shown in figures 8. According to Brunaur-Deming-Deming- Teller (BDDT) classification, the adsorption isotherm is of Type IV with two capillary condensations [Figure 8, Left]. Adsorption isotherm in the relative pressure range from 0.1-0.88; indicates low affinity for nitrogen adsorption and the presence of micropores in the material. Two hysteresis loops were observed at relative pressure between 0.8-1. It is easily presumed that these hysteresis loops differ in shape. In the relative pressure range 0.88-

0.92, $H_2$ type hysteresis loop is observed, which signifies ink bottle type pores in the material. At the highest relative pressure values, vis., between 0.92-1, the observed hysteresis loop is of type H3, suggesting the existence of slit like pores [5-10]. The area of first hysteresis loop is significantly smaller compared to the other, implying that ink bottle type pores are limited in the system. Corresponding pore size distributions is depicted in Figure 8 (Right). As indicated by the system, the sample contained micropores (< 2 nm), small meso pores (peak pore at ca.3.5nm) and large meso pores (3.9-31.2nm). The formation of porous structure is attributed to the aggregation of nanoparticles within the shell wall of individual nanostructures, thus confirming the existence of multilength scaled porous structures within the sample. The micro/ mesoporous structures are advantageous on many fields as they enhance the adsorption efficiency of adsorbate molecules and their flow rates [11].



(a)                                              (b)
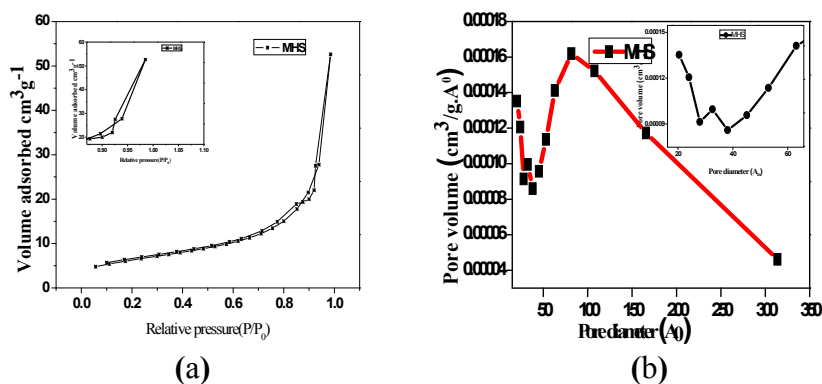
**Figure 8.** Nitrogen adsorption desorption isotherm (Left) and the pore size distribution curve (Right) of MHS

As determined by the nitrogen adsorption desorption experiments, BET surface area of the multi shelled nanostructure is obtained to be 22.33 $m^2$/g and the pore volume is 0.081$cm^3$/g. Both the surface area and pore volume are increased when compared to the starting precursor material ($TiO_2$ powder) which was10.17 $m^2$/g and 0.0394 $cm^3$/g respectively. It is clear the surface area value is almost doubled upon solvothermal processing, confirming the morphological change.

### 3.1.8 Morphology evolution and mechanism of formation of multishelled hollow spheroids

In order to understand the growth of these complex architectures, in-depth study is conducted by tuning the solvothermal reaction time which gives detailed awareness on the growth mechanism and morphology evolution of this mutishelled hollow nanospheroids. Insights in to the formation mechanisms were achieved by carrying out the reaction at time intervals 1, 2.5, 5, 6, 7, 9, 11, 13, and 14 hours. All other reaction parameters were kept constant and the resultant products at different reaction time duration were analyzed by transmission electron microscopy, so as to analyze the morphology transition at each stage.

Figure 9a represents the TEM image of solid nanosphere obtained after the solvothermal reaction for about 1 hour. The obtained particle is a hard one of size ~ 40 nm, as indicated by the image. Figure 9b shows the TEM image of the product after 2.5 hours of reaction time. Aggregation of small

particles of 5 nm on the exterior part of the solid sphere is evident in the image. On close observation we could see that the inner portion of this sphere has become lighter compared to the former hard one, which is obtained in the previous step. We assume that the nano particles found on the surface might have come out of the interior of hard sphere, thus constituting a transition stage during the evacuation of inner solid core. Its electron diffraction pattern (inset in Figure 9 b) revealed the polycrystalline nature of the sample. Figure 9c represents the TEM image obtained at 5 hours of reaction which indicated a yolk shelled structure for titania. Clear distinction between the comparatively thick walls and the inner hollow part can be made. The diameter of the structure has increased to about 170-175 nm. A multishelled nanostructure is obtained in the TEM image after 6 hours of solvothermal reaction [Figure 9d]. It was noticed that the core has diminished in size when compared to the yolk shell structure, and a gradual increase in diameter of the particle was observed. Besides, an increase in thickness of the shell wall is also observed as moving from outer to the interior region of the structure. The particle size of mutishelled spheroid after 7 hours of solvothermal reaction is about 180-200nm (Figure 9e). Shell number up to five is confirmed by this image. It is evident that the particle size increases in each stage implying that the shell growth occurs on the surface. The surface of these multi walled nano spheroid is composed of large number of aggregated nano particles which gave them a porous nature. This is in accordance with the FEG-SEM image shown in Figure 1a. There are different types of

pores within the system. Primary crystallites aggregates to form structures having intra aggregated pores between them. The inter aggregations of these porous structures resulted in larger inter aggregated nanostructures. The connections of these porous nanostructures are supposed to be formed by the condensation reactions of the hydroxyl groups on the surface of adjacent members. Profusion of of Ti-OH groups on the surface of titania promotes two adjacent titania particles to dimerize by condensation reactions catalyzed by base.

$$M\text{-}OH^{\delta-} + M\text{-}OH^{\delta-} + OH^- \longrightarrow M\text{-}O\text{-}M\text{-}OH + H_2O$$
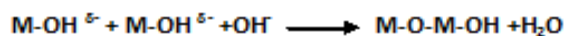
This secondary inter aggregation of titania particles gave them a chain like nature. Sometimes a cavity is formed inside as seen in the SEM (Figure 10a). This chain like nature is quite evident from the SEM, HR-TEM, and FEG-SEM depicted in Figure 10. This sort of chain formation creating chambered interior cavity was previously reported by Liu et.al also in alkaline medium [12]. These observations related to the porous nature of shelled system are consistent with the results obtained from FEG-SEM, TEM and Nitrogen adsorption desorption isotherm. The existence of these mesopores in a wide range in the structure can be invaded by hydolizable ligands, thus finding applications in drug delivery.
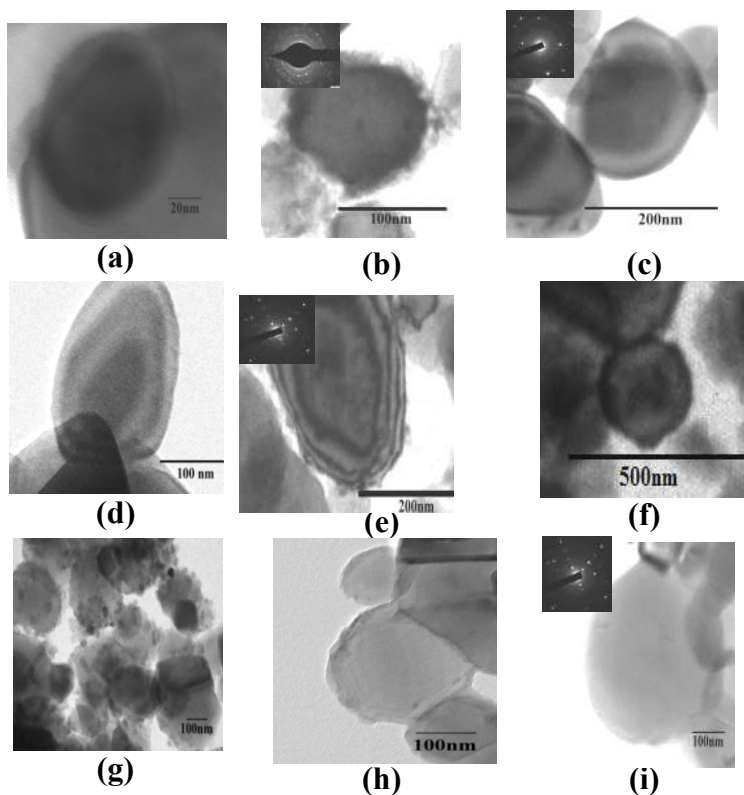
**Figure 9**.TEM images of the TiO$_2$ nano spheres obtained at different Reaction durations a) 1hr b) 2.5hrs c) 5hrs d) 6hrs e) 7hrs (f) 9hrs (g) 11hrs (h) 13hrs (i) 14hrs.

We conducted the synthesis at three more time intervals to attain an idea of things happening during complete hollowing process. Further increase in solvothermal reaction time led to the following observations. The multi walled nature has disappeared and the core has become very small after 9 hours (Figure 9f). Figure 9g is supposed to be the stage where the evolution of hollow structure with thin walls begins, at the expense of thick walls. Hollow spheres with thinner walls are more desirable since they offer good

permeability for solution or gas. Then gases and liquids can easily enter the nano pores and the inner chambers of these hollow spheroids which ensure high catalytic efficiency [13]. Figure 9h represents the TEM image of the oxide after solvothermal reaction for 13 hours where the thicker walls have completely faded away. As the dissolution from rigid areas continues; a thinner finer walled hollow structure of 260-275nm was achieved at 14 hours as seen in Figure 9i. Inset shows the SAED pattern confirming the single crystalline nature of the system. As evident from SAED pattern, it was quite interesting to note that all these hollow structures maintained single crystalline nature which adds increased significance for the work.



(a)                                    (b)



(c)
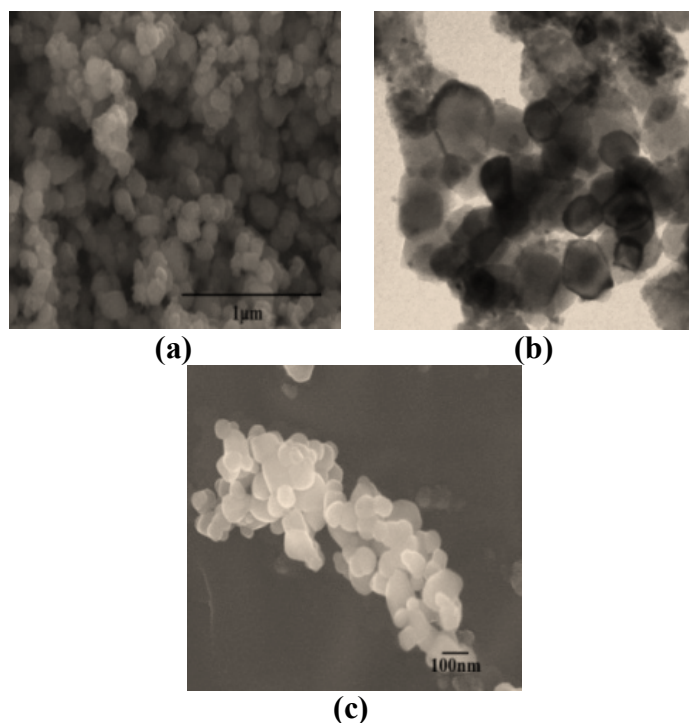
**Figure** 10. SEM (a); TEM (b); FEG-SEM (c); of MHS

The formation of titania hollow structures which passes through various complex structured interiors is explained on the basis of inside out Ostwald ripening processes. According to the IUPAC, this process refers to ''the growth of larger crystals from those of smaller size which have a higher solubility than the larger ones'' [14]. This type of ripening process is previously discussed in the preparation of complete hollow spheres [15-16]. Size changes in the wall thickness and the cavity span is observed in each stage which clearly confirms the inside out ripening process noticed in such situations. The slight deviation from spherical shape in the above mentioned morphologies is due to alkali etching. By considering all the above mentioned stages that occur during the transformation of a solid sphere to a hollow one, a plausible pathway to the final product can be made as discussed below.

Presence of methanol along with strong alkaline conditions is essential for the hollowing process. Under alkaline reaction conditions, the freshly formed anatase $TiO_2$ nanoparticles are in high local concentration and they quickly aggregate to form solid spheres so as to decrease the surface energy. The faster nucleation rate within the solid core leads to the formation of crystallites with smaller size while its peripheral part is packed with much bigger sized crystallites. Because of this non uniformity of crystallites, the concentration of solutes across the bulk solution varies. The homogenization of this concentration gradient will end in hollow structures by the complete dissolution of smaller crystallites and the growth of larger crystallites. The crystallinity difference within the

solid sphere caused by the surrounding polar medium may also facilitate the dissolution and crystallization process.

It is reported that during the preparation of hollow spheres via solvothermal process which used alcohol as one of the reactant, part of the alcohol is converted to ether and water by condensation reaction, the latter act as the hollowing process controller [17-18]. It can be recollected that the FTIR spectrum of the uncalicined sample has revealed the presence of organics on the surface of solvothermal product, which is denoted by the specific IR band at $1120cm^{-1}$ arising from the asymmetric streching vibrations of C-O-C bond in dialkyl ether [19-20]. It is understood that the Ostwald ripening process is promoted by the water generated during the solvothermal reaction. As the water is being continuously formed by the reaction of methanol on the surface of tiania [21], surface nanoparticles have higher crystallinity than inside. Less crystalline particles on interior are more likely to dissolve than those in the exterior.

During the evacuation process, surface crystallites act as nucleation sites for the creation of hollow cavity between the core and the shell. With the consumption of crystallites just below the surface and its recrystallization on the surface, a void is formed between the interior part and exterior surface. This empty space divides the sphere in to core and shell. Again, if the sizes of crystallites in the core are not exactly the same; the dissolution and recrystallization go on. That is secondary Ostwald ripening occurs, where the pre formed interior solid core is further divided in to

external shell and interior core. Meanwhile the shell initially formed by the cleaving of the core fades away, contributing towards outermost shell growth. The interior portions, including the solid cores and the inner shells are less stable thermodynamically. Hence after prolonged solvothermal reaction, completely finer thin walled hollow nanostructures with a diameter of about 275nm are evolved as the final product. Schematic illustration of the evolution of various hollow structures is given in Figure 11.
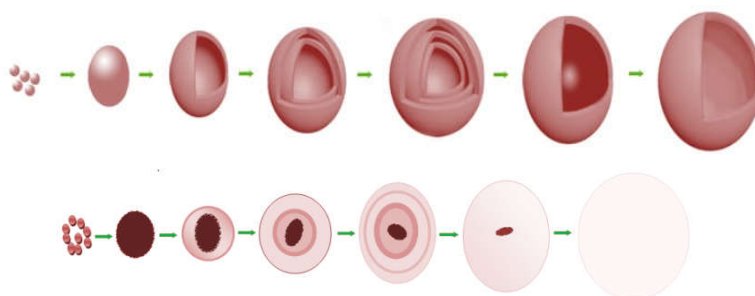


**Figure 11**. Schematic illustration of the formation of single crystalline titania hollow nano spheroids having various interiors (Top). Corresponding two dimensional representations (bottom)

It is clear from the scheme that the nanoparticle aggregation resulted in the formation of a hard solid sphere which inturn undergoes the above mentioned Ostwald ripening type of proliferation and recrystallisation resulting in yolk shelled spheroid. Secondary Ostwald ripening that leads to multishelled structure is followed, that finally ends up with the thin walled spheroid. Hence it is quite evident that time modulation in the solvothermal procedure can yield hollow structures of different interiors. In the present study we could attain a five shelled structure by adjusting

the duration to 7 hours. Such a high shell number through by this method is practically nil for single crystalline titania, to the best of our knowledge. Due to this core evacuation process, the shell of the nanospheroids has intercrystallite channels which are communicable and serve as the gateway for materials exchange between the interior cavity and exterior space, making it suitable for a variety of fine applications. It is reported that the reactions occurs more easily when the nanostructures itself form the moving pathway through which molecules moves in to and out [22-23]. We provide the first account of a versatile straight forward method to prepare a family of amazing single crystalline multishelled titania hollow nano spheroids of up to five continuous shells, via a low cost, template free solvothermal process under mild conditions. Achievement of single crystalline structures of uniform size through this synthetic route requires indepth study of the various reaction conditions and reagent concentrations.

## 3.2 Mesoporous assembled titania nanocuboids [MT]

Synthesis of mesoporous assembled titania nanocuboids have been done as discussed in section 2.3.2. Results of various characterisation techniques are discussed below.

### 3.2.1 Small angle Xray-diffraction pattern

Mesoporous character of the synthesized sample is confirmed first by the low angle XRD. Figure 12 represents the Small angle XRD pattern of the mesoporous material. The single

strong diffraction peak in the low-angle region indicated the presence of meso- structure. Meso-structures packed at random with more or less regular diameter often display a single peak in low angle XRD [24-25].
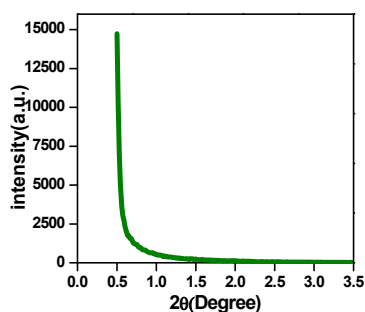


**Figure 12.** Small angle XRD pattern of mesoporous assembled titania nanocuboids (MT)

## 3.2.2 Nitrogen adsorption- desorption studies and BET-Surface area analysis
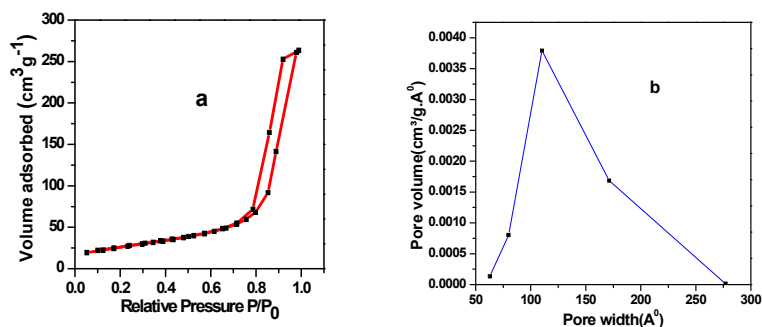


**Figure 13**. Nitogen adsorption - desorption isotherm (a) and the BJH pore distribution curve (b) of mesoporous assembled titania nanocuboids (MT)

The Nitrogen adsorption desorption experiment is another commonly employed technique to investigate the mesoporous characteristics. The isotherm represented in Figure 13a, is that of Type IV, typical characteristic of mesoporous material [26]. The hysteresis loop indicated the presence of mesoporous structure within the synthesised structure. The initial part of the isotherm is attributed to monolayer-multilayer adsorption. Presence of huge and steep condensation / evaporation steps with $P/P_0$ beyond 0.8 indicated the presence uniform and large mesopores and large pore volume [27]. Existence of narrow H1-type hysteresis loops indicated the formation of slightly constricted mesoporous structures. The Barret–Joyner–Halenda (BJH) pore size distribution (Figure 13b) determined from the desorption isotherm showed that the sample is having average pore width about 17.4 nm. Such a high pore size is rarely reported for mesoporous titania using P123 as template. The specific surface area of the sample, calculated by the multi-point Brunauer-Emmett-Teller (BET) method, is 93.54 $m^2$/g. The large pore diameter is responsible for this reduced surface area when compared to other reported meso-structured materials. The total pore volume taken from the adsorption branch of the nitrogen isotherm curve at $P/P_0$=0.994 single point is 0.407756 cm³/g. Thus we can confirm that the material possess mesopores of uniform pore channels throughout the nanostructures, which is an essential requirement for diverse applications [28].

## 3.2.3 Electron microscopy analysis

The morphology of the prepared samples was investigated through SEM and TEM analysis. Here it is worth to emphasize that the mesoporous structure arises in this synthesized photocatalyst due to the pores existed between the nanocrystalline $TiO_2$ particles owing to their aggregation, which is in the same line as the mesoporous $TiO_2$ reported in literature [29-34]. FESEM image (Figure 14a.) revealed uniform 10-15 nm sized units assembled together in certain direction. The FESEM image Figure 14b displays that the orientation of these nanounits resembles the arrangement of petals in a flower, again pointing out a particular axis directed growth. The structure as a whole when viewed from the top seems to be cuboidal due to the specific arrangement of the individual units. The red arrows shown in the FEG-SEM image (Figure 14b.) indicated the voids formed due to this peculiar arrangement. Figure 14c represented low resolution TEM image where the piling of primary blocks of size 10-15 nm is observed by sharing specific crystal faces. The red circles represented the various nanocuboids as appeared in the TEM. We can observe that most of them adopt cuboid structure. The interconnected fabrication of individual building blocks can be attributed to the solvent effect. A mixture of solvents water and ethanol has been used in the the sol- gel method adopted here. When the solvent is water due to the existence of large amount of hydroxyl groups on the metal oxide surface, the nano units may have a strong interaction with solvent by forming the hydrogen bonds. However, when using the mixed solvent of

H$_2$O and EtOH as reaction medium, the interaction of the hydrogen bond between hydroxyl groups on the TiO$_2$ surface is weakened because of the introduction of alkyl group which is responsible for the random aggregation. Figure 14 d displayed the low resolution TEM image of an individual nano cuboid.

.
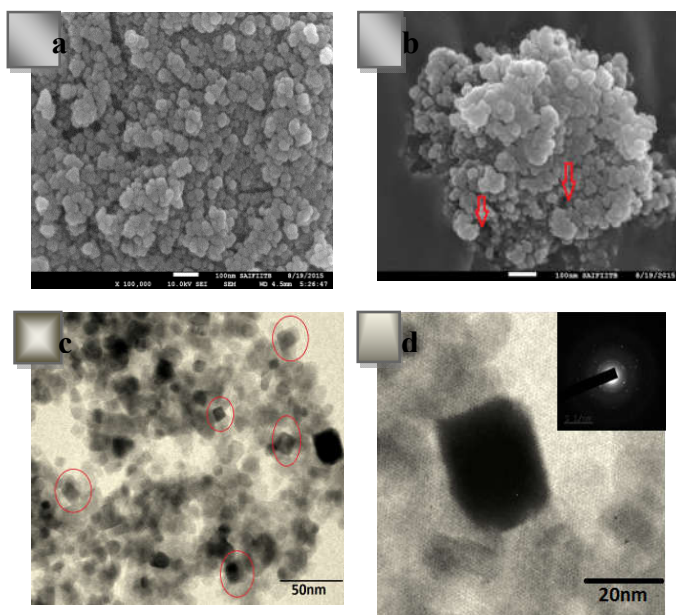


**Figure 14**. FE-SEM (a, b) and d) Low magnification TEM images of Mesoporous assembled titania nanocuboids (c, d)

The arrows in figure 15a pointed the perceived stacking of individual units. Some ordered arrangement of building units makes the observed vacant spaces in the TEM image. The observed bigger units appearing in the TEM are due to the 1D and 2D arrangement

of the primary units. Some vertices of the lower layered units are visible in figure 15b, which emphasized that certain axes are participating in the assembly confuting the others. The said fact is confirmed by the HRTEM image (Figure 15c). The white dotted line depicted the square tops and the right angled steps, as appeared in the high resolution TEM. The lattice fringes are clearly visible. Two sets of lattice fringes taken at two different places of cuboid are being observed in the HR-TEM image (Figure 15d). The common orientation among the nanocrystals can be visualized easily in the lattice image of Figure 15d. We can perceive a boundary as well as a region with perfect and imperfect attachments and alignments between particles. Aggregation of similar crystallographically oriented nanocrystals forming larger agglomerates and the presence of defects ensures the oriented allignment process in the predominant nanocrystal growth mechanism. Lattice fringe with d spacing value of 0.35 nm is that of 101 plane of anatase titania and 0.23nm is that of 001 plane. This synergy of 101 and 001 planes of anatase titania is favourable for the enhanced activity of anatase titania [35-36]. When the HRTEM image in Figure 15e is considered, faceted crystals with several geometries can be identified. Since the Wulff shape predicted for the anatase $TiO_2$ phase is truncated tetragonal bipyramidal, the 2-dimensional projection in different zone axes, objects appears to be in different geometries. TEM image is a bi-dimensional projection of a 3D object. Therefore, the alternative morphologies observed are due to the projection of the truncated bipyramid in different

zone axes. Figures 15f and 15g depicit observed isosceles trapezoidal and square top geometries in the HRTEM image. The d spacing value corresponding to the lattice fringes of the same are that of {101} and {001} planes respectively, confirming the isosceles trapezoidal 101 plane and square toped {001} planes of anatase titania. Figure 15h, represented the model how the side of the nanocuboid when observed from the top, which matched with the HRTEM (Fig 15f). Figure 15i is the 3 dimensional model showing the 101 facets on the sides and square shaped top (001 facets) of the nanostructure. Figure 15j portrays the piling units in 2 dimensional views. For convience, cuboidal geometry has been chosen for the pictorial representation.
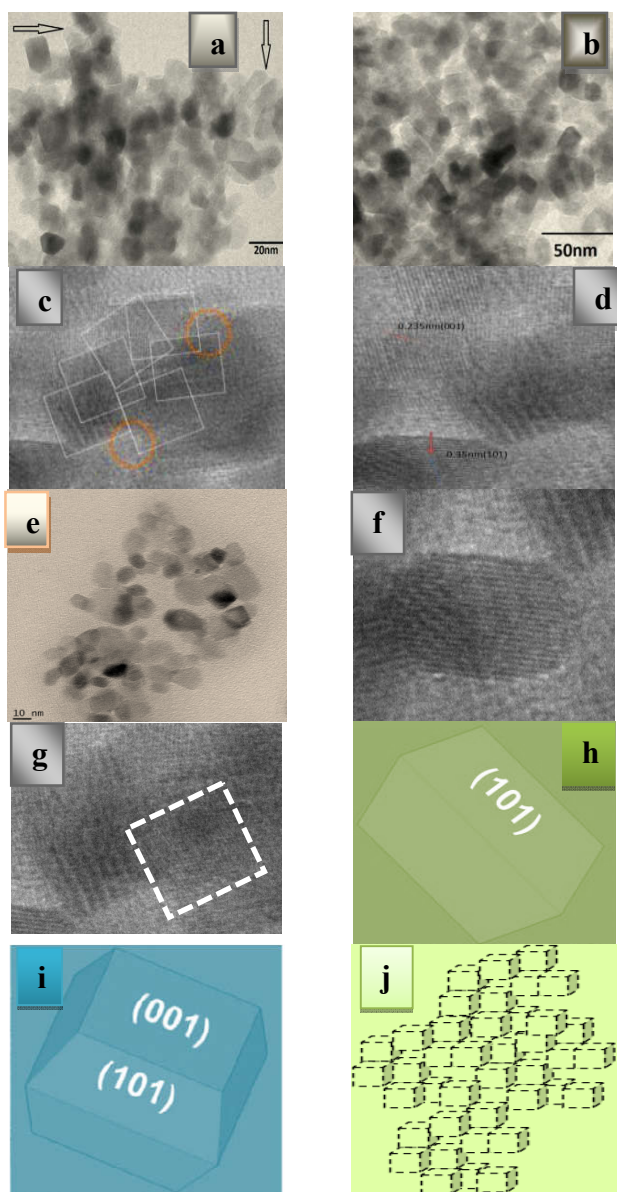
Figure 15. TEM images (a), (b), FEG-SEM image (c), TEM image showing lower vertices of cube (d), corresponding HRTEM image showing right angled steps (e), HRTEM image showing lattice distance spacing (f) , High resolution images and the corresponding 3D pattern of 101 plane (g , h) and 001 plane (i, j) Schematic development of nanostructure assemblies in 2D view (k)

## 3.2.4 Wide angle Xray diffraction pattern

Further confirmation regarding the planes is made from the wide angle XRD pattern. Figure 16 represents the wide angle XRD pattern of mesoporous assembled titania nanocubes. Diffraction peaks at $25.22°$, $37.8°$, $47.9°$, $53.9°$, $54.9°$, $62.6°$, $68.74°$, $70.12°$, $75.02°$ degrees correspond respectively to (101), (004), (200), (105), (211), (204), (116), (220) and (215) planes of $TiO_2$ in anatase phase (JCPDS card, No. 21-1272). Moreover, significantly enhanced peaks of (200) reflections confirm a preferred orientation [37]. The diffraction peaks from (103) and (105) planes that are parallel or quasi-parallel to the (001) plane were relatively small or not observed [38]. Besides compared to (101) and (200) peaks, (004) and (105) peaks are somewhat broad indicating small crystal size along 001 plane as well as oriented growth along special axis. The crystallite sizes were calculated with the Scherrer equation ($\Phi = K\lambda/\beta \cos \theta$ ), where $\Phi$ is the crystallite size, K is usually taken as 0.89, $\lambda = 0.154$ nm, which is the wavelength of the X-ray radiation; $\beta$ is the full width at half-maximum intensity (FWHM), and $\theta$ is the diffraction angle of the (101) peak for anatase ($2\theta = 25.2\circ$). Thus, the average crystallite size calculated is found to be 11.17 nm, which is consistent with the particle size derived from TEM analysis. In particular, the relative XRD intensity ratio of (004) and (200) peak i.e., $I_{(004)} / I_{(200)}$, is found to be 0.936, indicating the strong [001] oriented planes.
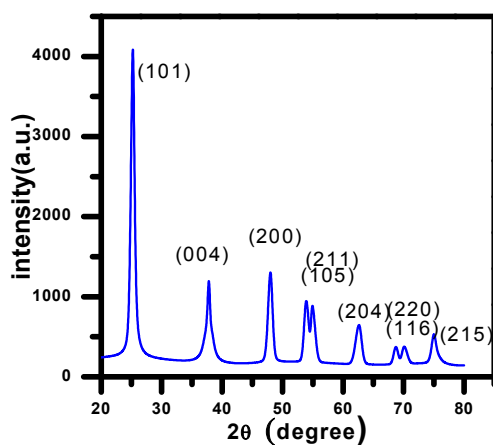
Figure 16 .Wide angle XRD pattern of calcined mesoporous TiO₂ sample

## 3.2.5 Raman spectroscopy
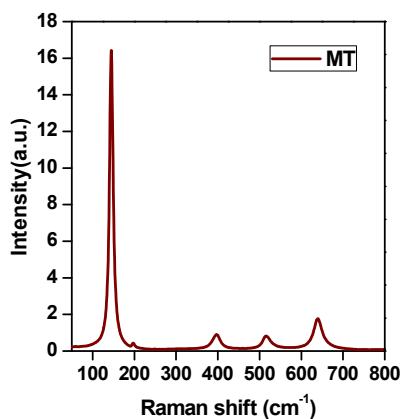


Figure 17. Raman spectrum of mesoporous assembled titania nanocuboids

Raman peaks of 145 cm$^{-1}$, 197 cm$^{-1}$, 397cm$^{-1}$, 514cm$^{-1}$ and 639 cm$^{-1}$ are attributed to the anatase peaks of titanium dioxide. These correspond to $E_{g(1)}$, $E_{g(2)}$, $B_{1g(1)}$, $A_{1g}$ and $E_{g(3)}$ Raman active fundamental modes. No other peaks are observed emphasisng the purity of sample as revealed from XRD analysis.

### 3.2.6 Fourier Transform Infrared Spectroscopy (FTIR)

The FTIR spectrum of the sample calcined at 500$^0$C (Figure 18) exhibited bands at 460 cm$^{-1}$, 620 cm$^{-1}$ and 910 cm$^{-1}$ in the range of 400- 1000 cm$^{-1}$ that are contributions from anatase titania [39]. The broad bands at 3400 cm$^{-1}$ and 1638 cm$^{-1}$ justify the presence of surface-adsorbed water and hydroxyl groups in titania. As there are no observable bands corresponding to surface adsorbed organics, we can confirm that the calcination temperature is sufficient to remove all the volatile impurities which are associated with the surfactant.
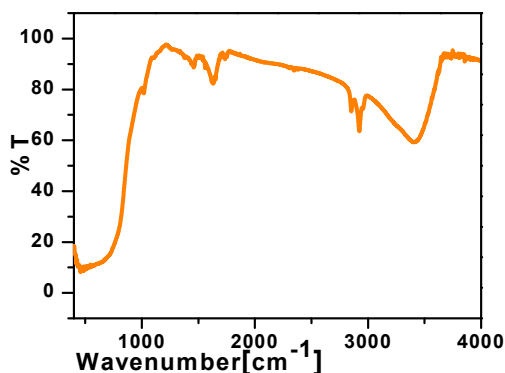


Figure 18. FTIR spectrum of mesoporous assembled titania nanocuboids (MT)

### 3.2.7 UV-Visible absorption spectrum and Kubelka-Munk Plot

Figure 19a represents the UV-Visible absorption spectrum of the prepared mesoporous assembled structure. It consists of a broad intense absorption around 389 nm (corresponding to band gap energy of 3.18 eV, calculated from the formula ( $\lambda = 1239.8/E_{bg}$) caused by the charge transfer from the valence band formed by 2p orbitals of the oxide anions to the conduction band formed by the 3d $t_{2g}$ orbitals of Ti $^{4+}$ cations. The band gap energies of the samples have been determined as per the equation (1) by extrapolation of a Tauc plot to the X-axis. The band gap value is found to be 3.2 eV.
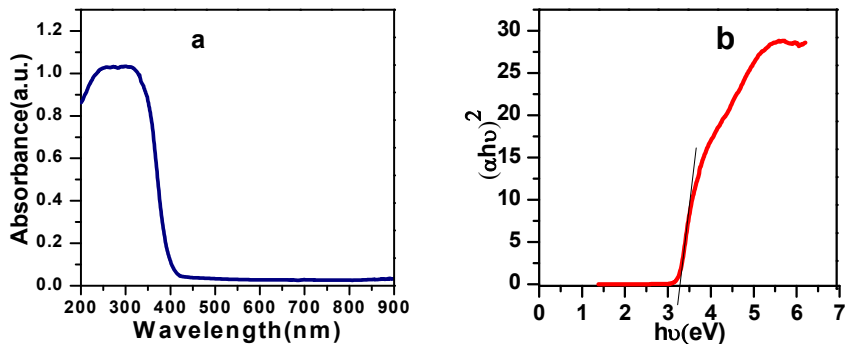


**Figure** 19. UV-Visible absorption spectrum (b) and corresponding Kubelka- Munk plot (c) of Mesoporous assembled titania nanocuboids (MT)

**3.2.8 Dynamic Light Scattering Analysis**

The particle size distribution curve (Figure 20) showed narrow distribution of particles. The histograms indicate that the particle size of the Titania made by the sol-gel method is about 146 ± 7 nm. This value is higher than what observed in the TEM images due to the measurement of large aggregates which are stacked by the oriented growth. The zeta potential and PDI value are found to be -36.1mV and 0.2097 respectively, implying considerable stability of the dispersion medium.
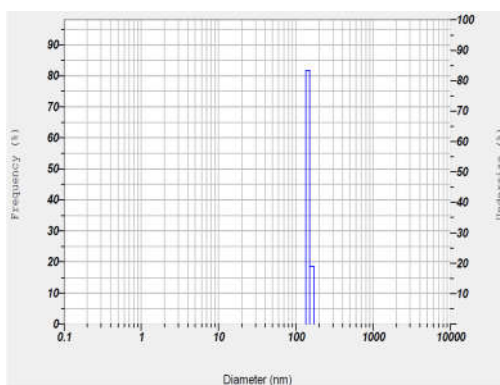


**Figure 20**. Particle size distribution curve of mesoporous assembled titania

**3.2.9 Possible mechanism leading to mesoporous assembled titania nanocubes with large pores**

In oriented attachment growth mechanism, spontaneous self-organization of adjacent nanounits occurs sharing a common crystallographic orientation. In the beginning the nucleation and growth of anatase nanocrystals takes place. Since the reaction

medium is in a semi- coagulated state, some attractive interactions between the nanocrystals must occur forming agglomerates by an ordered assembly of the nanoparticles; i.e., by the oriented attachment (OA) process. Again these smaller units interact to produce larger agglomerates with proper crystallographic interfaces. Origin of the attractive interaction between nanoparticles and agglomerates is not clear. However it is assuered that it can be a structural interaction promoted by the selective desorption process of the organic compounds (Here P123;) attached to the nanoparticle surface.

Aggregation-based growth is driven by reduction in surface free energy. Researchers have indicated that P123 ((PEO) 20–(PPO) 70–(PEO) 20) has advantages of tuning the texture and porous structures [40-41]. Anatase {001} plane which contains edge sharing octahedral with highest density of vertexes serve as place for the capping agent to bind [42]. Free P123 molecules selectively adsorb onto {001} plane of $TiO_2$ nanocrystals to suppress their intrinsic crystal growth along that face. Thus P123 stabilizes the structure by lowering its surface energy because of coverage of P123 on crystal surface [43]. Therefore P123 not only acts as a template for the formation of the porous structures, but also induces the reassembly of titania nanocrystallites. After the nanostructure Fabrication, P123 itself can be removed completely by calcination at $500^0C$ which is confirmed by the FTIR Spectrum. Solvent evaporation driven oriented assembly in the mixture of solvents having different boiling points also aids for the development of this

super structure. At the inter phase between water and alcohol, PPO-PPO-PPO /Titania micelles are formed thus reducing the surface tension. By constant evaporation of solvents (at $110^0$C), owing to the differed boiling points of the solvents, anisotropic aggregation occurs at 3 dimensions. During calcination, adjacent nanobuilding blocks are cross-linked by removing the surface hydroxyl groups and the oriented growth continues leading to 3Dimensional crystallographic fusion.

Obviously, P123 plays an important role in introducing mesoporosity in the texture of these assembled titania nanocubes. The structure directing function of P123 is well-known [44-45]. The mesopore diameter partly depends on the nature of the alkoxide groups of the inorganic precursors [46]. The hydrolysis of Ti(OBun)$_4$ results in the formation of n-BuOH in situ. It is well-known that butanol acts as a co-surfactant or swelling agent in block copolymer–water systems. Unlike short-alkyl-chain alcohols, long alkyl chain alcohols can spear more easily into the micelle poly (propylene oxide) core (high hydrophobic properties). The polar end of butanol located at the hydrophilic- hydrophobic interface between the poly (ethylene oxide) and PPO blocks and helps to stabilize it and determine its surface curvature. The pore size of the mesostructure is roughly determined from the size of hydrophobic core of the template. The pore size expansion due to BuOH could be explained by the increase in the hydrophobic core volume or the swelling in the hydrophobic to hydrophilic volume ratio of the block copolymer micelles [47].

## 3.3 Titania nanotubes [TNT]

Synthesis of Titania nanotubes have been done as discussed in section 2.3.3. The results of the characterisation techniques adopted are dicussed below.

## 3.3.1 Electron microscopic images

The electron microscopic images confirmed the nanotubular morphology. Figure 21a represented the high-magnification SEM image of the hydrothermally synthesied nanotube. Tubular bundles are seen in some region, which may be due to the aggregated nanotubes. A more vivid picture is obtained from the TEM image shown in Figure 21b. The tubes are hollow, multiwalled and open ended as revealed from the TEM images [represented by the the arrows in Figure 21c]. They possess more or less uniform inner and outer diameter along their length as observed in previous reports [48-49]. The inner diameter is about 7-8 nm with the interlayer spacing ~ 0.75 nm. The length of these tubes ranges from 100-250 nm. The yield of nanotubes were observed to be high by hydrothermal method.

The SAED pattern of TNT (Figure 22a) exhibits a diffuse and fussy diffraction ring due to the relatively amorphous structure. We can see from the HRTEM images (Figures 22 b, 22c, 22d) that two types of interplanar spacings are observed in a heretojunction, with 0.57 nm corresponds to the (200) plane of $TiO_2(B)$ phase and another with 0.35 nm which is the 101 plane of anatse titania.

Biphasic crystalline structures are highly beneficial to titania for various applications [50]. This type of generation of junctions and chemical potential gradients in the catalysts helps to separate the photogenerated electrons and holes into different locations on the catalyst, and thus increase the photocatalytic activity.
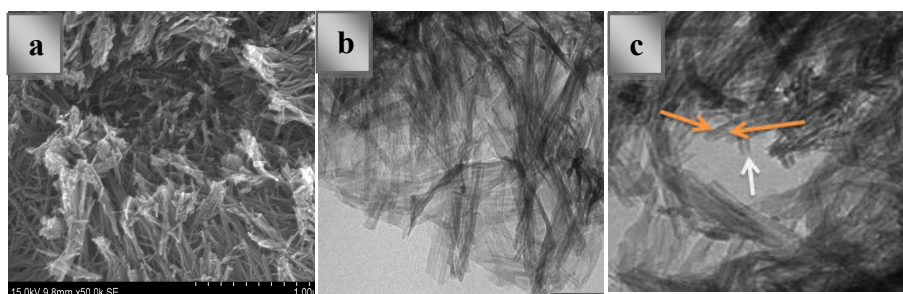


**Figure 21**. SEM image(a) ,TEM images (b, c) of Titania nanotube
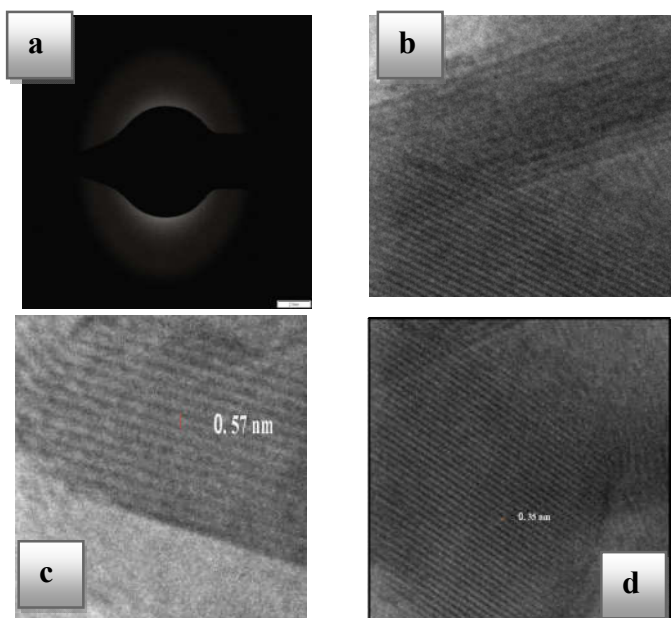


**Figure 22**. SAED pattern (a), HRTEM images of Titania nanotube

### 3.3.2 X ray diffraction pattern

Figure 23 depicites the XRD pattern of the prepared nanotubes. The peaks in the diffraction pattern of the nanotube is broadened due to confinement effect. The XRD pattern indicated a mixed phase of anatase and $TiO_2$ (B) phase in tubes. $TiO_2$ (B)is a metastable phase of titania with bandgap close to anatase. For the standard $TiO_2$(B) compound, the XRD diffraction peaks appeared around $2\theta = 14.2°$, $25.1°$, $28.5°$, and $48.53°$[(JCPDS 74- 1940 ] [51] Anatase titania exhibits peaks around $25.3°$, $36.6°$, $48.0°$, $54.5°$, $62.6°$ and $68.0°$ which are indexed to (101), (004), (200), (105), (204), and (116) planes of Anatase (JCPDS-00-021-1272). In this case, XRD pattern confirmed the biphasic structure of TNT and the diffraction peaks corresponds to both $TiO_2$ (B) and anatase.
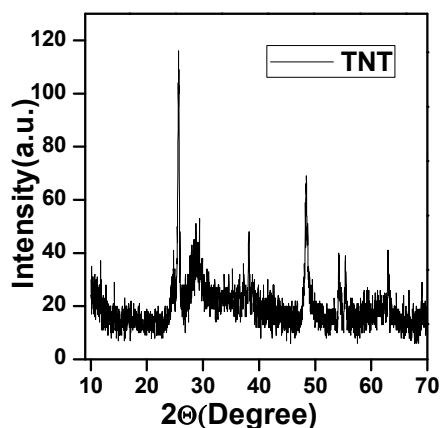


**Figure 23**. Wide Angle XRD Pattern of TNT

### 3.2.3 Raman spectroscopy

Figure 24 showed the raman spectrum of hydrothermally synthesized titania nanotube. The peaks corresponding to anatase and $TiO_2$ (B) phases are present. Anatase peaks are found around 144 cm$^{-1}$, 515 cm$^{-1}$ and 639 cm$^{-1}$ and that of $TiO_2$ (B) are at 123cm$^{-1}$, 162cm$^{-1}$, 195cm$^{-1}$ and 370 cm$^{-1}$. Presence of biphasic structure has wide applications when compared to single component systems for the well separation of photogenrated charge carriers.
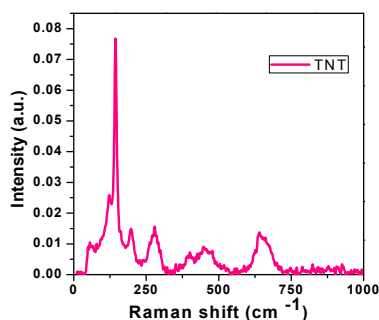


**Figure 24**. Raman spectrum of Titania nanotubes

### 3.3.4 Fourier Transforn Infra Red Spectroscopy (FTIR)

Figure 25 shows typical FTIR spectrum of titania nanotube. The presence of crystallographic water molecules in the sample is confirmed by the appearance of a characteristic peak at 1631 cm$^{-1}$, that can be assigned to the H–O–H deformation mode. The broad band observed at 3200.0 cm$^{-1}$ - 3600.0 cm$^{-1}$ represents the O-H stretching, indicating the presence of O-H functional groups. The broad band found at 497.05 and 646.77 cm$^{-1}$ was assigned to Ti–O

and Ti–O–Ti skeletal frequency region. The band around the wavenumber of 666.0 cm$^{-1}$, indicate the anatase phase of titanate [52]. Moreover, the one in at 460 cm$^{-1}$ could be interpreted by the presence of Ti-O-Ti crystal phonons due to the tubular structure exhibited by TNTs [53].
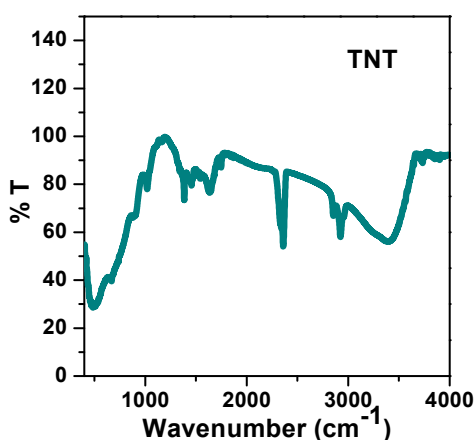


**Figure 25**. FTIR spectrum of titania nanotubes

3.3.5 UV-Visible absorption spectrum and Kubelka Munk plot

The UV-Vis absorption edge and band gap energies of the samples have been determined from the reflectance [F(R)] spectra using the KM (Kubelka–Munk) formalism and the Tauc plot. The absorption spectrum showed a very broad band in the range 245-295 nm. The extrapolation of a Tauc plot to the X-axis should yield the band gap energy of titania nanotube which is found to be 3.22 eV. The good absorption of this material in the UV region

proves the applicability of this product in medical application such as sunscreen protectors or as antiseptic ointments.
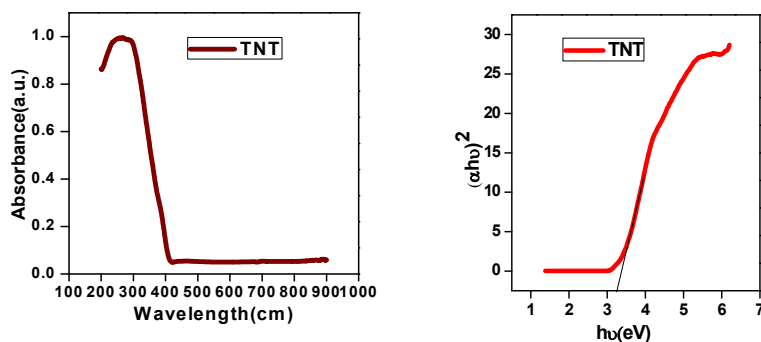


**Figure 26**.   UV-Visible absorption spectrum and corresponding Kubelka-Munk plot of TNT

## 3.3.6 Nitrogen adsorption desorption   Study and BET-Surface area analysis

Typical type IV isotherms with hysteresis loop caused by capillary condensation is observed at a relative pressure range of 0.5–0.9 in nanotubes [54]. The hystersis loop is identified to be in between H1 (at $0.5 < P/P_0 < 0.9$) and H3 ($P/P_0 > 0.9$). From the  isotherm it can be observed that hysteresis extended to $P/P_0 \sim 1$ indicates the presence of large pores, which are not being filled. Considering the morphology of the material by electron microscopy, smaller pores may signify the pores inside the nanotubes. and the  larger pores correspond to the pores between the nanotubes. The hysteresis loop is found to be broad, indicating a wide distribution of pore sizes. The pore volume distribution curve is found from the desorption data (with BJH algorithm). In the pore distribution curve (Figure 27

b) , the pores are found to be within mesoporous range, with peak centered at 10.9 nm. Surface area and Pore volume were found to be 84.79 m$^2$/g and 0.3465 cm$^3$/g respectively.
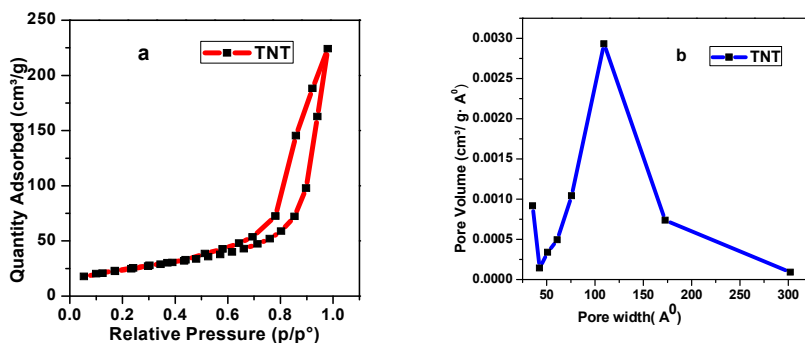


**Figure 27**. Nitrogen adsorption desorption isotherm and BJH pore distribution curve of TNT

### 3.3.7 Dynamic Light Scattering analysis

Figure 28 showed the particle distribution curve of titania nanotube. It revealed slightly broader distribution than from identical spherical particles. The zeta potential and Poly dispersity index value was found to be -52.05mV and 0.387. These value indicated that the dispersion is stable.
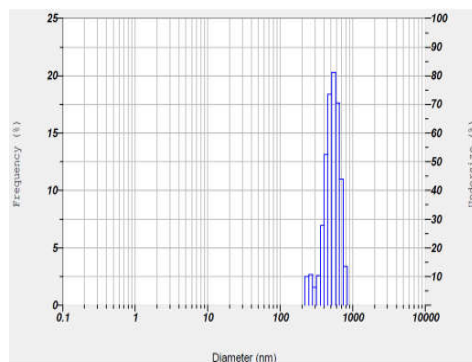
**Figure 28.** Particle Size distribution curve of Titania nanotube

### 3.3.8 The Formation of titania nanotube from nanoparticle by alkaline hydrothermal treatment
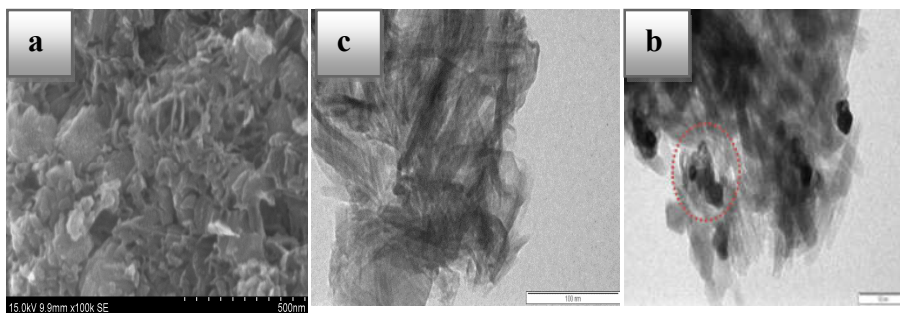


**Figure 29.** SEM image of Hydrothermally treated titania for short reaction time (a) TEM image (b) Nanotubes with end rolled (c)

The initial precursor to titania nanotubes were $TiO_2$ particles. To understand the formation mechanism of the $TiO_2$ nanotubes, , a short reaction time for hydrothermal processing was adopted. A per many reports, [53-57]. Some lamellar Titanium oxide products were observed as seen in Figure 29 a and Figure 29

b which emphasised the nanosheet fromation which is an intermediate step to tubular structure. Transformation of anatase $TiO_2$ to nanotube $TiO_2$ is accompanied by the dissolution and crystallisation of titanium dioxide. It was considered that Ti in alkali solution is in the monotitanate form $TiO_3^{2-}$ Or $TiO_2(OH)^{2-}$ , rather than polytitanates $Ti_nO_{2n+m}^{2m-}$

$TiO_2 + NaOH \rightarrow 2\ Na^+ + TiO_3^{2-} + H_2O$ (Dissolution of precusor)

$2\ Na^+ + TiO_3^{2-} \leftrightarrow [Na_2TiO_3]_{nanosheet}$ (Dissolution and crystallization)

$[Na_2TiO_3]_{nanosheet} + TiO_3^2 + 2\ Na^+ \leftrightarrow [Na_2TiO_3]_{nanotube}$ (Naosheet Curves)

$[Na_2TiO_3]_{nanotube} + 2\ H_2O \leftrightarrow [H_2TiO_3]_{nanotube} + 2NaOH$
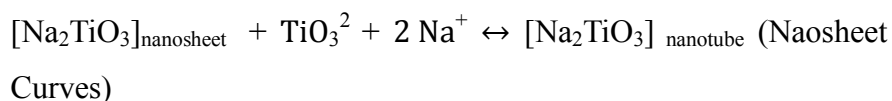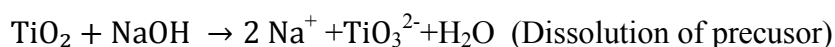
Thus, a model of 3D→2D→1D has been proposed for the formation mechanism of $TiO_2$ nanotubes. Anatase titania , 3D crystal produces lamellar structures [2D] upon reaction with alkali. When immersed in alkali, the dangling bonds on the surface of titania reacts with alkaline -OH groups. Then, the lamellar $TiO_2$ curls to saturate these dangling bonds. Multiple layered nanosheets in the nanotubes tend to curve to completely close, thereby leading to multiwall nanotubes.  Finally, the nanoscale tubular structure was achieved. The curvature is clearly visible in the TEM images represented by the dotted red circle Figure 29 c [58]. The pictorial representation showing the curling of nanosheet to nanotube upon hydrothermal treatment has been displayed below [Figure 30].
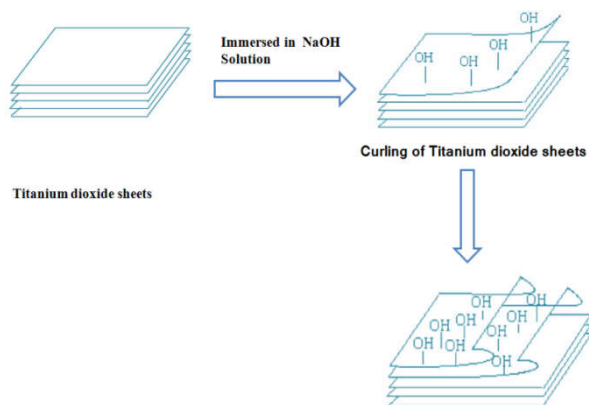
**Figure 30**. Schematic representation of the curling of nanosheet to nanotube upon alkaline hydrothermal treatment

The heterogeneous photocatalyst formed via self-transformation of a single material is highly feasible method. It was observed that the intensities of $H_2Ti_3O_7$ diffraction lines are more in the uncalcined sample and the intensities were less in the calcined sample confirmed the onset of phase change upon calcination. Armstrong **et al. [59]** have reported the first synthesis of titanium dioxide nanotubes with the $TiO_2$-B crystal structure by simple hydrothermal reaction and the nanotube yield is estimated to be 90%. Some authors reported that nanostructured $H_2Ti_3O_7$ transforms into a metastable $TiO_2(B)$ phase and into anatase/rutile upon calcination. **[60].** Transformation in to $TiO_2(B)$ phase passes through the following states as reported by Edisson et al.[61].

$H_2Ti_3O_7$ into $H_2Ti_6O_{13}$ and then $H_2Ti_6O_{13} \rightarrow H_2Ti_{12}O_{25} \rightarrow TiO_2(B)$
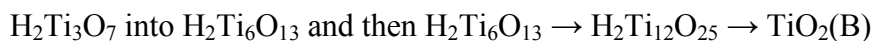
The retension of tubular morphology after phase change is usually difficult. Armstrong *et al* synthesized $TiO_2(B)$ nanotubes or nanowires by adjusting the hydrothermal synthesis conditions.

We also could successfully synthesise $TiO_2$ (B) nanotubes by hydrothermal treatment and calcination process.

## 3.4 Titania nanobelts [TNB]

**Synthesis of Titania nanobelts have been already discussed in section 2.3.4. The characterisation results are discussed below.**

### 3.4.1 Electron microscopy images
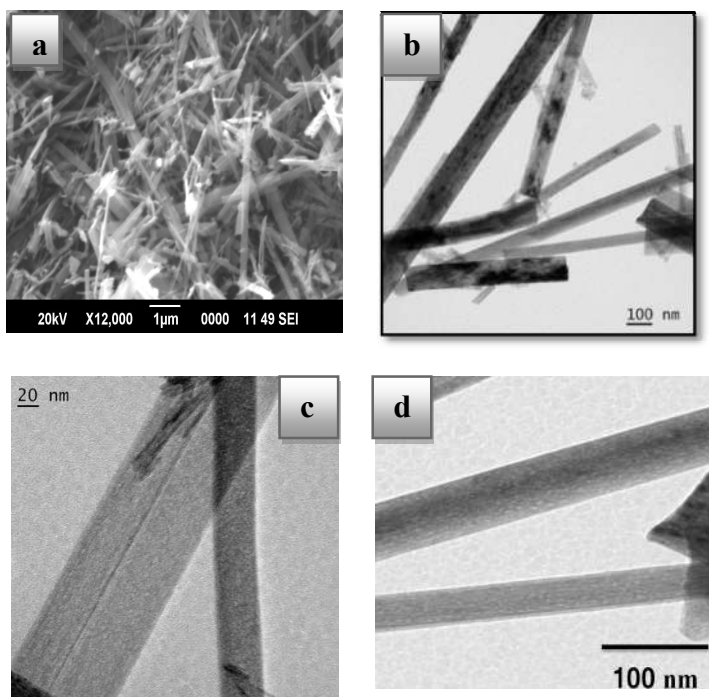


**Figure 31.** SEM,TEM images of synthesised titania nanobelt (TNB)

Electron microscopic images revealed the nanoblet morphology of the synthesised material. SEM images (Figure 31 a) revealed that the width of the nanobelt is about 50-200nm, several micrometers in length. They possessed 30-50 nm thickness and with clean surfaces. More idea about morphology can be gathered from TEM images (Figure 31 b). Figure 31 c represented the microtomed cross scetion TEM images of nanobelt which provide the top view. The rough surface is generated due to the post treatment process of the nanobelt after hydrothermal process [62]. We can observe uniformly distributed small pores all along the length of nanobelt [Figure 31d]. The HRTEM image shown in Figure 32a revealed lattice fringe spacing of 0.618 nm corresponding to the 010 plane of $TiO_2(B)$ Phase. The HRTEM exhibits discontinuous lattice fringes, characteristic of the mesoporous structure [63]. The SAED pattern (Figure 32b) reavealed the angle between (400) and (002) facets which was measured to be $\beta \sim 107°$, which is identical to the lattice parameters of monoclinic $TiO_2(B)$ ($\beta = 107°$).
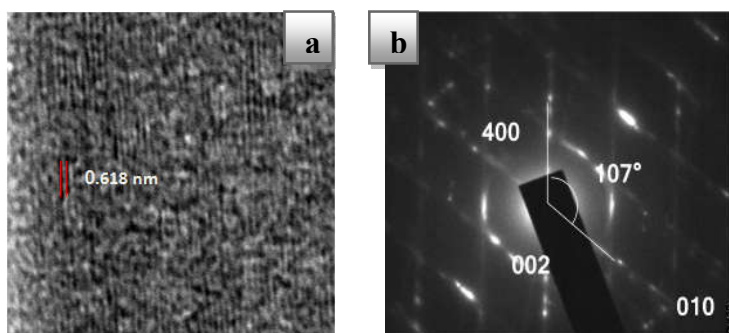


**Figure 32.** HRTEM images and SAED pattern (b) of Titania nanobelt

## 3.4.7 Dynamic Light Scattering Analysis

A narrow distribution of particle size was observed for nanobelts of titanium dioxide. The zeta potential value and poly dispersity idex was was found to be -43.75 mV and 0.673 respectively. These values of titania nanobelt indicates considerable stability of the dispersion medium.
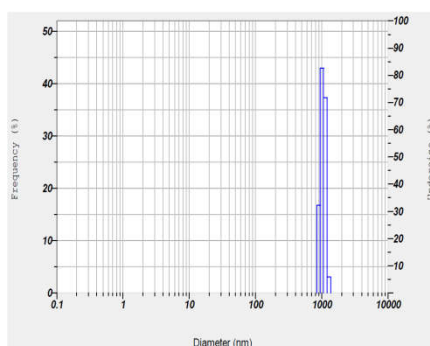


**Figure 33.** Histograms of the titania nanobelt size distributions

## 3.4.2 Xray diffraction pattern

The XRD pattern is obviously different from those of $TiO_2$ anatase and rutile forms. Peaks at 14°, 25°, 28.5°, 33.2°, 44°, 48.2° and 57.5° corresponding to (001)/(200), (110), (002), (310), (003), (020) and (022) planes of $TiO_2$ (B) phase. As already mentioned, the $TiO_2(B)$ is a metastable interphase between $H_2Ti_3O_7$ and anatase $TiO_2$, the presence of which is already due to the shape confinement effect of $H_2Ti_3O_7$ nanobelts having a layer structure, which has a similar crystal structure with $TiO_2(B)$. $TiO_2$-B can be distinguished from the titanate structure by its broad peak of multiple planes

between 28° and 34° [64]. One of the appealing structural feature of this phase lies in the characteristic parallel channels which are running along the [010] orientation. Apart from the phase, another characteristic feature in this pattern is the increased intensity of the (020) peak at 48.6 degrees relative to that of the predominant (110) peak. This result pointed to preferential exposure of the diffractive (020) facets of $TiO_2$ (B) [65]. It has been reported that Anatase peaks are observed when the calcination temperature are raised above 400°C [66-67]. The said fact is obvious from Figure 33b, that the peaks are clearly assigned to that of anatase when the calcination tempearture was raised to 700°C. This indicates that the crystal phase can be tuned by chosing appropriate calcination temperatures, as per the nature of applications.
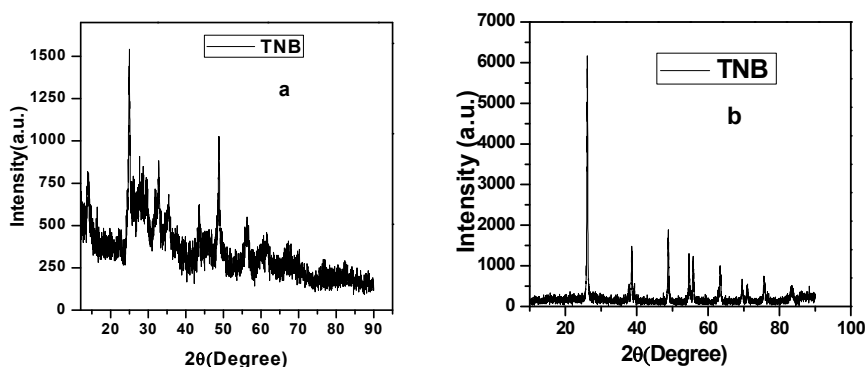


**Figure 34**. X-ray diffraction pattern of Titania nanobelt (TNB)

### 3.4.3 Raman spectroscopy

Figure 35 represented the raman spactrum of hydrothermally synthesised titania nanobelt. It can be identified that the bands at 123 cm$^{-1}$, 247 cm$^{-1}$, 195 cm$^{-1}$, 411 cm$^{-1}$, 471 cm$^{-1}$ and 640 cm$^{-1}$ are attributed to vibration of $TiO_2$ (B) [68-70]. No characteristic peaks of other phases are observed in the spectrum confirming the $TiO_2$ (B) phased nanobelt supporting the XRD data.
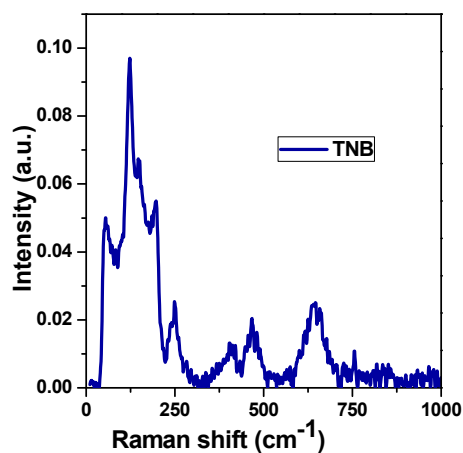


**Figure 35**. Raman spectrum of titania nanobelt (TNB)

### 3.4.4 UV-Visible absorption spectrum and Kubelka munk plot

Figure 36a displayed the UV-Visble absorption spectrum of titania nanobelt. The absorption spectrum of titania nanobelt is also seen in the UV region. The band gap value is calculated by the extrapolating the the curve (Figure 36 b.) to X axis. The value is

observed to be 3.07 eV which is indeed lower than the anatse titania (3.12 eV).
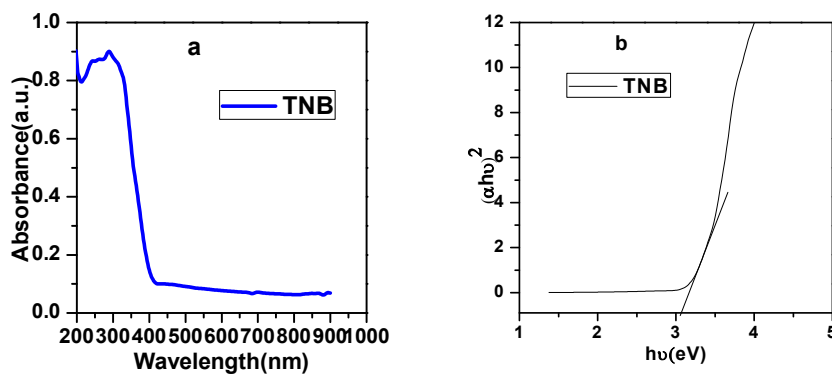


**Figure 36**. UV-Visible absorption spectrum (a) and Corresponding Kubelka-Munk plot (b) of TNB

### 3.4.5 Fourier Transform Infra Red Spectroscopy

The FTIR spectrum (Figure 37) shows band characteristic of OH groups at ~3400 and 1620 cm$^{-1}$. They are corresponding to OH stretching vibrations and and physically adsorbed water molecules respectively [71]. This indicated the presence of large amount of water as well as hydroxyl groups in the system. Sharp peaks at $v =$ 500 cm$^{-1}$ and $v = 900$ cm$^{-1}$ were attributed to the stretching of Ti–O found in the nanostructure.
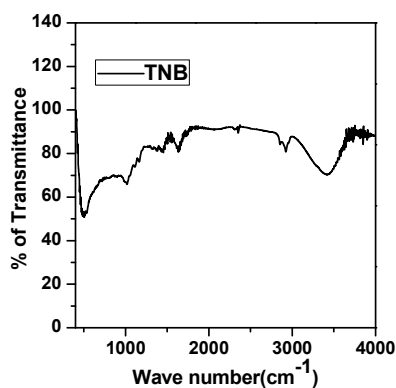
**Figure 37**. FTIR Spectrum of TNB

## 3.4.6 Nitrogen adsorption desorption studies and BET surface area analysis

Nitrogen adsorption/desorption analysis (Figure 38a) was used to characterize the surface data of synthesised $TiO_2$ (B) nanobelts. Adsorption isotherm is of type II with a very thin hysteresis loop which is indicative of a microporous/non-porous material. It is noteworthy that hysteresis loop in materials was not closed and the two branches are nearly parallel over a wide range of relative pressures especially the desorption curve is very close to that of the adsorption at very low relative pressures. The very low difference in the desorption step is not significant to be considered as a different behavior in nitrogen desorption. The low pressure hystersis can be assumed to be due to the presence of micropores [72]. The hystersis loop was identified to be of H4 type, characteristic of slit like micropores and mesopores. The BET surface area calculated for titania nanobelt is found to be 47.634

$m^2/g$. The surface area was quadrupled after the hydrothermal treatment of precusor titania (10.27 $m^2/g$). The BJH pore distribution curve (Figure 38 b) revealed that some pores are within the range 5-12 nm with mean peak value at 9nm. These pores might have resulted due to the aggregated single sheets coming together during nanobelt formation. Another set pores in the range 3-5 nm is attributed to the porous nature of nanobelt. There pores confirmed the presence of small mesopores within the nanobelt. The pore volume was calculated to be 0.057 $cm^3/g$. After nanobelt formation, the pore size is observed to be smaller than that of the precursor titania (about 3.58 nm), while the surface area is commentably increased.
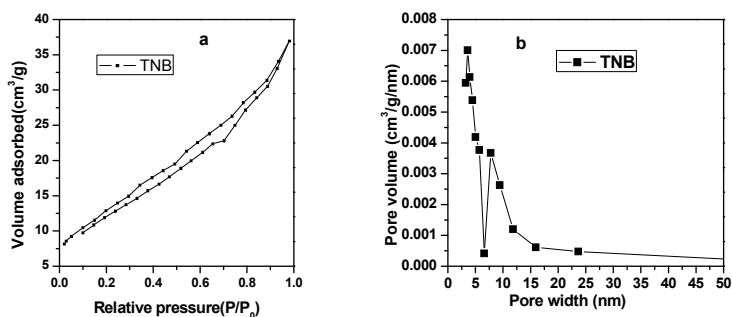


**Figure 38**. Nitrogen adsorption desorption isotherm (a) and BJH pore distribution curve (b)

### 3.4.8 Formation mechanism of TiO$_2$ (B) Nanobelts

The concentration of NaOH , reaction temperature, time, calcination temperature etc, all have decisive role in the formation of nanobelts. At hydrothermal temperature of $200^{\circ}C$ anatase

Titanium dioxide reacts with alkali to produce titanate nanoparticles [$M_2Ti_nO_{2n+1}$] having monoclinic lattice. The morphology largly depends on the hydrothermal reaction temperature at this stage as 110-150°C temperature yields titania nanotubes and higher temperatures yiled nanorods/nanobelts [73]. At high reaction temperatures, the fast rection of titania in alkaline solution results in titanate nanoparticles which grew along certain planes forming single layered nanobelt. The superposition of these single layered nanobelts resulted in the large titanate nanobelts. The specific orientation of grains to form belt/sheet like structure and its superpositions are evident in TEM images shown below.
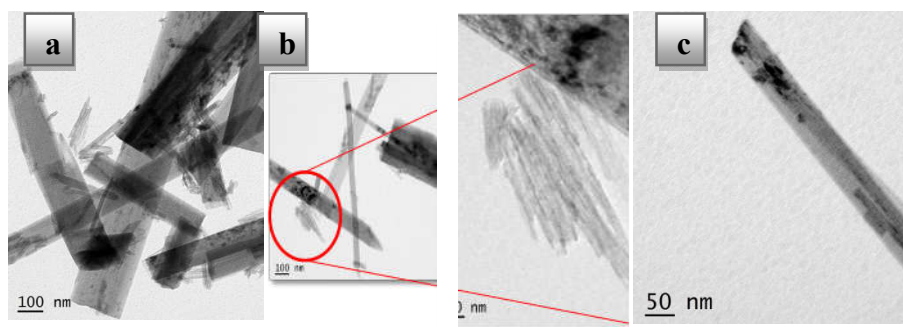


**Figure 39**. TEM images showing the proper allignment of titanate particles to form belt lie structure and its superpositions

The single layer titanate belt formed superpose each other , exchanging Na$^+$ ions with H$^+$ ions to form hydrogen titanate when they are treated with acid. The crystal structure of sodium titanate and hydrogen titanate with $TiO_6$ octahedra sharing edges to from belt like structure is shown below [Figure 40]. The blue dots

represents sodium and green dots represents Hydrogen. Since both of these titanate have similar structure, the acid washing step never alters its morphology. Calcination process dehydrates the titanante structure to form $TiO_2$ (B) nanobelts.
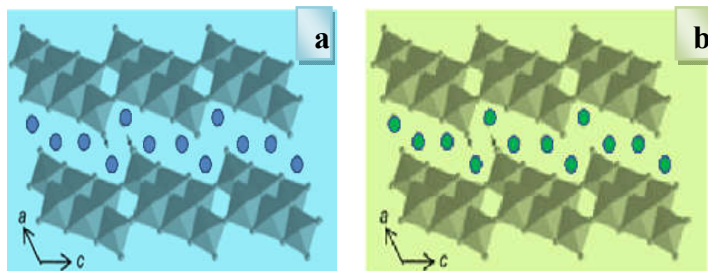


**Figure 40**. Crystal structure of Sodium Titanate (a) and Hydrogen titanate (b) where blue dots represents sodium ions and green dots denotes Hydrogen.

$TiO_2$ (B) is known as the metastable interphase between $H_2Ti_3O_7$ and anatase. As $TiO_2$ (B) possesses the same monoclinic crystal structure with the similar lattice structure along the c axis, the conversion of titanate to $TiO_2$-(B) phase takesplace with lower transformation energy. Similarly in the two phases namely anatase and $TiO_2$-B, former contains chains of edge-sharing octahedral in one orientation whereas the other polymorphs have chains in two orientations. $TiO_2$-B and anatase are thus structurally related. Therfore its easy transformation to anatse is readily observed at higher calcination temperatures which has been confirmed by the XRD pattern in Figure 33b. But coexistence of mixed phase anatase and $TiO_2$ B, with anatse as major portion are proven to be benficial

for photocatalysis [74-75]. When the calcination temperature is about 800°C, the titania nanobelt collapse to nanorods or cylindrical nanoparticles. [62].

## 3.5 Titania nanoparticles [TNP]

The procedure for the synthesis of titania nanoparticle have been discussed in section 2.3.5. The characterisation results are discussed in the following sections.

### 3.5.1 Electron microscopy analysis

The SEM images (Figure 41a) revealed nearly spherical nanoparticles in the range 20-30nm size. Agglomorated nanoparticles are observed from the TEM images. 15-20 nm particles are perceived from the TEM images (Figure 41b). Bigger nanoparticles observed may be due to the agglomeration of individual units. The SAED pattern (Figure 41c) reavealed the polycrystalline nature of the sol-gel derived nanoparticles.
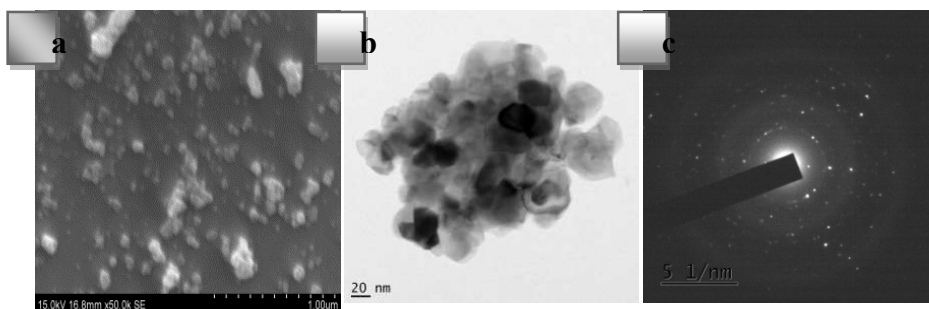


**Figure 41.** SEM , TEM, Electron Diffraction pattern of titania nanoparticle

Figure 42 represented the high resolution TEM images of the nanoparticle from different regions. The lattice fringes observed from the HRTEM images revealed the interfringe spacing of 0.352nm [(101) plane] and 0.32 nm [(110) plane] , which are identified to be that of anatase and rutile phase of titanium dioxide nanoparticle respectively.
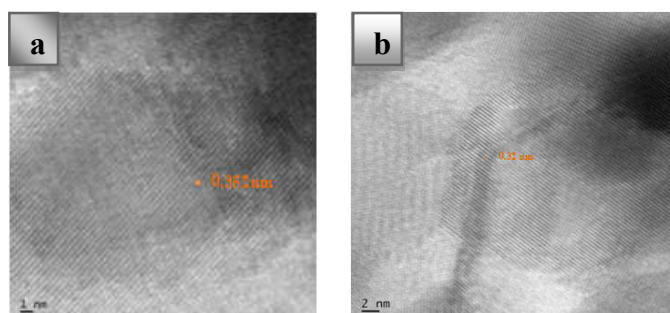


**Figure 42**. High resolution TEM images of synthesised titania nanoparticle

### 3.5.2 Dynamic Light Scattering analysis

Figure 43 represented the histogram showing the wide ranged particle size distribution of synthesised titania nanoparticle. The zetapotential value was found to be -43.75, exhibitng a considerable stability of dispersion medium.The poly dispersity index value was 0.416.
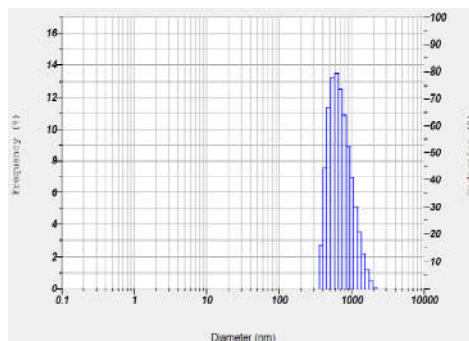
**Figure 43.** Particle size distribution curve of titania nanoparticle

### 3.5.3 X-ray diffraction pattern of Titania nanparticle

The XRD peaks are observed at 25.3(101), 37 (112), 48.1(200), 53.9(105), 55.1(211), 62.7(204), 68.8(116),70.3(220), 75.1(215) degrees. These correspond to diffraction peaks of anatase phase $TiO_2$. Anatase peaks are dominant in the crystal structure however some rutile peaks are also observed in the XRD pattern.
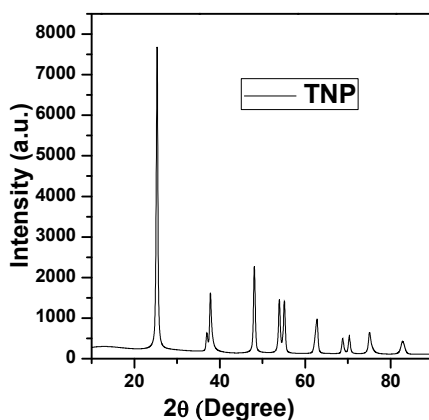


**Figure 44.** X-ray diffraction pattern of titania nanoparticle

### 3.5.4 Raman spectrum

In the raman spectrum of nanoparticle (Figure 45) , bands are observed at 144 $cm^{-1}$, 197 $cm^{-1}$, 396 $cm^{-1}$, 516 $cm^{-1}$ and 641 $cm^{-1}$ which emphasised the observation related to the Anatse character of the synthesised material, thus supporting the data observed from the XRD pattern revealing the crystal phase.
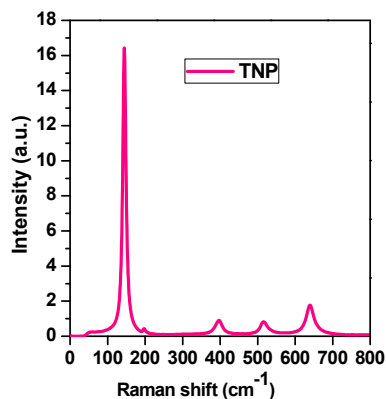


**Figure 45.** Raman spectrum of Titania naoparticle

### 3.5.5 Fourier transform infra red spectroscopy

FTIR spectrum of synthesised sample after calcination at $500^{\circ}C$ has been represented in figure 46. Peak at 3112 $cm^{-1}$ corresponds to the –OH streching vibration and that near to 1440 $cm^{-1}$ is due to O-H bending vibrations of water.Ti-O vibrations are observed at near 400-700 $cm^{-1}$ which are attributed to Ti-O stretching and Ti-O-Ti bridging stretching modes [76].
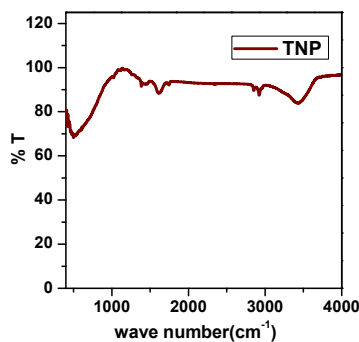
**Figure 46.** FTIR Spectrum of Titania nanoparticle

### 3.5.6 UV-Visble absorption spectrum and Kubelka-Munk plot

The UV-Visble absorption spectrum of titania nanoparticle has been shown in the figure 47 (left). The major absorption is in the UV region and adsorption edge slightly extending to visible region.The kubleka munk plot (Right) shown in figure give the band gap value as 3.1 eV  equivalent to 397 nm.
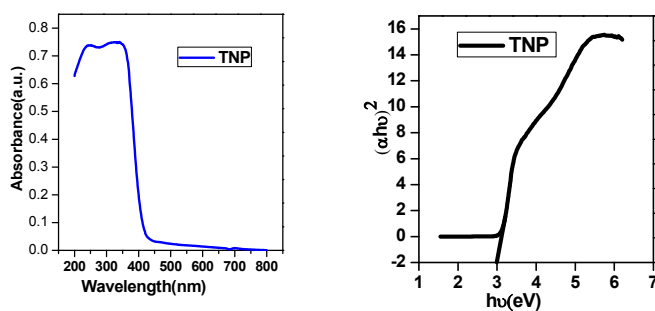


**Figure 47.** UV-Visible absorption spectrum (Left) and Kubleka-Munk plot (Right) of Titania nanoparticle

### 3.5.7 Nitrogen adsorption studies and B.E.T Surface area analysis

Nitrogen adsorption desorption isotherm and corrresponding BJH pore distribution curve are shown in Figure 48.The isotherm is of type V with H1 hystersis loop in the relative pressure region 0.4-0.9 (Left). A narrow pore size distribution is observed from figure 48 (Right). Pores had size in 3.4-14.9 nm with mean peak value at 7.9 nm. The BET surface area value is found to be 22.29 $m^2$/g. Single point adsorption total pore volume is 0.066726 cm³/g.
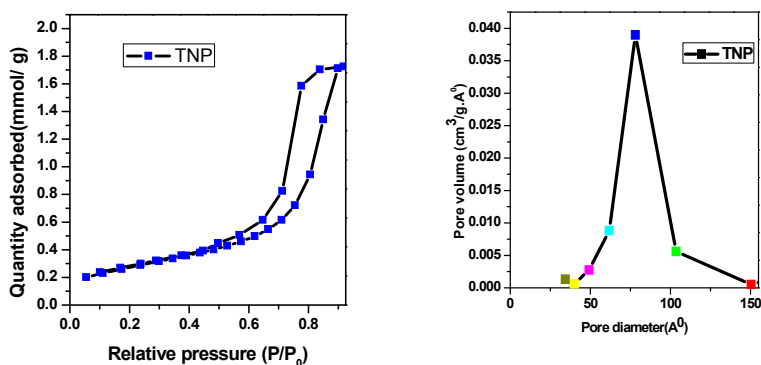


**Figure 47.** Nitrogen adsorption desorption isotherm (Left) and BJH Pore distribution curve (Right) of TNP

# References

1.  Y. Wang, Q. Zhu and H. Zhang, Chem. Commun., 2005, 41, 523.

2.  .HLiu, .YXu, .SWen, .JZhu, .LZheng, .MShen , .G ,Zhao .J ,Shi.Zhang and XPolym. Chem. 2013 ,4 ,1788.

3.  .H Cai, .XAn, .JCui, .JLi, .SWen, .KLi ,Zheng.L ,Shen.M ,Shi .Zhang and X.GACS Appl Mater Interfaces 2013 ,5 ,1722.

4.  ,Sarmento .Pintado and B .M ,Ferreira .D ,Silva .Da .B.S .2016,112 ,84,.Macromol.Biol.J.Int

5.  S. Liu, X. Sun, J. Li, X. Li, Z. Xiu and H. Yang, Langmuir, 2010, 26, 4546.

6.  L. Diamandescu, F. Vasiliu, D. Tarabasanu-Mihaila, M. Feder, A. M. Vlaicu and C.M. Teodorescu, Mater. Chem. Phys. ,2008 ,112 , 146.

7.  A.B. Murphy, Sol. Energ Mater. Sol C ,2007 ,91, 1326.

8.  J. G. Yu, J. C. Yu, M. K. P. Leung, W. K. Ho, B. Cheng, X. J. Zhao and J. C. Zhao, *J. Catal.* 2003, 217, 69.

9.  J. Yu, W. Liu and H. Yu, Cryst.Growth.Des. 2008, 8,930.

10. J.G. Yu, J.C. Yu, W.K. Ho, M.K.P. Leung, B. Cheng, G.K. Zhang andX. Zhao, J. *Appl. Catal., A* 2003, 255, 309.

11. J. Yu, W. Liu and H. Yu, Cryst.Growth.Des., 2008, 8, *930.*

12. S. Liu, J. Yu and S. Mann, Nanotechnology, 2009, 20, 325606.

13. Z. P. Xu and H. C. Zeng, Chem. Mater., 1999, 11, 67.

14. H. C. Zeng, Curr. Nanosci., 2007, 3, 177.

15. X.X. Yu, J.G. Yu, B. Cheng and M. Jaroniec, J. Phys. Chem. C, 2009, 113, 17527.

16. H. Sun, L. Wang, D. Chu, Z. Ma and A. Wang, Mater.Lett., 2015, 140, 35 .

17. A. Pan, H.B. Wu, L. Yu and X.W. Lou, Angew. Chem. Int. Ed. 2013, 52, 2226.

18. H. G. Yang and H. C. Zeng, J. Phys. Chem. B 2004, 108, 3492.

19. S. Shang, X. Jiao and D.Chen, ACS Appl. Mater. Interfaces 2012, 4, 860.

20. F .A. Cary, andR .M. Giuliano ,Organic chemistry, Mc Grow Hil, 2011, 8th edition , Newyork.

21. D.P. Woodruff, The chemical physics of solid surfaces, Elsevier, 2001, 9, Amsterdam, The Netherlands, **ISBN:** 9780444601308.

22. D. R. Rolison, *Science*, 2003, 299, 1698.

23. L. Zhang and J. Yu, Chem. Commun., 2003, 16, 2078.

24. Y. D. Wang, C. L. Ma, X. D. Sun, andH. D. Li, Mater. Lett. *,* 2002 ,54 ,359.

25. T. Y. Peng, A. Hasegawa, J. R. Qiu and K. Hirao, Chem. Mater. *,*2003 ,15 ,2011 .

26. K. S. W. Sing, D. H. Everett, R. A. W. Haul, L. Moscou, R. A. Pierotti, J. Rouquerol and T. Siemieniewska, Pure. Appl. Chem., 1985, ,57 603.

27. N. Dongthanh, W. Wei, L. Haibo and R. U. Hongqiang , Front. Mater. Sci. ,2016 ,10 ,23.

28. S. Zhongliang, Y. Xingman *and* Y. Shuhua, J. Rare. Earth. *,*2012 *, ,30*355.

29. Q. Sheng,Y. Cong, S.Yuan, J. Zhang and M. Anpo, Micropor.Mesopor.Mater.,2006,95 , 220 .

30. Y. Zhang, H. Zhang, Y. Xu and Y. Wang, J. Solid State Chem.,2004 ,177 ,3490.

31. J. Yu, J.C. Yu, M.K.P. Lueng,W. Ho, B. Cheng, X. Zhao and J. Zhao, J. Catal. ,2003 ,217 ,69.

32.  J.C. Yu, J. Yu, W. Ho and L. Zhang, Chem. Commun. ,2001 ,19 , 1942.

33.  Y. Zhang, A. Weidenkaff and A. Reller, Mater. Lett. ,2002 ,54 , 375.

34.  Y.V.Kolen'ko,V.D. Maximov, A.V. Garshev, P.E. Meskin, N.N. Oleynikov and B.R. Churagulov, Chem. Phys. Lett. ,2004 ,388 , 411.

35.  Y. Jiaguo Yu, L. Jingxiang, X. Wei, Z. Peng and J. Mietek, J. Am. Chem. Soc. ,2014 ,136 ,8839.

36.   N. Roy, Y.  Sohn and D .Pradhan, ACS nano ,2013 ,7 ,2532.

37.  Z. Xiaowei , J. Wenzui , C. Jinguang, Y. Jianfeng, L. Zhenhu, M. Yurong *and* L. Jinglin Xie *,*Adv. Funct. Mater.  ,2011 ,21 ,3554.

38.  J. L. Woo and M. S. Yun, Cryst. Growth Des.,2012 , 12 ,5792.

39.  G. Soler-Illia, A. Louis and C. Sanchez, Chem. Mater.  ,2002 ,14 , 750.

40.  M. Liu and H. Yang, Colloids Surf., A *,2010 ,*371,126.

41.  K. Zhang, Z. Fu and T. Nakayama, Mater. Res. Bull.  *,2011 ,*46 *,* 2155–2162.

42.  W. Donghai, L. Jiu, H. Qisheng, N. Zimin, L. Weigang, E. W. Rick and J. Ying Bing, J. Am. Chem. Soc.,2006 , 128 ,13670.

43.  Y. X. Gao, S. H. Yu, H. Cong , J. Jiang, A. W. Xu, W. F. Dong andH. Colfen, J. Phys. Chem .B.*,2006 ,* 110 ,6432.

44.  C. Gao, W. Zhang, H. Li, L. Lang and Z. Xu, Cryst. Growth Des.  ,  ,2008 8 ,3785.

45.  G. Wang, L. Zhang, H. Dai, J. Deng, C. Liu, H. He and C.T. Au, Inorg. Chem.,2008 , 47 ,4015.

46.  G. Calleja, D. P. Serrano, R. Sanz, P. Pizarro and A. Garcı´a, Ind. Eng. Chem. Res. ,2004 , 43 ,2485.

47.     L. Kesong, Z. Milin, S. Keying and F. Honggang, Mater. Lett. , 2005, 59, 3308.

48.     H. Yu, J. Yu, B. Cheng and J. Lin J. Hazard. Mater., 2007,147, 581.

49.     G.H. Du, Q. Chen, R.C. Che, Z.Y. Yuan, andL.P. Peng, Appl. Phys. Lett. ,2001 ,79 ,3702.

50.     ,Chattopadhyay .K.Ghosh and K .K.C ,Maiti .N.U ,Sarkar .D .6,127 ,2012 ,.Lett.Sci.Adv

51.     .C Liang.J , He,.Y Xiang,.P Gao,.J Fang, .J Zhao, .and W Shen, Synth. React. Inorg. Met.-Org. Nano-Metal Chem. 2009, 39, 480.

52.     .SMozia, .EBorowiak-Paleń,.J Przepiórski, B. Grzmil, T. Tsumura, M. Toyoda, J. Grzechulska-Damszel and A. W. Morawski, J Phys Chem Solids ,2010 ,71 ,263.

53.     M. N. Subramaniam , P. S. Goh , N. Abdullah , W. J. Lau , B. C. Ng and A. F. Ismail ,J. Nanopart. Res ,.2017 ,19 ,220.

54.     S. J. Gregg and K. S. W. Sing, Adsorption, Surface Area and Porosity, 2nd edn., Academic Press, London, 1982.

55.     .TKasuga, .M Hiramatsu,.A Hoson, .T Sekino .and K Niihara, Adv. Mater. ,199911, 1307.

56.     .S.SLiu,.K.C Lee,.C.H Chen,.C.C Wang.C.and L Juang, Chem. Eng. J. ,2009,147, 188.

57.     .Q.YWang,.Q.G Hu, .F.X Duan,.L.H Sun.K.and Q Xue, Chem. Phys. Lett. ,2002 365, 427.

58.     Y.F. Chen, C.Y. Lee, M.Y. Yeng and H.T. Chiu, Mater. Chem. Phys. , 2003, 81 , 39.

59.     .GArmstrong,.R .A Armstrong, .JCanales and .G.P Bruce , Chem. Commun*.,* 2005, 19, 2454.

60.     Jr .EMorgado,.S.A.M Abreu, .T.GMoure, .A.BMarinkovic, .M.PJardim and .S.AAraujo ,*Mater. Res. Bull.,2007 ,* 42 1748.

61.     E. Morgado Jr, P. M. Jardim, B. A. Marinkovic, F. C. Rizzo, M. A. de Abreu, J. L. Zotin and A. S. Araujo, Nanotechnology, 2007, 18, 495710.

62.     D. Wang ,F .Zhou ,C. Wang and W. Liu, Microporous and Mesoporous Mater ,2008 ,.116 ,658.

63.     L .Cui, F .Huang, M. Niu, L. Zeng, J .Xu and Y. Wang ,Journal of Molecular Catalysis A: Chemical,2010 , 326 ,1.

64.     W. A. Daoud, and G. K. H. Pang ,J. Phys. Chem. B, 2006, 110, 25746 .

65.     G. Xiang, T. Li, J. Zhuang and X. Wang, Chem. Commun., 2010, 46, 6801.

66.     R. Yoshida, Y. Suzuki and S. Yoshikawa, J. Solid State Chem., 2005, 178, 2179.

67.     T. P. Feist and P. K. Daviest, J. Solid State Chem., 1992, 101, 275 .

68.     K. Yamamoto, K. Tomita, K. Fujita, M. Kobayashi, V. Petrykin and M. Kakihana, J. Cryst. Growth, 2009, 311, 619.

69.     Y. V. Kolen'ko, K. A. Kovnir,  andA. I. Gavrilov  A.V. Garshev, J.  Frantti, O.I.  Lebedev, B.R.  Churagulov, G.  Van  Tendeloo and M. Yoshimura., J. Phys. Chem. B,,2006  110, 4030.

70.     W. Zhou, L. Gai, P. Hu, J. Cui, X. Liu, D. Wang, G. Li, H. Jiang, D. Liu, H. Liu and J. Wang, CrystEngComm, 2011, 13, 6643.

71.      .RWang,   .KHashimoto,.A   Fujishima,.M   Chikuni,  .A.E Kojima, .A Kitamura,  .MShimohi-goshi and  .TWatanabe, Adv. Mater ,1998,10 ,135.

72.     F. Collet , M. Bart, L.Serres and J. Miriel ,Construction and Building Materials  ,2008 ,22 ,1271.

73.     L. Kavan, M. Kalbácˇ, M. Zukalová, I. Exnar, V. Lorenzen, R. Nesper, M. Graetzel, Chem. Mater.,2004 , 16 ,477.

74. D.J. Yang, H.W. Liu, Z.F. Zheng, Y. Yuan, J.C. Zhao, E.R. Waclawik and X.B. Ke, H.Y. Zhu, J. Am. Chem. Soc. 2009, 131, 17885.

75. Y. Chimupala, P. Junploy, T. Hardcastle, A. Westwood, A. Scott, B. Johnson and R. Brydson, J. Mater. Chem. A, 2016, 4, 5685.

76. .M.APeiro, .J Peral,.C Domingo, .X Momenech.A.and J Ayllon, Chem. Mater. 2001, 13, 2567.

# CHAPTER IV
# PHOTOCATALYTIC APPLICATIONS OF TITANIA NANOSTRUCTURES

*Industrialisation and population growth not only resulted in the world wide environmental pollution but also in the energy crisis for present an upcoming generations. Thus, emergence of new and renewable technologies for environmental pollution remediation and energy production is highly welcomed at this stage. If the developing technologies rely on principles which never futher secondary pollute the nature by adopting environmentally friendly and inexpensive materials it is a boon to mankind. In this direction, semiconductor mediated photocatalysis mainly using Titania is found to be successful in meeting the requirements of energy and enivronmental issues.*

# CHAPTER IV
# SECTION A

## 4.1 TITANIA NANOSTRUCTURES FOR ENVIRONMENTAL CLEAN-UP

**Part 1. Photocatalytic activity of synthesised nanostructures for the removal of organic pollutant**

**Part 2- Antimicrobial activity of titania based nanostructures**

**CONTENTS**

*Semiconductor based photocatalytic process has been considered as the sustainable technology which is adorable due to its low cost, easy availability, environmentally friendliness with the "zero" waste scheme in the water/wastewater industry. For years this technology has been clearly proved its ability to remove a series of persistent, harmful organic compounds and microorganisms in environment. Manipulation of factors like morphology, crystal phases, surface area, exposed crystal facetes etc affects its photocatalytic activity to an considerable extent. Recently the beginning of a new era utilising the superhydrophillic property of photocatalysts for fabrication of self cleaning devices have been marked. Titania with its excellent photocatalytic ability to remove pollutants along with light induced superhydrophilicity is certainly an elite member in this series. This chapter presents a comparison of photocatalytic, antimicrobial activity studies of synthesised nanostructures and superhydrollic nature to be used for self cleanng applications.*

# Part 1. Photocatalytic activity of TiO$_2$ nanostructures for the removal of organic pollutant

In this section we have investigated the photocatalytic activity of titanium dioxide nanostructures taking methyleneblue as a target pollutant. The mineralisation was further confirmed by chemical oxygen demand analysis.The detailed experimental procedure is provided in chapter.

## 4.1.1 Introduction

The demand of clean water resources is increasing in an alarming rate nowadays. It has been found that global consumption of water is more than twice the rate at which the population is growing. The shooting up of industrialisation corresponding to the requirements of increased population and the long term drought due to the deforestation are some of the reason for the scarcity of clean water resoures. The major pollutants include chlorinated and nonchlorinated aromatic compounds, dyes, pesticides, insecticides, pharmaceuticals, detergents, toxic heavy metals etc; Bunch of works have been done in this direction to remove these contaminants using titanium dioxide photocatalysts.

Among these, Organic dyes constitute a major part of many industries producing materials for our day to day life ranging from textiles, paper, leather industries, furniture, plastics, carpets, rubbers etc [1]. These dyes colour their products consuming considerable volumes of water therefore, the generated wastewater will be certainly

coloured. The perception of water quality is greatly influenced by the color and it is the first contaminant to be recognized in wastewater [2] . The occurrence of very small amounts of dyes in water even less than 1 ppm is highly visible and undesirable [3]. India's Textile and Apparel industry is one of the oldest industries in Indian economy dating back several centuries. After agriculture, it is country's second largest employer providing direct employment to over 45 million people, 14 percent contributor to overall Index of Industrial Production (IIP), 4 percent to GDP (Gross deomestic product), 14 percent to export earnings. India is the second largest producer of cotton in the world and produces 23 percent of the world's total cotton production. The enormous amount of waste water generation is   naturally an anticipated result. Textile industry wastewater is needed to be treated due to the incomplete fixation of synthetic dyes during the dyeing process. 1-20 % of globally produced dyes are discharged in to the the water resources [4]. Some dyes itself are made from carcinogens and the production of toxic and carcinogenic by products in waste water phase caused by the weathering of some dyes[oxidation, hydrolysis and other chemical reactions] [5]. Baughman and et al reported that there are dyes which are made from known carcinogens such as benzidine and other aromatic compounds [6]. Chung et al. [7] illustrated the reduction of dyes in the intestinal environment, forming toxic amines, thus imparting its adverse effects on animal and human health. They may cause irritation to the skin, eyes and systemic effects including cyanosis, blood changes etc. An imbalance in ecosystem is observed in the aquatic environment in presence of these dyes (less than 1ppm for some dyes)   which blocks the water transprency,

sunlight penetration and oxygen dissolution [8-10]. Moreover, it cause adverse effects on the food source of aquatic lives as the photosynthetic activity of aquatic flora is affected by the presence of these dyes. As the solubility of dissoved oxygen is reduced, biological oxygen demand and turbidity increases and results in the complete destruction of food web in that particular region [11-12]. Resolving this problem not only relys on strict environmental legislations regarding the use of these dyes and the conservation of water resources, but also recovers the clean water from polluted water and sludege by proper treatment programms before they are admitted to the environment. Still, wastewater containing dyes is very difficult to treat, as these recalcitrant organic molecules are resistant to aerobic digestion, stable to light and temperature etc; [13]. In this direction, devising advanced materials for the development of newer technologies for viable environmental clean up has attracted tremendous attention.

Many techniques are practiced from years for recovering clean water. The most wdely used methods in this direction can be categorized as chemical, physical, biological. Physical methods included adsoption using activated carbon, peat, woodchips,silicagel, clay,ricehulls, flyash, other methods like membrane filtration, ion exchange, irradiation, electrokinetic coagulation etc;. Chemical methods are oxidative process like ozonation, fentons reagent, sodium hypochlorite, Cucurbituril, photochemical, electrochemical destruction, Some are filtration, sedimentation, adsoption or coagulation, nanofiltration, ultra filtration, active sludege biochemical

process, chemical precipitation, chlorination etc. Biological treatments are also availble which in liquid state fermentations, sometimes is incapable of removing dyes from sewage on a continuous basis due to the more time period required for decolourisation processes. The limitations of these techniques being, use of high cost materials, inability to completely eliminate the targets, most often reults in secondary pollution releasing mutagenic byproducts in to the environment which are needed to be further processed. For example commonly used method, adsorption and chemical coagulation do not result in dye degradation and the waste disposal problem persists. On the otherhand, the chemical oxidation treatments are found to be effective towards the demolition of chromophoric composition of dyes. Still a complete mineralization is not achieved. Chlorination and ozonisation effect decolorization through chemical reactions. But the most contraversial effect being the by-products of chlorination ie; chlorinated organics are more toxic even compared to the dye itself [14-15]. Another method is treatment with ozone included its instability, expensive nature, and its hazardous nature due to strong and non-selective oxidizing power. So a post treatment destruction unit is needed to put a stop to the unreacted ozone which escapes. Nowadays, due to the large degree of aromatics inherent in dye molecules and stability of modern dye, the above said treatments are found to be less effective for decolorization and mineralization [16]. As the textile industries are forced to treat their effluents before bumping in to the environment by the strict government legislations, developing technique which is cost effective, simple, and effective without producing any secondary pollution is highly desirable [17-19].

In this direction, advanced oxidation process (AOP) is one of most promising innovative water treatment technology which can provide almost total degradation of a wide range of organic compounds which are resistant to conventional technologies. Various agents used in AOP techniques include i) Ozone [20] ii) Hydrogen peroxide [21] iii) Photolysis [22] iv) Photocatalysis and v) Sonolysis [23]. A common feature shared by all these AOP s included the generated hydroxyl radical which has higher oxidation potential of 2.80 eV related to the oxidants like hydrogen peroxide (1.78 eV) atomic oxygen (2.42 eV) etc; [24]. The above said oxidants are usually most effective with UV light in order to enhance the degradation process. These •OH trigger sequence of reactions to break down the bigger pollutant molecules into smaller and less harmful products. Easy operating conditions and the production of less reiduals made this technique more popular among various quarters of scientific community.

Among these AOP's heterogenous photocatalysis using semiconductor metaloxides can be used to degrade a range of pollutants which mineralise them to less harmful products. And this technique is characterised by the generation of superoxide and hydroxyl radicals($OH^-$) produced by the catalysts up on irradiation. Photocatalysis in general is thought of as the catalysis of a photochemical reaction at a solid semiconductor surface [25-26]. This technology has potential to be used for degradation and mineralisation of of various organic pollutants, for air [ $NH_3$, CO etc] water purification, degradation of waste plastics, green synthesis of industrially important chemicals.

## 4.1.2 Working principle of Photoctalysis for pollutant removal

The basic steps involved in heterogenous photocatalytic process include i) Transfer of the reactants in the liquid phase to the surface of catalyst ii) adsorption of the reactant on the catalyst surface iii) The photocatalytic reaction in the adsorbate phase iv) desorption of the products from the catalyst surface v) removal of the products to the liquid phase.

When UV light with energy greater than the bandgap of titanium dioxide, falls on its surface of the catalyst, electrons are excited from valence band to the conduction band creating a pair of negatively charged electrons and positively charged holes in conduction band and valence band respectively. These migrated electron- hole pairs have strong reducing and oxidising ability. The electrons react with surface bound water to produce hydroxyl radicals. whereas holes produce superoxide radical on reaction with oxygen molecules adsorbed on the surface. These reactive species carry out the oxidation reduction reactions. Figure 1 represented the mechanism of photocatalysis.
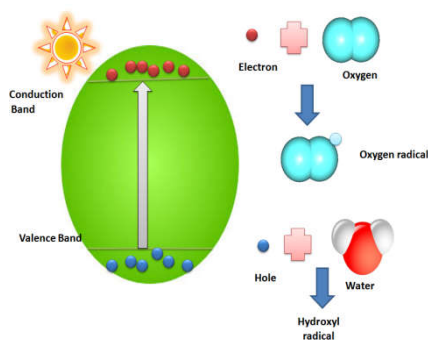


**Figure 1.** Mechanism of a semiconductor mediated photocatalysis up on UV irradiation

This photocatalytic dye degradation mechanism is possible in the presence of dissolved oxygen and water molecules which are responsible for the formation of reactive hydroxyl radicals. The suggested mechanistic pathways for a given photocatalytic reaction are named as direct and indirect photocatalytic pathways. Two different approaches have been suggested for direct photocatalytic pathway mechanism: (i) Heterogeneous photocatalysis—the Langmuir–Hinshelwood process ii) The Eley – Rideal process. In the former case, the production of electrons and holes produced by the photoexcitation of the catalyst are taken into account. The hole produced is trapped by the adsorbed dye molecule on the catalyst surface to form a reactive radical state which can decay as a result of recombination with an electron. The catalyst is regenerated in the process. The Langmuir–Hinshelwood (L–H) equation can be expressed as follows

$$1/v = 1/k_r + 1/(k_r k_a C)$$

Where $v$ is the reaction rate for the oxidation of reactant (mg/L min), $k_r$ is the specific reaction rate constant for the oxidation of the reactant (mg/L min), $k_a$ is the equilibrium constant of the reactant (L/mg) and C is the dye concentration. When the C ~ $C_0$, the equation can be simplified to an apparent first-order equation:

$$\ln C_0/C = kK = k_{app} \, t$$

Thus, plot with $\ln C_0/C$ versus time is a straight line, upon linear regression, the slope of which gives the constant $k_{app}$ for the first order equation. The Langmuir-Hinshelwood model describes the dependence of the observed reaction rate on the initial solute concentrations. In

Eley Rideal mechanism, upon excitation, the free charged carriers are fragmented and the holes produced are trapped by the surface defects. The surface active centers (S) can then react with the dye to form an adduct species which decompose to produce products or can recombine with electrons. The reaction scheme is represented below

$$\text{Catalyst} + h\nu \longrightarrow \text{electron} + \text{hole}$$

$$S + \text{hole} \longrightarrow S+$$

$$S^+ + \text{electron} \longrightarrow S$$

$$S + \text{dye} \longrightarrow (S\text{-}CP)^+$$

$$(S\text{-dye}) + \text{electron} \longrightarrow S + \text{Products}$$
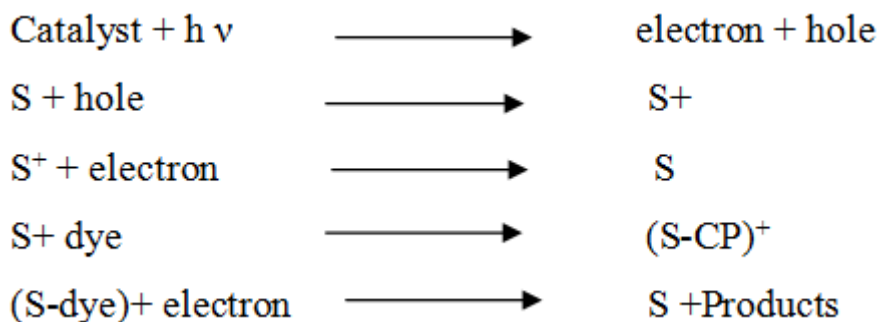
In indirect photocatalytic mechanism, electron hole pairs formed are trapped by molecular oxygen and water molecules to produce hydroxyl radicals and superoxide radicals. The hydroxyl radicals combine to form hydrogen peroxide and which attacks the dye molecules whereas the superoxide radicals also finally forms hydroxide radicals by chain reaction.

$$TiO_2 + h\nu \longrightarrow e^- + h^+$$

$$h^+ + H_2O \longrightarrow OH^\cdot + H^+$$

$$O_2 + e^- \longrightarrow O_2^{\cdot -}$$

$$O_2^{\cdot -} + H^+ \longrightarrow HO_2^\cdot$$

$$HO_2^\cdot \longrightarrow H_2O_2 + O_2$$

$$H_2O_2 \longrightarrow OH^\cdot + OH^-$$

$$OH^\cdot + Dye \longrightarrow CO_2 + H_2O$$
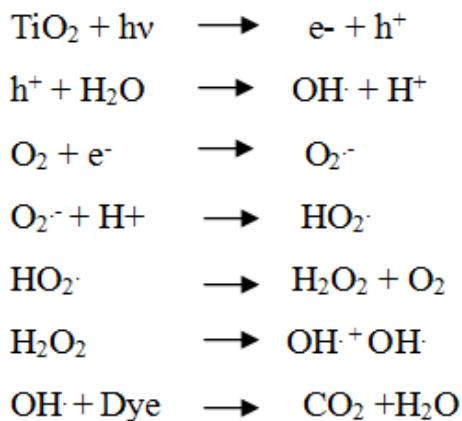
## 4.1.3 Titania based Photocatalysis for environmental clean up

A series of semiconductor photocatalysts have been explored for the photocatalytic degradation of various contaminants. $WO_3$, $TiO_2$, ZnO, $Fe_2O_3$, CdS, ZnS, $V_2O_5$, $ZrO_2$, $SnO_2$, $CeO_2$ and $Sb_2O_4$ include the explored metal oxides. Among the possible semiconductors that can be used in heterogeneous photocatalysis, Titanium dioxide, is widely accepted as the benchmark catalyst due to its inexpensiveness, environmental friendliness, photo and chemical stability, inertness etc. Demerits of many of the other photocatalysts include formation of chemically activated surface-bond intermediates, chemical and photocorrosion and degradation of catalyst during the repeated catalytic cycles. Therefore $TiO_2$ is considered to be the most suitable photocatalyst for widespread environmental applications.

Titania based photocatalysis is a widely investigated and most promising among the various dye degradation technologies due to the

complete removal of organic pollutant from waste water. It is the commonly employed and much effective process and among other Advanced oxidation processes. It is because $TiO_2$ is the most active photocatalyst in the photon energy of 300 nm< l < 390 nm, its chemical and thermal stability, mechanical properties, preservance in stability and activity after the repeated catalytic cycles [27-28]. The photocatalytic activity of titania was first reported to the world by Honda and Fujishima in 1972 through the water splitting reaction in presence of $TiO_2$ electrode. Since then identification as a photocatalyst for hydrogen production, $TiO_2$ photocatalysis drew attention of researchers and substantial efforts have been putforward in this direction. Though the reaction efficiency was high, but its absorption in the UV region was pointed as major drawback for Hydrogen production. Instead of $TiO_2$ various small band gap semiconductors were experimented which showed lower efficiency and stability. Therefore in the middle of 1980s, the enthusiasm in the research of the $H_2$ production was diminished to an extent. Instead, the research was shifted towards the light induced oxidation power of $TiO_2$ for organic pollutant removal. Frank and Bard in 1977 first reported the decomposition of cyanide in the presence of aqueous $TiO_2$ suspensions [29]. Thus studies utilising the oxidation power of $TiO_2$ for the degradation of contaminants increased to a substantial extent in the successive years. In the 1980s, detoxication studies many harmful compounds in water and air was demonstrated using powdered $TiO_2$ as potential purification methods of waste water and polluted air [30]. Later in 1987, immobilisation of $TiO_2$ powders on supports were studied in view of easy handling of photcatalysts [31].

Pruden and Ollis through different experiments demonstrated complete degradation of halohydrocarbons into $CO_2$ and HCl [32-33] Gianturco et al [34] have studied photomineralisation of dichloromethane, tetrachloroethylene, mono, di, and trichloro ethanoic acids. They found that the degradation rate of mono, di- and trichloroethanoic acids takesplace at a lower rate than tetrachloroethylene. Total organic carbon (TOC) analysis and chloride ion estimation confirmed the complete mineralisation of contaminants. Like wise, polychlorinated biphenyls which is considered as one of the twelve categories of persistant pollutant has been found to be degraded by titania based photocatalysts [35-37]. $TiO_2$ assisted photocatalytic degradation of aromatic and alicyclic (1,2-dimethoxy benzene, pyridine, morpholine and lindane) pollutants were examined by Pichat [38]. Crittenden et al [39] examined the photocatalytic removal of benzene, toluene, ethyl benzene and xylene. Ferry and co-workers studied the mechanism of photocatalytic reduction of nitro aromatics in sacrificial electron donars at the surface of titanium dioxide slurries [40]. Phenol and its derivatives constitute another major catergory of pollutant investigated in detail. Kawaguchi [41] investigated the photocatalytic decomposition of phenol using $TiO_2$ and detected hydroquinone and catechol as the main intermediates by HPLC. Carpio et al studied complete photocatalytic degradation of phenol by pellet or powder deposited $TiO_2$ on activated charcol in sunlight [42]. Phenolic compounds Chlorophenol and bisphenol A are identified as endocrine disrupting chemicals. Among the nitrophenols, US Environmental Protection Agency listed the priority pollutants 2-nitrophenol, 4-nitrophenol, and 2,4-dinitrophenol have strict recommendation for

their concentration in natural water bodies (10 ng/mL) [43]. Chiang et al found that Bisphenol A (BPA) was degraded photocatalytically by different $TiO_2$ photocatalysts and platinization was found to increase the rates of BPA degradation and mineralization [44]. Gu et al observed the photocatalytic degradation of 2,4 dichlorophenol by granular activated carbon supported $TiO_2$ and found that as the concentration of dichlorophenol increased, the removal efficiency was decreased due to multilayer of reactant molecules adsorbed on the catalyst surface preventing the contact between the molecules with photoinduced holes [45] .

Pollution due to pesticide residues are widespread and the potential chronic effects of these compounds are carcinogenesis, reproduction, neurotoxicity and effects cell development mostly in the early stages of life. Morover use of conventional oxidation processes result in the formation of mutagenic compounds. The term pesticide include herbicides, fungicides, insecticide, disinfectant, sanitizer etc; The most common of these are herbicides which account for approximately 80% of all pesticide use. Harada et al. studies the efficient degradation of Dichlorvos (2, 2-Dichloro Vinyl Dimethyl Phosphate) occurred with $Pt/TiO_2$ photocatalyst and $H_2O_2$ into $Cl^-$, $PO_4^{3-}$, $H^+$, and $CO_2$ [46]. Senthilnathan et al [47] observed the degradation of methyl parathion using $TiO_2$-P25 Degussa and $TiO_2$ doped with nitrogen, both in suspension under solar radiation. Anandan et al studies the decomposition of monochrotophos using Degussa P25 and $IO_3^-$ doped $TiO_2$ particles [48]. Malato et al. studied methamidophos decomposition on P25 titanium dioxide catalyst under

sunlight in a pre industrial pilot plant and the mineralisation was confirmed by TOC and $PO_4^{3-}$. In presence of electron scavengers, the mineralization was enhanced to 18 times related to that treated with $TiO_2$ alone [49]. The photocatalytic degradation of phenyl urea herbicide namely diuron, was carried out in the presence of platinized $TiO_2$ photocatalyst by Katsumata et al. and the rate of diuron degradation was found upon platinization along with the formation of chloride, nitrate and ammonium ions as end-products [50]. Topalov et al investigated the photocatalytic oxidation of fungicide, metalaxyl dissolved in water using $TiO_2$ and the intermediates formed were analysed by proton NMR spectra. On the basis of the TOC measurements the rate of metalaxyl decomposition can be explained in terms of the Langmuir–Hinshelwood kinetic model [51].

Matthews studied the photocatalytic degradation of coloured organics (methylene blue, rhodamine B, methyl orange and salicylic acid) using $TiO_2$ coated sand in a flat bed configuration [52]. Reeves et al investigated the photocatalytic destruction of organic dyes with solar energy and the complete mineralisation was confirmed by TOC. This work lightened the potential of utilising sunlight for semiconductor mediated photocatalysis in the removal of textile dyes from wastewater [53]. Kiwi observed that in photocatalytic degradation of anthraquinone-sulphonate dye, presence of oxygen increased the degradation efficiency and addition of hydrogen peroxide enhances the degradation rate considerably [54]. Nasr et al attempted visible light degradation of naphthol blue black (NBB) using $TiO_2$ nano particles [55]. The photocatalytic degradation of brilliant blue

dye which is biologically non degradable was completely mineralised by Ray and Beenackers in a novel photocatalytic reactor for water treatment in presence of $TiO_2$ and UV light [56]. Solar catalytic treatment of live waste water and biologically treated samples by Freudenhammer et al using non-concentrating thin film fixed bed reactor (TFFBR) suggested that in sunlight rich areas this method offers an economically viable method for treatment processes [57]. Sivekumar and Shanthi investigated the photocatalytic degradation of some textile reactive dyes (Procion Brilliant Magenta M-B(PBM), Procion Brilliant Yellow M-4G(PBY) and Procion Brilliant Orange M-2R (PBO) using different grades of $TiO_2$ and concluded that $TiO_2$ (Degussa P 25) was superior to any other grade [58]. Hasnat et al studied the visible light induced photocatalytic degradation of a cationic dye and an anionic dye, in $TiO_2$ dispersions. They pointed the necessity of adsorption and the extent of degradation was discussed in terms of the Langmuir– Hinshel wood model [59]. Belessi et al observed the photocatalytic degradation of Reactive Red 195 (RR 195) by $TiO_2$ nanoparticles and found that acidic pH promotes the electrostatic attractions between the positively charged surface of the adsorbent and anionic dye. [60].

### 4.1.4 Modifications of Titanium dioxide for better photocatalysis

Crystallinity, surface to volume ratio, manipulation of nanostructure with various modifications like porosity, its size, pore distributions etc. All these affect the photcatalytic activity of titanium dioxide in one way or in another way [61-62]. Tao *et al.*, prepared flower-like $TiO_2$ hollow spheres by the assembly of nanosheet [63]

possessed higher surface area (65 m$^2$/g) than commercial TiO$_2$ (7 m$^2$/g). Hence photocatalytic degradation of methyl orange (MO) by the flower-like TiO$_2$ hollow sphere is better than that of commercial TiO$_2$. Among the various polymorphs of titania, anatase phase is proven to exhibit higest photocatalytic activity [64-65]. It has been reported by ohtani et al that anatase titania with high degree of crystallinity and surface area significantly influence the photocatalytic activity[66]. Fabrication of photocatalysts with mixed TiO$_2$ phases have attracted significant attention, because they can exhibit much higher catalytic activity than either of its componet phases when present alone [67-68]. Construction of titania based nano architectures has significant influence in the catalytic activity of the material towards various reactions.

One dimensional nanostructures have already proved their excellence for photoctalytic activities. It has been reported by Asapu et al that compared to other powder forms, titania nanotube has higher photocatalytic activity due to its higher surface area and reduced recombination effect [69]. More or less similar conclusions were given by Hsien and shankar from their experiments [70-71] . Mozia et al reported that TNT is an excellent photocatalyst to degrade dyes, namely acid red 3B, and it can remove 98% of the dye [72]. The higher surface area rendered by the tubular structure of TNT is expected to improve the adsorption of pollutants, thus TNT is an ideal candidate for both adsorption and photocatalysis [73]. Vu et al has been reported that TNT exhibit 2.5 times higher photocatalytic activity compared to that of commercial TiO$_2$ [74]. For mixed phase TiO$_2$,

synergism between the anatase and rutile has proven to enhance photocatalysis [75]. The spatial separation of charge carriers are responsible for this higher activity. If the nanobelt is of single phase the photocatalytic activity is found to be lower, due to the presence of fewer active surface sites and higher rate of charge carrier recombination [76-78]. But Weija Zhou et al reported that $TiO_2(B)$/anatase interface heterostructure nanobelt had an enhanced photocatalytic ability comparing with pure $TiO_2(B)$ and anatase nanobelts [79], Yang et al. [80] synthesised $TiO_2(B)$ nanofibers with a shell of anatase nanocrystals and they observed that compared to pure phase or P25, they exhibited higher photocatalytic activity towards sulforhodamine B degrdation. Other one dimensional structure titania nanowire has received considerable photocatalytic research interests due to the unique and controllable electronic properties as well as the large surface-to-volume ratio. The terms "nanowhisker" and "nanofiber" are also frequently met in the literature. It has been observed that in the photocatalytic field, a continuous particle framework is beneficial for catalyst recovery when compared to separated nanoparticles [81]. mesoporous titania has received tremendous attention nowadays due to its high specific surface area and other favourable parameters for adsorption [82]. Mesocrystals, new class of nanostructured materials, built of crystallographically oriented nanoparticles [83] also has been explored. These mesocrystals have potential much higher than single and polycrystalline materials in photocatalytic field [84].

Engineering the $TiO_2$ nanostructures with specifically exposed crystal facets has established as an effective way for its photcatalytic activity enhancement. Based on this, the first report by Yang et al demonstrated the superior activity of uniform anatase single crystals with 47% {001} facets [85]. Numerous research has been devoted in this direction to tailor the morphology to get favourable $TiO_2$ facetes [86-88]. According to Han et al, due to the high density of active unsaturated Ti atoms and active surface oxygen atoms on the {001} facets, the photocatalytic activity of the facet is higher than that of {101} facets [89]. However, investigations by Jiaguo et al showed a decrease in the photocatalytic activity when an excess of {001} facets is present, and the reason was attributed to the electron overflow effect on {101} planes which is present in a small amount. The result is that the electrons are blocked within the {001} planes leading to increased charge recombination [90]. Thus the synergy of low energy {101} and high energy {001} planes is essential for an increased photocatalytic activity of $TiO_2$. The co-exposed {101} and {001} planes of anatase can form a surface heterojunction within a single $TiO_2$ particle where the {101} facets act as reduction sites and {001} facets as oxidative sites, which is beneficial for the transfer of photogenerated electrons and holes to the {101} and {001} facets, respectively. Thus the charge carriers are well separated increasing the photocatalytic performance of a system with coexposed facets [91]. The surface properties like Nanocavities which  are empty voids exposed on the surface of one dimensional $TiO_2$ nanostructured material are reported by praveen et al [92]. They have beneficial optical and electrical properties for efficient photocatalytic reactions. They reported the  formation of nanocavities on anatase $TiO_2$ nanobelts and nanotrods during the synthesis process [93].

Recently, hollow spheres with complex interiors have attracted immense research interest because of their higher order of structuring and novel physico-chemical properties that positively tune their applications, when compared to the same sized solid materials/hollow counterparts. The inner "nanospace" of these structures, when coupled with chemical functionality of boundary materials, creates both aesthetic beauty and scientific attraction [94]. Yanhui et al prepared anatse hollow spheres by hydrothermal method using carbon spheres as templates and the activity was found to be 6 times higher than that of degussa P25 titania [95]. Photoelectric activity depends not only on surface, but also combination of efffects are also utilised to enhance the properties. Hollow spheres with active exposed facets have been superior activity as reported by Yuzhu et al [96]. Among the various hollow architectures, multishelled hollow micro-nanostructures with three or more shell structures are expected to be better performing than the single or double shelled ones. However, fabrication of such super designs is quite tedious due to their complicated structure [97-100]. Other than the shape, delicate control over crystalline texture, shell porosity, interior complexity and chemical composition of hollow nanostructures bring additional tasks to their synthesis [101-106]. Multishelled hollow spheres nature imparts high specific surface area to the special morphology and thus improve the photocatalytic performance of $TiO_2$ [107]. It is documented that hollow spheres with curved surfaces can multireflect the incident light by means of their inner walls of shells and thereby increase light-harvesting efficiency in both photocatalysis and solar cells [108].

Literature shows that for the development of new functional materials with enhanced performance, rational design and preparation

of nanostructured materials are highly inevitable. Here we have synthesised five titania based nanostructures of varying morphologies which ofcourse differ in porosities and crystallinity. The activity of these systems is checked towards methylene blue dye degradation. The activity was compared with available reports in terms of catalyst doage and dye concentration.

## 4.1.5   Results and discussion

$10^{-5}$ M concentration of methylene blue dye was chosen as the model target pollutant for titania mediated photocatalytic degradation studies. Methylene blue (MB; $C_{16}H_{18}N_3SCl$) is a blue coloured tricyclic phenothizaine dye, with a molecular weight (MW) of 319.85 g/mol and absorbs in visible region at 663 nm. It is widely used in textile especially for dying cotton,wool and silk and in paper industry. Similar to other dyes MB also exhibits various harmful effects in humans like hypertension, vomiting, jaundice, and tissue necrosis etc; [109] The structure of the dye has been represented below.



**Figure 2**. Chemical structure of Methylene blue dye

The degradation of methylene blue dye using titanium dioxide photocatalyst in presence of light is effective and efficient process. Photocatalytic activity was checked in a photoreactor equipped with

light source as described in section 2. UV-Visible spectrophotometer was used used to moniter the concentration of the dye with irradiation time. The decrease in concentration of the dye in presence of light and photocatalyst is monitered using UV-Visible spectrophotometer under specific time intervals. The absorbance is correlated with concentration using standared curve of methylene blue dye in the desired range. In this experiment the catalyst dosage chosen was 0.25g/L, which is much lower when compared to most of the reports in literature with almost a same concentration of the dye solution. The experiment was done in dark, in presence of light without catalyst in presence of light with catalyst. The degradation was nill in the first two cases and considerable degradation was observed in presence of catalyst and light.

Figure 3 shows the UV-Visible absorption spectrum of methylene blue dye showing decrease in the absorbance of the dye in presence of light with increase of  irradiation time of multishelled titania hollow nanospheroids (MHS), mesoporous assembled titania nanocuboids (MT), Titania nanotubes (TNT), Titania nanobelts (TNB), Titania nanoparticles (TNP). We can observe a time dependent decrease in the absorbance of the peak at 662 nm for all the prepared systems. The absorbance value was correlated to the concentration of dye in the standard curve and percentage of degradation was calculated. Almost complete degradation was achieved by the multishelled titania hollow nanospheroids within 35 minutes whereas the degradation percentage of other systems namely MT, TNT, TNB and TNP being 87.72%, 87.01%, 81.7% and 69.45%. Figure 3i. showed the rate of degradation of the various phtocatalysts prepared with irradiation time. We can observe that the rate of degradtion is

higher for multi shelled titania hollow nanospheroids, MHS when compared to other systems.
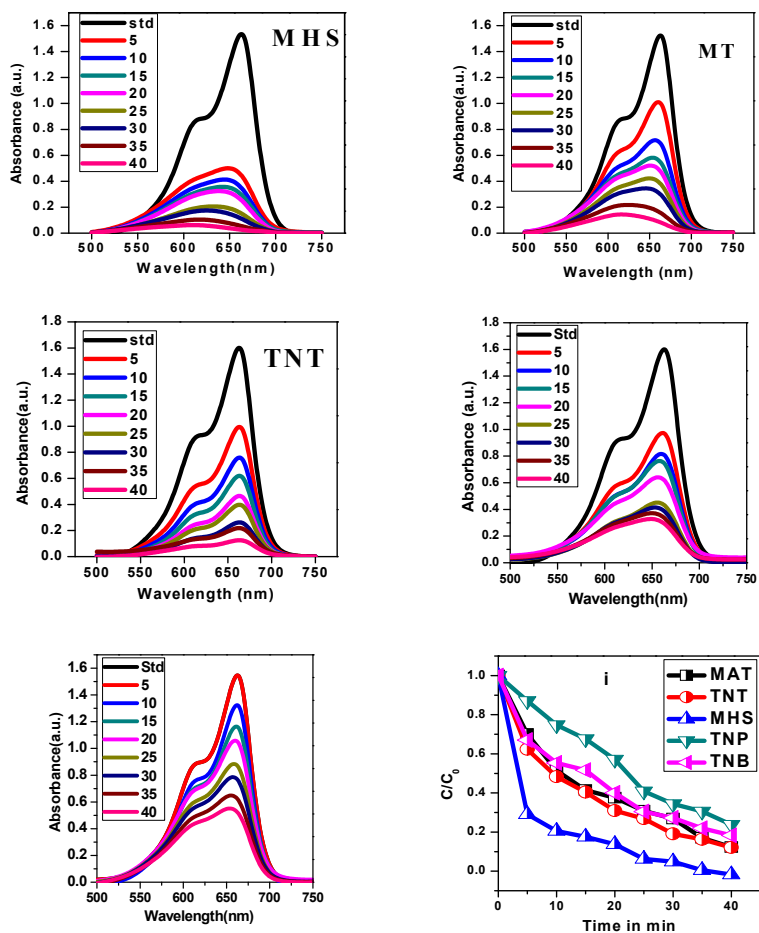


**Figure 3**. UV-Visible absorption spectra showing decrese in the Absorption peak of methylene blue dye with photocatalyst rate of degradation of prepared nanostructures, Plot of $C/C_0$ as a function of time (i)

The reaction data obtained can be fitted well with first order kinetic plots and the plot ln $C/C_0$ Vs time [Figure 4] upon linear fitting, the slope of the stright line will give the rate constant.
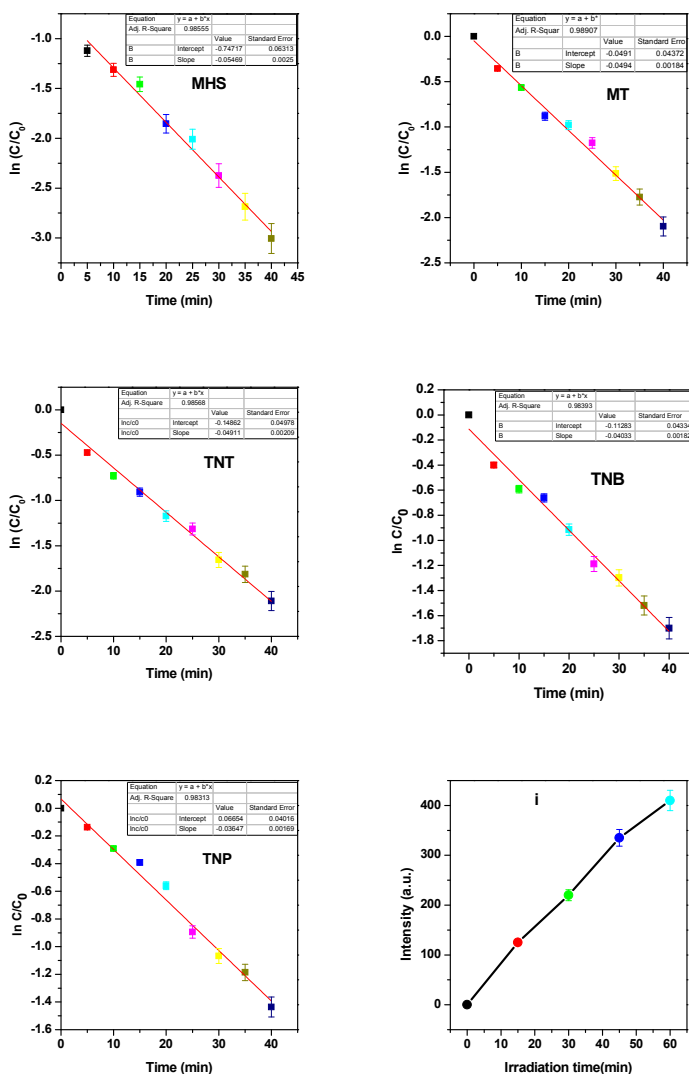


**Figure 4.** First order kinetic plots of Titania nanostructures and Plot of the induced fluorescence intensity at 426 nm against irradiation time for terephthalic acid on MHS (i)

The table1 displays the rate constants of the photocatalytic degradation of methylene blue dye with the corresponding nanostructures. These are in agreement with the activity observed for each system towards methylene blue dye degradation experiments.

| Systems | Rate Constant ($s^{-1}$) | Regression constant ($R^2$) |
|---------|--------------------------|------------------------------|
| MHS | $5.469 \times 10^{-2}$ | 0.9855 |
| TNT | $4.911 \times 10^{-2}$ | 0.9856 |
| MT | $4.944 \times 10^{-2}$ | 0.9890 |
| TNP | $3.647 \times 10^{-2}$ | 0.9831 |
| TNB | $4.033 \times 10^{-2}$ | 0.9839 |

**Table 1**. Rate constant for photocatalytic dye degradation of various nanostructures

Finally the formation of OH radical are confirmed by fluoresence intensity increase against the illumination time at 425 nm for the most active system MHS. We can see from the figure 4i that the fluoresence intensity increased by UVlight illumination in terephthalic acid solutions linearly with time. Therefore we can conclude that the hydroxyl radicals are formed on the surface directly proportional to the irradiation time. Finally we have compared the activities with a reference titania, Degussa P25 under the same experimental conditions and it was observed that the reference titania showed only 52.6% degradation within that stipulated time, which again showed the superior performance of the prepared nanostructures.Though the surface area of degussa P25 is 50 $m^2/g$, the higher photocatalytic

activity shown by the prepared systems clearly demonstated the morphological influence and crystal phases.

We can see that the multishelled hollow nanospheroids are having an commendable activity and superior to all the other structures. Generally, higher application potential of multi walled structures than their solid counterparts is attributed to the increased multiple reflections of light from the complex interiors due to its multishelled structure [110-111]. A detailed morphologycal analysis has been described in section 3.1 of third chapter. Figure 5 b demonstrates the possible ways of multiple reflections from the interiors of this multishelled structure. It was reported that the structure with many chambers allows the multiple reflections of UV light within. Thus photocatalytic activity is markedly increased because of the efficient use of light source. Besides the multiple reflections, the superior design of our catalyst may be providing easy and effective transport of the reactant molecules to get in to the active sites on the frame work walls and hence enhancing the reaction rate. Another point that favours the higher efficiency of the multiwalled structure is the increased surface area of the system, which was almost double the value of precursor titania powder. All these factors positively contribute to the excellent photodegradation activity of the multiwalled spheroids.
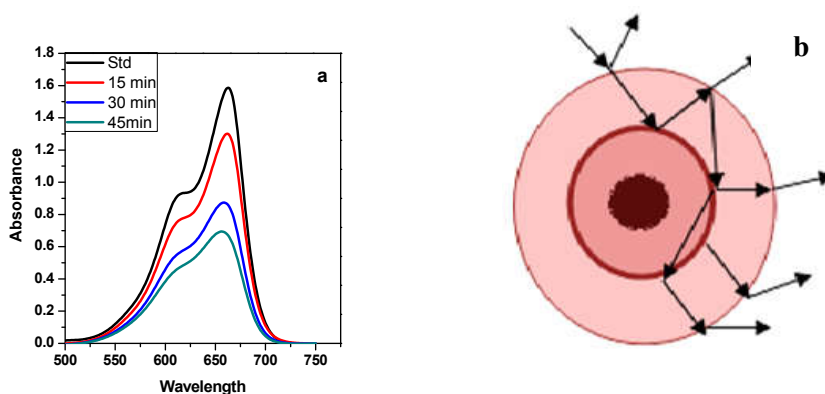
**Figure 5.** UV-Visible absorption spectra of commercial titania towards methylene blue degradation under identical experimental conditions (a) Schematic illustration of multiple reflection of light within the structure (b)

Mesoporous titania is also exhibiting a good photocatalytic degradation effciency. The higher activity may be attributed to the increased surface area of the mesoporous structures along with the synergy due to the existence of {101} and {001} planes on the nanostructured titania surface. It has already been said in chapter III of section 3.2 that MT has been derived from the oriented growth of nanocuboids with exposed active crystal facets. Among the various nanostructured materials, nanocuboids have the advantage of its large surface area, uniform size, low density, and equidistant sharp edges that facilitate highly localized pathways etc. The main benefit of cube like nanostructured materials is the pores which serve as pathways for the charge carriers to stab into interior of nanocubes which could enhance the performance of the photocatalyst by reducing the recombination rate. The high surface area is very much beneficial for photocatalysis by the increased surface sites. The higher activity of co-

exposed {001} and {101} planes has been well known. Figure 6 portraits the mechanism of photocatalytic degradation by the prepared mesoporous material. When {101} and {001} facets come in contact with each other, they form surface hereo junction. When the sample is irradiated with UV light, electrons migrate to {101} plane and holes to {001} plane of anatase titania. {101} plane acts as reduction and 001 act as oxidation sites, thus reducing the recombination of charge carriers on the surface. Ideally, the selective passage of photogenerated charge carriers to the specific exposed crystal facets, results in the spatial separation of redox sites on the anatase, which decreases the recombination rate of photogenerated electrons and holes and thus, enhancing the photocatalytic activity as observed in this case.
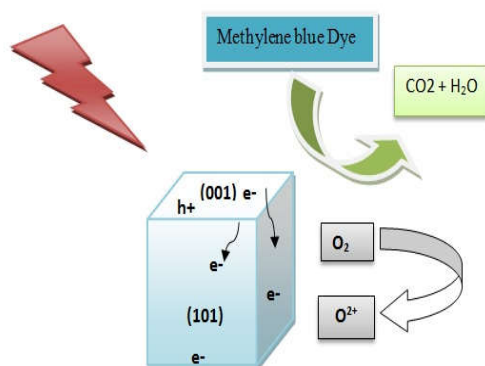


**Figure 6.** Mechanism of photocatalytic performance of mesoporous assembled titania nanostructure (MT)

Titania nanotubes also showed commendable activity due to the enhanced surface area and the biphasic crystalline nature of the titania nanotube. The detailed description of tubular morphology and biphasic

crystalline nature of titania nanotubes have been given in section 3.3 of third chapter. Usually the surface areas of anatse/$TiO_2$(B) heterojunctions are in the order of 1-5 tens of $m^2/g^{-1}$. Among the methods of synthesising anatase/$TiO_2$(B) heterojunctions, hydrothermal method involving protonated titanate nanostructures is well documented and its thermal treatment can induce topotactic transformation from monoclinic titanates to anatase $TiO_2$ through $TiO_2$(B) as an intermediate phase and lead to anatase/$TiO_2$(B) heterojunctions with a coherent interface [112-114]. But the thermal treatment above 400 °C most probably destroys the tubular morphology of nanotubes and we can observe a direct transformation to anatase phase of titania. Thus the development of an anatase/$TiO_2$(B) nanotube heterojunction with good surface area is highly desired. Certainly the photocatalytic efficiency of $TiO_2$(B) is observed to be lower than anatase and this metastable phase possesses a narrower bandgap, higher band edge potential (both conduction and valence band). Electrons in the valence band of titania in Anatase phase can absorb more photon easily because of its lower valnce band potential. If a heterojunction is fromed by $TiO_2$(B) and anatase the photogenerated electrons and holes could transfer to anatase phase and $TiO_2$(B) phase, respectively thus recombination is prevented [115-118]. Thus when a photocatalyst composed of two crystal phases, it may be beneficial to the separation of photogenerated holes and electrons, which will significantly improve the photocatalytic activity as in P25 [Mechanism has been depicited in figure 7.] The synergy of this biphasic Anatse/ $TiO_2$ (B) structure along with a good surface area value makes titania nanotube a good photocatalyst.
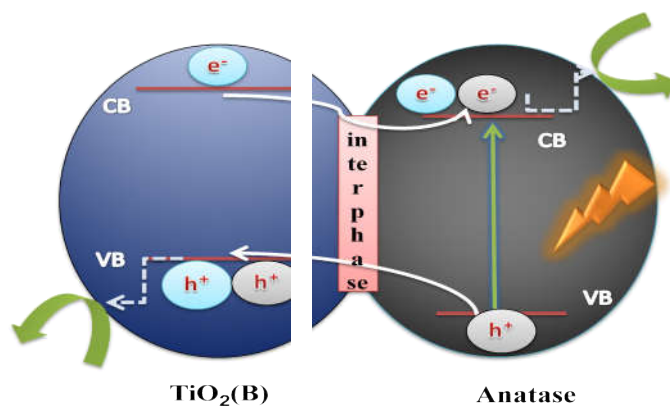
**Figure 7**. Mechanism of photocatalysis in a biphasic anatase $-TiO_2$ (B) interphase

It has been observed that titania nanobelt compared to other structures exhibit a little lower activity due to the presence of $TiO_2$ (B) phase alone in their crystal structure. The structure and crystal phase analysis have been done in section 3.4 of third chapter. It has been documented that one dimensional structures like nanobelt or nanowires exhibit lower photocatalytic activity due to lower active sites and higher recombination of charge carriers in a single phase nanostructure than in a combination Anatase/$TiO_2$(B) phase. Therefore a little lower activity compared to the tubular morphology is clearly due to this single phase structure of $TiO_2$(B). But the activity was observed to be reasonably high compared to the titania nanoparticle (TNP) with a surface area value of 21.62 $m^2$/g. The higher activity of Titania nanobelt than titania nanoparticle is substantiated by the peculiar morphology with a surface area value of 47.63 $m^2$/g. Among the synthesised systems, titania nanoparticle is found to possess the lowest surface area value and a highly agglomorated structure which

are responsible for its reduced activity. But the higher activity than the commercial titania is substantiated by the relatively lower amount of rutile peaks than degussa P25. We can observe just a single rutile peak in the XRD spectrum of titania nanoparticle as described in section 3.5 of third chapter.

One of the necessary criteria for heterogenous dimensional structures with large aspect ratio can be easily separated after the photocatalytic photocatalyst is the reusability of the catalyst as for practical photocatalytic process; the major problem faced being the reduced recoverable nature of the photocatalyst from the solution after the reaction [119-120]. Experiment conducted to this effect revealed that our systems especially one reaction by sedimentation or filtration and can be reused as well. Another factor which has concern for a catalyst is its recyclability. It is observed that the systems are efficient in this aspect also as seen from figure 8.
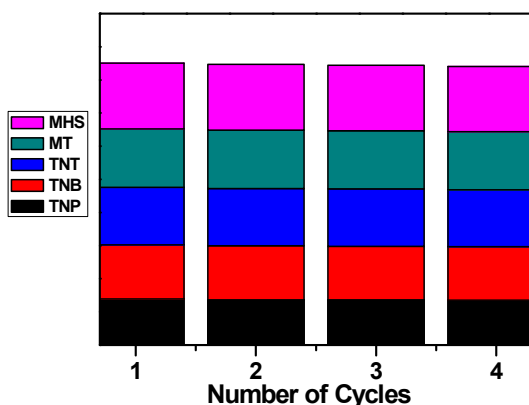


**Figure 8**. Recyclability of the prepared systems towards Methylene blue dye degradation

### 4.1.6 Chemical oxygen demand (COD) measurement

The chemical oxygen demand (COD) is used as the oxygen equivalent of the organic content in the dye sample that is inclined to oxidation by strong oxidant and formation of $CO_2$ and $H_2O$. High values of COD and BOD are observed for chemicals which are dark in colour which inturn leads to turbidity in the effluents and depletion of dissolved oxygen. Certainly this has an adverse effect on the marine ecological system. CODs of the dye solutions were estimated before and after reaction in presence of UV light with the photocatalysts. The decrease of COD values of the treated dye solutions implies mineralization of the dye molecules along with color removal. The Samples after 35 minutes of photocatalytic degradtion by different photocatalysts are shown in the figure 9. The corresponding COD value of commercial titania is also shown.



**Figure 9**. Dye solution evaluated for COD analysis after 35 minutes of photocatalytic degradation by Titania nanostructures

The obvious color change is observed in the case of multishelled titania hollow nanospheroids within that time but others exhibit much

higher range of blue colour. Usually the decolorization of a dye is different from the mineralisation. A dye completely decolorised does not mean that it has been completely mineralised. To eveluate the extent of mineralisation of the methyleneblue dye within that stipulated time, COD measurements were carried out by repeating the experiments under same conditions and the COD values obtained have been shown in the table 2. Each COD result is the mean of triplicate measurement. No obvious change was observed in the COD value when the dye was treated with UV light alone where as a significant change was observed when the experiment was repeated in presence of catalysts. The initial COD value of the dye was 48.4 mg/L. After 35 minutes of photocatalytic reaction, the COD was observed to be 24.2 mg/L for the multishelled hollow nanospheroids indicating that the complete mineralization is required in more time different from the methylene blue decolorization. The commercially available degussa P25 was also taken for a comparison and it was observed that the COD was found to be decreased only to 47.2 mg/L. In the case of preprared nanostructures, the results were. MHS showed almost 50% mineralization within 35 minutes. The COD value was found to increase in the order MHS < MT < TNT < TNB < TNP. The COD values were in accordance with the decolorization percentage measured by spectrophotometrically for various catalysts.

| Sl. No. | Sample Name | COD (mg/L) |
|:---:|:---:|:---:|
| 1 | Blank | 48.4 |
| 2 | MHS | 24.2 |
| 3 | MT | 33.9 |
| 4 | TNT | 36.3 |
| 5 | TNB | 43.6 |
| 6 | TNP | 46 |
| 7 | Comm.TiO$_2$ | 47.2 |

**Table 2**. Observed COD values of dye solution for various systems after photocatalytic treatment for a fixed time period

To summarise, the synthesised nanostructures showed absorption in the UV region but have different morphology, surface area, pore volume and crystal phases. Accordingly their photocatalytic activites were obviously different. The surface area value of the systems were in the order MT > TNT > TNB > MHS > TNP. Most active anatase phase was exhibited by both MHS and MT. Bicrystalline phases with TiO$_2$ (B) and Anatse interphase for Nanotubes and TiO$_2$(B) phase alone for Titania nanobelt. Titania nanoparticle exhibited anatse and some rutile phases as revealed from XRD spectra. The activity followed the order MHS > MT > TNT > TNB > TNP. Thus inspite of the lower surface area value, the intricate morphology which efficiently utilises the radiation along with photocatalytically active anatse phase are responsible for the higher activity of MHS. The activity was much higher with a lower catalyst doasage is highly commentable when compared to many other reported works. Here the catalyst dosage adopted were only ¼$^{th}$ the amount of

those reported in literature under identical experimental conditions. In addition to good surface area value and the porosity features, the synergy of {001} and {101} facets which reduces the charge carrier recombination process positvely tune the photocatalytic activity of mesoporous assembled titania. The bicrystalline phase [ $TiO_2$ (B) and Anatse] and good surface area value due to its one dimensional structure makes titania nanotube to exhibit a comparable activity to MT. Though having a single phased [$TiO_2$(B)] belt structure, the high surface area makes nanobelt a better photocatalyst than TNP. The lower activity of nanoparticle is attributed to its presence of rutile phase, lower surface area and highly agglomarated nature when compared to all the other systems.

### 4.1.7 Photoinduced superhydrophilicity measurement

The self-cleaning property for a $TiO_2$ photocatalyst coated surface is based on the photocatalytic oxidation activity, which decomposes organic contaminations, various microbes and along with photo-induced super hydrophilicity.Thus under UV radiation, $TiO_2$ decompose contaminants to less harmful products whereas its superhydrophilicity enables it to remove the contaminants along with water as they run off [Figure 4]. Usually $TiO_2$ coated self cleaning surfaces are mostly applied to exterior construction materials like tiles, glass, plastic films, etc. It is because of the super hydrophilicity offered by these titania coated surfaces when exposed to abundant sunlight and natural rainfall. The pioneer of $TiO_2$- based self-cleaning technology TOTO Ltd. (http://www.toto.co.jp/), ensures that $TiO_2$-based self-cleaning tiles remain clean for more than 20 years. Moreover, $TiO_2$-

based self-cleaning surfaces reduce air pollutants like nitrogen oxides (NOx) by photocatalysis, thus improving air quality [121].
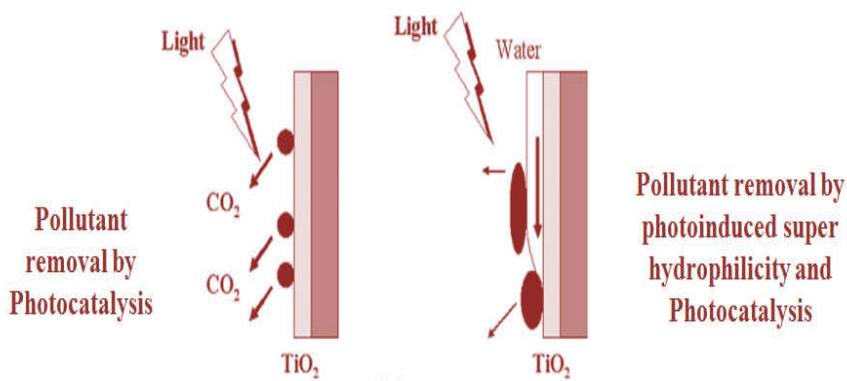


**Figure 4**. Schematic picture illustrating self cleaning mechanism by Titania coated surface for pollutant removal

It has been reported that titania based self-cleaning coating films prepared from unique morphological materials have shown improved self-cleaning effect. Shibata et al. [122] reported a very flat titania nanosheet-based surface which showed both photocatalytic oxidation activity and photo-induced hydrophilicity. Inspired by these works, we would like to check the superhydrophilicity nature of our synthesised multiwalled titania nanostructure and the the wetting characteristics are studied using contact angle measurement. A glass side (75 × 25mm) were ultrasonically cleaned in acetone and then dipped in absolute ethanol for 5 min, after which a thorough wash was carried out. In a typical protocol, a thin film of MHS was coated on a glass slide using alcohol and binder (Triton X-100) mixture to get a transparent film. Then the binder is removed with appropriate high temperature treatment and film was used for contact angle measurement. At zero hour of UV irradiation, the static contact angle

of MHS coated film was reduced upon UV irradiation sustantially. And the water droplet spreads on the surface [figure 5]. This showed the superhydrophilic property of MHS which can be used for fabricating self-cleaning materials in deomestic, hospitals and industrial applications in a large scale.
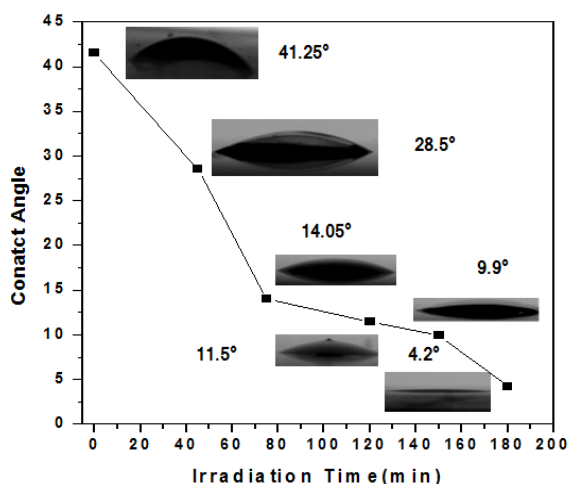


**Figure 5**. Static contact angles as a function of UV irradiation time. (Inset) Water droplets on MHS coated glass film

### 4.1.8  Concluding points of Part 1 - Applications in Photocatalysis

Titania nanostructures prpared are tested for organic pollutant removal taking methylene blue as the target dye. All the systems showed good activity towards dye degrdation. Multishelled titania hollow nanospheroids exhibited commendable activity among the nanostructures, completely degrading the dye within 35 minutes with a catalyst doasage commendable lower compared to many previous reports. The prepared structures are also tested for mineralisation

studies by COD analysis and it was observed to follow the same order as that of dye degradation studies. Commercially available degussa P25 was also tested for the same and is exhibiting the lowest decrease in COD value. The activity followed the order MHS > MT > TNT > TNB > TNP. The higher activity of mutiwalled structure is due to the multiple reflections of UVlight when light falls on the structure due to its multishelled nature which effectively utilises the light to boost up the photocatalytic process. The most active system, multishelled spheroids were found to be superhydrophillic also upon UV treatment. Hence it can be concluded thta the above mentioned system can serve as an efficient candidate for self cleaning applications.

# Part 2
# Antimicrobial activity of titania based nanostructures

Since the self cleaning materials have most applicablilty in the medical field and sanitary areas including self cleaning tiles/glass/walls/concrete/ equipments/fabrics, the study of the antimicrobial activity of the materials upon irradiation is also essential. Here we have investigated the antimicrobial activity of titanium dioxide nanostructures towards gram negative bacteria (E-Coli) and fungus (Candida ablicants). E.Coli method was used to evaluate the antibacterial activity and optical density method using ELISA micro plate reader was used to monitor the nanoparticles toxicity towards fungi. The detailed experimental procedure is provided in Chapter 2.

## 4.1.9   Introduction

Inactivation of microrganisms by nanomaterials is an another part of research where applications of photcatalysis has significant practical interest. Nowadays people are more concerned about the hygeine of materials they are using in a daily basis like food, cloths, drinks, sanitary devices other personal care products. Biomedical field is other area where atmost care is needed to wipe off  the infectious disease causing microrganisms. Bacterial infection in implantation of biomaterials often occurs and may lead to failure of surgery in this direction implants with antimicrobial properties are receiving sufficient attention. The emergence of new infectious diseases and the continuous development of antibiotic resistance among a variety of disease-causing bacteria pose a serious threat to public health worldwide. Eventhough the technological advancement is more

inclined to meet consumers demands and needs for improving the living standard of human beings, demand for fresh like, nutrient rich, additive free, minimal processed food materials is an area of hot research. This is due to the increased awareness about the loss of nutrients during processing of food and the possiblity of contamination in manufacturing and preserving. Therefore use of measures to control the harmful effects of microrganisms is a necessary. Antimicrobial agents  kill the microbes that contaminate by  the interaction with cell wall [123-124]. UV treatment in a desired range alone can be used to kill microorganisms as a mean of preservation of food [125]. But long treatment time required is the major shortcoming of this technology for practical purposes which can be reduced by combination technologies [126-127]. UV treatment alone will not destruct viruses and spores [128]. Various natural / synthetic antibacterial/antifungal agents are available nowadays; mainly include inorganic antibacterial agents, organic antibacterial materials and natural active antimicrobial substances. Organic antibacterial agents, including iodide, phenol etc are still in market due to their immediate and efficient bactericidal activity. The most applicable inorganic nano-structured materials as seen from Figure 1 can be grouped as follows: $TiO_2$ and its metallic /non-metallic nano-composites, silver, its nano-structured materials, antibacterial agents based on ZnO, Copper, Gold nano-particles, those based on Gallium, carbon nanotubes (CNTs), nano-clay and their modified species. Heavymetals (Silver, Copper, Zinc) are used but its use are  limited by bacterial resistance effects and human toxicity.  A comparitive study has been carried out by Azam et al [129] showed that antibacterial efficiency of nanostructured zinc oxide, copper oxide,

tin oxide and cerium oxide prepared by co- precipitation route exhibited a trend in activity which follows the decreasing trend as ZnO > $SnO_2$ > $CeO_2$ > CuO. Not only the structure but also the nature odf the meatloxides strongly influences the antibacterial efficiency. The unique properties of titania in antibacterial fields like stability, nontoxicity, broad spectrum of antibiosis make them a good candidate to investigate more by modfiying with various organic inorganic research moeties [130-134]. American Food and Drug Administration (FDA) have approved titanium dioxide for use in human food, drugs, cosmetics, and other food contact materials.
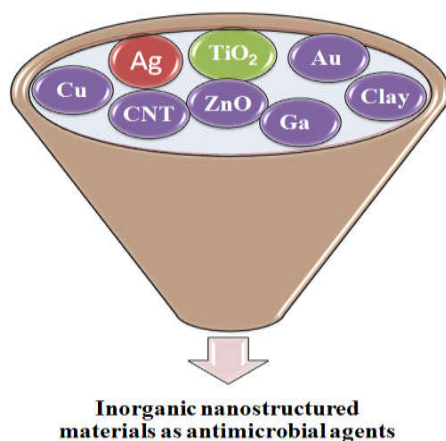


**Figure1**. Common examples for inorganic based nanostructured materials as antimicrobial agents

Photocatalytic disinfection of metal oxides microbes is usually attributed to the oxidative stress induced and cell membrane damage owing to the generation of reactive oxygen species, like hydroxyl radicals [135]. Some metal oxides can produce ROS in the dark and others only upon illumination. Reactive oxygen species will be

significantly higher upon illumination with light of energy higher than the band gap for metaloxides as in the case of titania. Other mechanisms of antimicrobial effect have been explained as the release of metal ions and its interaction with the cell wall like zinc oxide. A morphology dependent antibacterial activity was found to the titania nanostructures. Light dependent activity, size, aggregation, all depends on these interction with cell wall [136]. Many studies reports the generation of ROS as the possible mechanism of antibacterial effect. In the case of titanium dioxide, upon irradiation ROS produced will be higher therefore an increase in the antibacterial effect was observed. On contrary, MgO, the antibacterial effect was noticed without irradiation which underlines the some other complex mechanisms involved in the metaloxide generated antibacterial effect. Titania based bactericidal properties were reported since Matsunaga et al.[137] observed the bactericidal effect of $TiO_2$ photocatalytic reactions in 1985 because of its stable and strong bactericidal activity resulting from a series of free radical reactions. Though an early study by Carey et al towards the antimicrobial activity of primary waste water effluent showed no improved antimicrobial activity of $TiO_2$ [138]. Further studies have shown the usefulness of photocatalysis on $TiO_2$ for disinfection of water which included killing of waterborn bacteria and viruses from water supplies [139-141]. Makowski and Wardas reported that the production of highly reactive hydroxyl radicals can lead to removal of toxins from water and destruction of algae, bacteria, viruses and protozoa which normally are in water [142]. Titania based photocatalysis is well documented for a range of microorganisms including gram positive and gram negative bacteria, viruses,

endospores, protozoa,  fungi, and algae [143-147]. Almost all microbial toxins are destroyed except  Acanthamoeba cysts and Trichoderma asperellum coniodiospores which have been reported to be resistant.

Most frequently, it is insufficient to kill the bacteria as some of them produce endo and exotoxins in to the medium. Exotoxins are mostly heat sensitive proteins. Endotoxins are lipopolysaccharides usually produced within Gram-negative bacteria. They get released if the outer membrane becomes damaged. Even after the cells are dead these substances cause other medical problems. Photocatalytic microbial inactivation is mostly performed with gram negative bacteria Escherichia coli [148-150]. Effective studies based on the photcatalytic destruction of other gram negative bacteria are reported [151-152]. Usually it was observed that  compared to Gram-negative bacteria, Gram-positive bacteria were more resistant to photocatalytic disinfection [153-155]. The more complex triple layer cell wall structure of gram negative bacteria comprising of an inner membrane (IM), a thin peptidoglycan layer (PG) and an outer membrane (OM). Gram-positive bacteria have a thicker Peptidoglycan layer G and no OM. A few studies have also been reported that Gram-positive bacteria were more sensitive. Kangwansupamonkon et al. reported that Methicillinresistant Staphylococcus aureus and E. coli were more resistant than Micrococcus luteus [156]. Luo et al. [157] found that Enterococcus faecalis was more resistant than E. coli, but more sensitive than Pseudomonas aeruginosa. Van Grieken et al. (2010) saw that E. faecalis was more resistant in distilled water but no difference

in disinfection time was observed for E. coli and E. faecalis in natural waters [158]. Different affinites to $TiO_2$ and cell wall structure may be reponsible for these differences.

Fungi, algae, protozoa and viruses are also killed by photocatalytic degradtion mechanism of titania [159-162]. Fungal spores were generally more resistant and Giannantonio et al. [163] found that under experimental conditions used Trichoderma harzianum spores were resistant to killing. It was observed by Sökmen et al. [164] that cysts of Acanthamoeba exhibited significant resistance for killing but can be susceptable for complete deactivation depending on the treatment time.The fungicidal action of the $TiO_2$ photocatalytic reaction for control of Diaporthe actinidiae, a major fungal pathogen (kiwifruit) was recently revealed by the work of Hur et al. [165]. The antifungal activity of the $TiO_2$ photocatalytic reaction was tested against P. expansum. We observed that the viable colonies of P. expansum were apparently reduced in vitro when UVA was combined with $TiO_2$ [166]. Mammalian viruses including poliovirus 1, avian and human influenza viruses, and SARS coronavirus are susceptible to photocatalytic degrdation mechanism [167-169].

An understanding of the morphology of microbes will help in the design of more appropriate photocatalytic technologies for efficient disinfection applications. In this study bacteria and fungus are taken as the target substance for photcatalytic disinfection. Bacteria are typically procaryotic micro organisms not having any nucleus and DNA are not separated from cytoplasm by any specific membrane. As in higher plants and animals, the constituents of cell are not designated

for specific functions. Here respiration is taking place on cell membrane and observed morphologies are rod, spiral and spherical. Based on the ability of cell wall to be stained by gram stain, they are divided as gram positive and gram negative bacteria. In Gram positive bacteria, the cell wall which is about 20-80nm in thickness constitutes 80 % peptidoglycan whereas in gram negative bacteria, the peptidoglycan layer in cell wall only constitutes 10%. The outer membrane of 6-18nm thick constitutes lipopolysacharides, phospholipids, lipoproteins etc. The plasma membrane found below cell wall is mainly composed of phospholipid bilayer. This part has a series of vital functions related to the proper working of the cells like selectively permiting certain metabolites in and out of the cell, maintanance of osmotic equilibrium. The bacterial DNA is anchored on the cytoplasmic membrane thus serves as the binding site and is involved in the replication and segregation of DNA molecules during cell division. Moreover these constitutes the the enzymes for the synthesis, transport of cell wall components , machinary for electron transport and oxydative phosphorylation. Therefore changes to the cell membrane integrity has decissive role in determining the cell viability [170-171]. Some bacteria on their exterior surface contains other structures and materials such as slimes, sheaths, and cilia. The highly viscous slime layer or capsule of certain bacteria besides its protective function to cell wall stores food and infective capability. These enables bacteria to form biofilm on solid surfaces such as air filters, or to attach to dust particles and travel in air.

Other target species investigated for inhibition by titanium dioxide are eucaryotic organisms fungi whose genetic materials are enclosed in a nucleus which is surrounded by membrane. Unlike procaryotes its cytoplasm contains many organelles, each of which performs a specific cellular function. Here also the cytoplasmic membrane is surrounded by a cell wall structure as in bacteria. The fungal cell walls are lamellar. Principal constituents of the fungal cell wall are various types of polysaccharides with minor amounts of lipid and protein. Common polysacharide component of cell wall is Chitin and due to tougher cell wall structure, fungi can survive ih harsh conditions like high osmotic pressures, a wide range of pH and can extract water from solutions of high salt or sugar concentration . Even though fungal diseases are not as common as those caused by bacteria, they are harder to identify clinically and pose chronic health problem.

## 4.1.10  Mode of microbial inactivation

Matsunaga et al. in 1985 and 1988 proposed depletion of coenzyme A and subsequent respiratory inhibition as the reason for the photocatalytic deactivation of bacteria. Most of the subsequent studies showed membrane and cell wall damage as the major fate of the cells during the treatment. Sai et al [172] and Hu et al [173] showed leakage of ions from the cell as an evidence for membrane damage. Several studies confirmed the increased membrane permiability upon the photocatalytic reaction [174-176]. The microscopic images also showed bacterial cell wal damage on teatment with various forms of this photocatalyst [177]. Amezaga- Madrid et al [178] showed that damage to peptidoglycan layer leads to leakage from cell and

subsequent abnormal cell division. However study on killing of Eoli on $TiO_2$ Thin films showed that no visible destruction to peptidiglycan layer occured during this photcatalytic killing besided outer membrane degrades first followed by damage to cytoplasmic membrane [179]. Generally the antibacterial agents inactiviate cell viability. Endotoxin, lipopolysacharide of gram negative bacteria remain even after bacteria was killed. In aqueous solutions, endotoxin can not be eliminated rather requires techniques such as membrane filtration, adsorption techniques etc.Sundara et al found the decompostition of endotoxin of EColi.using titania photocatalyst that is $TiO_2$ in presence of UV light destroys the bacterial cell wall along with the cell viability[180]. It has been demonstrated by sunada et al that degradation of E.Coli endotoxin occus without damaging peptidoglycan layer. In the case of gram negative bacteria, cell disruption followed the order outer membrane, peptidoglycan layer, inner membrane. Due to the highly cross linked structure, peptidoglycan layer in microscopic images does not show a detectable damage. Amezaga-Madrid et al. [181] through their studies showed that the point of contact between the titania nanoparticle and the cell wall is reponsible for the localised damages observed in the microscopic images finally leading to its total rupture. studies by Yao et al. [182] suggested that damage of DNA was responsible for cell death. However, later studies revealed damage to DNA does occur on $TiO_2$ which may occur as a late event after cell death [183-185].

Linkous et al and Hong et al suggested that death of Algal species Oedogonium sp. and Chroococcus sp. was due to imprecise

collapse of cellular structures and membrane damage [186-187]. Further microscopic images taken after photocatalytic treatment of Candida ablicans revealed that damage to cell walls of Candida albicans suspended over a thin film of $TiO_2$ and on $TiO_2$-coated tissue conditioner [188-189]. Cell wall and membrane damage are the visible results of photocatalytically treatment of Giardia lamblia and the ciliate protozoan Tetrahymena pyriformis [190-191].

### 4.1.11  The killing mechanism of Microbes by photocalysis

Majority of studies show that reactive oxygen species are responsible for the microbial inactivation upon photocatalytic treatment. The OH radical scavengers completely removed the Titania based photocatalytic activity also introduction of materials which degrade $H_2O_2$ also reduce the phootkillling of microbes confirming that OH radicals and $H_2O_2$ are the species responsible for the inactivation [192-193]. Eventhough many racials are ivolved major action of photokilling of microbes is due to OH radicals as per the studies of Cho and Yoon et al. [194]. Intimate contact between nanotitania and bacteria intoduce more damage to the microbes.The fact is confirmed by many studies where higher extent of inactivation was obseved when $TiO_2$ was used in suspended form than in the immobilised phase [195-198]. Studies which used to increase or decrese the photokilling of bacteria is based upon the number of contacts between the nanoparticle on cell surface [199-200].

It has been proven that initial cellular changes upon photocatalytic treatment, followed the complete mineralisation of

microbes which were confirmed by various techiques.Wolfrum et al showed this fact using $C^{14}$ labelled cells.The total organic carbon analysis by cheng et al showed the complete photocatalytic oxidation of Legionella [201] total oxidation of cell organic matter by total internal reflection/ FTIR was showed by Nadtochenko et al.[202]. Thus the photocatalytic killing mechanism of microorganisms can be summerised as  below. Initially up on irradiation with light the ROS formed on contact with the cells resul in the membrane permeability which is reversible process. Further exposure leads to cell wall resulting in a series of irreversible processes like leakage of ions, cell death. Further membrane damage leads to the leakage of higher molecular weight components like proteins. localised damge is observed where titania is in contact with the cell and which is folllowed by the potrusion of the cytoplasmic membrane into the surrounding medium in the degraded areas of the peptidoglycan. Finally the degradation of the internal constituents of the cell results in the  complete mineralisation.

## 4.1.12  Results and Discussion

In this study we have checked the photocatalytic antibacterial and antifungal activity of titania nanostructures prepared. Antibacterial activity on photocatalytic treatment was done towards gram negative bacteria E.Coli. using colony counting method and antifungal activity by optical density method.

**Antibacterial activity towards E.Coli – Colony counting method**

E.Coli. , gram negative bacteria was chosen as a representative of gram negative bacteria and were treated with different concentrations of nanoparticle suspensions. As expected, all the $TiO_2$ systems were

found to be ineffective as antimicrobial coatings under dark conditions, since no reduction in bacterial growth could be observed even after one hour exposure to the systems. A fixed time of UV light is given to all the samples that is for15 minutes. Different concentrations of the same sample gave different values for viable colonies. Each nanostructures at this fixed course of light radiation, gave different inhibition to the bacterial colonies. The control provides too dense bacterial colonies on the cultural plate. The $TiO_2$ systems showed a significant decrease in bacterial growth. Again Irradiation within that stipulated time, the multiwalled structure exhibited almost complete inhibition, the concentration being commendably lower than that of the other systems.

The activity followed the order MHS > MT > TNT > TNB > TNP

It is interesting to observe that the activity followed the same order as we have seen the previous section II part A. This confirmed the involvement of hydoxyl radical mediated oxidation reactions. As mentioned earlier [Section 4.1.5, Figure 3] the ROS generation under UV light radiation by MHS hints its potential to serve as antibacterial agent also. The agar plates containing the bacteria that were recovered after exposure to $TiO_2$ systems in presence of UV illumination (15 minutes) are shown in figure 2.

The better antibacterial activity exhibited by the MHS with that fixed period of UV irradiation pointed to the dependence of the morphology in this bacterial elimination process. The combination of the multi-chambers with such hollow nano objects and porous shells bestows the system with such a superior bactericidal effect. This is achieved by the multiple reflection of light within the chamber which

effectively utilizes the light source when that compared to that occurs in a nanoparticle surface. Reactive oxygen species generated by this UV light is responsible for destructing the micro organism.

| Sample | Control | Viabile colonies at with incresing Concentration of Sample | | |
|--------|---------|---|---|---|
| MHS | | | | |
| MT | | | | |
| TNT | | | | |
| TNB | | | | |
| TNP | | | | |
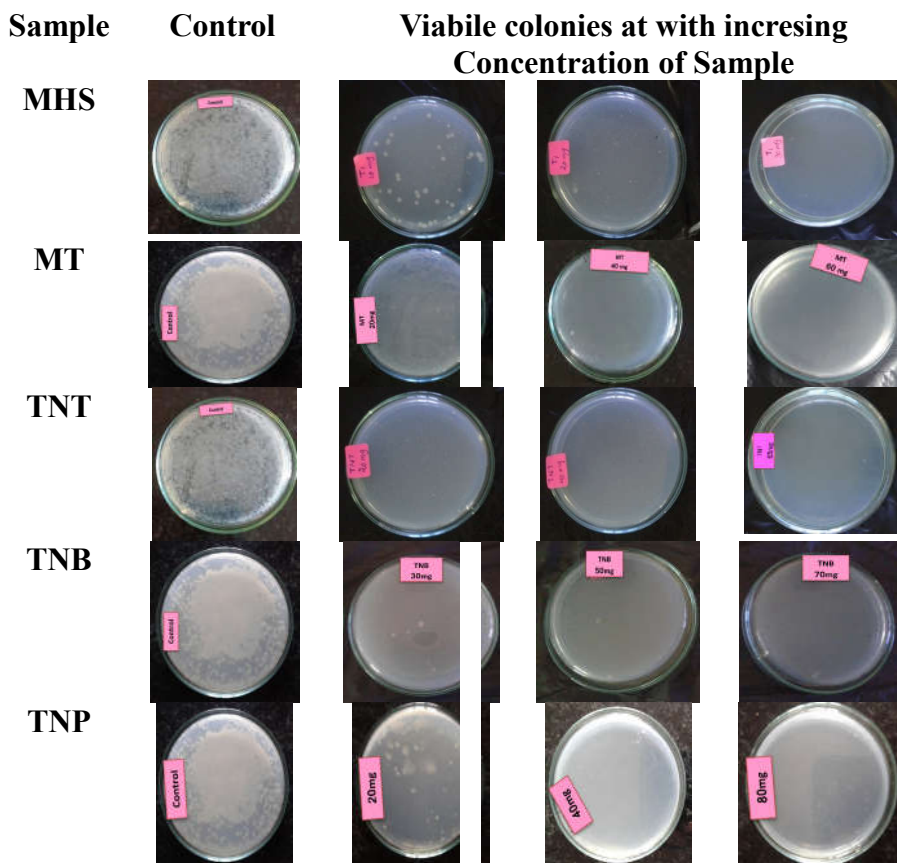


**Figure 2**. Decrease in the number of viable *E.Coli.* Bacteria after exposure to $TiO_2$ nano structures with UV light as a function of concentration

**Antifungal activity studies towards Candida ablicans**

Fungal cells are other disinfection targets. Hence photoinactivation tests on strains of fungi, Candida albicans was performed in the presence of titania nanostructures. The inhibition activity was examined by optical density measurement at 600 nm. It is rapid and nondestructive method for the evaluation of antimicrobial efficiency of materials. As the name implies, optical density is not a measure of absorbance instead it is a measure of the turbidity of the medium which inturn a measure of the density of microbial cells in the medium. The optical density of the scattered light from the medium is measured. Control experiments also have been done without the nanoparticles and it was observed to be higher. In the presence of antifungal agent in the medium, the fungal growth is inhibited and therefore the optical density of the medium decreases. The % growth inhibition was evaluated from the following equation using OD values of the control and the test compound;

$$\% \, I = \frac{ODcont - ODtest}{ODcont} \times 100$$ , where $OD_{cont}$ is the optical density of the control and $OD_{test}$ is the optical density of the test compound.

The comparison of Anitifungal activity of Titania nanostructures towards Candida ablicans made. The bacterial inhibition efficiency of Titania nanostructures towards staphylococcus aureus is depicted in bar diagram [Figure 3]. The corresponding optical density values are shown in Table 1. A concentration dependent activity has been observed towards the fungus. All the systems were

behaving differently towads the fungal inactivation which may be attributed to the particle size, morphology, preparation methods etc.
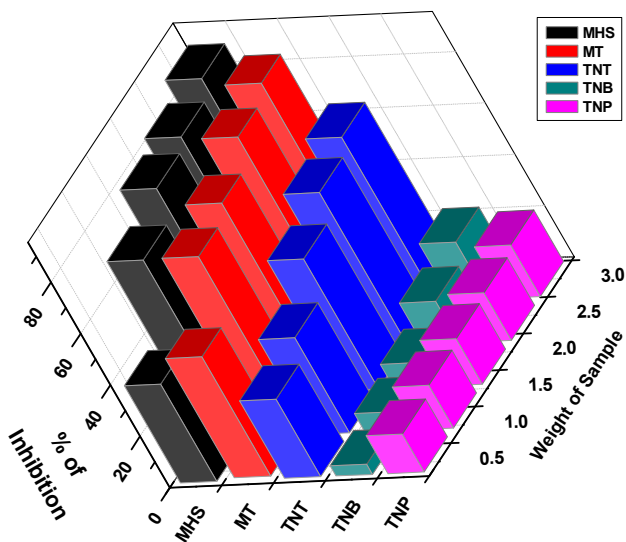


**Figure 3**.    Comparison of photcatalytic inhibition efficiency of different systems for Fungi inactivation

Here also the higher activity of mutishelled titania hollow nanospheroids is found to be exhibiting higher activity for each concentration. It is due to the higher light harvesting ability of these chambered structures which the produces more hydroxyl radicals for the degradation of pathogens. The higher surface area, mesoporous nature and small particle size is responsible for the good activity of mesoporous assembled titania nanocuboids. Titania nanotube, titania nanobelt are not so inferior towards the microbial inactivation as per the above said studies.

| Systems | Concentration of Sample (mg) | 0.6 | 1.2 | 1.8 | 2.4 | 3 |
|---------|------------------------------|-----|-----|-----|-----|---|
| | $OD_{Control}$ | $OD_{Test}$ | | | | |
| MHS | 1.062 | 0.661 | 0.328 | 0.213 | 0.182 | 0.122 |
| MT | 1.062 | 0.569 | 0.336 | 0.296 | 0.254 | 0.163 |
| TNT | 1.062 | 0.742 | 0.669 | 0.525 | 0.31 | 0.383 |
| TNB | 1.062 | 1.02 | 0.985 | 0.963 | 0.891 | 0.829 |
| TNP | 1.062 | 0.905 | 0.885 | 0.874 | 0.865 | 0.849 |

**Table 1.** Optical density values of different nanostructures in presence and absence of the test compounds

## 4.1.13 Concluding points of Part 2 – Antimicrobial activity study

Antibacterial and antifungal activity of prepared titania nanostructures have been evaluated towards bacteria and fungi for having a comparison. Titania exhibited antimicrobial activity due to its strong oxidizing property when exposed to light. ROS, such as hydrogen peroxide, hydroxyl radical and superoxide anions, generated on the photoilluminated titania surface are responsible for the complete removal of pathogenic systems. With a fixed time course of light radiation, multiwalled titania hollow nanospheroids showed maximum inhibition of gram negative bacteria E.Coli with minimal catalyst concentration. The antifungal activity of prepared nanostructures have been carriedout towards the fungi Candida albicans and a dose dependent activity was observed with multiwalled titania hollow nanospheroids showing the minimum number of viable cells with a predetermined concentration and fixed time of light irradiation

## 4.1.14  Conclusion of Section A

Titanium dioxide is widely used as a self-cleaning material owing to their excellent photocatalytic activity to remove various organic materials, pathogens etc combined with its photoinduced superhydrophilicity. The synthesised nanostructures are proven to be efficient to remove organic pollutant and various microorganisms. Among these, multishelled titania hollow nanospheroids is proven to be the best for methylene blue dye degradtion with a catalyst doasage amounts only to ¼$^{th}$ of the value reported in literature under identical experimental conditions. The antimicrobial activity studies also revealed the higher inhibition activity of multishelled system at a lower concentration with a fixed time course of radiation.   The higher photocatalytic activity exhibited by the system is due to the multiple reflections of light from its complex interiors thus effectively utilising the light falls on its surface. The contact angle measurement of the same also proved its hydrophilic nature upon UV treatment which is highly desiarble for the fabrication of a self cleaning device. Thus the synthesized multiwalled hollow nanospheroids ensured itself as a promising self-cleaning products for domestic, medical and industrial applications in large-scale.

## References

1.      A.L. Pruden and D.F. Ollis, Environ. Sci. Technol.,1983 , 17, 628.

2.      A.L. Pruden and D.F. Ollis, J. Catal.,1983 , 82, 404.

3.      F. Gianturco, L.V. Tatti, F. Rota, P. Bruzzi, L. Rivas, I.R. Bellobono, M. Bianchi and H. Muntau, Chemosphere, 1996, 33, 1531-1542.

4.      S. Tunesi S. and M.A. Anderson, Phys. Chem., 1991, 95, 3399 .

5.      P.E. Menassa, M.K.S.Makand and C.H. Langford, Environ. Technol. Lett.,1988 , 9, 825.

6.      X. Zhu & D. Zhou ,Y .Wang , L .Cang ,  G. Fang  and J. Fan,  J Soils Sediments , 2012, 12, 1371.

7.      P. Pichat, Wat. Sci. Tech., 1997, 35, 73.

8.      J.C. Crittenden, Y. Zhang, D.W. Hand, D.L. Perram and E.G. Marchand, Water Environ. Res.,1996 , 68, 270.

9.      L. John and H.G. FerryWilliam, Langmuir,1998, 14, 3551 .

10.     H. Kawaguchi, Environ. Tech. Lett., 1984, 5, 471.

11.     E. Carpio, P. Zúniga, S. Ponce, J. Solis, J. Rodriguez, W. Estrada, J. Mol. Catal. A: Chem. , 2005, 228, 293.

12.     D.T. Sponza, Ö.S. Kuscu, Process Biochem., 2005, 40,1679.

13.     K. Chiang, T.M. Lim, L. Tsen and  C.C. Lee, Appl. Catal. A, 2004, 261, 225.

14.      L. Gu, Z. Chen, C. Sun, B. Wei and X. Yu, Desalination, 2010, 263, 107.

15.     K. Harada, T. Hisanaga, and K. Tanka, Water Res., 1990, 24, 1415.

16.     J. Senthilnathan and L. Philip, Chem. Eng. J.,2011 , 172, 67.8

17.     S. Anandan, K. Kathiravan, V. Murugesan, and Y. Ikuma, Catal. Commun., 2009, 10, 1014.

18.     S. Malato, J. Blanco, C. Richter, and B. Milow, Chemosphere, 1999, 38, 1145.

19.     H. Katsumata, M. Sada, Y. Nakaoka, S. Kaneco, T. Suzuki, and K. Ohta, J. Hazard. Mater. , 2009, 171, 1081.

20.    A. Topalov, D. Molnár-Gábor and J. Canádi, Water Res. 1999, 33, 1371.

21.    M. Muruganandham, R. Amutha, G.J. Lee, S.H. Hsieh, J.J. Wu, M. Sillanpaa, J.Phys.Chem.C,2012 , 116, .12906

22.    I. M. Banat, P. Nigam, D. Singh, R. Marchant, Bioresour, Technol., 1996, 58, .217

23.    T. Robinson, G. McMullan, R. Marchant, P. Nigam, Bioresour.Technol., 2001,77 ,.247

24.    J.P. Jadhav, G.K. Parshetti, S.D. Kalme and S.P. Govindwar, Chemosphere, 2007, 68, 394.

25.    E.J. Weber, N.L. Wolfe, Environ. Toxicol. Chem.,1987 , 6, 911.

26.    G.L. Baughman and T.A. Perenich , Environ. Toxicol. Chem., 1988, 7, 183.

27.    K.T. Chung, G.E. Fulk, M. Egan, reduction of azo dyes by intestinal anaerobes, Appl. Environ. Microbiol., 1978, 35, 558.

28.    A. Houas, H. Lachheb, M. Ksibi, E. Elaloui, C. Guillard, J.-M. Herrmann, Appl. Catal. B,2001 , 31,14.5

29.    L. Davydov, E.P. Reddy, P. France, and P.G. Smirniotis, Appl. Catal. B, 2001, 32, 95.

30.    M. Zubair Alam, S. Ahmad, A. Malik and M. Ahmad, Ecotoxicology and Environmental Safety , 2010, 73, 1620.

31.    S. Daniela, Z. Carmen and M.Teodor, Cent. Eur. J. Chem., 2012, 10, 1913 .

32.    S. Malato, P. Ferna´ndez Ibanez, M.I. Maldonado, J. Blanco and W. Gernjak, W. Catal. Today, 2009, 147, 1.

33.    M.N.V Ravi Kumar, T.R. Sridhari, K.D. Bhavani and P.K. dutta, Colorage, 1998, 45, 25.

34.    Y. Liu, X. Che, J. Li and C. Burda, Chemosphere,2005 , 61, 11.

35.    C. Burda, Y. Lou, X. Chen, A.C.S. Samia, J. Stout and I.L. Gole, Nano Lett., 2003, 3, 1049.

36.    I. Arslan and I.A. Balcioglou, Dyes Pigm., 1999, 43, 95.

37.     J. Lu, T. Zhang, J. Ma and Z. Chen, J. Hazard. Mater. , 2009, 162, 140.

38.     M.A. Rauf, S.M. Qadri, S. Ashraf and K.M. Al-Mansoori, Chem. Eng. J., 2009, 150, 90.

39.     S. Zodi, O. Potier, F. Lapicque and J.P. Leclerc, Desalination, 2010, 261, 186.

40.     A.R. Tehrani-Bagha, N.M. Mahmoodi and F.M. Menger, Desalination, 2010, 260, 34.

41.     A.K. Abdessalem, N. Bellakhal, N. Oturan, M. Dachraoui and M.A. Oturan, Desalination, 2010, 250, 450 .

42.     F.H. AlHamedi, M.A. Rauf and S.S. Ashraf, Desalination, 2009, 239, 159.

43.     S. Merouani, O. Hamdaoui, F. Saoudi and M. Chiha, Chem. Eng. J.**,** 158, 2010, 550.

44.     O. Legrini, E. Oliveros and A.M. Braun, Chem. Rev.,1993 , 93, 671.

45.     M.R. Hoffmann, S.T. Martin, W. Choi and D.W. Bahnemann, Chem. Rev., 1995, 95, 69 .

46.     P.V. Kamat, Chem. Rev., 1993, 93, 267.

47.     Meng Nan Chong, Bo Jin , Christopher W.K. Chow and Chris Saint , Water Res., 2010, 44, .2997

48.     M. Stylidi, D.I. Kondarides and X.E. Verykios, Appl. Catal., B, 2003, 40, 271.

49.     S. N. Frank and A. J. Bard: J. Am. Chem. Soc., 1977, 99, 303.

50.     M. A. Fox and M. T. Dulay: Chem. Rev., 1993, 93, 341.

51.     R. W. Matthews: J. Phys. Chem., 1987, 91, 3328.

52.     R.W. Matthews, Water. Res.,1991 , 25, 1169.

53.     P. Reeves, R. Ohlhausen, D. Sloan, K. Pamplin, T. Scoggins, C. Clark, B. Hutchinson and D. Green, Sol. Energy, 1992, 48, 413.

54.     J. Kiwi, Environ. Toxicol. Chem.,1994 , 13, 595.

55.     C. Nasr, K. Vinodgopal, L. Fisher, S. Hotchandani, A.K. Chattopadhyay and P.V. Kamat, J. Phys. Chem.,1996 , 100, 8436.

56.     A.K. Ray and A.A.C.M. Beenackers, J. Environ. And Energy Eng. AIChE., 1997, 43, 2571.

57.     H. Freudenhammer, D. Bahnemann, L. Bousselmi, S.U. Geissen, A. Ghrabi, F. Saleh, A. Si-Salah, U. Siemon and V. Vogelpohl, Wat. Sci. Tech., 1997, 35, 149.

58.     T. Sivekumar and K. Shanthi , Indian J. Environ. Prot., 2001, 21, 101.

59.     M.A. Hasnat, I.A. Siddiquey and A. Nuruddin, Dyes Pigm.,2005 , 66, 185.

60.     V. Belessi, G. Romanos, N. Boukos, D. Lambropoulou and C. Trapalis, J. Hazard. Mater., 2009, 170, 836 .

61.     X. Hu, G. Li and J.C. Yu, Langmuir 2010, 26, 3031

62.     X. Chen, S. Mao, Chem. ReV. 2007, 107, 2891.

63.     Y.G. Tao, Y. Xu, J. Pan, H. Gu, C. Qin, and P. Zhou, *Materials Science and Engineering*: *B*, 2012, **177**, 1664.

64.     Y. Ohama, and D.V. Gemert, Applications of titanium dioxide photocatalysis to construction materials. Netherlands: Springer, .2011

65.     D.F. Ollis and H. Al-Ekabi, Photocatalytic Purification and Treatment of Water and Air; Elsevier: Amsterdam, 1993.

66.     B. Ohtani, Y. Ogawa and S.I. Nishimoto, J. Phys. Chem. B, 1997, 101, 3746.

67.      T. Kawahara, Y. Konishi, H. Tada, N. Tohge, J. Nishii and S. Ito, Angew. Chem., 2002, 114, 2935.

68.     D. C. Hurum, K. A. Gray, T. Rajh and M. C. Thurnauer, J. Phys. Chem. B, 2004, 108, 16483.

69.     R. Asapu, V.M. Palla, B. Wang, Z. Guo, R. Sadu and D.H. Chen, J. Photochem. Photobiol., A, 2011, 225, 81.

70.     Y.H. Hsien, C.F. Chang, Y.H. Chen and S. Cheng, Appl. Catal. B, 2001, 31, 241.

71.     K. Shankar, J.I. Basham, N.K. Allam, O.K. Varghese, G.K. Mor, X. Feng, M. Paulose, J.A. Seabold, K.S. Choi and C.A. Grimes, J. of Phys. Chem. C., 2009, 113, 6327.

72.     S. Mozia, E. Borowiak-Paleń, J. Przepiórski, B. Grzmil , T. Tsumura, M. Toyoda, J. Grzechulska-Damszel and A.W. Morawski, J. Phys. Chem. Solids, 2010, 71, 263.

73.     W.C. Lin, W.D. Yang, Z.J. Chung and H.J. Chueng , Appl Mech Mater., 2011, 117,786.

74.     T.H.T. Vu, H.T. Au, L.T. Tran, T.M.T. Nguyen, T.T.T. Tran, M.T. Pham, M.H. Do and D.L. Nguyen, J Mater Sci , 2014, 49, 5617.

75.      L. Liu and X. Chen, Chem. Rev., 2014, 114, 9890.

76.     H. Zhang, G. R. Li, L. P. An, T. Y. Yan, X. P. Gao and H. Y. Zhu, J. Phys. Chem. C, 2007, 111, 6143.

77.      J. Wang, D. N. Tafen, J. P. Lewis, Z. L. Hong, A. Manivannan, M. J. Zhi, M. Li and N. Q. Wu, J. Am. Chem. Soc., 2009, 131, 12290.

78.      X. B. Chen and S. S. Mao, Chem. Rev., 2007, 107, 2891.

79.     Z. Weijia, G. Ligang, H. Peiguang,  C. Jingjie, L. Xiaoyan, W. Dongzhou, L. Guohong, J. Huaidong, L. Duo,  L. Hong and W. Jiyang, CrystEngComm, 2011, 13, 6643.

80.     D. Yang, H. Liu, Z. Zheng, Y. Yuan, J. Zhao, E. R. Waclawik, X. Ke and H. Zhu, J. Am. Chem. Soc., 2009, 131, 17885.

81.     A. A. Ismail and D. W. Bahnemann, J. Mater. Chem., 2011, 21, 11686.

82.      P. Marco, S.F. Francesca, A. Marco, G. Francesco, G. Edoardo and B. Barbara,  Catal. Today., 2014, 227, 71.

83.     H. Co¨lfen and M. Antonietti, Angew. Chem., Int. Ed., 2005, 44, 5576.

84.     Z. Li, C. Jin, J. Chuan, Z. Lei  and O. Paul, CrystEngComm, 2013, 15, 5012.

85.     H.G. Yang, C.H. Sun, S.Z. Qiao, J. Zou, G. Liu, S.C. Smith, H.M. Cheng and G.Q. Lu, Nature, 2008, 453, 638.

86.     N.Q. Wu, J. Wang, D. Tafen, H. Wang, J.G. Zheng, J.P. Lewis, X.G. Liu, S.S. Leonard and A. Manivannan, J. Am. Chem. Soc., 2010, 132, 6679.

87.      H.G. Yang, G. Liu, S.Z. Qiao, C.H. Sun, Y.G. Jin, S.C. Smith, J. Zou, H.M. Cheng, G.Q. Lu, J. Am. Chem. Soc. 2009, 131, 4078.

88.    N. Murakami, Y. Kurihara, T. Tsubota, T. Ohno, J. Phys. Chem. C, 2009, 113, 3062.

89.    X. Han, Q. Kuang, M. Jin, Z. Xie and L. Zheng, J. Am. Chem. Soc., 2009, 131, 3152.

90.    Y. Jiaguo Yu, L. Jingxiang, X. Wei, Z. Peng and J. Mietek, J. Am. Chem. Soc., 2014, 136, 8839.

91.    N. Roy, Y. Sohn and D. Pradhan, ACS Nano, 2013, 7, 2532.

92.    D. Praveen Kumar, N. Lakshmana Reddy, M. Karthikeyan, N. Chinnaiah, V. Bramhaiah, V. Durga Kumari and M.V. Shankar, J. Colloid. Interface. Sci., 2016, 477, 201.

93.    D. Praveen Kumar, M.V. Shankar, M. Mamatha Kumari, G. Sadanandam, B. Srinivas and V. Durga Kumari, Chem. Commun., 2013, 49, 9443.

94.    H. G. Yang and H. C. Zeng, J. Phys. Chem. B, 2004, 108, 3492.

95.    Yanhui Ao, Jingjing Xu, Degang Fu and Chunwei Yuan, Catal, Commn., 2008, 9, 2574.

96.    Yuzhu Jiao, Chengxin Peng, Fangfang Guo, Zhihao Bao, Jinhu Yang, Lukas Schmidt-Mende, Ricky Dunbar,Yao Qin, and Zifeng Deng, J. Phys. Chem. C., 2011, 115, 6405.

97.    H. X. Li, Z. F. Bian, J. Zhu, D. Q. Zhang, G. S. Li, Y. N. Huo, H. Li and Y. F. Lu, J. Am. Chem. Soc., 2007, 129, 8406.

98.    Y. Zeng, X. Wang, H. Wang, Y. Dong, Y. Ma and J. Yao, Chem. Commun., 2010, 46, 4312.

99.    S. H. Hwang, J. Yun and J. Jang, Adv. Funct. Mater., 2014, 24, 7619. 17 H. Ren, R. B. Yu, J. Y. Wang, Q. Jin, M. Yang, D. Mao, D. Kisailus, H. J. Zhao and D. Wang, Nano Lett., 2014, 14, 6679.

100.   M. Yang, J. Ma, C. Zhang, Z. Yang and Y. Lu, Angew. Chem., Int. Ed., 2005, 44, 6727.

101.   J. J. Xu, M. D. Chen and D. G. Fu, Appl. Surf. Sci., 2011, 257, 7381.

102.    X. W. Lou, L. A. Archer and Z. C. Yang, Adv. Mater., 2008, 20, 3987.

103.    Y. H. Ao, J. J. Xu, D. G. Fu and C. W. Yuan, J. Hazard. Mater., 2009, 167, 413.

104.   C. F. Zhang, H. B. Wu, C. Z. Yuan, Z. P. Guo and X. W. Lou, Angew. Chem., Int. Ed., 2012, 51, 9592.

105.   H. X. Li, Z. F. Bian, J. Zhu, D. Q. Zhang, G. S. Li, Y. N. Huo, H. Li and Y. F. Lu, J. Am. Chem. Soc., 2007, 129, 8406.

106.   C. W. Guo, Y. Cao, S. H. Xie, W. L. Dai and K. N. Fan, Chem. Commun., 2003, 6, 700 .

107.   S. Li, J. Chen, F. Zheng, Y. Li and F. Huang, *Nanoscale*, 2013,**5**, 12150.

108.   J.H. Pan, X.W. Zhang, A.J. Du, D.D. Sun, J.O. Leckie, J. Am. Chem. Soc. 2008, 130, 11256.

109.   K.V. Kumar,V. Ramamurthi,S. Sivanesan, J. Colloid Interface Sci., 284 2005, .14

110.   Y. Zeng, X. Wang, H. Wang, Y. Dong, Y. Ma and J. Yao, Chem. Commun., 2010, 46, 4312.

111.   S. Ko, C. K. Banerjee and J. Sankar, Composites Part B, 2011, 42, 579.

112.   V. Kumar, J. H. Kim, J. B. Jasinski, E. L. Clark and M. K. Sunkara, Cryst. Growth Des., 2011, 11, 2913.

113.   G. L. Xiang, Y. G. Wang, J. Li, J. Zhuang and X. Wang, Sci. Rep., 2013, 3, 1411.

114.   T. Beuvier, M. R. Plouet, M. M. L. Granvalet, T. Brousse, O. Crosnier and L. Brohan, Inorg. Chem., 2010, 49, 8457.

115.   D. Yang, H. Liu, Z. Zheng, Y. Yuan, J. Zhao, E. R. Waclawik, X. Ke and H. Zhu, J. Am. Chem. Soc., 2009, 131, 17885.

116.   C. Yothin, J. Patcharanan, H. Trevor, W. Aidan, S. Andrew, J. Benjamin and B. Rik , J. Mater. Chem. A, 2016, 4, 5685 .

117.   Z. Zheng, H. Liu, J. Ye, J. Zhao, E. R. Waclawik and H. Zhu, J. Mol. Catal. A: Chem., 2010, 316, 75.

118.   H.H. Lo, N.O. Gopal, S.C. Sheu and S.C. Ke, J. Phys. Chem. C, 2014, 118, 2877.

119.   Y. Yu and D. Xu, Appl. Catal. B, 2007, 73,166.

120. H. Zhu, X. Gao, Y. Lan, D. Song, Y. Xi, J. Zhao, J.Am. Chem. Soc., 2004, 126, 8380.

121. T. Ibusuki and K. Takeuchi, J. Mol. Catal., 1994, 88, 93.

122. T. Shibata, N. Sakai, K. Fukuda, Y. Ebina and T. Sasaki, Phys. Chem. Chem. Phys., 2007, 9, 2413.

123. J.A. Calabria, W.L. Vasconcelos, D.J. Daniel, R. Chater, D. McPhail and A.R. Boccaccini, Constr. Build. Mater., 2010, 24, 384.

124. M.B. Patel, S.A. Patel, A. Ray and R.M. Patel, J. Appl. Polym. Sci., 2003, 89, 895.

125. V. Falguera, J. Pagán, S. Garza, A. Garvín and A. Ibarz, Food Res. Int., 2011, 44, 1580.

126. S.Y. Park and S. Ha, Food Bioprocess Technol., 2015, 8, 895.

127. C. Liu, X. Li, and H. Chen, Int. J. Food Microbiol., 2015, 214, 18.

128. T. Koutchma, Food Bioprocess Technol., 2009, 2, 138.

129. A. Azam, A.S. Ahmed, M. Oves, M.S. Khan, S.S. Habib and A. Memic, Int. J. Nanomedicine., 7, 2012, 6003.

130. J. C. Tiller, C.J. Liao, K. Lewis and A.M. Klibanov, Proc. Natl. Acad. Sci. USA., 2001, 98, 5981.

131. M. Ignatova, N. Manolova and I. Rashkov, Eur. Polym. J., 2007, 43, 1609.

132. Y. Zhao, Z. Wang, X. Zhao, W. Li and S. Liu, Appl. Surf. Sci., 2013, 266, 67.

133. T.R. Stratton, J.A. Howarter, B.C. Allison, B.M. Applegate and J.P. Youngblood, Biomacromolecules, 2010, 11,1286.

134. X. Zhang, H. Su, Y. Zhao and T. Tan, J. Photochem. Photobiol. A, 2008, 199,123.

135. P. Wu, J. A. Imlay and J. K. Shang, Biomaterials, 2010, 31, 7526.

136. T. Z. Tong, A. Shereef, J. S. Wu, C. T. T. Binh, J. J. Kelly, J.F. Gaillard and K. A. Gray, Environ. Sci. Technol., 2013, 47, 12486.

137. T. Matsunaga, R. Tomoda, T. Nakajima and H. Wake, FEMS Microbiol. Lett., 1985, 29, 211.

138.    J.H. Carey and B.G. Oliver, Water Pollut Res J Can, 1980, 15,157.

139.    J.C. Ireland, P. Klostermann, E.W. Rice and R.M. Clark, Appl. Environ. Microbiol. 1993, 59, 1668.

140.    R.J. Watts, S. Kong, M.P. Orr, G.C Miller and B.E. Henry, Water Res. 1995, 29, 95.

141.    C. Wei, W.Y. Lin, Z. Zainal, N.E. Williams, K. Zhu, A.P. Kruzic, R.L. Smith and K. Rajeshwar, Environ. Sci. Technol. 1994, 28, 934.

142.     A. Makowski and W. Wardas, Current Topics in Biophysics, 2001, 25, 19.

143.    I. Paspaltsis, K. Kotta, R. Lagoudaki, N. Grigoriadis, I. Poulios and T. Sklaviadis, J. Gen. Virol., 2006, 87, 3125.

144.    V.K. Yemmireddy and Y. Hung, Int. J.Food. Microbiol., 2015, 204, 75.

145.    E.F. Duffy, F.A. Touati, S.C. Kehoe, O.A. McLoughlin, L.W. Gill and  W. Gernjak, Sol. Energy, 2004, 77, 649.

146.    C. Chen, L. Wu, H. Chen, and Y.Chung, Water, Air, and Soil Pollut., 2010, 212, 231.

147.    A.R. Rahmani, M.T. Samadi and A. Enayati Moafagh, J. Res. Health. Sci. , 2008, 8, 55.

148.    C. Sichel, J. Blanco, S. Malato and P. Fernandez-Ibanez, J. Photochem. Photobiol., A. 2007, 189, 239–246.

149.    P.S.M. Dunlop, C.P. Sheeran, J.A. Byrne, M.A.S. McMahon, M.A. Boyle and K.G. McGuigan, J. Photochem. Photobiol., A. 2010, 216, 303.

150.    J. Marugan, R. Van Grieken, C. Sordo and C. Cruz, Appl. Catal., B, 2008, 82, 27.

151.    L. Muszkat, L. Feigelson, L. Bir, K.A. Muszkat, M. Teitel, I. Dornay, B. Kirchner and G. Kritzman, Phytoparasitica, 2005, 33, 267.

152.    B. Kim, D.  Kim, D. Cho and S. Cho, Chemosphere, 2003, 52, 277.

153.    D.W. Sheel, L.A. Brook, I.B. Ditta, P. Evans, H.A. Foster, A. Steele and H.M. Yates, Int J Photoenergy., 2008, 2008, Article ID 168185, 11 pp. ]

154.   E.V. Skorb, L.I. Antonouskaya, N.A. Belyasova, D.G. Shchukin H. Möhwald and D.V. Sviridov, Appl Catal B, 2008, 84, 94.

155.   L. Muszkat, L. Feigelson, L. Bir, K.A. Muszkat, M. Teitel, I. Dornay, B. Kirchner and G. Kritzman, Phytoparasitica, 2005, 33, 267.

156.   W. Kangwansupamonkon, V. Lauruengtana, S. Surassmo and U. Ruktanonchai, Nanomed. Nanotechnol. Biol. Med., 2009, 5, 240.

157.   L. Luo, L. Miao, S. Tanemura and M. Tanemura, Mater Sci Eng B, 2008, 148, 183.

158.   R. Van Grieken, J. Marugan, C. Pablos and A. Lopez, Appl Catal B, 2010, 100, 212.

159.   J. Lonnen, S. Kilvington, S.C. Kehoe, F. Al-Touati and K.G. McGuigan, Wat Res, 2005, 39,877.

160.   D. Sawada, M. Ohmasa, M. Fukuda, K. Masuno, H. Koide, S. Tsunoda and K. Nakamura, Mycosci, 2005, 46, 54.

161.   H. Ryu H, D. Gerrity, J.C. Crittenden and M. Abbaszadegan, Wat Res, 2008, 42,1523.

162.   L. Peng, D. Wenli, W. Qisui and L. Xi, Photochem. Photobiol., 2010, 86, 633.

163.   D.J. Giannantonio, J.C. Kurth, K.E. Kurtis and P.A. Sobecky, Int. Biodeterior. Biodegrad., 2009, 63, 252.

164.   M. Sökmen, S. Degerli and A. Aslan, Exp Parasitol, 2008, 119, 44.

165.   J.S. Hur, S.O. Oh, K.M. Lim, J.S. Jung, J.W. Kim and Y.J. Koh, Postharvest Biology and Technology, 2005, 35, 109.

166.   C. Maneerat and Y. Hayata, International Journal of Food Microbiology, 2006, 107, 99.

167.   W. Han, P.H. Zhang, W.C. Cao, D.L. Yang, S. Taira, Y. Okamoto, J.I. Arai and X.Y. Yan, Prog Biochem Biophys, 2004, 31, 982.

168.   R.J. Watts, S. Kong, M.P.Orr, G.C. Miller and B.E. Henry, Water Res, 1995, 29, 95.

169.   L. Zan, W. Fa, T. Peng and Z.K. Gong, J Photochem Photobiol B, 2007, 86,165.

170.    G. Gottschalk, "Biosynthesis *of Escherichiu coli* cells *from* glucose," Bacterial Metabolism. *Ed.* M.P. Starr. Springer-Verlag, New York, NY. 1979. pp. 34.

171.    B.D. Davis, R. Dulbecco, H.N. Eisen, H.S. Ginsberg, W.B. Wood, Jr., and M. McCarty, Microbiology. 2nd edition. Harper and Row, Publishers, Hagerstown, MD. 1973. pp. 201.

172.    T.Saito, T. Iwase, J. Horie, T. Morioka,1992, J Photochem Photobiol B 14, 369.

173.    C. Hu, J. Guo, J. Qu, X. Hu, Photocatalytic degradation of pathogenic bacteria with AgI/$TiO_2$ under visible light irradiation. Langmuir, 2007, 23, 4982.

174.    Z. Huang, P.C. Maness, D.M. Blake, E.J. Wolfrum, S.L. Smolinski, W.A. Jacoby, J Photochem Photobiol A, 2000, 130,163.

175.    G. Gogniat, M. Thyssen, M. Denis, C. Pulgarin and S. Dukan, FEMS Microbiol Lett, 2006, 258, 18.

176.    P. Wu, J.A. Imlay and J.K. Shang, Biomater, 2010, 31, 7526.

177.    T. Saito, T. Iwase, J. Horie and T. Morioka, J Photochem Photobiol B, 1992, 14,369.

178.    P. Amezaga-Madrid, G.V. Nevarez-Moorillon, E. Orrantia-Borunda and M. Miki-Yoshida, FEMS Microbiol Lett, 2002, 211, 183.

179.    K. Sunada, T. Watanabe and K. Hashimoto, J Photochem Photobiol A, 2003, 156, 227.

180.    K. Sundara,Y. kokuchi, K. Hashimoto, A.Fujishima, Environ. Sci. Technol., 1998, 32, 726.

181.    P. Amezaga-Madrid, R. Silveyra-Morales, L. Cordoba- Fierro, G.V. Nevarez- Moorillon, M. Miki-Yoshida, E. Orrantia-Borunda and F.J. Solis, J. Photochem. Photobiol., B. 2003, 70, 45.

182.    K.S. Yao, D.Y. Wang, J.J. Yan, L.Y. Yang and W.S. Chen, Surf. Coat. Technol., 2007, 201, 6882.

183.    X. Yang and Y. Wang, Build. Environ., 2008, 43, 253.

184.    Y. Wang, X. Yang and Z. Han, Trans Hong Kong Inst Eng, 2005, 12, 39.

185.     X.C. Shen, Z.L. Zhang, B. Zhou, J. Peng, M. Xie, M. Zhang and D.W. Pang, Environ. Sci. Technol., 2008, 42, 5049.

186.     C.A. Linkous, G.J. Carter, D.V. Locuson, A.J. Ouellette, D.K. Slattery and L.A. Smith, Environ. Sci. Technol., 2000, 34, 4754.

187.     J. Hong, H. Ma and M. Otaki, J. Biosci. Bioeng., 2005, 6, 592.

188.     K.P. Kühn , I.F. Chaberny, K. Massholder, M. Stickler, V.W. Benz, H.G. Sonntag and L. Erdinger, Chemosphere , 2003, 53,71.

189.     N. Akiba, I. Hayakawa, E.S. Keh  and A. Watanabe, J. Med. Dent. Sci., 2005, 52, 223.

190.     M. Sökmen, S. Degerli and A. Aslan, Exp. Parasitol., 2008, 119, 44.

191.     L. Peng, D. Wenli, W. Qisui and L. Xi , Photochem. Photobiol., 2010, 86, 633.

192.     F.M. Salih, J. Appl. Microbiol., 2002, 92, 920.

193.     C. Guillard, T.H. Bui, C. Felix, V. Moules, B. Lina and P. Lejeune, C .R. Chim, 2008, 11, 107.

194.     M. Cho and J. Yoon, J. Appl. Microbiol., 2008, 104, 759.

195.     M. Otaki, T. Hirata and S. Ohgaki, Wat.Sci. Technol., 2000, 42,103.

196.     V. Cohen-Yaniv, N. Narkis and R. Armon, Wat. Sci. Technol., 2008, 58, 247.

197.     M. Pratap Reddy, H.H. Phil and M. Subrahmanyam, Catal. Lett., 2008, 123, 56.

198.     C.L. Cheng, D.S. Sun, W.C. Chu, Y.H. Tseng, H.C. Ho, J.B. Wang, P.H. Chung, J.H. Chen, P.J. Tsai, N.T. Lin, M.S. Yu and H.H. Chang, J. Biomed.Sci., 2009, 16, 10.

199.     A.G. Rincón and C. Pulgarin, Appl. Catal. B, 2004, 51,283.

200.     P.A. Christensen, T.P. Curtis, T.A. Egerton, S.A.M. Kosa and J.R. Tinlin, Appl. Catal. B, 2003, 41, 371.

201.     Y.W. Cheng, R.C.Y. Chan, P.K. Wong, Wat. Res., 2007, 41,842.

202.     V.A. Nadtochenko, O.M. Sarkisov, V.V. Nikandrov, P.A. Chubukov, N.N. Denisov, Russ J. Phys. Chem. B, 2008, 2, 105.

# CHAPTER IV
# SECTION B

## 4.2 PHOTCATALYTIC ACTIVITY OF CO-CATALYST MODIFIED MESOPOROUS ASSEMBLED TITANIA AND TITANIA NANOTUBES TOWARDS HYDROGEN PRODUCTION BY WATER SPLITTING

**CONTENTS**

*The world has voracious appetite for energy with the increase in world population and the rampant unregulated industrial growth. In the development of new energy sources, hydrogen fuel has received substantial interest. The term evokes a vision of energy which is sustainable and environmentally friendly. The focus of photcatalysis is not only on the oxidation of various contaminants emerging as a threat to mankind, but also on the photoreduction reactions that produce sustainable energy sources such as hydrogen, and the reduction of nitro-aromatic contaminants etc; Thus development of photcatalysts which can solve both energy and environmental issues are highly desirable in the present scenario. Yet now the generation of hydrogen efficiently by photocatalytic splitting of water using sunlight remains as un-achieved aim from a technological perspective. To improve the visible light photocatalytic activity of $TiO_2$, number of approaches has been developed in recent years. In this section, we evaluate and compare the efficiency of titania nanostructures and its modified systems for production of hydrogen through water splitting reaction.*

## 4.2.1   INTRODUCTION

### Hydrogen - A Future Energy Carrier

Energy is the very essential core of today's society and economy. Our whole economic, social and physical welfare rely on the sufficient and uninterrupted supply of energy. We are enjoying the benefits that are preseved by our ancestors. Since worldwide appetite for energy are growing in an alarming rate, we should provide solutions for energy crisis for the coming genrations. The growth of modern technological era passed through age of fossil fuels, age of petroleum where the ascendance of wood, coal, oil rich societies has been observed. With respect to the growing population, the energy consumption from these sources had a detrimental effect on mankind. Today we have entered the stage where the inherited environmental pollution, related effect of greenhouse gases and the consequent climate changes are standing as a big problem to get solved. In order to save the coming generations from experiencing an energy vacuum, we are really in need of alternative, renewable and environmentally benign energy sources. Low efficiency of the available alternative energy sources such as wind, biomass, nuclear, solvothermal, geothermal and solar make them unfit for the purpose.

In this scenario there is a growing awareness on $H_2$, as a fuel for future to avoid potential energy crisis. Annual wold wide production of Hydrogen is more than 44.5 million tons (or 500 billion cubic meters) in the present time which are used for industrial purposes [1]. Hydrogen is not a primary fuel source. Like electricity, hydrogen

is an energy carrier ie; it is a means for transmitting energy from primary fuel source to users of benefit. It has an additional attribute that makes it more suited for some applications than electricity that it can be stored for latter use. This makes it attractive for powering vehicles and portable devices. Hydrogen powered vehicles/ fuel cell electric vehicles, FCEVs have been introduced as they might produce almost similar performance as that of petroleum based fuels; but with zero emission which is highly desirable. When this power source is on the way to enter into our daily life, we should search for proper and greener alternative resources to meet its high demand in future.

Hydrogen is the most abundant element in the universe. But its natural existence in elemental form in earth is nill. Hydrogen is locked up in enormous quantities in various resources such as biomass, natural gas, fossil fuels, water etc. Production of Hydrogen from these resources essentially require a source of energy which may vary (thermal, photolytic, electrolytic etc.). In thermal process, energy in resources including natural gas, coal, or biomass are utilized to produce hydrogen. And this included natural gas reforming, gasification, renewable liquid fuel reforming and high temperature water splitting. Natural gas steam reforming is the most commonly used hydrogen production methods explored by the researchers. Electrolytic processes use electricity to split water into hydrogen and oxygen in a unit called electrolyzer which consists of an anode and cathode separated by an electrolyte. Two electrolysis pathways for wide-scale hydrogen production are electrolysis using renewable sources and nuclear high-temperature electrolysis. In photolytic

process of Hydrogen production, light energy is used to split water to its constituents. Much investigations are undergoing in this area as they offer long-term potential for sustainable hydrogen production with low environmental impact. Photolytic processes included: photobiological Water Splitting, photoelectrochemical Water splitting. The word ''photo electrochemical'' refers to a scheme in which light is used to introduce an electrochemical process which includes, photoelectrolysis, photocatalysis' and photo assisted splitting.

Around 50% of the global hydrogen demand come by natural gas steam reforming, 30% met from oil reforming, 18% from coal gasification, 3.9% from water electrolysis, and 0.1% from other sources [2-4]. Many of the above said resources for producing Hydrogen are having detrimental effect on environment. For eg., the high temperature reaction between hydrocarbon and water during steam methane reformation concurrently generates hydrogen and carbon dioxide. Basically the basic intention of using greener Hydrogen power for reducing environmental pollution thereby global warming is violated as it releases the green house gas $CO_2$ Into the atmosphere.

When hydrogen is produced from water, not only the unwanted emissions are minimized but also it is considered as cost effective as it needs only the assistance of an external energy source. The approaches which used water as a material for hydrogen production included electrolysis, thermochemical water splitting, photo catalyzed water splitting and photoelectrolysis. Among these methods, photocatalytic production of hydrogen from water is projected as the most rewarding

work since the resources used are abundant, cheap and less toxic to environment. Water is abundant as well as renewable. Photocatalytic water splitting over semiconductor materials has been deemed as a promising approach for direct solar-to-hydrogen conversion and extensive research work is carried out in this direction. There are two types of configurations adapted to a photo catalyst that can be used for photochemical water splitting: (i) photoelectrochemical cells and (ii) particulate photo-catalytic systems. Photoelectrochemical cell set up involves two electrode; one of them is a photocatalyst exposed to light irradiation, and the other one immersed in an aqueous electrolyte. In particulate photocatalytic systems, the powdered photocatalysts are in the suspended in aqueous solution and each particle acts as micro photoelectrode performing oxidation and reduction reactions of water on its surface. The particulate photocatalytic systems are far simpler and cheaper than photo electrochemical cell.

Among the methods of generating the fue Hydrogen from renewable energy sources, photocatalysis on semiconductor metal oxides has become promising one due to the simplicity of concept and technical feasibility. The pioneering discovery by K. Honda and A. Fujishima, in 1972, unfolded the photosensitization effect of a $TiO_2$ electrode for the electrolysis of water into $H_2$ and $O_2$ using a Pt metal electrode (cathode) and a $TiO_2$ (anode) in presence of UV light. They observed that, unlike normal electrolysis, the electrolysis of water occured at a lower bias voltage under UV light irradiation of the $TiO_2$ electrode [5]. Later in 1977, G. N. Schrauzer et al. reported the photocatalytic decomposition of $H_2O$ on powdered Pt/Rh metal

decorated $TiO_2$ photocatalysts [6]. These observations lead to the fact that in semiconductor mediated photocatalysis charge separation of photogenerated electrons/holes is assumed to be the most important process. The electrons and holes move to Pt metal side and titania respectively inducing oxidation / reduction reactions [7-8]. The revolutionary works by Honda/Fujishima and Schrauzer/Guth, inspired various researchers for designing photocatalytic systems using various semiconductors, semiconductors incorporated with inert supports, colloidal semiconductors, binary oxide catalysts etc.

## 4.2.2 Basic Mechanism of semiconductor based photocatalytic water splitting for Hydrogen generation

Photogenerated electron/ hole pairs are involved in both photocatalytic water/ air purification and photocatalytic hydrogen production. An effective photocatalyst is the one that uses these electrons and holes efficiently. Nevertheless, the utilization of holes/electrons as well as the system processing are special for each. That is in photocatalytic water/air purification, the conduction band (CB) level is insignificant whereas valence band (VB) holes are the important elements that prompt the decomposition of contaminants. On the other hand, when photocatalysis is applied to perform water-splitting for the production of Hydrogen, the reducing CB electrons become keystones and protons are reduced to hydrogen molecules by these electrons. In general, the overall photo catalytic water splitting reaction producing Hydrogen involves three major steps: (i) absorption of light by a semiconductor to produce electron–hole pairs, (ii) charge separation and migration of photgenerated electron hole pairs to the

surface of the semiconductor, and (iii) surface reactions for $H_2$ or $O_2$ evolution. The hydrogen evolution reaction takes place on the surface of semiconductor materials. The availability of high surface area makes nanosized semiconductors a good candidate for enhanced adsorption and photoctalysis on their surface compared to their bulk counterparts. When an incident photon with energy equal to or higher than the band gap of material strikes, electrons in the valence band are excited to the conduction bands leaving holes in the valence band. The surface adsorbed water or protons are reduced by these electrons into molecular hydrogen. Water splitting reaction to hydrogen and oxygen is an uphill reation. The reaction is accompanied by a large positive change in the Gibbs free energy i.e., It is an uphill reaction.

$$H_2O \rightarrow \frac{1}{2} O_2 + H_2 \text{ ; } \Delta G = +237 \text{ KJ/mol}$$
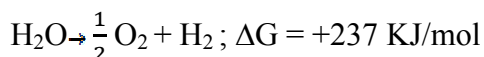
For water-splitting, the energy of the absorbed photon must be at least 1.23 eV $[E_i = \Delta G°_{(water)}/ 2N_A$ where $\Delta G°_{(water)} = 237.141$ /mol and $N_A =$ Avogadro's number $(6.022 \times 10^{23}$/mol)]. This means that during the photocatalytic water-splitting, photon energy is converted into chemical energy using the photocatalyst. To achieve efficient hydrogen production, using a single semiconductor, the CB level should be more negative than reduction potential of water to hydrogen while the VB should be more positive than oxidation potential of water to oxygen [9].
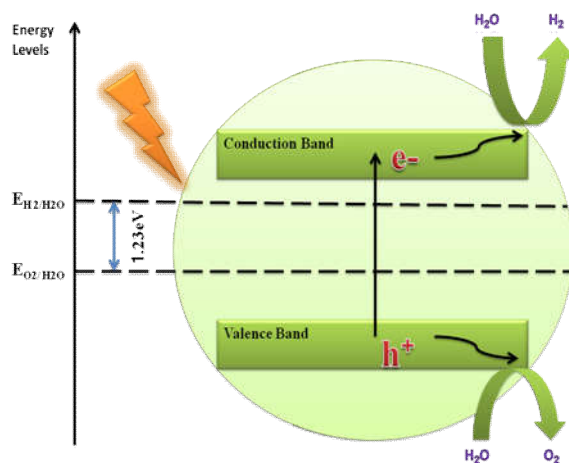
**Figure 1**. Mechanism of semiconductor based photocatalytic water splitting for Hydrogen generation

Metal oxides such as $TiO_2$, $ZnO$, $WO_3$, $ZrO_2$, $SnO_2$, $Fe_2O_3$, $RuO_2$, sulphides such as $ZnS$, $GaS$, metal (oxy)sulfide, metal (oxy)nitride, tantalates, niobates, Indates, Tungsten based materials, Perovskite type materils, Inorganic complexes, semiconductors containing elements such as Ga or In, compounds such as GaAs, CdTe and CdSe, etc. are invariably used in photocatalytic water splitting. Semiconductors with a small band gap, such as CdS and CdSe, were investigated, but their efficiency and stability were much lower than those of $TiO_2$ [10-13]. $TiO_2$ is one among the elite member of photocatalysts for water splitting owing to its appropriate energy band potential, long term stability against photo and chemical corrosion, non-toxicity, cost effectiveness and easy availability. But the hydrogen production efficiency is still quite low because of the following reasons.

   i)       Charge overpotential for Hydrogen and oxygen evolution makes titania less efficient for water splitting [14].

   ii)      Recombination of photo-generated electron-hole pairs before reaching surface to reduce water: Quick recombination of CB electrons with VB holes taking place.

   iii)     Possibility of the fast backward reaction: As the decomposition of water into hydrogen and oxygen is an energy increasing process, backward reaction (to form water) easily proceeds.

   iv)     Inability to exploit visible light: Since the band gap of $TiO_2$ is about 3.2 eV, it used only UV light for hydrogen production. The inability to utilise the visible light which accounts more in solar radiation, efficiency of solar photocatalytic hydrogen production is limited.

In view of rectifying these limitations and thus to produce good yield of Hydrogen by visible light driven photocatalytic water splitting, research has largely been directed to this area by introducing many photocatalyst modification techniques and chemical additives. As a whole, approaches like proper selection of the structure, the crystallinity, the particle size, surface area, addition of sacrificial agents, doping with metals/ nonmetals/ other semiconductors etc. substantially improve the hydrogen evolution by Titania.

## 4.2.2 Modification of semiconductor photocatalyst – contolling the shape

Majority of the studies focussed on Hydrogen production activity of nanoparticles. Modification of the semiconductor photocatalst is an improved and optimized approach for efficient photocatalysis. Crystal structure of the material (crystallinity, defects, etc;) indeed influences the separation and transfer of photogenerated charge carriers. For example, considering the hydrogen generation in powder photocatalysis, anatase (EG = 3.2 eV) gives better results than rutile (EG ¼=3.0 eV) . The reason being the higher reduction potential of photogenerated electrons in the former one than in the latter [ bottom of the conduction band of anatase is located 0.1V more negative than that of rutile] [15]. Also surface properties ( particle size, surface structure, active reaction sites, surface area) are related to the morphology of the semiconductor. Keeping all these in mind, researchers strive to produce well defined nanostructured semiconductors with differed morphology to raise the charge carrier separation yield and, hence the hydrogen evolution reaction (HER) activity [16-20]. Tuning of morphology has attracted considerable attention as the change in material morphology that can modify charge carrier diffusion pathways.  Various attempts have been made in this direction for designing nano-structured $TiO_2$ with different surface morphologies such as mesoporous structure, nanorod, branched nanowires, bamboo like nanotube, nanosheets etc [21-27].

Creating semiconductors with porous structure thereby increasing the surface area continus to be a topic of interest for

effective heterogenous catalysis. mesoporous materials persuade efficient absorption of solar light and electron delocalization properties and offer a large number of surface active sites available for photocatalytic reactions. It is usually observed that the use of a high surface area mesoporous oxide support offers some beneficial effects on the catalytic performance rather than a commercial support for noble or transition metals [28-31]. One-dimensional nanostructured $TiO_2$, for example nanotubes, nanofibers etc, are of particular importance due to their superior electronic/magnetic/optical/catalytic, and mechanical properties, and their versitile applications in various fields [32]. It is identified that Titania nanotubes possess large specific surface area and efficient electron conductivity [33]. The reports suggest that Titania nanotube is a good candidate to enhance the  HER activity by adding metal oxide composites or low cost metals on $TiO_2$ nanotubes [34-36]. Similarly Titania based Hollow / core shell/ multiwalled structures are found to be another potential candidate owing to its low density ,tunable thickness of the shells, pore volume, high surfce area, efficient light harvesting ability etc. [37-39]. These properties are indeed beneficial. Thus we can conclude that tuning the morphology is an important factor in the enhancement of photocatalytic processes.

### 4.2.4   Reaction with sacrificial agents

In later 1970 s, several experiments were conducted for the simultaneous production of $H_2$ and $O_2$ in the powder systems, but the reaction efficiency was very low. Kawai and Sakata examined the reasons for this lower efficiency and concluded that in the powder

system, the produced $H_2$ and $O_2$ gases might recombine to regenerate water molecules. It is because the production sites of each gas are located close to each other. Further, addition of organic compounds to the aqueous suspension of platinized $TiO_2$ enhanced the quantum yield to a considerable extent. In this case, the organic compound is oxidised instead of water by photogenerated holes at the $TiO_2$ sites and Hydrogen is produced at Pt sites [40].

An additional factor that makes photocatalysis productive is the ability of the solvent to suppress the undesired electron–hole recombination, by capturing the valence band holes or the conduction band electrons. when Additives like electron donars/acceptors are introduced into the reaction solution, their irreversible consumption occurs instead of water. These added materials are called sacrificial agents. As electron acceptors ($Ag^+$, $Ce^{4+}$, $Fe^{3+}$) in hydogen evolution are less significant, in water splitting reactions, mostly the sacrificial agents are electron donars [41] . There are inorganic systems ($S^{2-}/SO^{3-}$, $Br^-$, $CN^-$, $Ce^{3+}$, $Fe^{2+}$ , $I^{3-}$ etc) and organic sacrificial reagent system ( methanol, ethanol, lactic acid etc). Among them methanol was most widely used [42-45]. In the case of $TiO_2$ in presence of sacrificial agents, upon irradiation, the photogenerated electrons transferred from the conduction band of $TiO_2$ to the empty orbital of the electron acceptor. Thermodynamically, the potential of the electron acceptor shuld be below the conduction band potential of $TiO_2$. In the case of elecron donars, the electrons are transferred from the filled orbital of donar to recombine with the holes in the valence band which is possible when the potential of electron donar is above the valence band

potential of $TiO_2$. Considering the potential of methanol oxidation by hole is $E^0_{(.CH2OH/CH20)}$= -0.95V, and potential for water oxidation is $E^0_{(H2O/O2)}$ = 1.23V, the energy difference between the valence band potential of $TiO_2$ ($E^0(ox)$=2.94V) and methanol oxidation is higher, the holes easily oxidise methanol thus making available the electrons free from recombination. In Hydrogen generation by photocatalytic water splitting, the oxidation of water by holes is a much slower process than the reduction by electrons. Once the holes are scavenged from the photocatalyst surface by the sacrificial electron donars, the longer decay time of surface electrons would make the reduction of protons in the solution easy [46].

## 4.2.5   Photocatalyst modification for visible light harvesting

The easily tunable band gap of titania makes it a suitable candidate for absorption of light in the visible light wavelength region to operate effectively under natural sunlight irradiation. Investigations by various researchers towards increased the hydrogen production by semiconductor metaloxides including attempts to increase the visible light response together with efficient charge migration and separation. General Strategies in this direction included, band gap engineering (metallic or/ and non metal ion doping) [47-54] coupling with semiconductors [55-58], dye sensitization [59], surface plasmonic enhancment [59-61] surface modification via organic materials [62], creating oxygen vacancies and disorder [63-67] single phase narrow band gap smeiconductors [68-69], cocatalyst loading [70-71]etc; Here we have adopted the co-catalyst modification as a mean for visible light harvesting of nanostructured titania.

### 4.2.6    Co-Catalysts for Phtocatalytic Hydrogen evolution

Most of the semiconductors do not result in a good and relaible Hydrogen evolution rate even in the presence of a sacrificial agent due to the easy recombination of charge carriers combined with the comparatively slow surface reactions. Presence of appropriate cocatalyst on the light harvesting semiconductor certainly promote the photocatalytic pathway. The role of cocatalysts in semiconductor based water splitting reactions can be categorized as i) These cocatalysts decreases the activiation energy or overpotential for $H_2$ or $O_2$ evolution reactions. ii) It increases the robustness of the semiconductor by suppressing its photocorrosion. This can be achieved by extracting the holes which are responsible for the self decomposition of many semiconductors by photo oxidation. [72-73] iii) Cocatalysts effectively separate the photogenerated charge carriers. In presence of cocatalyst, the photogenerated electrons are transferred from the semiconductor metaloxides to the cocatalyst, reducing protons to hydrogen molecules along with the oxidation of electron donar by holes if any. The readiness of cocatalyst to trap the electron from semiconductor and its ability to reduce $H^+$ ions on the surface are are taken in to account while selecting the cocatalysts to assist in good $H_2$ production. The relative energy level formed at hereojunction between the semiconductor and the cocatalyst determines the effective separation of photogenerated electrones. The heretostructure with a shorter distance between the semiconductor and cocatalyst is beneficial. It is because this will reduce the transport distance of electrons between the two energy levels making the recombination in bulk difficult [74-78].

In general, in situ photoreduction, chemical reduction and impregnation-calcination/reduction methods are the usually employed preparation methods to load these metals as clusters/ nanoparticles (NPs) on semiconductors. The photo deposited electrons act as electrodes within nanosize which accumulate the photogenerated electrons, reduce the water reduction overvoltage, and increases the recombination of Hydrogen atoms [79-80]. The process of charge transfer between a host catalyst and the cocatalyst have been represented in figure 2.
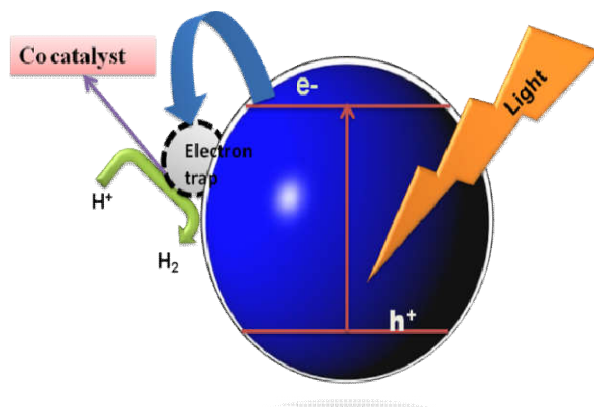


**Figure 2. Charge transfer between a host catalyst and the cocatalyst**

The metal concentration on the surface of $TiO_2$ also has influence on the photocatalytic hydrogen yield. According to literature, very low and very high concentrations have detremental effect on the hydrogen production activity in the case of cocatalyst loaded systems. The possible reasons put forward to explain the decreased activity at high concentrations are i) Partial blocking of active sites on the surface of titania by these deposited metals ii) Possibility of light filtration by

the deposited metals iii) The decrease in the surface properties of the nanoparticles deposited with increse of their size growth which diminishes its the electronic contact thus decrease charge transfer rate.

Noble metals, transition metals, nonmetal oxides like transition metal sulfides, nanocarbon based materials like carbon nanotube, graphene etc are often emplyed as efficient cocatalysts for water reduction. Untill now the hydrogen production from water using visible light radiation is highest in the case of platinum based cocatalysts loaded on semiconductors. Generally the work function of the noble metals are sufficiently larger than many semiconductors. Therefore, upon excitation, the charge carriers of $TiO_2$ are easily trapped by noble metals due to their lower fermi energy level. Platinum, having the lowest Fermi level among the noble metals is the best to trap these photgenerated charge carriers. Some other noble metals proven to be  efficient to produce hydrogen enrgy by water splitting are silver, ruthenium, gold, rhodium, and palladium [81-85]. Most of the noble-metal based co-catalysts are too limited and expensive to be used for large-scale energy production. Therefore, alternative cocatalysts based on nonprecious metals and metal-free materials with high efficiency and low cost have been actively pursued.

In recent years, many kinds of novel cocatalysts based on cheap and earth-abundant elements have been developed for hydrogen production by water splitting. Among the transition metal based co catalysts, cobalt, copper and nickel have been investigated more. In these systems also creation of a schottkey barrier at

metal/semiconductor interface promotes the separation of photogenerated charges [86]. Smaller the schotkey barrier height, higher will be photocatalytic hydrogen production ability due to the easy transfer of electrons to metal from the photocatalyst. Though the bulk form of these metaloxides have high overpotential compared to noble metals, these metals in nanoscale offer intrinsic electrocatalytic activities due to the increased active sites and interfacial interactions thereby efficient charge transfer from semiconductor to cocatalyst. The activities of some systems are comparable to Pt based systems. Recently, Zong et al. found that loading $MoS_2$ as a co-catalyst on CdS significantly enhanced the rate of $H_2$ evolution. The activity was even better than a Pt-loaded sample [87]. Besides when compared to Pt , the cost of these metals is at least three orders of magnitude lower, which is an added advantage in practical applications. Another limitation when noble metals are used as cocatalysts is that they catalyse the backward reaction. Additives such as sodium hydroxide, sodium carbonate etc can be used to suppress these backward reaction [88-91]. On the other hand transition metals do not require any additives as they do not promote backward reaction [92]. Thus transition metal based cocatalysts can be suggested an alternative choices for hydrogen production by water splititng.

Amongst the transition metal /transition metal oxides, copper/copper oxides based catalysts have received immense attention. Its non toxicity, cost benefits and low band gap energies (1.4-2.3eV) make them eventual candidate for low-cost photocatalytic applications. Boccuzzi etal [93] observed that copper containing $TiO_2$ showed

higher photocatalytic activity in gas pollutant removal when compared to noble metal loaded ones. These results motivated the use of this photocatalyst for energy applications in an economic point of view. Later, Sreethawong [24] reported that hydrogen evolution rate of Cu loaded $TiO_2$ was approximately two fold higher compared to the optimum value of the Ni loaded case. Xu et al. [94] found that the as-prepared $CuO/TiO_2$ exhibited a good yield of photocatalytic $H_2$ production rate in aqueous solution of methanol which is even higher than that of some Pt/Pd incorporated $TiO_2$ systems. It was reported by Xu et al.[95] that more effiecient charge transfer takesplace when Cu species exist on the surface of $TiO_2$ than those in $TiO_2$ lattice. Since Redox potentials $E_{(M^{z+}/M^0)}$ of copper(II) is 0.34V,comparing it with the $E_{CB}(TiO_2)$ [-0.55 V], revealed that the photocatalytic reduction of copper metals by the $TiO_2$ conduction band electrons is preferred until complete conversion of the dissolved metal salts[96].

Among the noble metals at the nanoscale, silver is an extremely attractive metal due to its low cost, easy preparation, notable catalytic activity, size/shape-dependent optical properties, antimicrobial activity ,its applications in sensing (chemical and biological ) which is based on surface-enhanced Raman scattering and localized surface plasmon resonance [97-99]. Since redox potentials $E_{(M_z^+/M^0)}$ of silver (II) is 0.80V, comparing it with the $E_{CB}(TiO_2)$, revealed that the photocatalytic reduction of silver metals by the $TiO_2$ conduction band electrons is favorable until complete conversion of the dissolved metal salts [96]. Various reports emphasised that silver is a promising candidates for improving the photoreactivity of titanium dioxide by

transferring electron from conduction band of titania to Fermi level of Ag nanoparticles. Thus recombination of charge carriers has been prevented which in turn responsible for the degradation of various polutants[100-103] . These studies revealed its potential to be used as a photocatalyst to produce energy by utilising the entrapped electrons for the reduction of water in presence of light. Jae-Woo Park et al. [104] have reported methanol photo decomposition over the mixture of $Ag_2O$ and $TiO_2$. Later Park and kang have examined the hydrogen production by the decomposition of 50% aqueous methanol solution over $Ag/TiO_2$ photocatalyst with low energy UV lamps [105] Photocatalytic studies by Sadanandan et al over silver impregnated titania in aqueous solution of glycerol, showed observed the existence of $Ag_2O$-Ag phase structure on the surface of $nanoTiO_2$ is beneficial for high hydrogen production in sunlight compared to the presence of mere Ag phase. Very few studies have been reported on the effects of silver deposition on visible light-induced photocatalysis on $TiO_2$ to produce Hydrogen energy.

The nanostructured metal oxide when incorported by the co-catalyst, the structural benefits are also exploited for activity enhancement. Some recent reports have shown that copper loaded $TiO_2$ nanotube shows excellent hydrogen production actiivty due to the movement of photogenerated charge carriers along the length of the tube [106-107]. The structural dimensionality is thus an important factor related to the photocatalytic activity. Anna et al evaluated the photocatalytic activity towards Hydrogen production over metal/$TiO_2$ Photocatalysts.They have observed that the efficiency was much

higher when compared to the metal/Degussa $TiO_2$ systems [96]. As the capability of mesoporous titania to accumulate Ti(iii) under illumination has been reported and can be visually observed by grey blue coloration of nanoparticle suspension, by the reduction of Ti(IV) ions by the conduction band electrons [108]. Thus we can assume that the captured conduction band electrons in the form of Ti(III) ions migrate to the surface of catalyst where they can be transferred to the cocatalyst if present to participate in the water reduction. Therefore, it is desiarble to introduce metallic cocatalyst into the pores of mesoporous titania to improve the efficiency of the photocatalytic hydrogen evolution. In their study, among the series of metal photodeposted (Pd, Cu, Ag, Ni, Co, Cd, Zn, Fe, Pb) on the surface of $TiO_2$, commendable activity was observed in the case of Pd, Cu, Ag, Ni photdeposited systems. The catalytic activity of photodeposted copper was near to that of palladium doped systems. Thus as a result of different chemical reactivity of the metal oxide with diverse nanostructures, a beneficial charge carrier separation may results and hence better photocatalytic activity can be expected.

In this piece of study we have investigated the photocatalytic activity of copper and silver photodeposited nanostructured titania in terms of cost effectiveness, low toxicity and ease of preparation. For convenience, two of the high surface area systems among the synthesised nanostructures have been adopted namely titania nanotube and mesoporous assembled titania naocuboids. Optimization studies based on the concentration of metals have been carried out and 0.5 %

loading (by weight) was adopted for incorporation in the photocatalyst. Detailed experimental setup has been explained in chapter 2.

### 4.2.7 Activity studies

Silver and copper loaded mesoporous assembled nanocuboids were denoted as AgMT and CuMT whereas silver and copper loaded titania nanotubes were denoted as AgTNT and CuTNT respectively.

The copper/silver content in titania nanostructures was analysed using ICP-AES and the data is presented in the table 1. It has been observed that the copper and silver content is in good agreement with the calculated values (0.5 Wt %).

| Sl No | Sample Name | Observed wt % |
|-------|-------------|---------------|
| 1 | CuMT | 0.450 |
| 2 | AgMT | 0.405 |
| 3 | CuTNT | 0.454 |
| 4 | AgTNT | 0.424 |

**Table1.** The ICP-AES analysis of cocatalyst loaded titania nanostructures.

## 4.2.7.1 characterisation of modefied analogues

Raman spectral lines of mesoporous assembled titania (Figure 3a) showed all the characteristic raman active modes[144cm$^{-1}$, 197cm$^{-1}$, 399 cm$^{-1}$, 514 cm$^{-1}$, 639 cm$^{-1}$] of anatase titania. Figure 3b shows the raman spectrum of hydrothermally synthesized titania nanotube. Peaks corresponding to anatase and $TiO_2$ (B) phases were evident in the figure. Anatase peaks are located at 144 cm$^{-1}$, 197cm$^-$1, 515 cm$^{-1}$, and 639 cm$^{-1}$ while that of $TiO_2$ (B) are seen at 123 cm$^{-1}$, 162cm$^{-1}$ and 196cm$^{-1}$. Anatase is a common impurity of $TiO_2$(B) phase. XRD pattern of mesoporous assembled titania agrees well with anatase phase of $TiO_2$ (JCPDS No. 21-1272), and no other phase impurities are observed. Co-catalyst loaded mesoporous assembled titania ie; CuMT and AgMT do not show any other specific peaks indicating their highly dispersed state [Figure 3c.]. XRD pattern of titania nanotube after annealing at 400$^0$C, [Figure 3 d] confirmed the biphasic structure of Titania nanotube, TNT ie; diffraction peaks corresponds to both anatase (JCPDS no.21-11272) and $TiO_2$ (B) [JCPDS no. 74-1940]. Peaks at 24.7$^°$, 28.4$^°$, and 48.5$^°$ are assigned to be that of (110), (002), and (020) reflections of $TiO_2$ (B) whereas peaks at 25.6$^°$, 38.1$^°$, 54$^°$, and 55$^°$ correspond to anatase titania. Presence of anatase impurity is proved to be beneficial for better photocatalytic acitivity due to the interphase interactions of $TiO_2$ (B) and Anatase domains [109]. Like mesoporous assembled nanostructure, the XRD pattern of the cocatalyst samples also do not show any specific patterns different from that of Tube,TNT which can be attributed to the low content of

the metal (0.5 %; probably below the detection limit of the X-ray diffractometer), and also shows high dispersion of components in the samples [110-111].
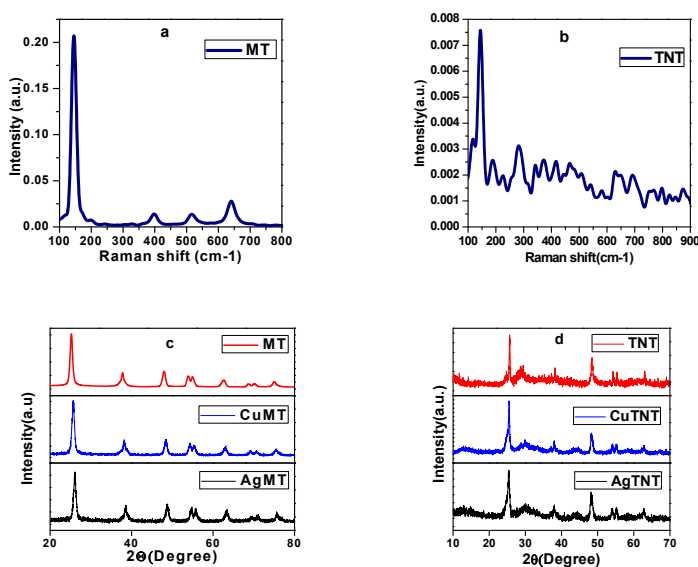


Figure 3. Raman spectra (a,b) of Mesoporous assembled titania, Titania nanotube, and XRD pattern (c,d) of mesoporous assembled titania, MT and titania nanotube, TNT with their doped systems

Nitrogen adsorption/ desorption analysis was used to characterize the porosity features of the synthesized nanostructures. The types of $N_2$ adsorption-desorption isotherms and hysteresis loops were classified by the nomenclature of Brunauer-Deming-Deming-Teller and International Union of Pure and Applied Chemistry. Figure 4a showed the nitrogen adsorption desorption isotherm of mesoporous assembled titania nanostructure and inset represented its pore distribution curve. The sample shows hysteresis

loops at relative pressures close to unity, type IV isotherm, characteristic of mesoporous materials with H1 hysteresis loop. Huge and steep condensation / evaporation steps with $P/P_0$ beyond 0.8 indicated the presence uniform and large mesopores and pore volume. The pore distribution curve (Inset of figure 3a) again confirmed that pores are within the mesoporous range (6.2 nm- 27.6 nm). The pore volume for the system is obtained to be 0.407756 $cm^3/g$. The high surface area (93.54 m²/g) is highly beneficial, as photocatalytic water splitting needs high specific surface area, porosity, and large pores for the catalyst to improve its performance.
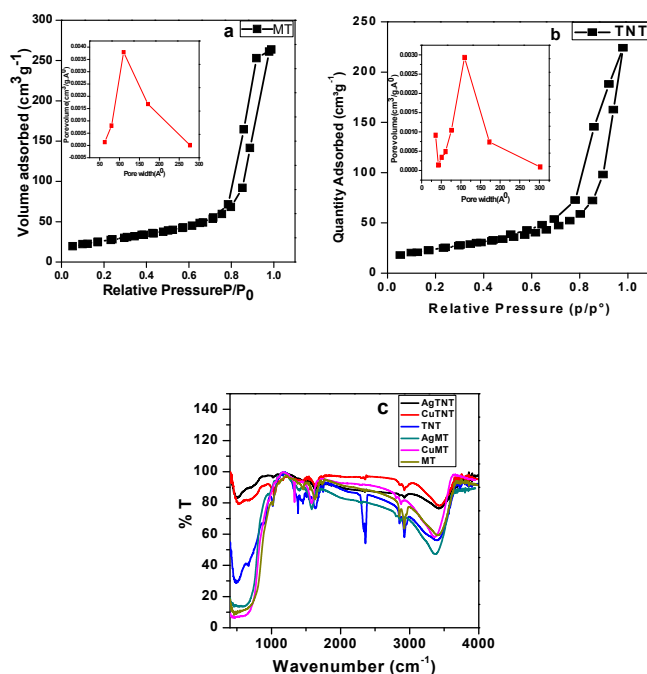


Figure 4. Nitrogen adsoption desorption isotherm and corresponding pore distribution curves (inset) of mesoporous assembled titania(a) and titania nanotube(b) FTIR spectra of the prepared photocatalysts (c)

Figure 4b represented the nitrogen adsorption desorption isotherm of hydrothermally synthesized titania nanotube. The isotherm shows monolayer adsorption at low values of relative pressures ($P/P_0$), followed by multilayer adsorption and capillary condensation. Hystersis loop is identified to be in between H1 (In the region at $0.5 < P/P_0 < 0.8$) and H3 (In the region $P/P_0 > 0.8$). In addition, the area of the hysteresis loops was relatively large, reflecting the presence of regular pore structures [112]. Two distinct peaks are observed in the pore distribution curve shown in the corresponding inset. The pores are found to be within the mesoporous range that is 3.5 nm- 30 nm. Considering the morphology of the material as observed by electron microscopy, the smaller pores correspond to the pores inside the nanotubes and the larger pores correspond to the pores between the nanotubes. The relative broad hysteresis loop indicates a wide distribution of pore sizes, thus ruling out the speculation about the shape of the pores in relatively high pressure ranges [113]. Pore volume distribution curve was obtained from the desorption data using the BJH algorithm and it is found to be 0.3465 cm$^3$/g. As both ends of the tubes are open and for the surface area measurement, the inner volume of the tube structure is accessible to $N_2$ molecules. The major contribution towards total pore volume is observed to be from mesopore volume which clearly indicates the mesoporous nature of the material. The plot of volume of $N_2$ adsorbed against the thickness of the nitrogen layer ($V_A$-$t$ plot) of the sample showed linearity in the $t$ plot region indicating the mesoporous nature of the titania nanotubes [Figure not shown] [114]. The surface area value of

nanotubes was observed to be 84.7972   m²/g. It can be seen that both the structures are in a possession to accommodate foreign bodies on account of their high surface area and porous nature. After doping, the decrease in the surface area value was observed for only titania nanotube based systems and it was insignificant for mesoporous assembled titania.

| Cocatalysts loaded samples | BET surface area (m²/g) |
|---|---|
| AgMT | 92.633 |
| CuMT | 93.2342 |
| AgTNT | 71.2344 |
| CuTNT | 70.614 |

**Table 2**. BET surface area of cocatalysts loaded samples

Figure 4c represented the FTIR spectra of the prepared nanostructures. Band at 1631 and 3415 cm$^{-1}$ is due to the bending vibrations of H-O-H and stretching vibrations of O-H bonds which suggest the presence of adsorbed water and surface hydroxyl group. The band observed in the lower frequency range (400-900cm$^{-1}$) is due to the Ti-O-Ti and O-Ti vibrations.

### 4.2.7.2 Morphology and Structure of the synthesized samples

The TEM image of Mesoporous assembled titania (Figure 5a) revealed uniform sized interconnected nanoparticles (10-15nm) whose ordered arrangement in certain direction created mesopores within the assembly. The clear contrast in the TEM image indicated the presence

of void spaces in the nanostructures. Structural mesoporosity evolution of these cuboids with co-exposed facetes have been reported earlier [115]. Figure 5b represented the TEM image and corresponding SAED pattern (insets) of copper decorated mesoporous structures. Most of the vacant spaces in between the mesoporous assembly are occupied as revealed from in the stacked areas. The voids observed in the cocatalyst loaded samples are comparatively less when compared to the parent nanostructure. More or less uniform distributions of nanoparticles are observed in the copper loaded systems than the silver loaded ones where much more aggregations are observed. The concentric ring structure in Figure 5b revealed the polycrystalline nature of copper decorated MT. HRTEM image [Figure 5c] of copper doped mesoporous assembled titania and its inset showed the inter fringe spacing to be 0.24nm , which is attributed to [001] plane of anatase titania appeared as square toped in HRTEM as reported earlier [115]. Interfringe spacing of 0.18 nm which corresponds to (200) facet of metallic copper is also observed. The TEM image of silver decorated mesoporous assembled nanostructures has been portrayed in Figure 5d. HRTEM image of the same is displayed in Figure 5e. The interfringe spacing of circled portion was measured to be 0.35nm (inset) corresponds to the (101) plane of anatase titania. The grey coloration of the catalyst is also the indicative of metallic copper deposition.

Multilayered nanotubular geometry is perceived in the TEM image (Figure 5f) of hydrothermally synthesised titania nanotube. Length of the tubes are noted to be > 200nm. The tubes are

characterized by uniform diameter along its length and open at both ends. Inner and outer diameters of the nanotubes were 6-7 nm and 8-12 nm, respectively. The interlayer spacing of multilayer nanotubes is found to be < 4 nm. After calcination at $400^{\circ}$C the tubular geometry was not destroyed as perceived from the TEM image. It can be concluded that the alkaline hydrothermal treatment and calcination process had completely transformed the precursor nanoparticles into $TiO_2$ nanotubes. The TEM images of copper and silver loaded titanium dioxide nanotubes (Figure 5g & 5k) depicted that as a consequence of the adopted cocatalyst loading procedures the length has been decreased when compared to the parent nanotubes. It has been noted that even after doping the multiwalled nature of nanotubular geometry is maintained to an extent as seen from Figure 5h. Randomly distributed aggregations of nanotubes and metal nanoparticles are evident from the image.
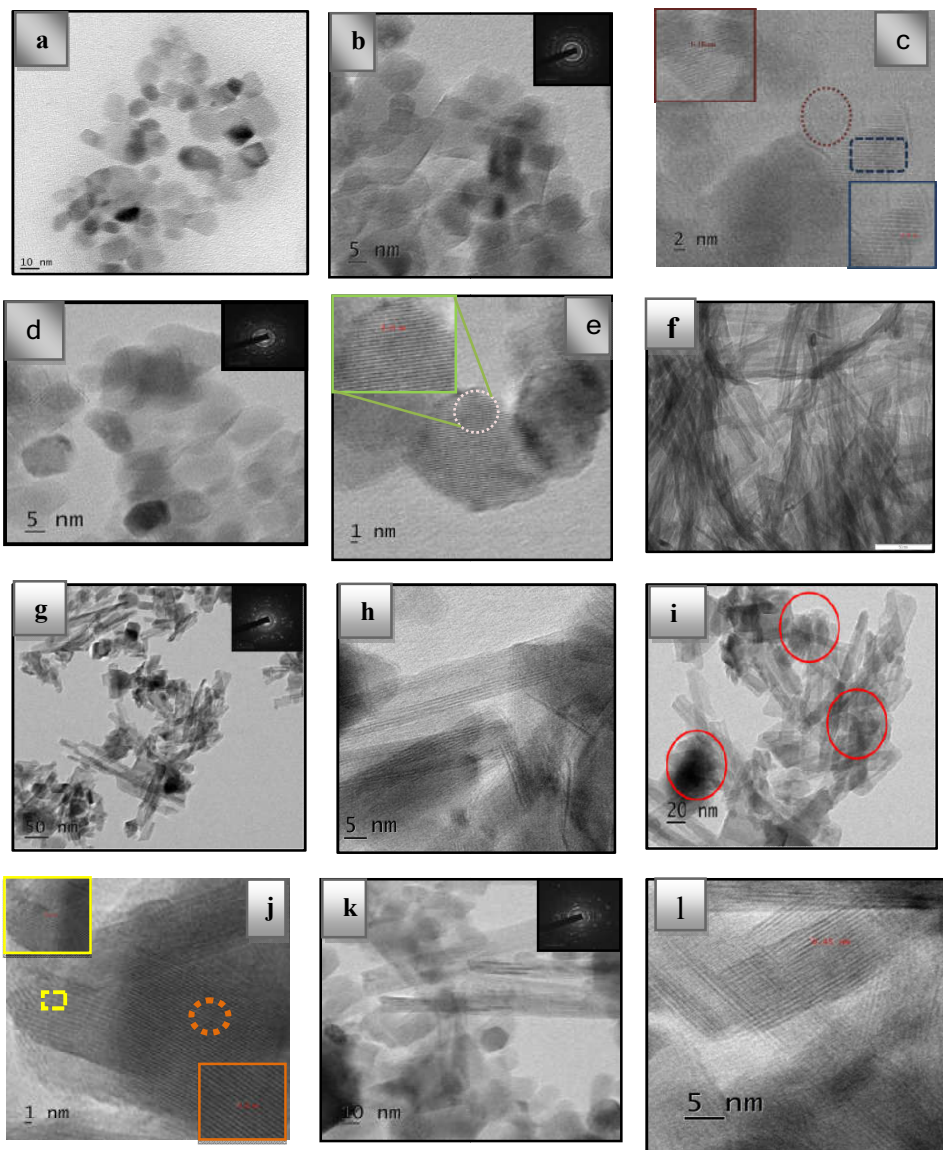
Figure 5. TEM, HRTEM, SAED patterns of mesoporous assembled titania nanostructure, titania nanotubes and their copper and silver doped analogues

In the copper decoarated nanotubes (Figure 5g) we can see that these nanoparticles are wrapped by these nanotube networks. The red circles indicated interlocked areas in the TEM image (Figure 5i). As the titanium dioxide nanotubes formed by the hydrothermal method are not well oriented (as in the case of nanotube arrays prepared by anodization) they have a tendency to aggregate themselves. Some nanoparticles are entrapped within this nanotube aggregation. These trapped nanoparticles owing to multipoint contacts with the nanotube networks serve as efficient channels for charge carrier migration. In the case of copper loaded nanotube, CuTNT, the copper nanoparticle detectable in the TEM image was few which confirmed the fine dispersion of tiny nanoparticles on the nanotubular surface. The HRTEM images (Figure 5j) showed an interfringe spacing equal to 0.65nm and 0.31nm which are corresponding to phase $TiO_2$ (B). The TEM image of silver loaded nanotube, AgTNT (Figure 5k) showed that metal nanoparticles have been deposited on the surface of nanotubes and the nanoparticle tends to aggregate more than to make a contact with nanotube surface. Number of nanoparticles in contact with the nanotube surface is less when compared to that of copper loaded one. The lattice fringes observed from HRTEM image (Figure 5l) was that of $TiO_2$ (B) phase [0.45nm].

## 4.2.7.3 The optical response of Prepared catalysts
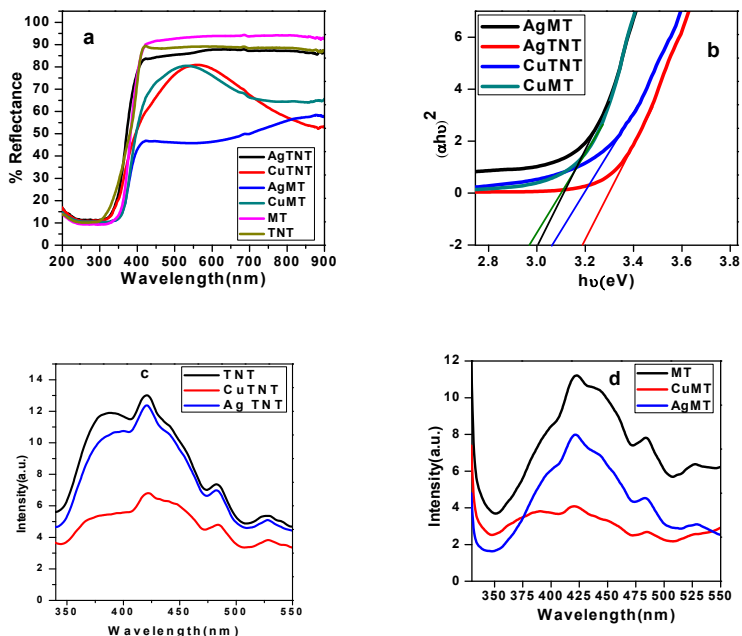


Figure 6. UV-DRS spectra (a) Kubelka munk plot (b) PL spectra(c, d) of synthesized samples

The difference in the activities of a photocatalyst can be substatiated by the UV Visible diffuse reflectance and PL spectra [Figure 6]. The optical diffuse reflectance spectra were used (200 to 800 nm) to determine the position of the absorption edge of photocatalyst and to analyse whether it has been extended to the visible region. The diffuse reflectance spectra of the cocatalyst loaded photocatalysts along with their parent systems are shown in Figure 6a. For the parent nanostructures, the reflectance onset is sharp while its variation is gradual for the cocatalyst loaded systems. It is evident that the

introduction of cocatalyst in the nanostructure matrices shifts the absorption of light to slightly higher wavelength ie; towards the visible region. Band gap values (Table 3) obtained by the extrapolation of hv Vs $(\alpha \; hv)^2$ (Figure 6b) were found to be lower for the metal loaded systems when compared to the parent systems. This in turn assures their suitability as a visible light photocatalyst. The absorption shift is justified by the introduction of additional energy levels by the metal naoparticles which are below the conduction band of parent systems [116-117]. These nanoparticles create additional bands within the band gap of titania and thus the charge carriers are trapped in these levels preventing their recombination. The reduced recombination is also substantiated by the decrease in PL intensity of the doped systems. Room temperature PL emission spectra of pure and doped titania nanostructures are represented in Figures 6cand 6d. The emission all of the samples were recorded at an excitation wavelength of 300 nm, under similar excitation conditions. PL signals were at the same positions for both the parent and cocatalyst loaded systems except that the PL intensity is decreased in the region of 455-550 nm in the case of latter series. The peak region represents the excitonic PL indicating the presence of surface oxygen vacancies and defects in the solid. The electron- hole pairs are well separated due to the participation of additional levels introduced by the cocatalysts. As the photogenerated electrons are trapped by the cocatalysts, these cannot be used for additional exciton emissions, thus leading to reduced PL intensity. Thus a decrease in PL intensity is symbolic of reduced charge carrier recombination and hence a higher photocatalytic activity.

| Photocatalyst | Bandgap energy (eV) |
|:---:|:---:|
| MT | 3.2 |
| TNT | 3.21 |
| Cu MT | 2.96 |
| Ag MT | 3.00 |
| Cu TNT | 3.02 |
| Ag TNT | 3.18 |

**Table 3.** Band gap energies of synthesized nanostructures

## 4.2.7.4 Photocatalytic degradation of methylene blue dye with the prepared catalysts

In order to check the visible light activity of the prepared systems, dye degradation experiment were conducted. Methylene blue, a heterocyclic aromatic cationic dye was chosen as a target pollutant to study the photocatalytic activity of the prepared nanostructures .The high solubility of the dye creates serious disposal problems to dye industry. In addition to that its presence in aquatic environment is highly detrimental to the living beings. It was observed that the activity of the nanostructure prepared was higher when compared to the commercially available Degussa P25. It emphasised the influence of morphology towards photocatalytic activity as indicated in many reports [118-120]. Figure 7 represented the rate of degradations of methylene blue dye in presence of various photocatalysts, which clearly indicated decrease in concentration of dye with increase in irradiation time.
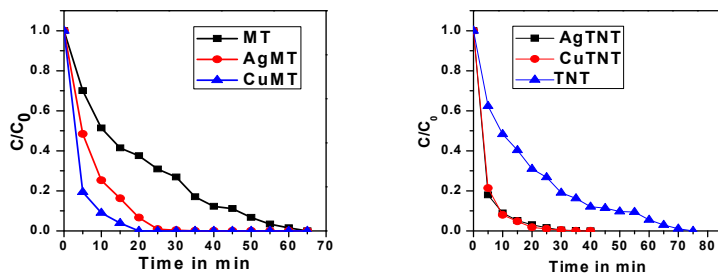
Figure 7. Photocatalytic degradation of methylene blue dye in presence of mesoporous assembled titania and titania nanotube along with their cocatalyst loaded analogues

As seen from the Figure, the copper and silver decorated systems of both the nanostructures showed better degradation ability when compared to the parent nanostructures. Both the nanostructures mesoporous titania, MT and titania nanotube, TNT took more than one hour for the complete degradation while the copper loaded mesoporous nanostructures degrade the dye within 25minutes. Silver loaded system took 35 minutes for achieving the same results. When the experiment was repeated with copper and silver decorated titania nanotube, the concerned durations were 35 min and 40 minutes respectively. Proximity in the surface area values  may be responsible for the more or less similar pathway for the degradation of methylene blue dye by the doped tubular nanostructures. Thus we can see that the cocatalyst loading with copper and silver is found to be effective for both the titania nanostructures in shifting its visible light response which is discussed in the following sections. It is worthy to mention here that the catalyst dosage chosen is 0.25g/L which is commendably

low when compared with previous reorts under sunlight using titania based systems under identical experimental conditions [120,121-126].

The benefits of the prepared catalysts when compared to Degussa P25 can be expressed in terms of catalyst separation also. It was very difficult to separate catalyst from the reaction mixture in the case of Degussa P25. At the same time the parent nanostructures namely titania nanotube, TNT, mesoporous structure, MT, and their copper /silver loaded analouges could be centrifugally separated even at a relatively low rotation speed. The schematic representation of the mechanism by which photocatalytic degradation of pollutant occurs on these nanostructured semiconductor surfaces has been represented in Figure 8.
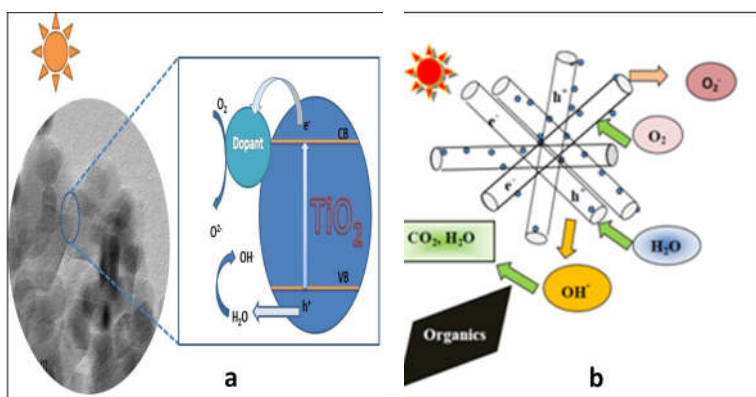


Figure 8. Mechanism showing photocatalytic degradation carried out by metal decorated mesoporous assembled titania (a) and Titania nanotube (b).

### 4.2.7.5 Photocatalytic activity study towards hydrogen production

The appreciable photodegradation efficiency of the doped systems towards methylene blue dye indicated the potential of the materials in photocatalytic hydrogen evolution. Hence the photocatalytic activity of all the samples towards the said reaction was compared under constant flux of Visible light. Control experiments were conducted and were found that there is no appreciable hydrogen evolution without either photocatalyst or irradiation. Figure 9 represents the efficiency of catalysts for water splitting in presence of visible light. The photocatalytic hydrogen yield is proportionally enhanced with light irradiation time. It was noticed that pure nanotube, TNTs and mesoporous assembled nanostructures are not active to produce hydrogen under visible light irradiation due to their very large band gap which is suitable for UV absorption.



Figure 9. Amount of hydrogen produced as a function of time for copper, silver loaded mesoporous assembled titania nanostructures (Left) and Titania nanotube (Right)

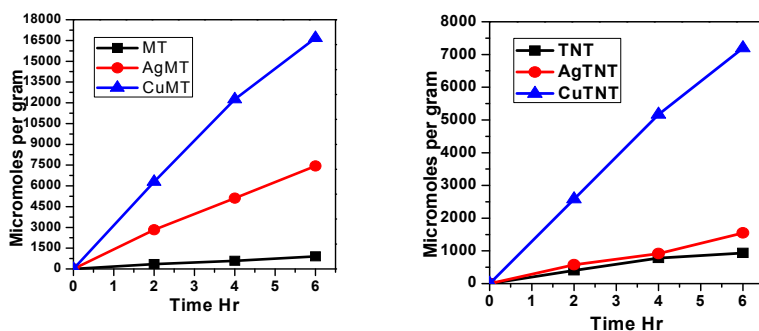Figure 9 [Left] shows the hydrogen yield in presence of mesoporous assembled structures and their copper and silver decorated analogues. Upon cocatalyst loading, a substantial improvement in activity is observed in the case of mesoporous assembled structures. It is worth noting from the TEM images that effective interaction between the dopants and $TiO_2$ existed in these systems. Such a close interconnection is particularly important for photocatalytic applications where the interfacial electron transfer from dopants to $TiO_2$ is believed to enhance the charge carrier separation and, thus, the photocatalytic efficiency. In addition, the presence of mesoporous and exposed facetes on the catalyst surface provides more accessability of active sites for the reactants and products to diffuse through, resulting in increased activity [127]. Maximum conversion of 7432.7 micromoles per gram and 16673.2 micromoles per gram is observed for silver and copper decorated samples respectively in 6 hours, with no signs of decay. The higher activity of copper decorated mesoporous structures again highlights its usage as a less expensive catalyst for future hydrogen energy production. The activity of copper loaded mesoporous assembled structures was found to be superior when compared to various reports under more or less similar experimental conditions [128-138]. Thus signifying the relevance of the study. Figure 9 [Right] illustrates the hydrogen yield as a function of time for titania nanotube based sytems. It can be seen that the hydrogen production rate was higher for the cocatalyst loaded systems when compared to the parent nanotubular structure TNT.

The reduced grain boundary in one dimensional tubular nanostructures facilitates the fast transfer of electrons. Thus charge carrier recombinations are decreased which is favorable to photocatalytic activity. Hydrogen production by silver and copper decorated systems in 6 hour was found to be 1546.9 micromoles per gram and 7198.4 micromoles per gram respectively. When same weight percentages of metals were employed, copper decorated nanotubes produced highest hydrogen yield. The reduced hydrogen production by silver loaded nanotube is assumed to be due to the larger aggregation of nanoparticles observed in the system as evident from the TEM images which acts as recombination sites when compared with the copper loaded additive. Another possible reason may be the reduced numbers of surface contact between the nanoparticles with the nanotube surface, which is also gathered from the TEM data. The higher activity of copper decorated system than the silver loaded one makes it an alternative choice for the noble metal catalyst.

## 4.2.7.6 Mechanism of Photocatalysis towards Hydrogen production by water splitting in cocatalyst loaded nanostructures

Among the prepared nanostructures mesoporous titania based photocatalysts are shown to be good in hydrogen production by water splitting. The fraction of electrons captured migrates to the inner pore surface of mesoporous titania where they are in contact with cocatalysts. Thus effective transfer of electrons takes place due to their proper contact which reduces the electron hole recombination rate in cocatalyst loaded mesoporous structures. In the case of cocatlyst loaded Titania nanotubes the TEM images showed that some

nanoparticles are entrapped within the nanotube aggregation. These entrapped nanotube/nanoparticle systems are higher in copper decorated systems than the silver based ones. These facilitate multipoint contacts with the nanotube network thus more paths are available for electrons to be transferred to the nanotubular network. Presence of efficient channels for charge carrier migration imparts higher activity for the cocatalyst loaded tubular structures. In the case of silver loaded titania nanotubes, higher aggregation of silver nanoparticles can be observed from the TEM images which acts as recombination centers thus reduces the availability of photogenerated electrons for the reduction of water molecules. The tendency of the powder to aggregate certainly reduces the surface area [evident from the surface area value of nanotube, TNT and its doped systems] exposed to the solution and the overall reactivity.

Both these cocatalysts have high electronegativity compared to the host metal. Thus will be positively affecting the proton reduction ability by these active sites thereby enhancing the hydrogen production activity. But it has been noticed that among the cocatalysts loaded systems, copper based systems are proven to be with higher activity in both the nanostructures, meso and tube. The photcatalytic activity of metal nanoparticles on the surface of titania nanostructures rely on many factors like relative affinity of the metal ions to the surface of titania, physical, chemical, electronic charatceristics of the contacts, size and surface structure of the metal nanoparticles. The studies on electronic interactions of photdeposited copper/silver metal nanoparticles on titania surface showed that at low weight percentage,

copper nanoparticles interact more strongly with the surface of $TiO_2$ as compared with silver nanoparticles. Studies revealed that as the surface states associated with $TiO_2$–$Ag_n0$ electronic contact lie within the band gap of titanium dioxide. The surface states associated with copper are much lower which made clear evidence for stronger interaction between the semiconductor and Copper metal. Diebold [139] also reported the higher electronic affinity of copper clusters to the surface of titanium dioxide related to silver. More advantageous energetics of $TiO_2$–copper contacts, related to silver based system, are responsible for the efficient capture of the photogenerated electrons by surface states transferring the same to metal nanoparticles. Thus recombinations are suppressed accelerating the total photocatalytic reaction [140-142]. Moreover, the significantly high electron affinity of silver (125.6 KJ/mol)compared to copper (118.5 KJ/mol) and Ti (7.6 KJ/mol), may cause undesiarable effects that impart difficulty in releasing trapped electrons to reduce water molecules thus reducing the photoctalytic activity.

## 4.2.8 Conclusion of Section B – Photocatalytic Water splitting

Photocatalytic water splitting reaction producing Hydrogen energy with the help of semiconductor photocatalyst in presence of visible light is believed to be one of the most promising renewable technologies. During the past decade, for making hydrogen production more economic and competitive, great efforts have been made in this direction in identifying non-precious catalysts due to the scarcity and expensiveness of Pt based catalysts though they are proved to be efficient. Cocatalyst loading on nanostructured titania based systems

for Hydrogen evolution rate (HER) has been investigated in this chapter. Two nanostructured titanium dioxide, namely nanotube and mesoporous assembled structures are selected for the same owing to their high surface area value. Both of them are decorated with silver and copper coacatalysts using photo-deposition method. UV-Visible absorption spectra of the cocatalyst modified system shows extended absorption towards visible region related to the parent nanostructures. As a preliminary examination, the photocatalytic activities of the cocatalyst loaded systems are examined towards dye degradation using methylene blue dye as a target pollutant which proved their excellent candidature. Hydrogen production by water splitting reactions in presence of visible light have been carried out which emphasised their visible light response. Both the cocatalyst modified systems were found to be effective in reducing the recombination of charge carriers which is a main drawback of titania based photocatalysts as are revealed by the photoluminascent spectra. Among the sysnthesised systems, the activity of copper decorated mesoporous assembled structures was found to be much higher which produced 16673.2 µmoles/g of Hydrogen. This catalyst outperforms the mesoporous assembled structures by a factor of 18 under identical conditions. Based on the results we can conclude that copper loaded titania nanostructures are cost-effective and efficient catalysts compared to other noble metal based titania systems in the relm of photocatalytic water splitting.

**References**

1.	M. Wang, Z. Wang, X. Gong and Z. Guo, Renewable Sustainable Energy Rev., 2014, 29, 573.

2.	N.Z. Muradovand T .N. Veziroglu, Int. J. Hydrogen Energy 2005 ,30 , 225.

3.	D.B. Levinand R . Chahine ,Int. J. Hydrogen Energy 2010 ,35 ,4962.

4.	A.H. Awadand T .N. Veziroglu ,Int. J. Hydrogen Energy 1984, 9 , 355.

5.	A. Fujishimaand K . Honda ,Nature 1972, 238, 37.

6.	G.N. Schrauzerand T .D. Guth, J. Am. Chem. Soc. 1977, 99, 7189.

7.	M. Anpo,K . Chiba,M . Tomonari,S . Coluccia, M. Cheand M .A. Fox, Bull. Chem. Soc. Jpn. 1991, 64, 543.

8.	M. Halmann, Nature ,1978, 275, 115.

9.	E.O. Frank ,Chem. Mater. ,2008, 20 ,35.

10.	M.J. Sang ,H.B .Pramod ,G.K .Hyum ,W.H .Dong ,S.J . Jum ,W.B . Sangand S .L. Jae ,Phys. Chem. Chem. Phys. ,2005, 7 ,1315.

11.	M. Kocaand M . Sahin ,Int. J. Hydrogen Energy ,2002, 27,363.

12.	 L.C. Gian ,S .Elenaand F . Lucio ,Appl. Catal., B: Environ. , 2008 , 84 ,332.

13.	N.  Meng ,K.H.L Michael ,Y.C.L .Dennisand K . Sumathy , Renewable and Sustainable Energy Rev., 2007, 11 ,401.

14.	A. Linsebigler, G.Q. Lu and J.T. Yates, Chem. Rev. ,1995, 95 ,735.

15.	 L. Kavan, M. Gra¨zel, S. E. Gilbert, C. Klemenz and H. J. Scheel ,J. Am. Chem. Soc. ,1996 ,118 ,6716.

16.	D. Jing, Y. Zhang and L. GuoChem. Phys. Lett., 2005, 415 ,74 .

17.	 F. E. Osterloh, Chem. Soc. Rev., 2013, 42, 2294.

18.	 W. Fan, Q. Zhang and Y. Wang, Phys. Chem. Chem. Phys., 2013, 15, 2632.

19.    Y. Quab and X. Duan, Chem. Soc. Rev., 2013, 42, 2568.

20.    M .P. Kapoor, S. Inagaki and H. Yoshida, J.Phys.Chem.B, 2005, 109, 9231

21.    C. Cheng,W . Renand H . Zhang ,Nano Energy 2014 ,5 ,132.

22.    B . Evrimand Y . Birgu ,Int. J. Hydrogen Energy ,2016 ,41 ,2498.

23.    S .T. Nishanthi,B . Sundarakannan,E . Subramanianand D .P. Padiyan ,Renew. Energy 2015 ,77 ,300.

24.    T. Sreethawong and S. Yoshikawa ,Catal. Commun., 2005, 6 ,661.

25.    Y . Jiaguo, Q. Lifang, and J. Mietek ,J. Phys. Chem. C ,2010, 114, 13118.

26.     G. Liu,C . Sun,H .G. Yang,S .C. Smith,L . Wang,G .Q. Lu,H .M. Cheng, Chem. Commun. 2010, 46, 755.

27.    K. Pongtanawat,P . Pairatand G . Nurak ,Int. J. Hydrogen Energy , 2013 ,38 ,15992.

28.    M. R. Gholipour, C.T. Dinh, F. Belandb and T.O. Do, Nanoscale, 2015, 7, 8187.

29.     I. Tamiolakis, I. T. Papadas, K. C. Spyridopoulos and G. S. Armatas, RSC Adv., 2016, 6, 54848-54855.

30.    T. Sreethawong, Y. Suzuki and S. Yoshikawa ,J. Solid State Chem., 2005, 178 ,329.

31.    N.L. Wu, M.S. Lee, Z.J. Pon and J.Z. Hsu ,Photochem. Photobiol. A, 2004, 163 ,277.

32.    D. V. Bavykin, S. N. Gordeev, A. V. Moskalenko, A. A. Lapkin, and F. C.Walsh, J .Phys. Chem. B, 2005, 109, 8565.

33.    S .Sakulkhaemaruethai and T .Sreethawon ,Int. J. Hydrogen Energy , 2011 ,36 ,6538.

34.    S.J. Jum,H .C. Sun,H .K. Dong,W .J. Ji,S .L. Kyung, andS .L. Jae ,J. Phys. Chem. C., 2009, 113, 8990.

35.    L . Caolong,Y . Jian, H. Bingyan,J . Liand S . Wenfeng ,Int. J. Hydrogen Energy ,2010 ,35 ,7073.

36.  C. Yubin,W . Lianzhou,M .L. Gaoqing,Y . Xiangdong and G. Liejin , J. Mater. Chem., 2011, 21, 5134.

37.  C.Y. Yang,Z . Wang, T.Q. Lin, H. Yin, X.J. Lü, D.Y. Wan,T . Xu, C. Zheng, J.H. Lin, F.Q. Huang, X.M. Xieand M .H. Jiang, J. Am. Chem. Soc. 2013, 135, 17831.

38.  J. Chattopadhyay, H. Rok Kim, S. Bong Moon and D. Pak ,Int. J. Hydrogen Energy,2008 , 33 ,3270.

39.  J. Chattopadhyay, R. Srivastava and P. K. Srivastava, J. Appl. Electrochem., 2013, 43, 279.

40.  T. Kawai and T. Sakata ,Nature ,1980, 286 ,474 .

41.  G. R. Bamwenda, T. Uesigi, Y. Abe, K. Sayama and H. Arakawa, Appl. Catal. A: Gen. 2001, 205, 117.

42.  S. Xu and D. D. Sun, Int. J. Hydrogen Energy 2009, 34, 6096.

43.  R. Sasikala, A. Shirole, V. Sudarsan, T. Sakuntala, C. Sudakar, R. Naik and S. R. Bharadwaj, Int. J. Hydrogen Energy 2009, 34, 3621.

44.  N. Strataki, V. Bekiari, D. I. Kondarides, P. Lianos, Appl. Catal. B: Environm. 2007, 77, 184.

45.  X. Yang, C. Salzmann, H. Shi, H. Wang, M. L. H. Green and T. Xiao, J. Phys. Chem. A 2008, 112, 10784.

46.  D.W. Hwang, H.G. Kim, J. Kim, K.Y. Cha, Y.G. Kim and J.S. Lee, J. Catal.,2000 ,193 ,40.

47.  R. Asahi, T. Morikawa, T. Ohwaki, K. Aoki and Y. Taga, Science, 2001, 293, 269.

48.  C. Z. Wen, Q. H. Hu, Y. N. Guo, X. Q. Gong, S. Z. Qiao and H. G. Yang, Chem. Commun., 2011, 47, 6138.

49.  S. In, A. Orlov, R. Berg, F. Garcia, S. Pedrosa-Jimenez, M.S. Tikhov, D.S. Wrightand R .M. Lambert, J. Am. Chem. Soc. 2007, 129, 13790.

50.  R. Dholam, N. Patel, M. Adami and A. Miotello Int. J. Hydrogen Energy,2009 , 34 5337.

51.  M.A. Khan, S.I. Woo and O.B. Yang ,Int. J. Hydrogen Energy, 2008, 33, 5345.

52.    M.M. Momeni, Y. Ghayeb and Z. Ghonchegi, Ceram. Int. ,2015, 41, 8735.

53.    Y. Li, T. Wang, S. Peng, G. Lu and S. Li, Acta Phys.Chim. Sin. , 2004, 20,1434.

54.    S. Bingham and W. A. Daoud, J .Mater. Chem, 2011, 21, 2041.

55.    H. Park, Y. K. Kirn, and W. Choi, J. Phys. Chem. C, 2011,115, 6141.

56.    W.W. So, K.J. Kimand S .J. Moon. ,Int. J. Hydrogen Energy 2004 , 29 ,229.

57.    Z. Ning, H. Tian, C. Yuan, Y. Fu, H. Qin, L. Sun and H. Agren, Chem. Commun., 2011, 47, 1536.

58.    Y. B. Chen and L. J. Guo, J. Mater. Chem., 2012, 22, 7507.

59.    A. Naldoni, M. D'Arienzo, M. Altomare, M. Marelli, R. Scotti, F. Morazzoni, E. Selli and V. Dal Santo, Appl. Catal. B: Environ. , 2013 ,239, 130.

60.    A. Primo, A. Corma, and H. Garcia, Phys. Chem. Chem .Phys., 2011,13, 886.

61.    Z. Liu, W. Hou, P. Pavaskar, M. Aykol, and S. B. Cronin, Nano Lett.,2011 , 11, 1111 .

62.    D. Jiang, Y. Xu, B. Hou, D. Wu, and Y. Sun, J. Soli. State Chem., 2007, 180, 1787.

63.    X. B. Chen, L. Liu, P. Y. Yu, and S. S. Mao, Science, 2011, 331, 746.

64.    X.H. Zhang,U . Veikk, J. Mao, P. Caiand T .Y. Peng ,Chem Eur J., 2012 ,18 ,12103.

65.    K. Hirano, A.E. Suzuki, T. Ishikawa, H. Moroi and M. Kaneko Shiroishi ,J. Photochem. Photobiol. A Chem., 2000, 136, 157.

66.    S.K. Choi, H.S. Kim and H.Park, Appl. Catal. B Environ. ,2012 ,121 , 206.

67.    E.A. Malinka,G .L. Kamalov,S .V. Vodzinskii, V.I. Melnik,  and Z. I. Zhilina, J. Photochem. Photobiol., A ,1995, 90, 153 .

68.     Z. Yi, J. Ye, N. Kikugawa, T. Kako, S. Ouyang, H. Stuart- Williams, H. Yang, J. Cao, W. Luo, Z. Li, Y. Liu and R. L. Withers, Nat. Mater., 2010, 9, 559.

69.     C. A. Caputo, M. A. Gross, V. W. Lau, C. Cavazza, B. V. Lotsch and E. Reisner, Angew. Chem., Int. Ed., 2014, 53, 11538.

70.     M. Murdoch, G. I. N. Waterhouse, M. A. Nadeem, J. B. Metson, M. A. Keane, R. F. Howe, J. Llorca and H. Idriss, Nat. Chem., 2011, 3, 489.

71.     Mizukoshi, Y., Sato, K., Konno, T.   J.,    and Masahashi, N. Appl. Catal., B, 2010, 94, 248.

72.     I. Tsuji, H. Kato and A. Kudo, Angew. Chem., Int. Ed., 2005, 44, 3565.

73.     M. Sathish, B. Viswanathan and R. P. Viswanath, Int. J. Hydrogen Energy, 2006, 31, 891.

74.     X. Zong, H.J. Yan, G.P. Wu, G.J. Ma, F.Y. Wen, L. Wang and C. Li., J. Am. Chem. Soc. 2008, 130, 7176

75.     J.S. Jang, D.J. Ham, N. Lakshminarasimhan, W.Y. Choi and J.S. Lee, Appl. Catal. A: Gen. 2008, 346, 149.

76.     K. Maeda, K. Teramura, D. Lu , N. Saito, Y. Inoue and K. Domen, Angew. Chem.,Int. Ed. 2006, 45, 7806

77.     K. Maeda, K. Teramura, D. Lu, N. Saito, Y. Inoue and K. Domen, J. Phys. Chem. C 2007, 111, 7554.

78.     M. Yoshida, A. Yamakata, K. Takanabe, J. Kubota, M. Osawa and K. Domen, J. Am. Chem. Soc. 2009, 131, 13218.

79.     A.I. Kulak, Electrochemistry of Semiconductor Heterostrucrures (In Russ.), Universitetskoye, Minsk, 1986.

80.     M. Gr¨atzel (Ed.), Energy Resources through Photochemistry and Catalysis, Academic Press, New York, 1983.

81.     N. Bao, L. Shen and T. Takata, Chem. Mater. 2008, 20, 110.

82.     K. T. Ranjith,T. K.Varadarajan and B. Viswanathan, J. Photochem. Photobiol. ,A 1995, 89, 67.

83. X. G. Hou, M. D. Huang, X. L. Wu and A. D. Liu, Chem. Eng. J. 2009, 146, 42.

84. W. Sun, S. Zhang, Z. Liu, C.Wang, Z. Mao, 2008, 33 ,1112.

85. T. Sreethawong, S. Yoshikawa, Int. J. Hydrogen Energy ,2006, 31 , 786.

86. R. Jingrun,Z . Jun,Y . Jiaguo,J . Mietek and Z.Q. Shi, Chem. Soc. Rev., 2014, 43, 7787.

87. X. Zong, H. Yan, G. Wu, G. Ma, F. Wen, L. Wang and C. Li, J. Am. Chem. Soc. 2008, 130, 7176.

88. K. Sayama and H. Arakawa, J. Phys. Chem. 1993, 97, 531 .

89. K. Sayamaand H . Arakawa, J Chem Soc, Chem Commun .,1992 ,2 , 150.

90. K. Sayama, H. Arakawa, J. Chem. Soc. Faraday Trans. 1997, 93, 1647.

91. K. Yamaguti and S. Sato, J. Chem. Soc. Faraday Trans. 1 1985, 81, 1237.

92. K. Maeda, K. Domen, J. Phys. Chem. Lett. 2010, 1, 2655.

93. F. Baccuzzi, E. Guglielminotti, G. Martra and G. Cerrato, J Catal. , 1994 ,146 ,449.

94. S. P. Xu and D. D. Sun, Int. J. Hydrogen Energy, 2009, 34, 6096.

95. S. P. Xu, J. W. Ng, X. W. Zhang, H. W. Bai and D. D. Sun, Int. J. Hydrogen Energy, 2010, 35, 5254.

96. V.K. Anna ,I.E .Natalia, L.S. Alexander, K.B. Viktor,E .R. Alexandra, I.L. Valentina, Y.K. Stepan,G .I. Vladimirand A .M. Piotr ,J. Photochem .Photobiol., A: ,2008, 198,126.

97. Z. M. Bugarcic, V. M. Divac, M. P. Gavrilovic, Monatsh. Chem. 2007, 138, 985.

98. T. Gleitsmann, B. Stegemann, T.M. Bernhardt, Appl. Phys. Lett. 2004, 84, 4051.

99. J. Keleher, J. Bashant, N. Heldt, L. Johnson, Y. Li, W. J. Microbiol. Biotechnol. ,2002, 18 ,133.

100.   L. .KYu, W.C. Huaand Y . Ku ,Thin Solid Films 2007 ,515 ,3461.

101.   Y.C. Li and H.S. Lee, J. Hazard. Mater. ,2010, 179 ,462.

102.    C. Suwanchawalit, S. Wongnawa, P. Sriprang and P. Meanha, Ceram. Int. 38 ,2012 ,5201.

103.    A. Vamathevan, R. Amaland D . Beydown. ,J. Photochem. Photobiol.,A, 2002,148,233.

104.   J.W. Parkand M . Kang ,Int. J .Hydrogen Energy 2007 ,32 ,4840.

105.   M.S. Parkand M . Kang ,Mater. Lett. 2008 ,62 ,183.

106.   D. P. Kumar, M. V. Shankar, M. M. Kumari, G. Sadanandam, B. Srinivas and V. Durgakumari, Chem. Commun., 2013, 49, 9443.

107.   M. Wang, L. Sun, Z. Lin, J. Cai, K. Xie and C. Lin, Energy Environ. Sci., 2013, 6, 1211.

108.   V.I. Yatskiv, A.V. Korzhak, V.M.Granchak, A.S. Kovalenko and S.Ya. Kuchmiy,    Theor. Exp. Chem. ,2003, 39 ,167.

109.   k. Lalitha ,G .Sadanandam,V .D. Kumari ,M .Subrahmanyam ,B . Sreedharand N .Y. Hebalkar, J. Phy.s Chem. C., 2010 ,114 ,22181.

110.    S.P. Xu, A.J. Du, J. Liu, J. Ng and D.D. Sun, Int. J. Hydrogen Energy ,2011, 36 ,6560.

111.   M .J. Jung,E . Jeong,Y . Kim,and Y .S. Lee, J. Ind. Eng. Chem. , 2013, 19, 1315.

112.   D .V. Bavykin ,V.N .Parmon ,A.A .Lapkinand F .C. Walsh ,J Mater Chem., 2004, 14 ,3370.

113.   S. Lowell and J.E. Shields, Powder Surface Area and Porosity (3rd ed.) Chapman and Hall, London 1991,2 , 77.

114.   Z. Zhao, Z .Sun, H .Zhao, M .Zheng, P .Du, J .Zhaoa and H .Fan ,J. Mater. Chem., 2012, 22, 21965.

**115.**   M.P.Nikhila and N.K.Renuka  ,CrystEngComm, 2017**,**19, 511.

116.   J. Navas, A. Sanchez-Coronilla, T. Aguilar, N.C. Hernandez, D.M. de los Santos, J. Sanchez-Marquez, D. Zorrilla, C. Fernandez-Lorenzo, R. Alcantara, J. Martın-Calleja, Phys. Chem. Chem. Phys. , 2014, 16, 3835.

117. V .Krishnakumar ,S .Boobas, J .Jayaprakash, M .Rajaboopathi, B.Han, M. L .Kultanen, J Mater Sci: Mater Electron ,2016 ,27 ,7438.

118. M.P.Nikhila and N.K.Renuka, RSC Adv., 2016, 6, 24210 .

119. X. Han, Q .Kuang, M. Jin, Z. Xie, and L. Zheng ,J. am. Chem. Soc. 2009, 131, 3152.

120. X. Yu, J. Yu, B. Cheng and B. Huang, Chem.–Eur. J., 2009, 15, 6731.

121. W. Donga, Y. Sunb, Q. Maa, L. Zhua, W. Huac, X. Lub, G. Zhuanga, S. Zhanga, Z. Guoa and D. Zhaoc, J. Hazard. Mater., 2012, 229, 307.

122. H. Huang, X. Liu and J. Huang, Mater. Res. Bull., 2011, 46, 1814.

123.  X. Wang, L. Li, Y. Lin and J. Zhu, Ceram. Int., 2013, 39, 5213.

124. A. Syoufian and K. Nakashima, J. Colloid Interface Sci., 2007, 313, 213.

125. A. Syoufian, O. H. Satriya and K. Nakashima, Catal. Commun., 2007, 8, 755.

126.  B. Chi, L. Zhao and T. Jin, J. Phys. Chem. C, 2007, 111, 6189  .

127. T .Puangpetch ,T .Sreethawong ,S .YoshikawaS and . Chavadej ,J. Mol. Catal. A: Chem.,2009 ,312, 97.

128. P. Khemthong, P. Photai, N. Grisdanurak ,Int. J. Hydrogen Energy , 2013 ,3 8 ,15992.

129. B. Chai, T. Y. Peng, P. Zeng and J. Mao, J. Mater. Chem., 2011, 21, 14587.

130. Y. B. Chen, L. Z. Wang, G. Q. Lu, X. D. Yao and L. J. Guo, J. Mater. Chem., 2011, 21, 5134.

131. S. K. Apte, S. N. Garaje, S. S. Arbuj, B. B. Kale, J. O. Baeg, U. P. Mulik, S. D. Naik, D. P. Amalnerkara and S. W. Gosavi, J. Mater. Chem., 2011, 21, 19241.

132. P. Larios, R. Lopez, A. Hernandez-Gordillo, F. Tzompantzi, R. Gomez, R. Torres-Guerra ,Fuel ,2012, 100 ,139.

133. K.M. Parida ,S. Pany ,B. Naik ,Int. J. Hydrogen Energy, 2013 ,38 , 3545.

134.    A.L. Ortiz, M.M. Zaragoza, J.S. Gutiérrez, M.M. da Silva Paula, V. Collins-Martínez ,Int. J. Hydrogen Energy ,2015, 4 0,17308.

135.    B. Chai, T. Y. Peng, J. Mao, K. Li and L. Zan, Phys. Chem. Chem. Phys., 2012, 14, 16745 .

136.    W. Fan, Q. Lai, Q. Zhang,Y . Wang, J. Phys. Chem. C., 2011, 115, 10694.

137.    C. C. Lin, T.Y. Wei, K.T. Lee and S.Y. Lu, J. Mater. Chem., 2011, 21, 12668 .

138.    Si-yao Guo, Song Han, Bo Chi, Jian Pu, Jian Li ,ACS Appl. Mater. Interfaces 2014, 6, 4743.

139.    U. Diebold, Surf. Sci. Rep. ,2003 ,48,53  .

140.     A. V. Korzhak, N. I. Ermokhina, A. L. Stroyuk, V. K. Bukhtiyarov, A.E. Raevskaya, V.I. Litvin, S.Y. Kuchmiy, V.G. Ilyin, P.A. Manorik , J. Photochem. Photobiol., A, 2008, 198, 126.

141.    A.I. Kulak, Electrochemistry of Semiconductor Heterostrucrures (In Russ.), Universitetskoye, Minsk, 1986.

142.    E.A. Streltsov, R.M. Lazorenko-Manevich, V.P. Pakhomov, A.I. Kulak, Electrochemistry (Russ. Ed) 19  ,1983 ,1148.

# CHAPTER V
# BIOLOGICAL APPLICATIONS OF TITANIA NANOSTRUCTURES

*In the past decades due to cancer disease prevalence there is an increasing interest in nanotechnology and nanomedicine. These two fields combine their power to develop new substances capable to irradicate cancer and also vehicles for delivering the chemotheraputic drugs in an effective and targeted manner. TiO$_2$ nanomaterials with their unusual stability, biocompatibility and excellent photoactivity have a unique place in biomedical applications of the future. Designing newer materials with newer ways to target the pathologically altered tissues lowers the side effects offered by the marketed anticancer drugs. This chapter deals with the in vitro cytotoxic studies of synthesised titania nanostructures towards human brest cancer cells and their drug and folic acid incorporated systems. The encapsulated anticancer drug and folic acid modifications were found to enhance the anticancer potential of nanotitania based systems. The modified systems are well characterised and the cell killing mechanisms of these cytotoxic agents are studied.*

## 5.1 **INTRODUCTION**

Cancer, the malignant crab like cellular malfunction where the cells multiply at bewildering speed is the second most leading cause of death worldwide after the cardiovascular diseases. According to WHO 8.8 million people worldwide died from cancer in 2015. Deaths from this dreadful disease worldwide are projected to continue rising, 14 million in 2012 to 22 million within the next two decades (www.who 2015). In India, occurrence of cancer is also high with, 5,50,000 cancer deaths and growth of 8,00,000 new cancer cases every year. The impact of cancer is considerably greater than the number of cancer cases. Its diagnosis causes immense emotional trauma and its treatment a major economic burden. Normally, human cells will not grow and divide to form new cells as cells grow old or become damaged and they die. Normal cells may become cancer cells. Before cancer cells structure in tissues of the body,the cells go through abnormal changes called hyperplasia and dysplasia. In hyperplasia, there is an increase in the number of cells in an organ or tissue that appear normal under a microscope. In dysplasia the cells look abnormal under a microscope but are not cancer. Hyperplasmia and dysplasia may or may not become cancer. When cancer develops, however, this orderly process breaks down. As cells become more and more abnormal, old or damaged cells survive when they should die, and new cells form when they are not needed. These extra cells can divide without stopping and may form growths called tumors. All tumors are not cancerous. Tumors can be benign or cancerous. A benign tumor is localized and wont spread to other parts. Normally benign type won't return when removed from

body. Malignant tumors on the other hand are cancerous. It is characterized by its invasion to nearby tissues by means of lymph and blood systems and spread to other parts of the body. As these tumors grow, some cancer cells can break off and travel to distant places in the body through the blood or the lymph system and form new tumors far from the original tumor. The spreading of cancer from one part of the body to another is called metastasis which is considered as the major cause of death. Internal factors like hormones, inherited mutations, mutations that occur from metabolism, immune conditions and external factors like tobacco, chemicals, infectious Organisms, radiation etc are the main causes of cancer.

Cancer can be sorted into three different stages: local, regional and distant. Local stage is described as the initial stage of malignant cancer where it is limited only to its primary organ (origin), which can be cured by chemotherapy. The advancement of cancer towards the surrounding organs, can be controlled. Sometimes it would proceed towards its second stage i.e. the regional stage affecting the neighboring tissues, organs and the regional lymph nodes. Distant stage is recognized as metastatic cancer when many lymph nodes from different parts of the body are affected and there are a little chances of endurance in this stage [1]. There are more than 100 types of cancer. Types of cancer are usually named for the organs or tissues where the cancers form. For example, lung cancer starts in cells of the lung, and brain cancer starts in cells of the brain. Cancers also may be described by the type of cell that formed them, such as an epithelial cell or a squamous cell. Main categories of cancer include Carcinoma, Sarcoma, Central

nervous system cancers, Leukemia, Lymphoma and myeloma. For certain types of cancer, e.g. cancer of the breast, testis, uterine corpus, and melanoma, advanced forms of treatment may produce a 5-year survival rate of 75% or more**. B**ut the Survival rates are generally less than 15% for the cancer of pancreas, liver, stomach, and lung (www.who.org). Lung, prostate, colorectal, stomach and liver cancer are the most common types of cancer in men, while breast, colorectal, lung, cervix and stomach cancer are the most common among women. The top five cancers in humans account for 47.2% of all the cancers; these cancers can be prevented, screened for and/or detected early and treated at an early stage [2]. Breast cancer is the most commonly occurring malignancy in women in the developed countries and the second most common in women in the developing countries and it comprises of almost one third of all malignancies in females. The lifetime risk of a woman developing invasive breast cancer is 12.6 %. Breast cancer is an alarming health problem of India. The survey by Indian Council of Medical Research (ICMR) in the metropolitan cities from 1982 to 2005 has shown that the incidences of breast cancer have almost doubled [3].

## 5.2 Treatment for cancer- Chemotherapy and its limitations

Various therapeutic treatment strategies for cancer are available at present, including surgery, chemotherapy, radiation and biological therapies. Out of which chemotherapy is the extensively followed in the present scenarios. Effectiveness of these treatments depends on the tumor type and its development stage. **R**adiation therapy and

Excision/removal of the tumor **are** helpful when cancer cells have not metastasized. If cancer cells have metastasized**,** single or combination of chemotherapy is used **[4]**. Chemotherapy is a category of cancer treatment that uses one or more anticancer drugs /chemotherapeutic agents as part of a standardized chemotherapy treatment. Chemotherapy may be given either with a therapeutic intent or it may intend to prolong life or to trim down the symptoms known as palliative chemotherapy. The chemotherapeutic drugs can be either given orally, intravenously or as an intramuscular injection in which the drug directly enters the bloodstream called systemic chemotherapy. Whereas in regional chemotherapy as the drugs are placed directly into the organ, a body cavity such as abdomen or cerebrospinal fluid it mainly affects cancer cells in those area. Traditional chemotherapeutic agents are cytotoxic in the sense that it can damage or stress cells, leading to cell death if apoptosis is initiated. Many of the side effects of chemotherapy can be traced to damage to normal cells that divide rapidly. The common medications affect mainly the quick dividing cells of the body, such as blood cells and the cells lining the mouth, stomach, and intestines. Less common side effects include dry skin, red skin, damaged finger nails, a dry mouth, water retention, and sexual impotence. If we are successful in diagnosing the cancer at its earlier stage, directing the specified chemotherapeutic agents to arrive at its target site releasing the required dose within we can eradicate these most dreadful disease to an extent.

5.3 **Need for drug delivery systems in Cancer** treatment

One of the major challenges faced in chemotherapy is the delivery of the cytotoxic drug in effective dose to the tumour site with minimal harmful side effects. These challenges initiated the quest for safer and effective drug delivery choices to enhance the benefit-to-risk ratio in cancer chemotherapy. Generally speaking, an ideal drug-delivery system should comprise two elements: **(i)** the ability to target the tissue of interest and **(ii)** to control the drug release. This targeting and controlled release will ensure high efficiency of the drug to be administrated and reduce the side effects associated. The targeted drug delivery/ smart drug delivery [5] is a method in which the drug is delivered in the desired part of the body with a concentration being gradually raised at each time. The scientific desire to treat the cancer cells in a methodical approach has resulted in the development of advanced drug delivery systems based on nanotechnology. The goal of a targeted drug delivery system is to prolong, localize and target the protected drug to the diseased tissue with properties of biocompatibility, biodegradability, selectivity, non-toxicity, and non-immunogenicity. Interestingly, nanomaterials seem to have the potential to satisfy all these requirements.

## 5.4 Nanomaterials in cancer therapy - Advantages

Chemotherapy, as the most widely used treatment approach in cancer patients, is usually faced with drug resistance, non-specificity and insufficient efficiency of drug delivery into the malignant cells [6-7]. When exploring new strategies for the treatment of cancer, one

possibility is the use of nanomaterials. The anticancer activity of nanoparticles towards tumor is either related to their intrinsic properties like anti oxidant activity or their response related to external stimuli such as Infrared rays, magnetic fields etc. Besides these inherent properties of metal nanoparticles, they can encapsulate or bind a range of therapeutic agents like proteins, hydrophobic/ hydrophilic drugs, etc. due to the high surface to volume ratios. Thus issues related to their soluability stability and other difficulties when the drug was used as such can be wiped off. These inherent properties of nanomaterials have been exploited in therapeutic antitumor approaches in photodynamic therapy and in hyperthermia [8]. Use of nanomaterials in drug delivery regimes are being strongly investigated which combat severe weaknesses of anticancer drug administration.

These nanomaterials can be easily transferred through leaky blood capillaries since they are 100 to 1,000 fold smaller than mammalian cancer cells. Moreover, these materials show relatively longer blood circulation that is beneficial as the loaded drugs are effectively utilized during this time. These have many advantages like easy preparation methods, effective tuning of size, shape and porosity, efficient protection of encapsulated entities from denaturation resistance to swelling or porosity changes with pH, easy functionalisable surfaces and benefit of ultra low size to evade the RES (reticulo-endothelial system) of body. One benefit of using nanoparticles is their tunable size which should be large enough to stop their quick leakage into blood capillaries and should be small enough to escape from the capture by fixed macrophages that are located in the

reticuloendothelial system, such as the liver and spleen. The approximate size of the sinusoid in the spleen and fenestra of the Kuffer cells in the liver varies from 150nm- 200 nm and the size of gap junction between endothelial cells of the leaky tumor vasculature may vary from 100nm - 600 nm. Therefore, the size of nanoparticles should be up to 100 nm to reach tumor tissues considering the passage through these two vascular structures [9-10]. Since the cancer cells are fast growing , they are in urge for new blood vesseles or rerouting the existing vessels for the supply of oxygen and other nutrients. Therefore an imbalance in the secretion of angiogenic regulators like growth factors and matrix metallo proteinases occurs. These processes make tumor vessels appear to be highly disorganized and dilated with numerous pores as shown in the figure 1. with enlarged gap junctions between endothelial cells and lymphatic drainage. Maeda et al have reported that because of the difference in structure between tumor and normal tissue, drug delivery nano system with the size below 200 nm will accumulate much more at the tumor than at the normal tissue [11]. As a result, a few pioneering nanoparticles based therapeutic products have been introduced into the pharmaceutical market which is superior to that of the currently available delivery options [12]. Different classes of nanomaterials like quantum dots, dendrimers, nanoshells, polymer drug conjugates, hydroxy apatite, calcium phosphate, carbon nanotubes (CNTs), fullerenes, gold and silver nanoparticles, liposomes and micelles have been evaluated for the potential medical application for simultaneous *invivo* imaging, drug delivery, cancer diagnosis & treatment [13-14]. Among these, unique structural characteristics and

properties of inorganic nanoparticles make them a suitable candidates to be used in medical field. Surface of the inorganic nanoparticle can be modified with several functional groups ranging from saturated and unsaturated hydrocarbons to carboxylic acids, thiols, amines, and alcohols. Premanathan et al have observed the anticancer acitivty of Zinc oxide nanoparticles against human myeloblastic leukemia cells [15]. Nickel oxide nanoparticles are found to exhibit anticancer activity against human lung carcinoma cells [16].
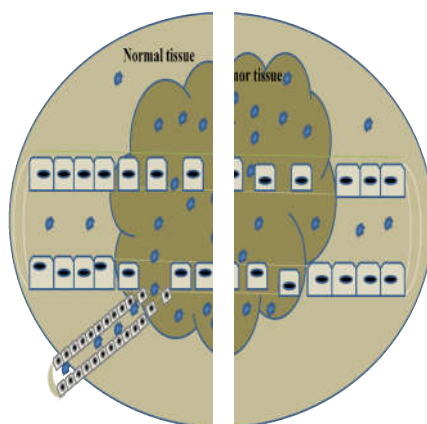


**Figure 1**. Hyperpermeable angiogenic tumor vasculature allows preferential extravasations of circulating nanoparticles.

The effect of morphology, size and chemical properties of inorganic nanoparticles are very important in determining its anticancer activity. Reports claim that the anticancer activity of nanoparticles varies with the size and surface area of the nanoparticles . For example, specific surface area of the nanoparticle is shown to be influenced by its cytotoxic activity as reported by Rabolli et al[17]. Cytotoxicity is the

cell-killing property of a chemical compound (food, cosmetic, or pharmaceutical) or a mediator cell (cytotoxic T cell). Increased surface activities like ROS generation, protein absorption etc imparted by high surface area of the nanopartcle are actually responsible for this cytotoxicity. As porosity of the particles considerably enhances the total surface area, constructuion of porous structures is preferred which significantly increased the potential to contribute to cytotoxicity [18]. But there are contravesial reports as shown by Hori et al that if a nanoparticle is basically inactive [physically and chemically] the benefit of high surface area will not contribute to its cytotoxic effects [19]. Thus, indentification of direct cytotoxic factors is rather important for the cytotoxic evaluation of nanoparticles rather than the value of specific surface area.

## 5.5 Targeted drug delivery

For most of the therapeutic agents, only a small portion of the medication reaches the desired organ, as in chemotherapy roughly 99% of the drugs administered do not reach the tumor site [20]. Efficiency of an anticancer drug in cancer treatment depends on its ability to reach the tumour tissues penetrating the barriers with minimal loss of its volume in blood circulation. Besides after reaching the desired tissue, it should selectively kill the cancer tissues without affecting the normal cells. Targeted drug delivery often called as smart delivery is one in which the nanoparticles are loaded with drugs and targeted to particular parts of the body where only diseased tissues are present, thus preventing the interaction with healthy tissues. Targeting drug to a

specific area not only increases the therapeutic efficacy of drugs but also decreases the toxicity associated with drug by allowing lower doses of the drug to be used in therapy. Drug can be targeted to an organ, particular cell/tissue, intracellular sites,viruses/bacteria cells etc. Thus the goal of a targeted drug delivery system is to extent, localize, and target drug interaction with the diseased tissue. There are two kinds of targeted drug delivery; namely, active targeted drug delivery and passive targeted drug delivery.

The nanoparticles are recognized as foreign bodies by the phagocytic cells and are rapidly removed from blood circulation mainly by macrophages located in the reticuloendothelial system (RES) [21]. Attempts like chemically attaching or adsorbing polymers like PEG at the surface, in order to keep the drugs for long time in blood circulation by avoiding RES recognition. Adding PEG on the surface of nanoparticle gave hydrophillic nature This allows water molecules to bind with oxygen on PEG by hydrogen bonding, thus making the nanoparticle antiphagocytic as hydrophobic interactions are natural to the reticuloendothelial system (RES)].The drug-loaded nanoparticle is able to stay in circulation for a longer period of time and extent the circulation time of encapsulated drugs in the bloodstream [22-23].

Physical signals, for instance magnetic fields and thermal energy which are externally applied to the mark sites may be utilized for active targeting. Inorganic (ceramic) particles with entrapped biomolecules have potential applications in active targeted drug delivery [24-25]. Incorporation of such targeting moieties helps to

actively target the drug to the sites of interest[26]. Reinforcement of to the effect of passive way was accomplished completely by this mode of active targeting. They interact with tumor-specific proteins present on the surface as well as in the cell interiors. These interactions include antigen– antibody and ligand–receptor binding. One confront we are facing in targeting cancers is that the defective cells are very similar in characteristics to their adjacent healthy tissue. Thus the task involves differentiating such cells, by designing ligands which have specificity for receptors that are over expressed on cancerous cells. On the contrary, these receptors are normally or minimally expressed on normal/healthy cells. Cell specific ligands can usually be utilised by the nanoparticle to bind specifically to the cell that has the complimentary receptor.targeting ligands like peptides, aptamer, antibodies, and other small molecules stimulate the cancer cell specific uptake [27-30]. For example, transferrin was conjugated to the nanoparticle to target tumor cells that possess transferrin-receptor mediated endocytosis mechanisms on their membrane. Thus targeting was found to increase uptake when compared to non-conjugated nanoparticles [31]. The folate receptor protein (FR) is also a well recognized tumor antigen / biomarker exploited for the use in diagnostic and therapeutic fileds for the treatment of cancer. Thus The passive and active targeting together not only assist enhancing the drug concentration at the tumor sites but also increases the cellular uptake of drug thus leading to better therapeutic efficacy.

Owing to its biocompactibility, low cost, non toxicity and tunable size, shape and crystal structure nanoTitanium dioxide comes in

top line among the engineered inorganic nanomaterials for biomedical applications. And the porous structure of these nanotitania endow them with a physical encasement a molecular payload (drug) from degradation or denaturization. $TiO_2$ is relatively stable over broad ranges of temperature and Ph. However lack of biodegradation and slow dissolution raise safety questions, especially for long- term administration.

## 5.6 Folate targeting

In targeted drug delivery, the surface of nanoparticles is modified with small functional groups, antibodies and other cancer specific receptors that increase targeting potential. Potential ligands like transferrin, lectins, folic acid, epidermal growth factor, antibody etc can be attached to this effect. Incorporation of various biological ligands or antibodies into $TiO_2$ NPs has improved the cytotoxicity towards the tumor cells. Xu et al. conjugated $TiO_2$ with a specific antibody against the carcinoem-bryonic antigen (CEA) of human LoVo cancer cells that could recognize cancer cells [32]. Similarly RGDC peptide was used to modify $TiO_2$ which could induce less damage to plasmid DNA and more toxicity to the cancerous cells [33]. Though these modifications certainly improved the specificity of $TiO_2$ towards tumor tissues, limitations being the immunogenicity and the recognition of monoclonal antibody by one specific antigen. Their practical applications are also limited by the cumbersome functionalization procedure and usage of several organic solvent in the synthesis process. Moreover, the relatively high-cost of antibodies and RGDC peptides

cause another serious economic burden. One of the most studied cancer-targeting ligands, FA has been known to target FA receptors (FAR) that are over expressed in several human carcinomas including breast, ovary, endometrium, kidney, lung, head and neck, brain, and myeloid cancers [34-37]. Moreover, highly stable folic acid has received promising concern among the active targeting moeties due to its non-immunogenicity, low cost and its faster internalization kinetics through cellular membrane [38]. Folic acid is a water soluable vitamin B with chemical formula $C_{19}H_{19}N_7O_6$. The structure of the same is displayed in Figure 2.
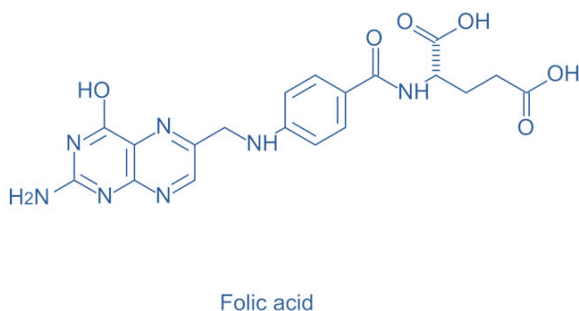


Folic acid

**Figure 2**. Folic acid molecule

The folate receptor (FR), also known as the folate binding protein (FBP or Folbp), is a glycopolypeptide with a high affinity ($Kd >> 10^{-10}M$) for folic acid [39]. Over expression of FR on many cancer cells obviously identifies this receptor as a potential target for ligand directed cancer therapeutics by a nondestructive endosomal path [40]. Folate Receptor can internalize its ligand into the cytosol, as it is associated to the lipid region of the cell membrane. The acidic microenvironment of interior is responsible for the dissociation of FR

from the folateincorporated Nanomaterials. Thus folate attached nanomaterials are released into the cytosol of the tumor cells. The advantages of FR among the available tumor targets/markers is that it can bind effectively to folic acid, FR expression in most proliferating normal tissues is limited to the luminal surface of certain epithelial cells, where it is inaccessible to the circulation while it is constantly expressed in specific types of major malignant tumors and leukemic cells where it is accessible via the circulation [41]. Also the attachment of drug does not interfere with the binding of folate for its receptor. As folate-targeting has been effectively proven to increase the efficiency of cancer therapy, consistently, a number of drugs have been used to target tumor tissues through a variety of FA-conjugated NPs. The cell specificity of folic acid-modified $TiO_2$ nanoparticles was evident. In the case of CHO cells , both unmodified and folic acid modified $TiO_2$ are internalised equally well, whereas modified with folic acid form promted the cellular uptake of titania in to HeLa cells due to the overexpresses folate receptors [42]. Results suggest that the folic acid modified $TiO_2$ is practically useful for the cancer therapy [43]. Figure 3 shows a schematic picture showing the active targeting mechanism by folate conjugated nanocarriers.
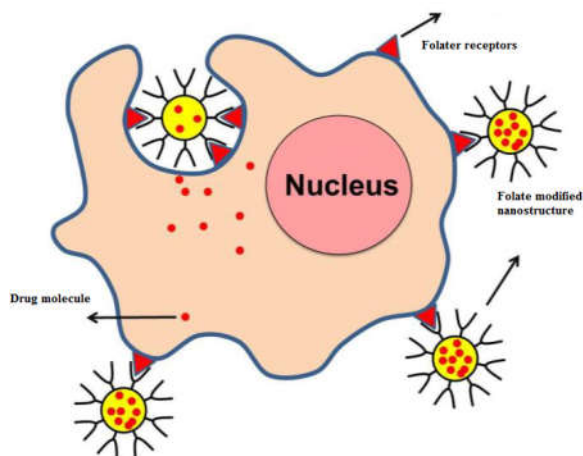
**Figure 3.** Schamatic showing the mechanism of Active targeting

## 5.7 TiO$_2$ – Toxicological properties

Recently, studies based on the toxicity evaluation of nanoparticles have increased dramatically, and many more are in progress. But the results of these investigations about the cytotoxicity of nanoparticles are not always clear. Occasionally there are contradictory reports on the cytotoxicity induced by nanoparticles. Titanium dioxide based cancer therapy is an emerging technique used for the treatment of variety of cancers due to its high therapuetic efficiency and reduced harmfulness to healthy tissues. World Health Organization working group concluded that the epidemiological studies on TiO$_2$ as an inhalation hazard in humans did not provide compelling evidence of carcinogenicity, although experiments in rodents suggested some evidence of carcinogenicity [44]. Results of several toxicological studies and similar in vitro and invivo studies have shown that metal

nanoparticles do not penetrate the human skin and it was considered not much dangerous using cosmetic products containing metal nanoparticles [45]. Thevenot et al in their studies revealed that the viable cells are different for JHU prostrate tumor cells and LLC cells with concentrations 0.1 mg/mL and 1 mg/mL respectively [46]. Gurr et al. [47] reported that anatase $TiO_2$ nanoparticles induced an increase of intracellular reactive oxygen species (ROS) level, malondialdehyde (MDA) level, and DNA oxidation on BEAS-2B cells and that oxidative stress was also induced by rutile $TiO_2$ fine-particles (200 nm in diameter). However, other authors reported that anatase $TiO_2$ fine-particles did not induce oxidative stress; high concentration of 3 mg/mL of anatase $TiO_2$ nanoparticles showed slight cytotoxicity on HDF and A549 cells; and rutile $TiO_2$ nanoparticles did not show cytotoxicity [48-49]. There are also reports that $TiO_2$ nanoparticles did not induce oxidative stress on mouse macrophage-like RAW 264 [50]. Very small bare anatase Titania nanoparticles in size range 10-20nm without photoactivation can induce higher hydrogen peroxide production, oxidative lipid peroxidation, DNA damage, and micronuclei formation in a human bronchial epithelial cell line [47]. On exposure to $TiO_2$ nanoparticles. Decrease in viability for BV2 microglia cell lines observed is faster compared to N27 neuronal cell lines implying that microglia are more prone to $TiO_2$ nanoparticles. Gerloff et al investigated the potential of a range of nanosized materials to induce cytotoxicity in Caco-2 cells. Titania nanopaticle with combined anatase and rutile phases exhibited low cytotoxic effects. Without photactivation, this particular material do not show any significant

DNA damage even after 4 h of treatment with a dose of 20 µg/ cm$^{2.}$ [51]. Geroff et al [51] analysed five TiO$_2$ samples for their cytotoxicity in human intestinal Caco-2 cells. Anatse /rutile samples showed higher toxicity per unit surface area than pure anatse samples [52]. These studies demonstrate that the toxicity of TiO$_2$ particles depends on its concentrations , surface functionality, size, crystallinity,  cell types etc [53]. Sokwong et al [54] demonstrated that TiO$_2$ particles increased the reactive oxygen species generated by alveolar macrophages and phagocytes. Titania nanoparticle with different sizes and with varying concentrations have been found to be non toxic in cell monolayer uptake model in vitro[55], in vivo, and inhalation models [56]. In vivo toxicities are exhibited as per some studies [57-58]. When rats are exposed to nanosized titania rods, it produced transient cell injury and inflammatory responses and these effects were almost like that caused by large sized titania nanoparticle exposure [59]. The discrepancies may be due to the lack of  correlation between in vivo and in vitro studies related to  TiO$_2$ nanoparticles [60]. Though in vitro studies indeed give several mechanistic information thus reveal the cell type specific responses, they fail to monitor several  intercellular effects in inflammatory cells and their signaling occur in its natural state [61].The predominant evidence suggests that TiO$_2$ nanoparticles are benign except when inhaled at very high levels [62].

## 5.8 TiO$_2$ - in cancer cell treatment

Inspite of the wide applications of Titanium dioxide in various fileds, in biomedical field its applications have been regarded as an

emerging one.The first nanotitania based biomedical applications was recorded by Fujishima and his coworkers in the early nineties of 20 th century. They reported the photodynamic therapeutic applications of nanotitania for killing cancer sellss (HeLa) [63]. Also at the same time a report by Ellingsen suggested the successful use of nanoTiO$_2$ as a coating on the surface in medical implants. These finding gave lime light to the use of nanotitania in biomedical relms. The cell killing properties of titania has been reported which showed that the reactive species will desrupt the cells and various viral forms [64-69]. In nano sized, TiO$_2$ may penetrate into the cell and this process may take place in the interior [70]. Nanocomposites which are increasingly applied for anticancer studies include silver doped TiO$_2$(Ag/TiO$_2$), gold doped TiO$_2$ (Au/TiO$_2$), and platinum doped TiO$_2$(Pt/TiO$_2$). The conjugation of noble metals increases its activity as observed by Mamun et al. They found that related to TiO$_2$ nanoparticles, silver doped TiO$_2$ nanocomposite exhibited 80 % more efficiency for killing human HeLa cells [71].

The use of nanostructured reservoirs for drug delivery has been focused mainly to the treatment of neurodegenerative diseases as epilepsy or cancer tumors. The engineering of the porosity in nanostructured materials (TiO$_2$, SiO$_2$, etc.,) is considered as an area of technological and scientific interest [72-73]. Surface properties of titania has significant influence on its cell-particle interaction like cellular uptake, internalisation of nanoparticles, extent of activity inside the cell, membrane binding etc. Research has been increased to a substantial extent in this direction by adopting various modifications of titania. Hollow nanostructures have received considerable attention in

practical applications of medicinal field due the possible encapsulation of biochemical molecules like Drug, DNA, dyes etc within the void structures [74-75]. Many titania nanostructures including titania nanoparticles, titania nanotubes, titania whiskers, titania matrices and titania capsules have been utilised successfully for delivery of a range of anticancer drugs like Temozolomide (TMZ), Gambogic Acid (GA), Doxorubicin (DOX), cisplatin and valproic acid [76]. Lopez et al [77] have shown that the anti tumor efficiency of Temozolomide (TMZ), a therapuetic drug for brain gliomas, can be improved by titania nanostructures  Also, successful encapsulation of valproic acid into Sol-gel derived $TiO_2$ nanostructures has been reported [78-79]. Incorporation of DNR and GA has been proven to improve the antitumor efficiency in human leukemia K562 cells compared to when the drug was administrated alone for the treatment[ 80-81]. Sodium phenytoin was observed to be co-gelled with titania for drug delivery applications as observed by lopez et al.[82] Recently, Garcia-Valverde reproted that Coating of carbon on Titania nanotube improved its biomedical applications [83]. Also, Wang et al observed that titania nanowhiskers possesses synergistic effect for carrying the anticancer drugs  to cancerous tissues and the PD therapeutic effect with UV light irradiation. Thus this structures can play roles important roles in various disease theranostics [84]. Another approach implements drug into the mesoporous materials thus preventing the undesired distribution throughout the body and reducing the side effects [85-86]. The reactive oxygen species generated are toxic for the cancer cells [87]. The porous space of nano $TiO_2$  has been widely investigated as

scaffold for drug delivery system. Recently Wang et al observed that polyethylineimine modified porous $TiO_2$ nanoparticles encapsulated with an anticancer drug specifically delivered to the target tissue by conjugating with folic acid.The porous $TiO_2$ nanoparticles not only generated the ROS but also released the chemotherapeutic agent upon photoactivation [88]. Feng et al [89] proved the excellent biocompactibility of $FA/TiO_2$ nanocomposite and its incorporation to human nasopharyngeal carcinoma cells. Venkadasubbu et al [90] proved that cellular uptake of $FA/TiO_2$ composite is enhanced by FA receptors in HeLa cells.

In aerobic cellular mechanism reactive oxygen species generation is an inherent element and it performs many important functions like regulation of protein phosphorylation, control over intracellular $Ca^{2+}$ concentration etc. But when the production of ROS is elevated and the cellular antioxidant defense system is not capable of controlling them, oxidative stress occurs resulting in the destruction of cellular components like lipids, proteins, and DNA [91-92]. Metal oxide nanoparticles can spontaneously generate ROS based on material composition and surface characteristics whereas other nanomaterials produce ROS only in the presence of selected cell systems. Oxidative stress is the important underlying factor which is responsible for the adverse biological effects of titania based photoactive semiconductors. The primary mechanism of the anticancer activity in this case is supposed to proceed by generation of ROS which is responsible for induction of apoptosis. Apoptosis is the programmed cell death and is a normal physiologic process that probably takes place during

embryonic development and in the continuing process of tissue homeostasis in the adult animals. It induces death of cells by the fragmentation of DNA, cell shrinkage, leading to cell fragmentation and the formation of apoptosis bodies. Any dysregulation of apoptosis always result in abnormality, disease and finally death [93]. Cancer also is consequence of improper pathway in apoptosis as well as uncontrolled cell proliferation [94]. Recently, researchers have used inducers of apoptosis in cancer therapy. In cancer cells, the cytotoxic drugs kill the defective cells by this mechanism and is considered an key process of evaluation for the clinical effectiveness of many anti-tumor drugs.

In the past few years, materials such as one- , two- , and three-dimensional crystal architectures, microcapsules, nanotubes, and hollow nanoparticles have attracted much attention because of their capable applications in the encapsulation of drugs, inks, flavors, and other chemical reagents [95-97]. Since titania based systems are widely investigated in nanomedicine, especially in anticancer therapy, the in-vitro cytotoxic properties of pure titania nanostructures synthesised via different pathways are assessed towards MCF-7 cancer cell lines. The results of characteriszation have shown that the synthesised titania nanostructures exhibit fine porosity features. In view of utilising the porosity of the synthesised nanostructures, these nanostructures are incorporated with an anticancer drug  5 Fluoro uracil. 5-FU which is widely used in the treatment of a wide range of cancers, including colorectal, cancers of the aerodigestive tract, skin cancers breast cancers etc. This anticancer drug is an analogue of uracil with a fluorine

atom instead of Hydrogen at the C-5. Further, for targeted drug delivery to desired tissues these nanostructured systems were modified with folic acid. Substantially increase in the cytotoxicities were observed for all the systems compared to their parent matal oxide structures and its drug loaded forms. The in vitro anticancer activity of folate modified systems is compared and the underlying mechanisms of most active Folate modified 5FU-loaded system were examined against human cancer cells.

## 5.9 Results and discussion

The synthesis procedure of various nanostructures and its anticancer drug/ folic acid incorporated forms have been described in chapter 2. The drug loaded systems are given prefix 'D' and folic acid modified systems, 'FD'. 5FU represents the anticancer drug 5Fluorouracil.

## Morphology after drug incorporation

Figure 4 represented the FE-SEM images of 5 fluoro uracil modified titania nanostructures. Compared to the parent nanostructures, no obvious change in morphology were observed. Drug loaded nanoparticle, mesoporous structure and multiwalled structure showed previous morphology itself, vis., almost spherical. Similarly the tubular and belt structures of titania maintain their morphology after drug encapsulation. After drug loading, increased aggregation is observed due to the adsorption of drug molecules. The porous structure can

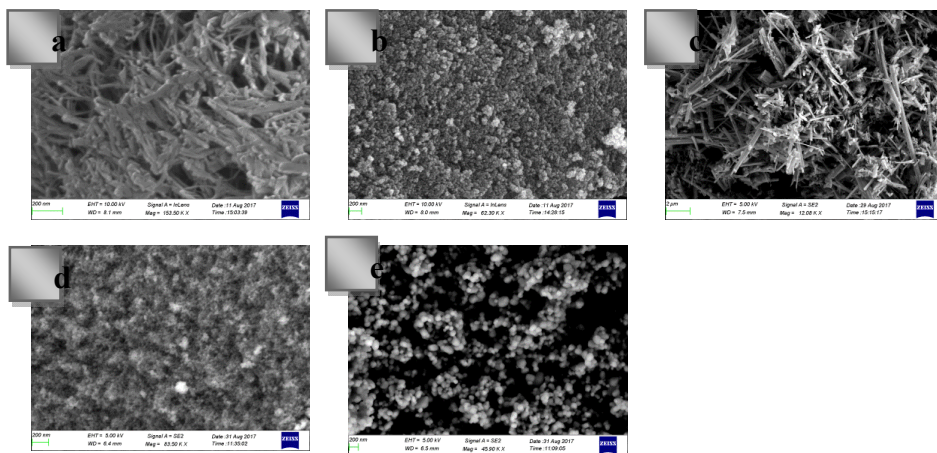accomodate significant amount of drug which are quantitatively measured by HPLC.



**Figure 4**. FESEM images of anticancer drug loaded nanostructures DTNT(a), DMT (b), DTNB (c), DTNP (d), DMHS (e)

**Calculation of drug content**

The entrapped drug efficiencies of the drug loaded systems were evaluated using HPLC. Table 1 shows the porosity features and drug loading of various titania structures. The highest drug uptake was shown by mesoporous assembled structures which is attributed to its highest surface area and pore volume among the nanostructures. More over, the porous network accomodates more additives than the other systems. Remaining systems followed the order, TNT > MT > MHS > TNB > TNP. Titania nanotube takes the second place which is also in accordance with the surface area and pore volume. However, mesoporous system was in the third place. The mesoporous structure is in a position to accomodate the drug molecules in their mesopores created by their nanocuboids. Drug uptake by Multishelled system was

higher than that of titania nanobelt and nanoparticle though its surface area was lower. Higher drug uptake by titania nanobelt compared to particles is owing to the increased number of active sites and higher pore volume which can adsorb drug molecules.This type of porous structures are proven to be performing better as a host for drug molecules than nanoparticle based systems [98].

| Nanostructures | Surface area $(m^2/g)$ | Pore volume $(cm^3/g)$ | Drug content per mg of DTiO$_2$ [ppm] | Drug content per mg of FDTiO$_2$ [ppm] |
|---|---|---|---|---|
| MT | 93.54 | 0.4077 | 8.3757 | 2.508 |
| TNT | 84.79 | 0.3465 | 3.497 | 2.500 |
| TNB | 47.634 | 0.05716 | 1.510 | 1.304 |
| TNP | 22.29 | 0.0667 | 1.321 | 1.110 |
| MHS | 22.33 | 0.0813 | 2.411 | 1.397 |

**Table 1.** Comparison of surface area and pore volume of nanostructures and their drug uptake

Further characterisation of 5Fluorouracil loaded titania nanostructures and its folic acid modified systems have assessed by Xray diffraction pattern [Figure 5]. A significant decrease in the intensity of the diffraction peaks was also observed after the loading 5FU, when compared to the parent materials. This is probably due to the blocking of the dispersion centres by the organic fragment    for

diffractograms of Titanium dioxide materials [99]. No additional peaks are observed indicating highly dispersed state and a much lower dosage of of the additives. We can conclude that, presence of 5-Fu does not customize the crystal structure of the Titania nanostrctures. In view of studying the addition of 5FU in $TiO_2$ matrix, analysis of the position of XRD peak revealed a shift of 2Ө value to a lower angle. This fact signifies the increase in the interplanar spacing (d value).
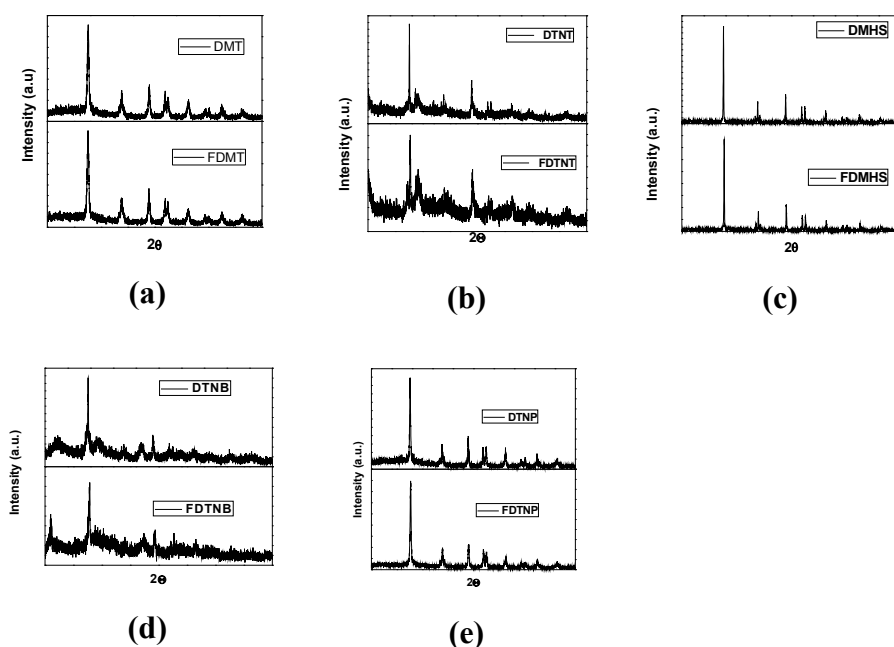


(a)　　　　　(b)　　　　　(c)



(d)　　　　　(e)

**Figure 5**. Xray diffraction pattern of anticancer drug loaded systems

The incorporation of 5FU can also be confirmed by comparing FTIR Specta of mesoporous assembled titania (MT), drug incorporated form (DMT) and pure 5FU [Figure 6] . This provides an idea about the possible chemical bonds formed during the synthesis. While

considering the FTIR spectum of pure 5FU, bands at 1721 cm$^{-1}$ and 1671 cm$^{-1}$ are due to the streching vibrations of C=O where as band at 1247 cm$^{-1}$ is due to the C-N strching vibrations. The C-F steching vibrations are observed at 1438 cm$^{-1}$. In drug loaded system, bands are observed at 1247 cm$^{-1}$, 1438 cm$^{-1}$, 1633 cm$^{-1}$, 1720 cm$^{-1}$. The presence of above bands in addition to the characteristic bands of Titanium dioxide confirmed the presence of 5-Fu on the surface of Titanium dioxide. The observed blue shifts for C=O groups in Drug incorporated mesoporous structure  may be attributed to the Ti-O bond formation. Similar Blue shift for C=O groups was observed for the all the Titania nanostructures which have been decorated with 5 fluorouracil, confirming the physical adsorption of anticancer drug in the metal oxide matrix [100].
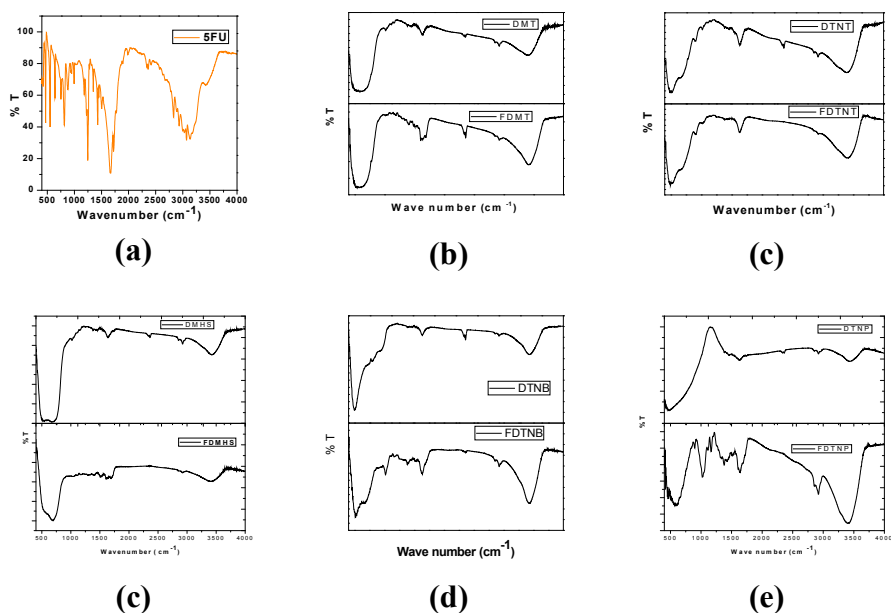


**Figure 6.** FTIR spectra of Drug incorporated nanostructures

Figure 7 illustrate a schematic illustration for the preparation of drug loaded mesoporous assembled titania nanocuboids.
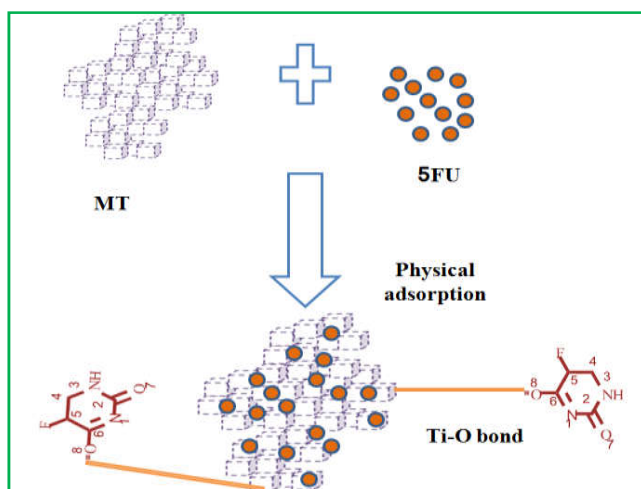


**Figure 7.** Schematic illustration of the preparation of drug loaded mesoporous titania

Since large fraction of human cancer cells are characterised by their over expression of folate receptors on their surface, modification of Titania with folic acid is highly desiarble. Folic acid surface modified titanium dioxide nanoparticles were proven to have enhanced anticancer activity compared to the mere $TiO_2$ nanoparticles [101]. This functionalization may effectively avoid or at least minimize the toxicity of $TiO_2$ NPs. Folic acid is a biocompactible redox active chromophore with facile anchoring groups for immobilisation on semiconductor surface [102]. Folic acid is composed of pteroic acid and glutamic acid linked through amide bond. The pteroic moety has the ability to form hydrogen bonds either within them or with other molecules [103]. Strong chemisorption of folic acid on $TiO_2$ surface have been already

reported and its slow desorption from surface occurs only at high pH. Since $TiO_2$ has high affinity for –COOH groups, chemisorption of folic acid on $TiO_2$ occurs through carboxylate groups of glutamate side chain [104-105]. The –$NH_2$ group in FA shows the – NH stretching vibrations at 1605 cm$^{-1}$. Since the –$NH_2$ group in FA has no interaction with 5-FU or $TiO_2$, the peak appears as such. Also, as there is no interaction between the –NH group of 5-FU and $TiO_2$/Folic acid, the –NH bending peak at 1398 cm$^{-1}$ appears as such in the spectra for DMT and FDMT. In the FTIR Spectra of $FDTiO_2$, the band at 1723 cm$^{-1}$ for –CO group disappears in the spectra for $FDTiO_2$. This hinted that the interaction between 5-FU with $TiO_2$ and folic acid in $FDTiO_2$ system. (Folic acid modified drug incroporated Titania) It was due to the formation of inter molecular hydrogen bond using the –CO group of 5-FU. These observations indicated the successful incorporation of folic acid and 5-fluorouracil in the system [106]. Schematic representation of folic acid modified 5-FU incorporated titania mesoporous assembled titania is given in Figure 8.
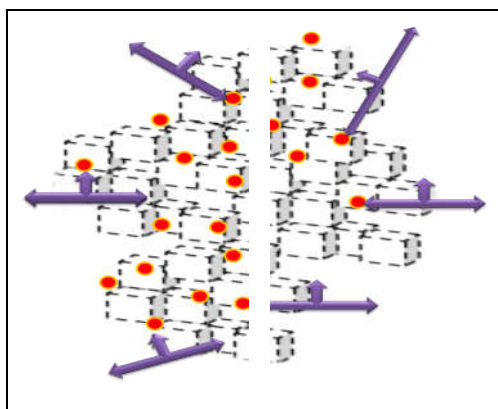


**Figure 8**. Schematic picturisation of Folic acid modified,5-FU loaded mesoporous assembled titania nanocuboids [Orange dots – 5FU molecule, triple headed blue arrow – Folic acid moeity]

## 5.9.1   In vitro cytotoxicity assay of nanostructures towards MCF-7 cancer cell lines

To verify whether the $TiO_2$ nanostructures possess the potential for cellular toxicity, cell viability assays were performed which is based on the reduction activity of methyl thiazolyl tetrazolium (MTT). The mitochondrial dehydrogenases in living cells reduce MTT to a blue-magenta colored formazan crystals. The absorption of dissolved formazan in the visible region associated with the number of intact alive cells. Cytotoxic additives have the ability to damage and destroy cells, and consequently diminish the reduction of MTT to formazan. Detailed description of MTT assay has been given in section 2.9.2.3. The resulting data are shown in Figure 9. The viability of untreated cells was assumed to be 100%. Cell viability was lowered as a function of concentration for all the nanostructures.
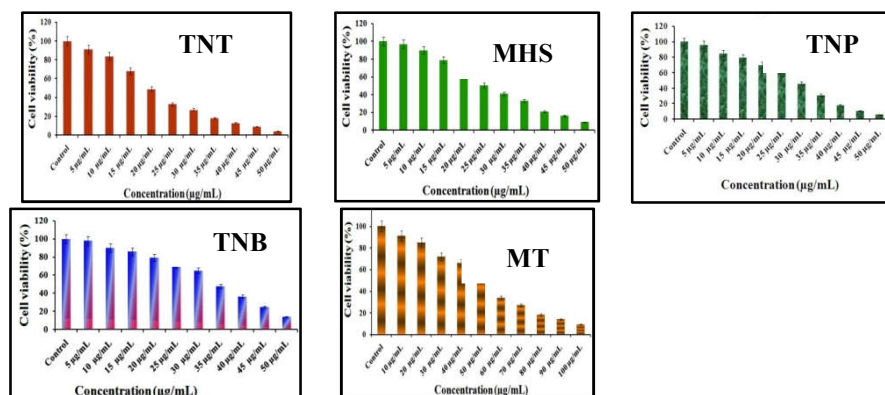


**Figure 9**. The MTT assay associated with cell viability after a 24 h incubation time period with varying concentrations of nanostructures. All measurements are averages of three replicas. Error bars represent standard deviations of three replicates of data taken.

Fifty percentage of cell death, which determines the inhibitory concentration ($IC_{50}$) value of nanostructures against cancer cells in 48 h is shown in Table 2. $IC_{50}$ is the concentration of drug at which 50% of cancer cells are inhibited. Lower the $IC_{50}$ value more potent the molecule.

| Sl. No. | Nanostructure | $IC_{50}$ value |
|:-------:|:-------------:|:---------------:|
| 1 | TNT | 22.11 µg/mL |
| 2 | MHS | 25.12 µg/mL |
| 3 | TNP | 30.23 µg/mL |
| 4 | TNB | 35.15 µg/mL |
| 5 | MT | 50.01 µg/mL |

**Table 2.** $IC_{50}$ values of the synthesised nanostructures obtained by MTT assay

The $IC_{50}$ values were found to be decreasing in the order MT > TNB > TNP > MHS > TNT. Therefore the inhibition activity follows the order MT < TNB < TNP < MHS < TNT. The trend of decreasing the number of viable cells with nanomaterial concentration was comparatively lower for mesoporous assembled strucutres as revealed from MTT assay and hence it is having the higher $IC_{50}$ value. Conversely, Titania nanotubes were found to be more toxic towards cancer cells and the number of viable cells measured at each concentration was lower than other nanostructures.

### 5.9.2    Morphological Analysis

Microscopic observations [Figure 10 [set i]] were monitored using Nikon light inverted microscope in which the control cells appeared normal whereas the treated cells showed distinct cellular morphological changes signifying unhealthy cells. In this experimental part, the cells were treated with $IC_{50}$ and $IC_{25}$ concentrations of nanoparticles. The nanostructure treated cells appeared to shrink and cell spreading patterns were restricted which are quite different from that of control cells. Among these, cells treated with $IC_{50}$ concentration of nanoparticles have appeared to be more affected to the action as seen from the images due to the higher concentration of the dosage form. DAPI is a popular nuclear counter stain and nanoparticle induced fragmentation was observed by this method. It stain both normal and dead or apoptic cells, but the effectiveness is low in the case of normal cells whereas it passes through cell membrane through the cells which have lost cell intergrity. Therefore the defective cells show much higher fluorescence than the normal ones. The bright field and fluorescence microscopic images are shown. As shown in the set ii of figure 10, the strong bluish fluorescence and cellular uptake observed in the imaging studies with nanostructures reveal that these molecules have high potency against breast cancer cell lines (MCF-7). The untreated cells appeared normal nuceli whereas the treated cells appeared to be fragmented and condensed chromatin representing apoptic bodies. As the applied concentration of nanostructures are increased, the total number of apoptic cells are also found to be higher.
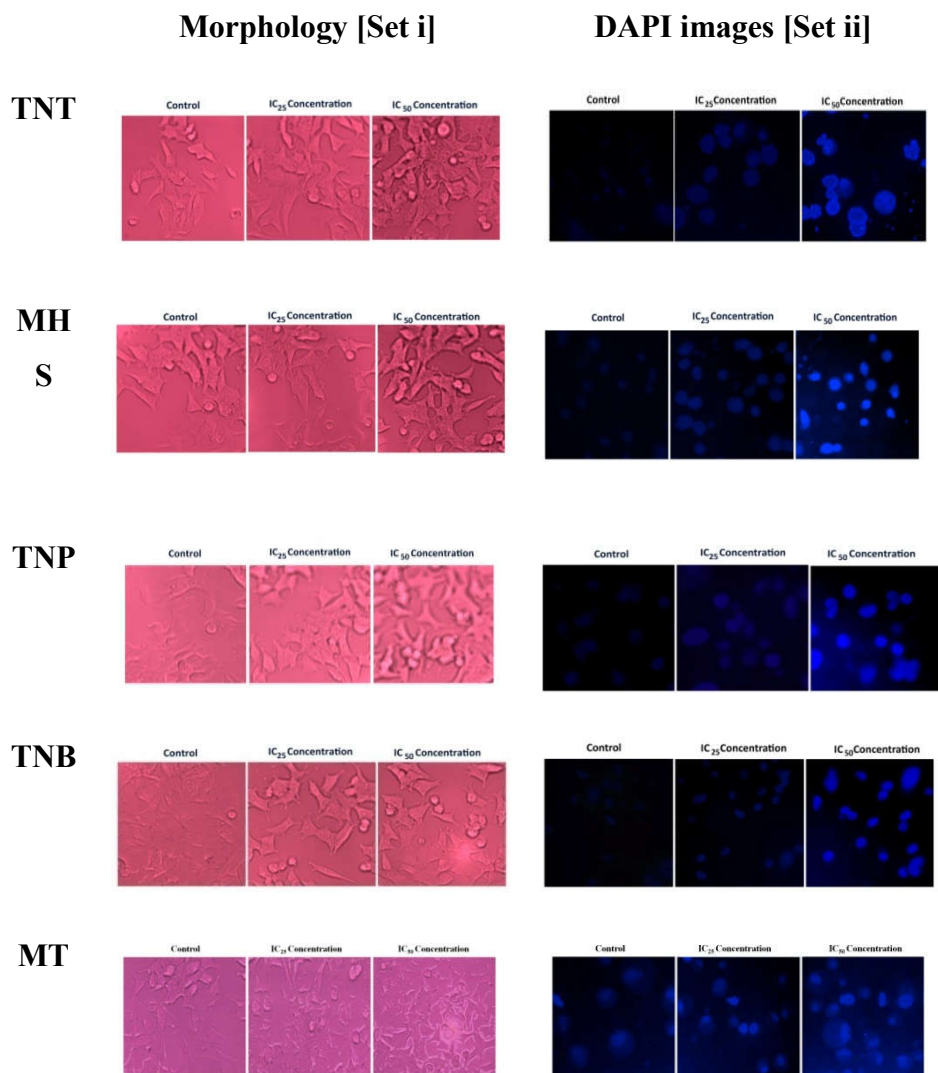
**Morphology [Set i]**     **DAPI images [Set ii]**

TNT

MHS

TNP

TNB

MT



**Figure 10.** The morphological characterization of control, MCF-7 cancer cells treated with nanostructures and corresponding DAPI-nuclear staining images of the same

### 5.9.3 Cytotoxic studies of anticancer drug loaded nano systems in DLA Cell lines

The cytotoxic studies of these nanostructures towards cancer cell lines gave an idea of utilising these diverse porous systems for targeted drug delivery. Thus these nanostructures are loaded with an anticancer drug namely 5 fluoro uracil.

As preliminary examination, to check of the effectiveness of anticancer activity of these anticancer drug entrapped nanostructures, cytotoxicity assay was carried out in mice cancer cell lines. Daltons Lymphoma Ascites (DLA) cell lines from tumor bearing mice were investigated by Trypan blue exclusion method.In this method the cells treated with the dye stain the dead cells blue. Detailed expertimentl procedure has been discussed section 2.9.2.1. The data in this regard are shown in Table 3.

| Concentration of Drug (Micro gram per mL) | % Cytotoxicity of Drug loaded titania nanostructures | | | | |
|---|---|---|---|---|---|
| | DTNT | DMT | DTNB | DTNP | DMHS |
| 500 | 42.13 | 56.21 | 40.13 | 42.17 | 45.24 |
| 250 | 28.14 | 30.24 | 26.23 | 20.22 | 24.21 |
| 200 | 20.16 | 19.15 | 18.23 | 10.13 | 14.14 |
| 100 | 12.21 | 14.21 | 10.21 | 4.16 | 7.18 |
| 50 | 8.23 | 7.12 | 4.17 | 2.21 | 5.13 |

**Table 3.** The trypan blue cytotoxic assay of 5-FU loaded titania nanostructures in DLA cells

In, Tripan blue assay the drug loaded systems were incubated for 3 hour at $37^{\circ}$C. We can see that the materials are showing a significant cytotoxicity only at higher concentrations and very low activity at low concentrations. This is probably due to the fact that as this assay is performed for a short time, the drug may not be released in to the medium upto a good level to show inhibition of cells at a low concentration. Thus we tried to extent the incubation time which is carried out using the MTT assay of the same systems in MCF-7 cancer cell lines. The cytotoxicity assay results have been shown in the succeeding sections. As said before the attachment of folic acid to the nanosystems were observed to be potential for the targeted drug delivery, we also examined the cytoxicity assay of folic acid modified systems of the titania nanostructures also.

### 5.9.4 Cytotoxic studies of drug encapsulated and Folate modified drug incorporated TiO$_2$ systems

The Cell viability assay [ Figure 11] of anticancer drug loaded TNT at different concentrations incubated for a period of 24 hours also showed a concentration dependent cytotoxicity. The IC$_{50}$ value was found to be 18.96 µg/mL and when compared with the MTT assay of parent tubular titania, the IC$_{50}$ value was observed to be lower due to the incorporated anticancer drug. The good anticancer activity exhibited by the drug loaded system compared to the previously mentioned trypan blue assay may be due to the higher incubution time of 24 hours, which is sufficient to release the drug to make the more cells nonviable. This results pointed to the slow release of the drug

from the drug loaded systems which is beneficial in view of theraputic efficiency.

The cell morphology observed using a light microscopic study assesses the extent of cell shrinkage with that of control cells at two different concentrations of nanosystems. [IC$_{25}$ and IC$_{50}$]. As seen from the figure 10., the control cells are less affected where as DTNT Nanosystem treated cells are more vulnarable to morphological change in a dose dependent manner. Cells with apoptotic nuclear condensation and fragmentation were obvious from the DAPI –nuclear staining [Third panel Figure 11]. The cell viability assay of folic acid modified anticancer drug loaded systems shows that the cells are more prone nonviable. The observed lower value for  IC$_{50}$ [10.82 μg/mL] also confirmed the above said fact. The higher in vitro anti tumor activity of FDTNT when compared to parent and drug loaded system is due to the potential targeting enabled using the folic acid moeties. Since folate receptors are over expressive on cancer cells, the folic acid modified system can effectively target and deliver the drug to the desired tissue with much lower concentration. Morphological changes of the cells were also studied to confirm apoptosis. The strong bluish fluorescence and cellular uptake have been observed in the imaging studies . The treated cells are affected more by the modified drug loaded system than the control , also the apoptic nucei are higher compared to the parent system as seen from DAPI nuclear staining.
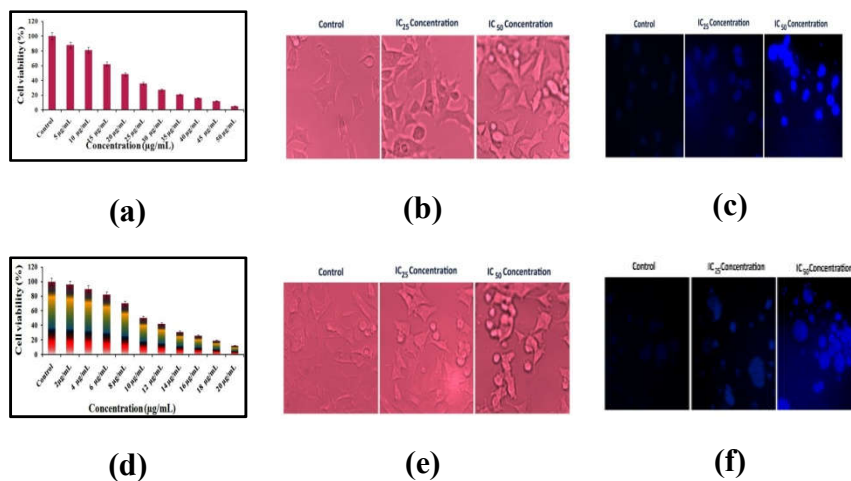
(a)          (b)          (c)

(d)          (e)          (f)

**Figure 11**. Cell viability assay, morphological change and DAPI nuclear staing of DNT (a,b,c) and FDTNT(d,e,f).

Further An in vitro cytotoxicity assay for drug loaded MHS and iths folic acid modified system were conducted using an MTT reduction assay[Figure 12 a and Figure 12 d]. Compared with the parent nanostructure, both DMHS and FDMHS exhibited higher cytotoxicity and the effect were more pronounced when the concentrations were increased. The observed $IC_{50}$ Value for DMHS and FDMHS were 20.31 µg/mL and 10.60 µg/mL respectively which were obviously higher compared to the cytotoxic effect parent multiwalled structure [$IC_{50}$= 25.12 µg/mL]. The decreased cell viability is due to the incorporated anticancer drug in the case of DMHS and the effective targeting ability of folic acid moeties as in FDMHS.   Folate functionalized nanosystem  could significantly enhance the cellular uptake of the drug delivery system in MCF-7 cells indicating good

breast cancer targeting potential of the system. The morphological changes observed when the cells were treated with $IC_{25}$ and $IC_{50}$ concentrations of DMHS and FDMHS have been displayed in figure 12 b and e. Control cells were observed to be irregular confluent aggregates with rounded and polygonal cells. The most recognizable morphological changes of treated cells observed in this study were the cytoplasmic condensation, cell shrinkage, production of numerous cell surface protuberances at the plasma membrane blebbing and hyper condensed chromatin. Untreated MCF 7 cells had normal morphology with intact round nucleus emitting a weak fluorescence. However, cells treated with both DMHS and FDMHS showed apoptotic nuclei, recognized by reduced nuclear size, condensed chromatin gathering at the periphery of the nuclear membrane and a total fragmented morphology of nuclear bodies as evident from the DAPI images [Figure 12 c, Figure 12f].
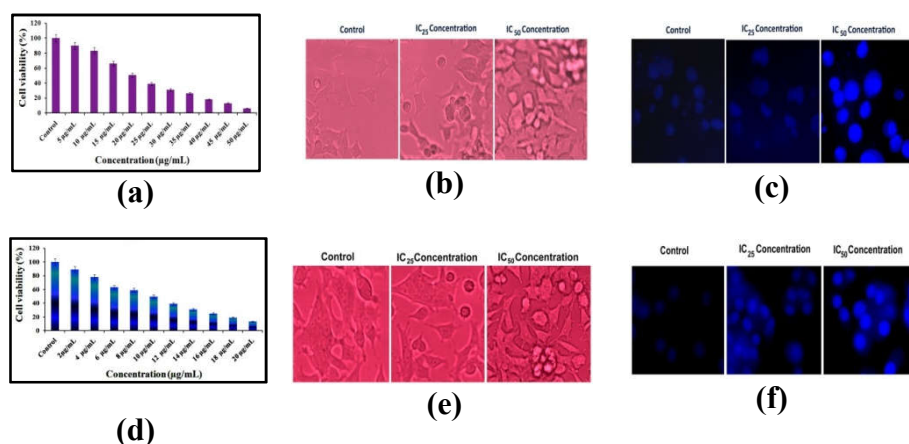


**Figure 12**. cell viability assay, morphological change and DAPI nuclear staing of DMHS (a,b,c) and FDMHS(d,e,f)

The relevant $IC_{50}$ values of DTNP and FDTNP on MCF-7 cancer cell lines have been investigated by MTT assay and found to be 25.05µg/mL and 14.20 µg/mL (Figure 13). The folic acid modified systems exhibit significant higher cellular uptake and cytotoxicity in breast cancer cell lines and the cytotoxicity exhibited was much higher compared to parent nanoparticle [$IC_{50}$ = 30.23µg/mL] due to the combined effect of incorporated anticancer drug and the active targeting of folic acid moeties. The cell blebbing and membrane disintegrity were observed using phase-contrast light microscopy to evaluate the level of cell shrinkage at the $IC_{50}$ and $IC_{25}$ concentration of both modified nanosystems after 24 h of incubation [Figure 13b, Figure 13e]. Moreover, the results of nuclear staining using DAPI also confirmed the visible nuclear changes of treated cells related to the normal ones[ Figure 13c, Figure 13f].
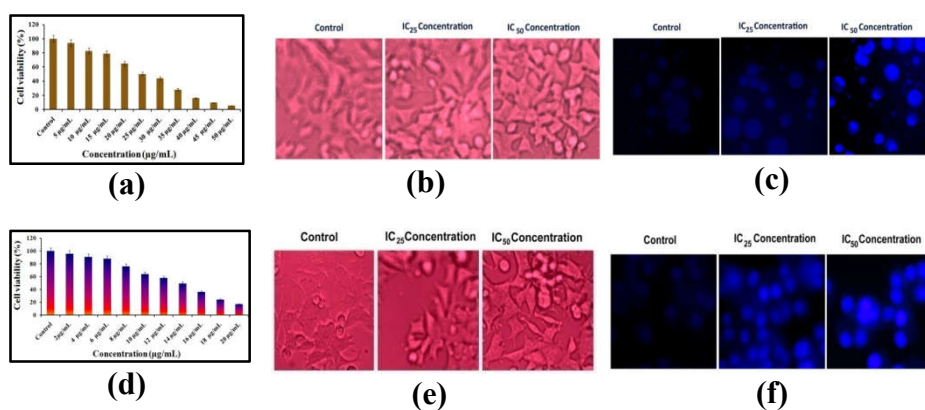


**Figure 13**. cell viability assay, morphological change and DAPI nuclear staing of DTNP (a,b,c) and FDTNP(d,e,f)

The quantitative results of cytotoxic assay of DTNB and FDTNB with MCF 7 cell lines were displayed in figure 14a and d respectively. This trend of survival decreasing with exposure concentrations is similar to those shown above and the folic acid modified system has been shown to have good potential for cancer cell targeting evident from the lower $IC_{50}$ value [$IC_{50}$ =12.23 µg/mL]compared to the parent nanoparticle [$IC_{50}$ = 35.15 µg/mL and the drug modified systems [$IC_{50}$ = 25.25µg/mL]. This is further confirmed from the morphological image of MCF-7 cancer cells treated with DTNB and FDTNB systems (Figure 14b, Figure 14e). These image shows that the cancerous cells were damaged more effectively by anti cancer loaded nanosystem and the effect was more pronounced in the folic acid modified form confirming enhanced anticancer activity when loaded onto TNB, which in turn, shows the practical utility of the present nanostructure. The fluoresecent DAPI images also confirmed the above said fact displaying apoptic nuclear bodies and condensed nuclear chromatin representing the damaging cells upon treatment with different concentrations of modified nanostructures [ Figure 14c, Figure14f].
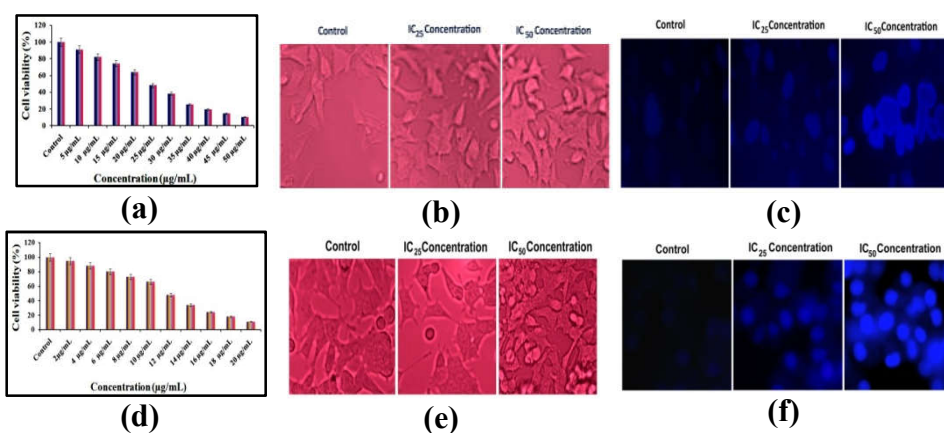


**Figure 14**. cell viability assay, morphological change and DAPI nuclear staing of DTNB (a,b,c) and FDTNB(d,e,f)

The viability studies [Figure 15 a, d] demonstrate that combining the anti cancer drug 5 Fluoro uracil to mesoporous assembled nanostructure decreased the cell viablity to an extent. It is clearly evident from the $IC_{50}$ values of parent and drug incorporated systems the values being 50.01 µg/mL and 30.21 µg/mL. And when the nanostructure was modified with targeting group folic acid the system exhibited higher cytotoxicity signifying higher cellular uptake. Thus folate functionalized nanosystem could significantly enhance the cellular uptake of the nanosystemin MCF-7 cancer cells indicating good breast cancer targeting potential of the system with an $IC_{50}$ value of 8.03 µg/mL . The morphologies of nanostructure reated systems showed apoptotic characteristics such as cell shrinkage, membrane blebbing, rounding, and so forth and as the concentration was raised to $IC_{50}$ value, few cells remained adherent and many detached from the substratum In contrast, control cells that were treated were well spread with a flattened morphology [Figure 15 b, e]. The DAPI stained nuclear morphology analysis showed normal nucei to untreated cells whereas characteristic apoptotic changes, such as fragmentation of the nucleus, and related formation of apoptotic bodies in the MCF-7 cancer cells were observed in the treated cells.Cells treated with the folic acid modified nanosytem form more number of apoptic nuceli as seen from the images as the concentration was raised to $IC_{50}$ value [Figure 15f].
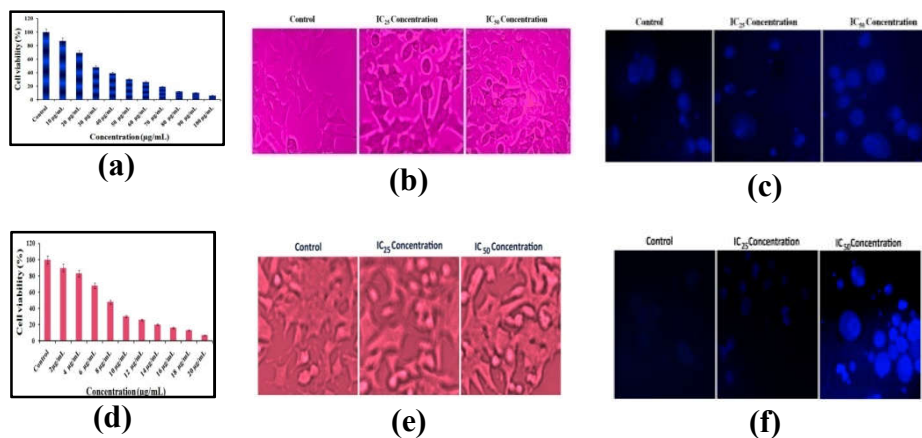
**Figure 15**. cell viability assay, morphological change and DAPI nuclear staing of DMT (a,b,c) and FDMT(d,e,f)

**Identification of the best system**

The intracellular uptake of all the folic acid modified systems were found to be higher than the parent nanostructures and its drug incorporated forms. This revealed the significant influence of folate moeties on MCF -7 cell lines to increase the uptake by receptor mediated endocytosis. It is established that folic acid, either in solid nanosheets structure or in aqueous solution, does not exhibit any cancer inhibition activity [103]. The added efficacy may be attributed to the increased drug accumulation in tumor cells due to the targeted delivery function and also the synergetic effect of two drugs mesoporous assembled titania nanocuboids, MT and 5 Fluorouracil, 5-FU. A comparison of anticancer activity of all the parent systems, drug loaded samples, folic acid modified drug incorporated systems in terms of $IC_{50}$ value is provided in Table 4. Among all the series the $IC_{50}$ value of folic

acid modified 5FU incorporated mesoporous titania is found to be lowest (8 µg/mL). The value decreased to be considerable extent from 50.01 µg/mL (MT) to 30.21 µg/mL (DMT) when 5-FU was incorporated and then reduced to 8 µg/mL on attaching folic acid. The leap from 50.01 µg/mL to 30.21 µg/mL is certainly due to the high loading efficiency of mesoporous assembled titania towards the anticancer drug. Drug uptake per milligram of drug loaded titania system was highest for MT [Table 1]. For other systems, the incorporation of anticancer drug certainly decreased the $IC_{50}$ value, but to a lesser extent than that of DMT. When we compare the drug (5-FU) content of DMT and FDMT, it was almost half in the latter one. But the $IC_{50}$ value was observed to be much lower. This clearly signifies the targeting ability of folate receptors on the $TiO_2$ surface. Effective targeting at a much lower dosage is achieved by Folate modified 5-FU incorporated mesoporous assembled titania when compared to other structures. Hence the present study points to the decisive role of porosity in assigning targeted drug delivery and anticancer activity of the prepared systems. The underlying cell killing pathway in the tumour tissues were further carried out using this system, FDMT only.

**Toxicity of Titania towards Normal cells**

In order to project as a good therapeutic agent, It is essential to evaluate the cytotoxicity of these mesoporous assembled titania towards normal cell lines. Hence in vitro cytotoxic effects of mesoporous structure were evaluated against normal cell lines with MTT assay [Figure 16]. Normal breast cancer cell line HBL-100 was

selected for the viability assay. It has been observed that the the toxicity of the nanostructure toward human normal cells (HBL-100) showed no significant deduction in cell viability for 24 h of incubation. The inhibition activity of 50 µg/mL of MT was only 86±1.17 indicating the considerable biocompatibleility of the system.
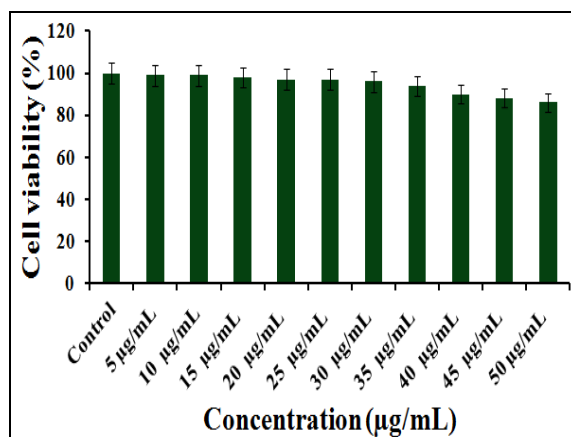


**Figure 16**. The cytotoxicities of mesoporous assembled titania nanostructure against HBL-100 Cell lines

**Intra cellular mechanisms – induction of Apoptic cell death by Folic acid modified 5-FU decorated mesoporous titania**

Under normal conditions, apoptosis is the programmed cell death and is a normal physiological process. Cancer is the dysregulation in the proper functioning of apoptosis resulting in uncontrolled growth of the cells. Nowadays apoptic inducers are introduced in cancer therapy to arrest the growth of destruction the cancer cells / destructu the cells. Here induced apoptosis is programmed for cancer cell killing by various cytotoxic agents.

Multitudes of distinctive morphological and biochemical features are used to characterise a cell undergoing apoptosis ie, for mointering the cell degeneration. Accordingly variety of cytometric methods have also been developed to recognize apoptotic cells, identify particular events of apoptosis and probe mechanisms associated with this mode of cell death. Anticancer drug 5 fluorouracil is also found to trigger cancer cell death through apoptic mediated pathway. Therefore we moniter some of these mathods including (i) AO/EtBr staining, (ii) Annexin V-FITC/PI Staining (iii) Comet assay (iv) DNA fragmentation (v) Rhodamine 123 staining (vi) Western blot analysis (vii) DCFH-DA flurescence assay etc, to study the cellular alterations upon anticancer treatment. These have been explained in detail in the following sections.

## 5.9.5    AO/EtBr staining

The induction of apoptosis, after the treatment with $IC_{50}$, $IC_{25}$ concentrations of Folic acid modified anticancer drug loaded mesoporous titania for 24 was evaluated by fluorescence microscopy after staining with acridine orange/ethidium bromide (AO/EtBr). The images of untreated and folic acid modified systems treated MCF-7 cancer cells are presented in Figure 16. Acridine orange is a vital dye and will stain both live and dead cells whereas Ethidium bromide will stain only cells that have lost membrane integrity. Acridine orange penetrate the normal cell membrane and the fluorescence microscopic analysis reveal that untreated cells were stained with a uniform green fluorescence [Left, Figure 17].  Early-stage apoptotic cells [beginning

of apoptosis], marked by crescent-shaped or granular yellow-green AO nuclear staining, and were observed in the experimental group treated with $IC_{25}$ concentration [Middle, Fifure 17]. Late apoptotic cells will also incorporate ethidium bromide and therefore stain orange [Right, Figure 17]. Cells treated with $IC_{50}$ concentration appeared to be in that stage. Necrotic cells increased in volume and showed uneven orange-red fluorescence at their periphery. The cells appeared to be in the process of disintegrating as revealed from the images.
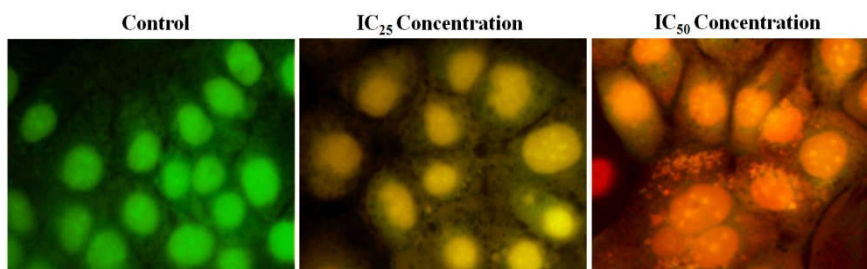


**Figure 17**. MCF-7 cancer cells treated with different concentrations $IC_{25}$ concentration (Middle) and $IC_{50}$ concentration (Right) of FDMT further stained with AO/EtBr

## 5.9.6 Annexin V-FITC/PI Staining

The apoptotic cell death are further confirmed and quantified by flow cytometric analysis of annexin V-FITC/PI stained MCF-7 cancer cell lines. One of the earliest apoptotic features involved the Phosphatidylserine (PS), membrane phospholipid translocation from the inner to the outer layer of plasma membrane. The annexin V-FITC/PI stained cells indicated damage to cell membrane resulting in nuclear staining. It has been reported that cells with both FITC

Annexin V and PI negative is considered viable while cells with both FITC Annexin V and PI positive is considered necrotic. And cells with FITC Annexin V positive and PI negative are considered apoptotic. Annexin V which has high affinity to phosphatidylserine and binds with it as PS is exposed by flipping from the inner to the outer layer of plasma membrane. Moreover, the necrotic cells [ fully damaged cells] are detected by the nuclear stain, propidium iodide (PI). Thus apoptosis and necrosis can be detected using the double staining with FITC-annexin V and PI. The distinguishable four phenotypes were; viable (lower left quadrant, Q3), early apoptotic (lower right quadrant, Q4), late apoptotic and necrotic (upper right quadrant, Q2), and damaged cells (upper left quadrant, Q1). The control system (Figure 18, Left) did not show any apoptosis indicating any negative impact on the cell lines. Figure 18 also shows the apoptotic profile at $IC_{25}$ and $IC_{50}$ concentrations of nanosystem. Compared to control cells, early apoptotic cells are raised to 15.85 % and 21.18 % for $IC_{25}$ and $IC_{50}$ concentrations of test sample. The late apoptotic cells were raised from 9.07 % to 27.12 % when the concentration was raised. The percentage necrotic cells at $IC_{50}$ concentration was 3.34% while 0.98 % for $IC_{25}$ concentration treated cells.
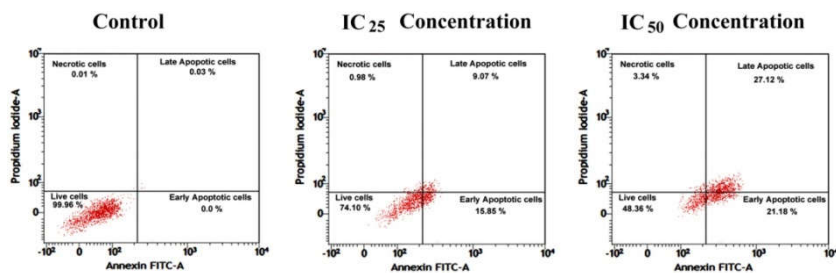


**Fgure 18**. Annexin V-FITC/PI Staining of Control (Left), $IC_{25}$ (Middle) and $IC_{50}$ Concentration of FDMT

### 5.9.7   Comet assay

Analysis of apoptotic inducing effect of Folic acid modified 5FU incorporated mesoporous titania on MCF-7 cancer cells was assessed by comet assay. In commet assay, nanoparticles were found to increase the DNA tail length which measures extent of DNA strand breaks also alkali labile sites. The induction of DNA single strand break is often used to predict oxidative damage of tumor cells. The results show the DNA damage (according to tail length) in MCF- 7 cells exposed to two different concentrations for 24 h (Figure 19). Microscopic images reveal that control cells do not exhibit any specific tail formation. But, a clear induction of comet tail was observed upon treatment with $IC_{25}$ concentration of FDMT and whose length was almost doubled/tripled when the cells were treated with its $IC_{50}$ concentration. It has been established that highly reactive radicals attack cellular components including DNA, lipids, and proteins leading to oxidative damage of the same.
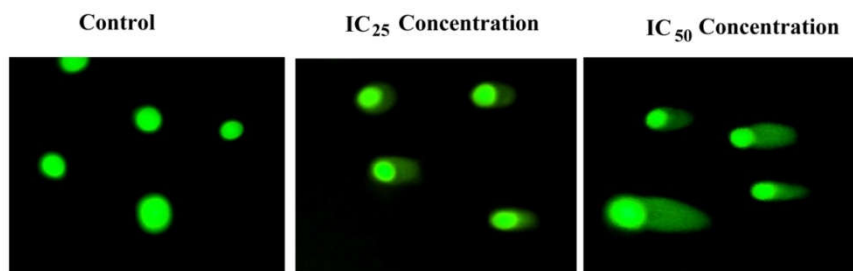


**Figure 19**. Analysis of apoptotic inducing effect of FDMT on MCF-7 cancer   cells   assessed   by   comet   assay.   Control (Left),   $IC_{25}$ concentration (Middile) and $IC_{50}$ (Right) concentatrion

### 5.9.8   DNA fragmentation

Ladder formation due to DNA fragmentation is  widely accepted as a hall mark of final stage of apoptosis [107]. In the present study, the DNA fragmentation was examined by extracting DNA from MCF-7 cancer cell lines treated with FDMT followed by detection in agarose gel. Laddering pattern was observed in cells treated with $IC_{50}$ value [Figure 20, lane 3]. On the other hand cells treated with $IC_{25}$ concentrations of the test system are shown in the lane 2 which does not produced any detectable ladder pattern. These results are consistent with the flow cytometric data of apoptosis in FDMT treated MCF-7 cancer cells. Collectively, these data confirm that the cell death proceeds through apoptotic pathway.
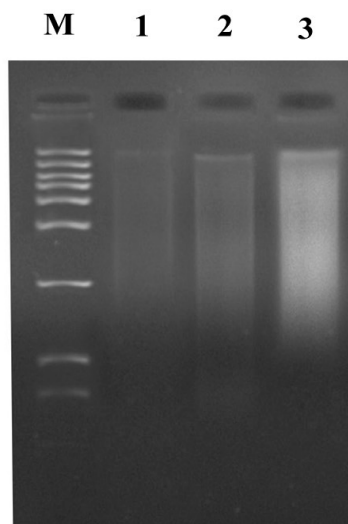


**Figure 20.**  DNA laddering assay of nontreated (lane 1), $IC_{25}$ (lane 2) and $IC_{50}$ (lane 3) FDMT treated MCF-7 cancer cells. Lane M: Marker

### 5.9.9    Rhodamine 123 staining

Figure 21    represented the depolarised membrane structure of mitochondria in FDMT treated MCF-7 cancer cells. The structure of mitochondria was observed to be normal and uniform in control cells. Rhodamine 123 is a cationic dye which is lipohilic and it is easily sequestered by the mitochondrial membrane revealing the  structural information. A diminished fluoresence indicated the mitochondrial membrane depolaristion. The ROS propagation inside the cells activates mitochondrial membrane permeabilization. Generally, ROS occurs as a byproduct of oxidative metabolism in mitochondria but when this drug encapsulated titania generates ROS, the normal physiological redox system collapses leading to mitochondrial rupture. The mitochondrial respiratory chain is itself a potential source of ROS, such as hydrogen peroxide and superoxide and its breakage further enhances the ROS level [108]. This rupture also releases Cytochrome C from the mitochondrial intermembrane space, stimulating the caspase dependent apoptosis pathway [109]. From figure 21,  a reduction in mean fluorescence intensity was observed following the treatment of cells with FDMT. The fluorescence images of treated cells revealed the loss of mitochondrial membrane potential due to mitochondrial membrane depolarization.This step was considered to be an initial and irreversible step of apoptosis.
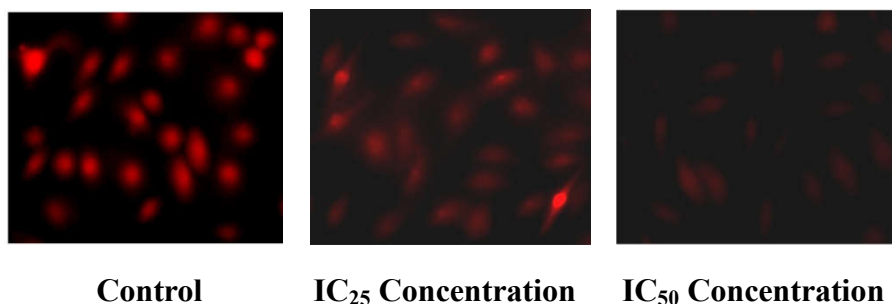
| Control | IC$_{25}$ Concentration | IC$_{50}$ Concentration |

**Figure 21.** The mitochondrial membrane potential loss of cancer cells analyzed using the dye, Rh-123

## 5.9.10 Western Blot Analysis - Expression of apoptosis-related proteins

Most of the anticancer drugs trigger apoptosis through mitochondrial mediated pathway. Here the 5FU incorporated folic acid modified mesoporous titania also postulated to follow the same pathway. For this expression levels of mitochondrial dependent apoptotic proteins namely caspase-3, caspase-9, Bcl-2, cytochrome C have been evaluated by western blotting. The β- actin was monitored as an internal Control.  It has been described that bcl-2 members (e.g., bcl-2) guard against multiple signals that lead to cell death while bax members (e.g., bax) induce apoptosis [110]. The down regulation of anti-apoptotic protein Bcl-2 was found to intiate the release of cytochrome C from mitochondria to cytosol and it is considered as the essential step in the induction of apoptosis. This is followed by the activation of caspase cascade like caspase-3, caspase-9 which are important in implementing apoptosis. These are responsible for the proteolytic cleavage of many important  proteins. Thus it is remarkable

to speculate the analysis of Bcl-2, Bax, cytochrome c, and caspases-3 and 9 gene expressions. The results in figure 22 revealed a considerable reduction in the expression of Bcl- 2 and significant increase in the expression of bax, cytosolic cytochrome c and caspase-3 and caspase- 9 in a dose dependent manner in the treated MCF-7 cancer cells compared to control cells. Thus, we can conclude that the induction of apoptosis is closely related to the down regulation of bcl-2, up-regulation of bax, loss of mitochondrial membrane potential, discharge of cytochrome c into cytosol, and following activation of caspase cascades.
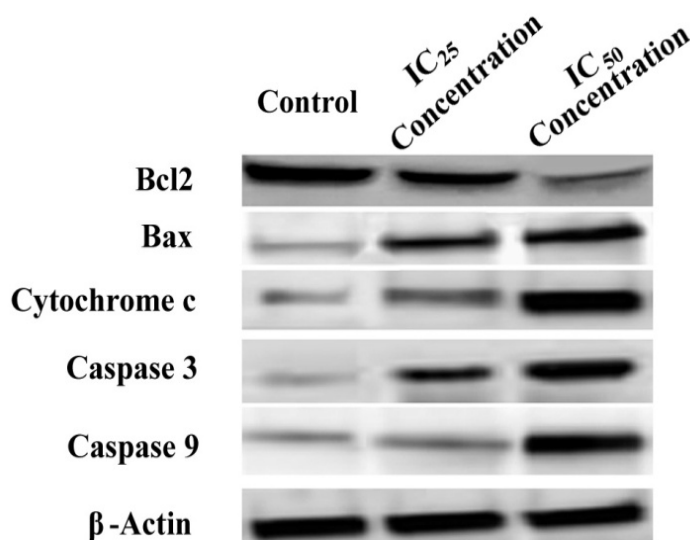


**Figure 22**. Relative expression of Caspase 3, Caspase 9, Bax, Bcl-2 expression in breast cancer MCF- 7 cells by western blot analysis. β-actin is the internal control.

## 5.9.11 DCFH-DA assay – Reactive Oxygen Species [ROS] Generation

We investigated the potential role of FDMT in inducing oxidative stress in MCF-7 cancer cells by measuring intracellular ROS by DCFH-DA assay using spectrofluorometry. 2,7-Dichlorofluorescein diacetate is deacetylated leading to DCFH which in presence of intracellular ROS converted into a highly fluorescent DCF having green fluorescence. It is because mitochondrial dysfunction and the induction of apoptosis is related to the generation of intracellular ROS [108]. ROS has been reported as an important regulator of mitochondrial function [111]. As shown in figure 23, after 24 h exposure to the nanosystem, an increase in the ROS level was observed which is in a concentration dependent manner. This indicated the up-regulation of intracellular ROS levels. The treated cells showed enhanced intensity of the green fluorescence in the treated cells when compared to the control and the flurescent intensity was strongly increased for the cells treated with $IC_{50}$ concentration. It has been well established that the generation/external addition of ROS result in cell death by two distinct pathways, viz. apoptosis or necrosis [112-113]. These results suggest that FDMT -induced apoptosis in MCF-7 cancer cells is ROS-dependent.
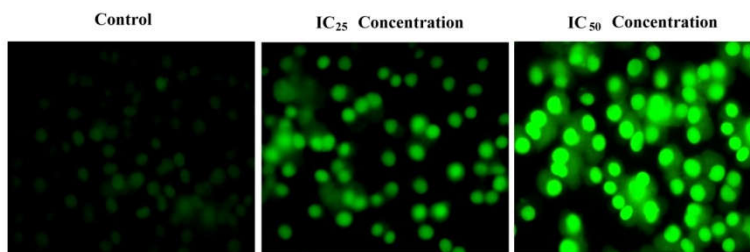
**Figure 23.** The DCFH-DA fluorescence levels of Control cells and Cells exposed to FDMT

Figure 24 represented the schematic representation of intra cellular mechanisms leading to the apoptosis and cancer cell death upon treatment with FDMT. Nanoscale size and the presence of folic acid molecule on the surface enables folic acid modified 5fluorouracil loaded mesoporous assembled titania readily enters inside the cancer cells through the leaky blood vessels. The acidic pH inside the tumor cells triggers the release of the anticancer drug and biomolecule functionalised titania system in to the cytoplasm. The resulting ROS generation inside the cell is responsible for the DNA fragmentation and mitochondrial membrane potential disintegration. The cytochrome C released from the intermitochondrial membrane space is responsible for the activation caspase cascade. Therby triggering apoptosis and then to cell death.
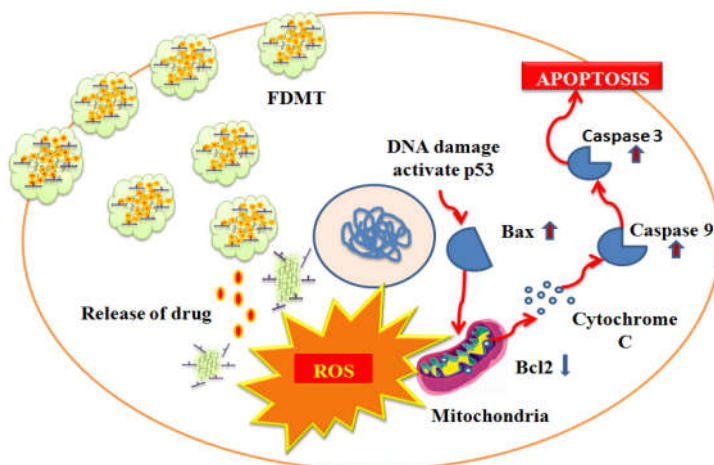
**Figure 24.** Schamatic representration of various intracellular mechanism leading to cell death

      To the best of our knowledge, no study has been carried out on $TiO_2$ based nanostructures, comparting the cytotoxicity of pure nanostructures, their 5fluorouracil drug loaded forms and Folate modified anticancer loaded forms in the biomedical realms so far. Additional adavantage of the study is the anticancer activity is achieved without the aid of external light source. Furthermore, if UV irradiation has been provided, enhanced mortality of cancer cells could be achieved. The cytotoxicity of nanomaterial $TiO_2$ towards cancer cells should be considered for further researches, and this certainly will have promising biomedical application in cancer therapy, such as Photo DynamicTherapy. Photodynamic therapy (PDT) is a nonsurgical treatment that utilises a photosensitizer (PS) followed by irradiation with wavelengths specific for its absorbance spectrum, in the presence of oxygen. This will induce cytotoxic effect generating cytotoxic reactive oxygen species which are capable for the destruction of diseased cells and tissues. Thus we can conclude that folate modified 5-

Fu loaded TiO$_2$ systems could be developed as novel apoptosis inducers against cancer cells.

## 5.10    Conclusion

+    Synthesised titania nanostructures were assessed for in vitro cell toxicity studies in cancer cells and found that all are exhibiting different extent of  cytotoxicity.The inhibition activity followed the order TNT > MHS > TNP > TNB > MT. cytomorphology analysis and DAPI images gave clear evidence for the unhealthy cells in the treated ones compared to the control cells.

+    Encapsulation of drug, 5-Fluorouracil into the porous structures of these nanostructures is achieved by simple incubation and the cell toxicity measures was in accordance with their drug uptake. Compared to the parent systems, all the drug loaded samples showed a lower IC$_{50}$ values. This increased inhibition activity was due to the presence of cytotoxic drug 5-Fluorouracil. Our results showed that 5FU surface decoration significantly enhanced the cellular uptake of Titania nanostructures through endocytosis. Among these, mesoporous assembled structures exhibited much higher drug acceptance than others.

+    Since folate receptors are overexpressed on many cancer cells, modification of the same will target the cancer tissues effectively. Thus we have modified titania systems with folic acid and followed by attaching the anticancer drug to the system.The cell viability assay of the folate modified anticancer

drug incorporated systems revealed that the $IC_{50}$ values were decreased to a considerable extent when compared to the mere drug loaded samples. The extra efficacy of the folate modifies 5-FU titania systems may be certainly achieved by the enhanced accumulation of anticancer drug due to the targeting moeity folic acid and partially due to the synergetic effect of two cytotoxic agents Titanium dioxide and 5-Fluorouracil.The folic acid can specifically target the cancer tissues releasing the drug molecules in the acidic pH. Folic acid modification not only enhances the biocompactibility of titanium dioxide, accumulate the metaloxide specifically in the cancer cells than the normal cells where the folate receptors are low. Thus this type of biomolecule-based nanstructures would be beneficial for smart multifunctional nanomedicine systems.

- The Anticancer activity increases among the folate modified systems in the order FDTNP ($IC_{50}$ = 14.20 µg/mL) < FDTNB ($IC_{50}$ = 12.23 µg/mL) < FDTNT ($IC_{50}$ = 10.82 µg/mL) < FDMHS ($IC_{50}$ = 10.60 µg/mL) < FDMT ($IC_{50}$ = 8 µg/mL). Among the folate modified series, the highest cancer inhibition activity was observed for folate modified 5-FU incorporated mesoporous assembled titania nanocuboids, $IC_{50}$ value being 8 µg/mL.

- Further investigation on the cance intracellular mechanism revealed that cell death is progressing through the activation of

apoptosis. And the fact was supported by various intracellular assays.

- AO/EtBr staining revealed the induction of apoptosis in the treated cells. Further confirmation was given by Annexin V-FITC/PI staining. The higher proportion of Annexin V-FITC positive cells for FDMT treated group was mainly attributed to the higher intracellular uptake of the $TiO_2$.

- DNA damage was confirmed by Commet assay and the DNA ladder formation was found only in the case of $IC_{50}$ concentrations supporting the flowcytometric results.

- Further experiment revealed the Mitochondrial membrane potential damge leading to the activation of apoptosis. Western blot analysis confirmed a remarkable higher expression of cytochrome C which initiate the caspase cascade. The treated cells showed upregulation of apoptic proteins Bax, caspase3, Caspase 9 and down regulation of antiapoptic protein Bcl2.

- The ROS overproduction is confirmed by DCFH-DA assay which is responsible for the mitochondrial dysfunction and induction of apoptosis. Thus we can conclude that Foilc acid modified anticancer drug loaded system, FDMT triggered apoptosis in MCF-7 cancer cells through mitochondria-mediated pathways, and the system can be developed a a novel apoptosis inducers against cancer cells.

# References

1.      K.A.V. Zubris, Kimberly Ann Veronica. Boston University, ProQuest, Dissertations Publishing, 2011.

2.      D. Sarnath and A. Khanna , Biomed.Res. J., 2014; 1, 1.

3.      I. Ali, W.A. Wani and K. Saleem, Cancer Therapy, 2011, 8, 56.

4.       **C.** Li, Adv. Drug Deliv. Rev. 2002, 54, 695.

5.      N. Korin, M. Kanapathipillai, B. D. Matthews, M. Crescente, M. Brill, A. Brill, T. Mammoto, K. Gosh, S. Jurek, S. A. Bencherif, D. Bhatta, A. U. Coskun, C. L. Feldman, D. D. Wagner and D. E. Inqber, Science. 2012, 337, 1453.

6.      R. Ortiz, C. Melguizo, J. Prados, P.J. Álvarez, O. Caba, F. Rodriguez-Serrano,F.Hita and A.Aranega, Recent Pat Anticancer Drug Discov. 2012, 7, 297.

7.      N. Bertrand and J.C. Leroux, J.Control Release. 2012,161,152.

8.      F.Caputo, M. de Nicola and L. Ghibelli, Biochem. Pharmacol. 2014, 92, 112.

9.      E. Wisse, F. Braet, D. Luo, R. De Sanger, D. Jans, E. Crabbe and A. Vermoesen, Toxicol. Pathol., 1996, 24, 100.

10.     F. Yuan, M. Dellian, D. Fukumura, M.Leunig, D.A. Berk, V.P.Torchillin and R.K.Jain, Cancer Res., 1995, 55, 3752.

11.     H. Maeda, G.Y. Bharate and J. Daruwalla, Eur. J. Pharm. Biopharma, 2009, 71, 409.

12.     X. Wang, L. Yang, Z.G. Chen and D.M. Shin, CACancer J. Clin. 2008, 58, 97.

13.     A. Tan, H. De La Pena and A.M. Seifalian, Int. J. Nanomedicine, 2010, 5, 889.

14.     E. Y. Hleb, N. A.Yakush, J. H.Hafner, R. A. Drezek, J. A. McNew and  D. O. Lapotko, Nanotech 2009, 2, 158.

15.     M. Premanathan, K. Karthikeyan, K. Jeyasubramanian, and G. Manivannan Nanomedicine: NBM, 2011, 7, 184.

16. M. Horie, K. Nishio, K., Fujita, H. Kato, A. Nakamura, S. Kinugasa, S., Endoh, A. Miyauchi, K. Yamamoto, H. Murayama, E. Niki, H. Iwahashi, Y. Yoshida, and J. Nakanishi, Chem. Res. Toxicology, 2009, 22, 1415.

17. V. Rabolli, L.C. Thomassen, F. Uwambayinema, J.A. Martens, and D. Lison, Toxicol. Lett., 2011, 206, 197.

18. G. Oberdorster, A. Elder and A. Rinderknecht, J. Nanosci. Nanotechnol. 2009, 9, 4996.

19. M. Horie, H. Fukui, K. Nishio, S. Endoh, H. Kato, K. Fujita, A. Miyauchi, A., Nakamura, M.Shichiri, N.Ishida, S.Kinugasa, Y.Morimoto, E.Niki, Y.Yoshida, and H. Iwahashi, J. Occup. Health , 2011, 53, 64.

20. A. Trafton, MIT Tech Talk. **2009**, 53, 4.

21. T.M. Saba, Arch. Intern. Med., 1970, 126, 1031.

22. L. Klibanova, K. Maruyama, V.P. Torchilin, L. Huang, FEBS Lett., 1990, 268, 235.

23. A. Sawhney, C. Pathak, J. Hubbell, Biomaterials, 1993, 14, 1008.

24. R.L. Gutman, G. Peacock, D.R. Lu, J. Control. Release, 2000, 65, 31.

25. T.K. Jain, I.Roy, T.K.De and A.Maitra, J. Am. Chem. Soc., 1998, 120, 11092.

26. I. Roy, S.Mitra, A.Maitra and S.Mozumdar, Int. J. Pharm., 2003, 250, 25.

27. S.M. Moghimi, A.C.Hunter and J.C.Murray, Pharmacol. Rev., 2001, 53, 283.

28. C. Yates, S.Sharp, J. Jones, D.Topps, M.Coleman, R. Aneja, J.Jaynes and T.Turner, Biochem. Pharmacol. 2011, 81, 104.

29. G.P. Adams, L.M. Weiner, Nat Biotechnol 2005, 23, 1147.

30. A. Gabizon, H. Shmeeda, A.T. Horowitz, S.Zalipsky, Adv Drug Deliver Rev , 2004, 56, 1177.

31. P. Alvin, D. Thompson, K.B. Ryan, A. Mccarthy, A.C. Moore, C.S. Burke, M.Dyson, B.D. Maccraith, Y.K. Gun'Ko, M.T. Byrne, Y.

Volkov, C. Keely, E. Keehan, M. Howe, C. Duffy, R. Macloughlin, Cell. Mol. Life Sci. 2011, 69, 389.

32.    J. Xu, Y. Sun, J. Huang, C. Chen, G. Liu, Y. Jiang, Y. Zhao, Z. Jiang, Bioelectrochemistry, 2007, 71, 217.

33.    Y. Yin, W.W. Zhu, L.P. Guo, R. Yang, X.S. Li, Y. Jiang, J. Phys. Chem. B, 2013, 117, 125.

34.    C.P. Leamon and A.L. Jackman, Vitam. Horm., 2008, 79, 203.

35.    H.S. Yoo and T.G. Park, J. Control. Release, 2004, 96, 273.

36.     C.P. Leamon and J.A. Reddy, Folate-targeted chemotherapy, Adv. Drug Deliv. Rev., 2004, 56, 1127.

37.    N. Parker, M.J. Turk, E. Westrick, J.D. Lewis, P.S. Low and C.P. Leamon, Anal. Biochem. , 2005, 338, 284.

38.    L.W. Christen, C.A. Rebecca, K.A.R. Deborah, N. Wendel and D.A. Ronald, Gynecol. Oncol. , 2013, 131, 493.

39.    A.C. Antony, Annu. Rev. Nutr., 1996, 16, 501.

40.    B.A. Gruner and S.D. Weitman, Invest. New Drugs, 1999, 16, 205.

41.    C.P. Leamon and P.S. Low, Drug Discov. Today, 2001, 6 , 44.

42.    R.J. Lee and P.S. Low, Biochim. Biophys. Acta , 1995, 1233,134.

43.    T.Y. Lai and W.C. Lee J. Photochem. Photobiol., A, 2009, 204, 148.

44.    R. Baan, K. Straif, Y. Grosse, B. Secretan, F. Ghissassi and V. Cogliano, Lancet Oncol. 2006, 7, 295.

45.    F. Furukawa, Y. Doi, M.Suguro,O. Morita, H.Kuwahara and T.Masunaga, Food Chem.Toxicol. , 2011, 49, 744 .

46.    P. Thevenot, J. Cho, D. Wavhal, R.B. Timmons, and L. Tang, Nanomed. Nanotechnol. Biol. Med., 2008, 4, 226.

47.    J.R. Gurr, A.S. Wang, C.H. Chen, and K. Y. Jan, Toxicology, 2005, 213, 66.

48.    C.M. Sayes, R. Wahi, P.A.Kurian, Y. Liu, J.L. West, K.D. Ausman, D.B. Warheit, and V.L.Colvin, Toxicol. Sci., 2006, 92, 174.

49.     M. Horie, L.K. Komaba, H. Kato, S. Endoh, K. Fujita, K. Nishio, A. Nakamura, A. Miyauchi, S. Kinugasa, Y.Hagihara, Y. Yoshida and H. Iwahashi, Nano Biomed., 2010, 2, 182.

50.     T. Xia, M. Kovochich, J. Brant, M. Hotze, J. Sempf, T. Oberley, C. Sioutas, J.I. Yeh, M.R. Wiesner, and A.E. Nel., Nano Lett., 2006, 6, 1794.

51.     K. Gerloff, C. Albrecht, A.W.Boots, I. Fö rster, and R. P. F. Schins, Nanotoxicology, 2009, 3, 355.

52.     G. Kirsten, F. Ivana, C.Emanuele, K.Julia, A.Catrin, W.B. Agnes, F. Irmgard, and P.F.S. Roel Chem. Res. Toxicol.*,* 2012, 25, 646.

53.     H. J.Johnston, G. R.Hutchison, F. M.Christensen, S. Peters, S. Hankin, and V. Stone, Part. Fibre Toxicol., 2009,6, 1.

54.     P. Sukwong, K.Somkid, S. Kongseng, D. Pissuwan, and K.Yoovathaworn, IET Micro Nano Lett., 2016, 11, 183.

55.     A.V. Pansare, D.K. Kulal, A.A. Shedge, and V.R. Patil, Dalton Trans., 2016, 45, 12144.

56.     P. Kocbek, K. Teskač, M.E. Kreft, and J. Kristl, Small, 2010, 6, 1908.

57.     E. Bermudez, J.B. Mangum, B.A. Wong, B. Asgharian, P.M. Hext, D.B. Warheit and J.I. Everitt, Toxicol. Sci., 2004, 77, 347.

58.     H.W. Chen, S.F. Su, C.T. Chien, W.H. Lin, S.L. Yu, C.C. Chou, J.J. Chen and P.C. Yang, FASEB J. 20,2393.

59.     D.B. Warheit, T.R. Webb, C.M. Sayes, V.L. Colvin and K.L. Reed, Toxicol. Sci., 2006, 91 227.

60.     C.M. Sayes, K.L. Reed and D.B. Warheit, Toxicol. Sci., 2007, 97, 163.

61.     H.C. Fischer and W.C. Chan, Curr. Opin. Biotechnol., 2007, 18 ,565.

62.     K. Schilling, B. Bradford, D. Castelli, E. Dufour, J.F. Nash, W. Pape, S. Schulte, I. Tooley, J. van den Bosch and F. Schellauf, Photochem. Photobiol. Sci. 2010, 9, 495.

63.     R. Cai, K. Hashimoto, K. Itoh, Y. Kubota and A. Fujishima, Bull. Chem. Soc. Jpn., 1991, 64, 1268.

64. Z.X. Lu, L. Zhou, Z.L. Zhang, W.L. Shi, Z.X. Xie, H.Y. Xie and P. Shen, Langmuir, 2003, 19, 8765.

65. L. K. Braydich-Stolle, N. M.Schaeublin, R. C. Murdock, J. Jiang, P. Biswas, J.J. Schlager, and S.M. Hussain, J. Nanopart. Res., 2009, 11, 1361.

66. K. Onuma, Y. Sato, S. Ogawara, N. Shirasawa, M. Kobayashi, J. Yoshitake, and F. Okada, The American journal of pathology, 2009, 175, 2171.

67. C. Hu, J. Guo, J. Qu, and Hu, Langmuir, 2007, 23, 4982.

68. Q.C. Xu, Y. Zhang, M.J. Tan, Y. Liu, S. Yuan, C. Choong and T.T.Y. Tan, Adv. healthcare mater., 2012, 1, 470.

69. K.C. Yoo, C.H. Yoon, D. Kwon, K.H. Hyun, S.J. Woo, R.K. Kim, E.J. Lim, Y. Suh, M.J. Kim, T.H. Yoon and S.J. Lee, Int. J. Nanomedicine., 2012, 7, 1203.

70. T. López, M. Alvarez, R.D. González, M.J. Uddin, J. Bustos, S. Arroyo and A. Sánchez, Adsorption, 2011, 17, 573.

71. M. Abdulla-al-Mamun, Y. Kasumoto, T. Zannat and M.S. Islam, Appl. Catal., A Gen., 2011, 398, 134.

72. D. Tian, S. Blacher, P. Dubois, J.P. Pirard and R. Jérôme, J. Sol–Gel Sci. Technol., 1998, 13 , 415.

73. O. Dulub, M. Batzilln, S. Solovev, E. Loginova, A. Alchagirov, T.E. Madey and U. Diebold, Science, 2007, 317 ,1052.

74. J. Zhu, J.Tang, L. Zhao, X. Zhou, Y. Wang and C. Yu, Small 2010, 6, 276.

75. T. Zhang, J. Ge, Y. Hu, Q. Zhang, S. Aloni and Y. Yin, Angew. Chem., Int. Ed. 2008, 47, 5806.

76. Z.F. Yin, L.Wu, H.G.Yang and Y.H. Su, Phys Chem. 2013, 15, 4844.

77. T. Lopez, J. Sotelo, J.Navarrete and J.A. Ascencio, Opt. Mater. 2006, 29, 88.

78. M. Uddin, D.Mondal, C.A. Morris, T. Lopez, U. Diebold and R.D. Gonzalez, App Surf Sci. 2011, 257, 7920.

79.     T. Lopez, E. Ortiz, P. Quintana and R.D. Gonzalez, Coll. Surf. A , 2007, 300, 3.

80.     P. Xu, R. Wang, J. Ouyang and B.Chen, Nanoscale Res Let. 2015, 10, 1.

81.     H. Zhang, C.Wang, B. Chen and X. Wang, Int. J. Nanomedicine. 2012, 7, 235.

82.     T. López, P. Quintana, E. Ortiz-Islas, E. Vinogradova, J. Manjarrez, D.H. Aguilar, P. Castillo-Ocampo, C. Magana and J.A. Azamar, Mater. Charac., 2007, 58, 823.

83.     M. García-Valverde, R. Lucena, F. Galán-Cano, S. Cárdenas and M. Valcárcel, J. Chromatogr. A, 2014, 1343, 26.

84.     X. Li, X. Wang, H. Lu, H. Tian, H. Jiang, G. Lv, D. Guo, C. Wu and B. Chen, Biomaterials, 2009, 30, 4708.

85.     M. Arruebo, WIREs Nanomed.Nanobiotechnol, 2011, 4, 16.

86.      M.V. Regi, F. Balas and D. Arcos, Angewandte Chemie, 2007, 46, 7548.

87.     S. George, H. Gardner, E.K. Seng, H. Chang, C. Wang, C.H. Yu Fang, and W.K. Chan, Environ. Sci. Technol., 2014, 48, 6374.

88.     T. Wang, H. Jiang, L. Wan, Q. Zhao, T. Jiang, B. Wang and S. Wang, Acta Biomater, 2015, **13**, 354.

89.     X. Feng,S.Zhang, H.Wu and X. Lou , Colloids Surf., B, 2015,  125, 197.

90.     G.D. Venkadasubbu, S. Ramasamy, V. Ramaksrishnan and J. Kumar, Adv Powder Technol.,2013, 235, 437.

91.     T.C. Long, N. Saleh, R.D. Tilton, G.V. Lowry, and B. Veronesi, Environ. Sci. Technol., 2006, 40, 4346.

92.     J. Lovric, S.J. Cho, F.M. Winnik, and D. Maysinger, Chem. Biol., 2005, 12, 1227.

93.     J.W. Wilson, C. Booth, and C.S. Potten, "Apoptosis Gene", Kluwer, Academic Publisher, Boston, Dordrecht/London, 1998.

94.     L. Jia, M.G. Macey, Y. Yin, A.C.Newland, and S.M. Kelsey, Blood, 1999, 93, 2353.

95.     L.Y. Wang, G.H. Ma and Z.G. Su, J.Controlled Release,  2005, 106, 62.

96.      S.Han, B. Jang, S.M. Oh and T. Hyeon, AdV. Funct. Mater. 2005, 15, 1845.

97.      D.H. Gracias, J. Tien, T.L. Breen, C. Hsu and G.M. Whitesides, Science 2000, 289, 1170.

98.     W. Wei, G. H. Ma, G. Hu, D. Yu, T. Mcleish, Z.G. Su and Z.Y. Shen, J. AM. CHEM. SOC. 2008, 130, 15808.

99.     K. Rajesh, B. Ayan Kumar, P. Sanjiv, F.  Mariano, B. David, R.D. Antonio, P.  Chitta and G.R. Santiago, Biomater. Sci., 2016, 4, 448.

100.    W. Liu, X. Li, Y.S. Wong, W. Zheng, Y. Zhang, W. Cao and T. Chen, ACS Nano, 2012, 6 , 6578.

101.    J.W. Ai., b. Liu and W.D. Liu, Mater.Sci.Eng C Mater. Biol. Appl., 2017, 76, 1181.

102.    F. Seker, K. Meeker, T. F. Kuech and A. B. Ellis, Chem. Rev. 2000, 100,  2505 .

103.    Y. Wang, C. Zhang, H. Li, G. Zhu, S.-S. Bao, S. Wei, L.-M. Zheng, M. Ren and Z. Xu, J. Mater. Chem. B, 2015, 3, 296.

104.    U. Diebold, Surf. Sci. Rep. 2003, 48, 53.

105.    S. Gawe̜da, G. Stochel and K. Szaciłowski, Chem. – Asian J., 2007, 2, 580.

106.     E.M. Manjusha, C.M. Jithin, K. Manzoor, S.V. Nair, H. Tamura and R. Jayakumar, Carbohydr. Polym., 2010, 80, 442.

107.     R.T. Allen, W.J. Hunter and D.K. Agrawal, J. Pharmacol. Toxicol. Methods 1997, 37, 215.

108.    S. Fulda and K.M. Debatin, Oncogene 2006, 25, 4798.

109.    K.Apel and H. Hirt, Annu. Rev. Plant. Biol. 2004, 55, 373.

110.    R. Vivek, V. Nipun Babu, R. Thangam, K. S. Subramanian and S. Kannan, Colloids Surf., B, 2013, 111, 117.

111.    A. Dhanasekaran, S. Kotamraju, C. Karunakaran, S.V. Kalivendi, S. Thomas, J. Joseph and B. Kalyanaraman,    Free Radic. Biol. Med. 2005, 39, 567.

112.    M. Ott, V. Gogvadze, S. Orrenius and B. Zhivotovsky, Apoptosis, 2007, 12, 913.

113.    S. Ueda, H. Masutani, H. Nakamura, T. Tanaka, M. Ueno and  J. Yodoi, Antioxid. Redox. Sign., 2002, 4, 405.

# CHAPTER VI
# SUMMARY AND SCOPE OF FUTURE WORK

## SUMMARY

6.1     Titanium dioxide (TiO₂) has been the most intensively investigated binary transition metal oxide in the past four decades. The apparent merits of TiO₂ including elemental abundance, good chemical and thermal stability, nontoxicity, easy synthesis, flexibility to get tuned in diverse morphologies etc. have attracted much research interest. In this work, we have synthesised five nanostructured titanium dioxide, namely multishelled titania hollow nanospheroids, mesoporous assembled titania nanocuboids, titania nanotubes, titania nanobelts and titania nanoparticle adopting various synthesis procedures.

The first chapter begins with advancements in nanotechnology applied to metal oxides, with special emphasis on titanium dioxide. This includes a brief history of photocatalysis and also explains the importance of titania as photocatalyst. Details on its structure, different methods of preparation as well as some relevant applications are addressed here. The necessity for modification of titanium dioxide, various strategies adopted in this direction to enhance the application potential and merits of these modification procedures are also heighlighted in this section citing appropriate literature. An outline of present research work was also incorporated.

Chapter 2 contains a detailed description of chemicals/reagents used, the experimental conditions for the preparation of various titania

nanostructures and its modifications techniques alongwith catalyst notations. Here we also discussed the theory and experimental basis behind various characterisation techniques adopted here. The experimental set up for the measure of photocatalytic activity studies and biological studies is well discussed in this part.

The third chapter summarised the results of various characterisation techniques of these synthesised titania nanostructures. Various microscopic analysis confirmed the size and morphology of the synthesised nanostructures. Crystal phases were analysed by XRD and Raman spectra. Mesoporous nature was further confirmed with low angle XRD and nitrogen adsorption desorption isotherms. Nitrogen adsorption desorption studies light on the porosity aspects, which are important in tuning the activity. UV- Visible diffuse reflectance spectrum showed that absorption of the synthesised nanostructures are in the UV-range. Various crystal planes are observed from the high resolution transmission electron microscopic images. Crystsalline/amorphous nature was revealed from the SAED images. The dynamic light scattering analysis provided an idea about particle size distributions, zetapotential and polydispersity index of the synthesised systems. This chapter also included the formation mechanism of various nanostructures prepared, with appropriate literature status.

The fourth chapter deals with the photocatalytic applications of titania nanostructures. This chapter is divided into two sections, Section A and Section B. First part of Section A described the UV light assisted photocatalytic degradation of organic pollutant taking methylene blue

dye using the synthesised $TiO_2$ photocatayst nanostructures. All the prepared systems showed good phootcatalystc activity activity towards dye degrdation while multishelled titania hollow nanospheroids was observed to be the superior one,   completely degrading within 35 minutes The highlight of this study is that the photocatalytic activity is achieved with a catalyst doasage which is commentable low compared to many previous reports. Much superior dye degradation efficiency was noticed for multishelled system where the catalyst amounts only to ¼$^{th}$  of the value reported under identical experimental conditions. Mineralisation studies by COD analysis were also conducted and it followed the same order. Commercially available $TiO_2$ was tested for dye degradation and is observed to be having the lowest value. The higher activity of mutiwalled structure is due to the multiple reflections of UV light when falls on the structure due to its sphere in sphere nature which effectively utilises the light to boost up the photocatalytic process. Mesoporous assembled titania nanocuboids is exhibiting good photocatalytic activities due to its high surface area and exposed active facetes. The biphasic strucutre and reasonable surface area value make titania nanotubes a better photocatalyst than Titania nanobelt. Among the synthesied systems, titania nanoparticle shows the lower activity owing to the presence of rutile phase snd lower surface area of the systems, towards dye degradation. Second part of section A comprises the photocatalytic antibacterial and antifungal studies of the prepared nanostructures. E.Coli, gram negative bacteria and the fungus Candida ablicans were chosen as the microbes for the experiment. All the Titanium dioxide systems exhibited antimicrobial activity due to its strong oxidizing property when exposed to light. With a fixed time course of light radiation, multiwalled titania hollow nanospheroids exhibited maximum inhibition of gram negative bacteria E.Coli with

minimal catalyst concentration. Further the antifungal activity was evaluated by Optical Density method and the multiwalled titania hollow nanospheroids itself show the minimum number of viable cells with a predetermined concentration and fixed time course of light irradiation. The commendable activity to remove organic pollutant and pathogenic organisms highlights the applicability of multishelled system as a self cleaning material in walls and tiles of house, kitchen, hospitals, etc. Hence contact angle measurement was also performed to examine the hydrophilicty under UV radiation and it was observed that the contact angle was decrased to a considerable extent showing the hydrophilic nature of titania based systems upon UV irradiation.

Section B of the fourth chapter describes the characterisation and photocatalytic water splitting ability of cocatalysts loaded mesoporous assembled titania nanocuboids and titania nanotubes. The cocatalysts, copper and silver were loaded using photodeposition method. Excellent candidature of these systems was proved by visible light assisted photocatalytic removal of methylene blue dye. Hydrogen production by water splitting reactions in visible light emphasised their visible light response. The cocatalyst modified systems were found to be effective in reducing the charge carrier recombination as evident from the photoluminascent spectra. Among the synthesised systems, the activity of copper decorated mesoporous assembled structures was found to be much higher which produced 16673.2µmoles/g of Hydrogen. Based on the results we can conclude that copper loaded titania nanostructures are cost-effective and efficient catalysts in the relm of photocatalytic water splitting.

The fifth chapter deals with the invitro cytotoxic studies of the synthesised systems in human breast cancer cell lines [MCF-7]. The

order of $IC_{50}$ value being TNT < MHS < TNP < TNB < MT as per MTT Assay. Morphology analysis and DAPI images confirmed visible evidence for the unhealthy cells in the treated ones compared to the control cells. Inorder to utilise the porosities of the synthesised nanostructures, Encapsulation experiments were done using the drug, 5-Fluorouracil. All the drug loaded samples showed lower $IC_{50}$ values related to their parent systems due to the presence of cytotoxic drug. Drug uptake per milligram of drug the loaded sample were analysed by HPLC. Highest uptake was shown by mesoporous assembled structures and correspondingly its $IC_{50}$ value (30 µg/mL ) was decreased to a considerable extent than its parent system, MT (50.01 µg/mL). The over expression of folate receptors on cancer cells are utilised to specifically kill the tumour tissues by modifiying the systems with folic acid. $IC_{50}$ values were found to decrease to a considerable extent when compared to the mere drug loaded systems. Targetting effect of folic acid and the synergetic effect of two cytotoxic agents namely Titanium dioxide and 5-Fluorouracil. Thus this type of biomolecule-based nanstructures would be beneficial for smart multifunctional nanomedicine systems. As folate modified 5-FU incorporated mesoporous assembled titania nanocuboids showed lowest $IC_{50}$ value, further investigation on the cancer intracellular mechanism were done using the system. Finally we concluded that system triggered caspase-dependent and ROS-dependent apoptosis in MCF-7 cancer cells through mitochondria-mediated pathway. Such a system can be developed as a novel apoptosis inducer against cancer cells.

## 6.2 Future Scope

➢ Achievement of single crystalline multishelled titania hollow nanostructures of uniform size through the sysnthesised requires indepth study of the various reaction conditions and reagent concentrations. Investigation on the effect of reagent concentrations and nature of alkali on the size and morphology of this complex hollow structure can be pursued.

➢ The photocatalytic activity of multishelled titania hollow nanospheroids  can be extended to the visible region by doping with appropriate metals, nonmetals etc.

➢ Hydrogen production by photocatalytic water splitting using copper cocatalyst loaded multishelled titania hollow nanospheroids and titania nanobelt can be monitored.

➢ Scope of nano titania for biomedical applications can be further increased if the oxide is made more biocompatible. This will also enable to perform in vivo studies using the system.

➢ 5Fluorouracil is reported to be stable against skin enzymes which make it a good candidate for transdermal delivery. Certainly nanocarriers could improve skin targeting, enhancing the drug's ability to reach and penetrate into tumor tissues. Besides nanocarriers reduce the skin irritation by avoiding the intimate contact of the drug with skin surface and also increase the drug stability. It has been concluded from the study that the titanium dioxide nanostructures especially mesoporous

assembled titania entrapped with anticancer drug has significant cytotoxic effects. We have developed a folic acid based gel which can entrap sufficient amount of drug and these 3 Dimensional network ofcourse result in slow release of the drug. Hydrogels in general have got more attention in the drug delivery industry because of their tunable chemical and three-dimensional (3D) physical structure most attractive features are their high water content, biocompatibility and environment responsiveness. When nanoparticle entrrapped anticancer drug was dispersed in this gel, it can effectively release drug in a sustained manner. It has been proven that Folic acid is a good candidate for topical micronutrient delivery as its bioactive forms is useful in the maintenance of genomic integrity via enhancement of DNA synthesis, DNA repair, and maintenance of epigenetic regulation. Folic acid has been reported to form supramolecular gel varying its composition with the ratio of DMSO to water solvent mixture. And this drug can entrap molecules which can be released in the medium. The prepared folic acid gel and its ability to encapsulate molecules are evident from figure shown below (Figure1).

Figure 1. Folic acid based supramolecular gel [Left] and the gel encapsulated Rhodamine dye [Right]

The gel comprises the solvents water, dimethyl sulfoxide and DMSO. When applied to skin, it penetrates and will pass into the tissue. The release of 5-FU from titanium dioxide to the gel network imbibes the drug and thus enter into the skin. Actually, 5-FU cream and solution have been used to treat skin cancers in clinical settings. Therefore, the development of the Folate targeted 5-Fu loaded titania nanostructures as a topical therapeutic agent could be an achievable design for treatment of melanoma. However, pharmaceutics studies are needed to realize this Design.

# PRESENTATIONS

1.  Poster presentation in UGC sponsored National seminar on Advances in Nanomaterials and Ploymers at Bharathmatha college,Thrikakara.

2.  Poster presentation in First National Conference on Advanced Nanomaterials at Nirmalagiri college Koothuparambhu, Kannur**. [** ISBN No. 978-81-931227-0-9**]**

3.  Oral presentation in the National Conference on advanced nanomaterials at N.S.S College Manjery. (ISBN No. ISSN 0974-2115)

4.  Poster presentation at the Fourth Inernational Conference on Frontiers in Nanoscience and Technology, COCHIN NANO 2016 at CUSAT Cochin.

5.  Oral presentation in 29th Kerala Science congress 2017

6.  Oral presentation at International conference on energy environment and advanced materials for sustainable future, ICEEAMSF-2017 at Kongu Engineering college,Erode **[**ISBN No. 978-81-933005-2-7].

# PUBLICATIONS

1.   M. P. Nikhila and N. K. Renuka\*, Novel Template Free Synthetic Strategy to Single Crystalline Multishelled Hollow Nanospheroids of Titania with Boosted Application Potential, RSC Adv., 2016, 6, 24210–24217

2.   M. P. Nikhila, A. K. Akhila, T. Divya, M. Anju, T. V. Arsha Kusumam and N. K. Renuka\*, P123 and solvent-assisted synthesis of titania nanocuboids with co-exposed {101} and {001} planes, CrystEngComm, 2017, 19, 511-518.

3.   N.K. Renuka and M.P. Nikhila, Synthesis, characterisation and photocatalytic activity of titania nanotubes, JCPHS, ISSN: 0974-2115

4.   T.V. Arsha Kusumam, Thasleena Panakkal , T. Divya , M.P. Nikhila , M. Anju , K. Anas , N.K. Renuka\* , Morphology controlled synthesis and photocatalytic activity of zinc oxide nanostructures , (2016), 42, 3769-3775.

5.   M. Anju, T. Divya, M. P. Nikhila, T. V. Arsha Kusumam,  A. K. Akhila, V. A. Ansi and N. K. Renuka\* An elegant and handy selective sensor for ppt level determination of mercury ions, RSC Adv., 2016, 6, 109506-109513

6.   Divya T., Nikhila M.P., Anju M., Arsha Kusumam T.V., Akhila A.K., Ravikiran Y.T., Renuka N.K.\*, Sensors and Actuators A , 2017, 261,85–93**.**